IMPLICATIONS OF ATMOSPHERIC TEST FALLOUT DATA FOR NUCLEAR WINTER

DISSERTATION

George H. Baker III
Defense Nuclear Agency

DEPARTMENT OF THE AIR FORCE
AIR UNIVERSITY
AIR FORCE INSTITUTE OF TECHNOLOGY

Wright-Patterson Air Force Base, Ohio

AFIT/DS/ENP/87-1

IMPLICATIONS OF
ATMOSPHERIC TEST FALLOUT DATA
FOR NUCLEAR WINTER

DISSERTATION

George H. Baker III
Defense Nuclear Agency

AFIT/DS/ENP/87-1

Approved for public release; distribution unlimited

AFIT/DS/ENP/87-1

IMPLICATIONS OF ATMOSPHERIC TEST FALLOUT DATA FOR NUCLEAR WINTER

DISSERTATION

Presented to the Faculty of the School of Engineering

of the Air Force Institute of Technology

Air University

In Partial Fulfillment of the

Requirements for the Degree of

Doctor of Philosophy

George H. Baker III, B.A., M.S.

Defense Nuclear Agency

February 1987

Approved for public release; distribution unlimited

AFIT/DS/ENP/87-1

IMPLICATIONS OF ATMOSPHERIC TEST FALLOUT DATA FOR NUCLEAR WINTER

George H. Baker III, B.A., M.S.

Defense Nuclear Agency

Approved:

Charles J. Bridgman — March 5, 1987
C. J. Bridgman, Chairman

D. L. Auton — 2/28/87
David L. Auton

George John — 3/9/87
George John

Ronald F. Tuttle — 3/9/87
Ronald F. Tuttle, LTC USAF

Dennis W. Quinn — 3/9/87
Dennis W. Quinn

Accepted:

J. S. Przemieniecki — 12 Mar 87
J. S. Przemieniecki
Dean, School of Engineering

Preface

The purpose of this research has been to revisit the atmospheric nuclear test data of the 1950's and 1960's in order to gain information germane to nuclear winter. I have concentrated on resolving the size distribution of the debris ensemble because particle size strongly governs the magnitude and duration of sunlight attenuation. By modeling the removal of nuclear debris from the atmosphere, it has been possible to bound the admissible distribution of lofted particulates. In addition, I have shown how gravitational cloud stratification creates particle populations approximated by a power law distribution. The results should be useful for fallout and dust effects modeling as well as nuclear winter studies. I was frustrated by time limitations-- there is much more to be learned from the ~400 events which have occurred in our atmosphere.

I am greatly indebted to my research advisor, Dr. Charles J. Bridgman, whose original calculation of optical attenuation vs. particle size distribution was the genesis of this project, and whose advice and encouragement enabled its completion. The excellent work of Dr. Marcel Nathans (LLNL), Dr. Ernest Bauer (IDA), and Dr. Alan Mason (LASL) provided the foundation for much of what I have done. I am most grateful for their advice and counsel during several meetings and telephone conversations. Capt Norm Davis (USMC) provided valuable assistance during the course of his masters' research. In addition, without the material provided by Mr. Al West of the DNA Technical Library and Mssrs. Bill Alfont and Dick Rowland of KAMAN TEMPO my research would not have been possible. The interest and assistance of LTC Ron Tuttle of AFIT and Dr. David Auton of the Defense Nuclear Agency was most appreciated. Special thanks are due to Dr. Marvin Atkins, Dr. Gordon Soper, COL William Adams, COL Ray Bellem, Dr. R.C. Webb and Mr. Bron Cikotas of the Defense Nuclear Agency who most graciously released me for the time necessary to complete my degree.

I must finally thank my wife, Donna and children, Matthew, Jeffrey, and Virginia for their patience, faith, and encouragement during the course of this endeavor.

George H. Baker

Table of Contents

Table of Contents, continued

Table of Contents, continued

List of Figures

List of Figures, continued

List of Figures, continued

List of Tables

ABSTRACT

Atmospheric test fallout data have been used to determine admissible dust particle size distributions for nuclear winter studies. The research was originally motivated by extreme differences noted in the magnitude and longevity of dust effects predicted by particle size distributions routinely used in fallout predictions versus those used for nuclear winter studies. Three different sets of historical data have been analyzed:

1) Stratospheric burden of Strontium-90 and Tungsten-185, 1954-1967 (97 contributing events),
2) Continental U.S Strontium-90 fallout through 1958 (75 contributing events), and
3) Local Fallout from selected Nevada tests (16 events).

The contribution of dust to possible long term climate effects following a nuclear exchange depends strongly on the particle size distribution. The distribution affects both the atmospheric residence time and optical depth. One dimensional models of stratospheric/tropospheric fallout removal were developed and used to identify optimum particle distributions. Results indicate that particle distributions which properly predict bulk stratospheric activity transfer tend to be somewhat smaller than number size distributions used in initial nuclear winter studies. In addition, both ^{90}Sr and ^{185}W fallout behavior is better predicted by the lognormal distribution function than the prevalent power law hybrid function. It is shown that the power law behavior of particle samples may well be an aberration of gravitational cloud stratification. Results support the possible existence of two independent particle size distributions in clouds generated by surface or near surface bursts. One distribution governs late time stratospheric fallout, the other governs early time fallout. A bimodal lognormal distribution is proposed to describe the cloud particle population. The distribution predicts higher initial sunlight attenuation and lower late time attenuation than the power law hybrid function used in initial nuclear winter studies.

IMPLICATIONS OF ATMOSPHERIC TEST FALLOUT DATA FOR NUCLEAR WINTER

I. Introduction.

A. Background.

The possibility of serious climatic consequences of a nuclear war has been recently investigated by several groups (1,2,3,4,5). Perhaps the best known investigation, and one with the most cataclysmic predictions, was by R. P. Turco, O. B. Toon, T.P. Ackerman, J.B. Pollack, and C. Sagan. The "TTAPS" group concluded that attenuation of incoming solar radiation leading to subfreezing land temperatures could occur over the northern hemisphere due to vast amounts of dust and smoke aerosols injected into the atmosphere during a major nuclear exchange. Their initial calculations (1, see figure 1 inset) were based upon a 9800 megaton baseline exchange between the superpowers but indicated that the yield threshold for major optical (and therefore climatic) effects may be as low as 100 megatons. The outcome the TTAPS baseline scenario is a peak 35° C temperature drop of roughly 6 month duration (figure 2). A subsequent, independent evaluation of these findings by the National Research Council (3) questioned the plausibility of certain of the TTAPS assumptions (e.g. treatment of smoke injection), but confirmed the possibility of large and prolonged temperature drops across the northern hemisphere leading to what the TTAPS group dubbed "nuclear winter." Ramaswamy and Kiehl (abbreviated R-K), in a recent parametric evaluation of the optical properties of dust and smoke, also calculated significant temperature drops (5). In these initial studies, smoke appears to dominate dust because of its higher absorption properties, and the large fuel densities assumed for targeted urban areas. Thus most of the research to date has been devoted to verifying smoke effects. This lopsided attention to smoke has also been warranted by the large number of variables in the fire problem which has left much more room for interpretation and hence much larger uncertainties. Differing

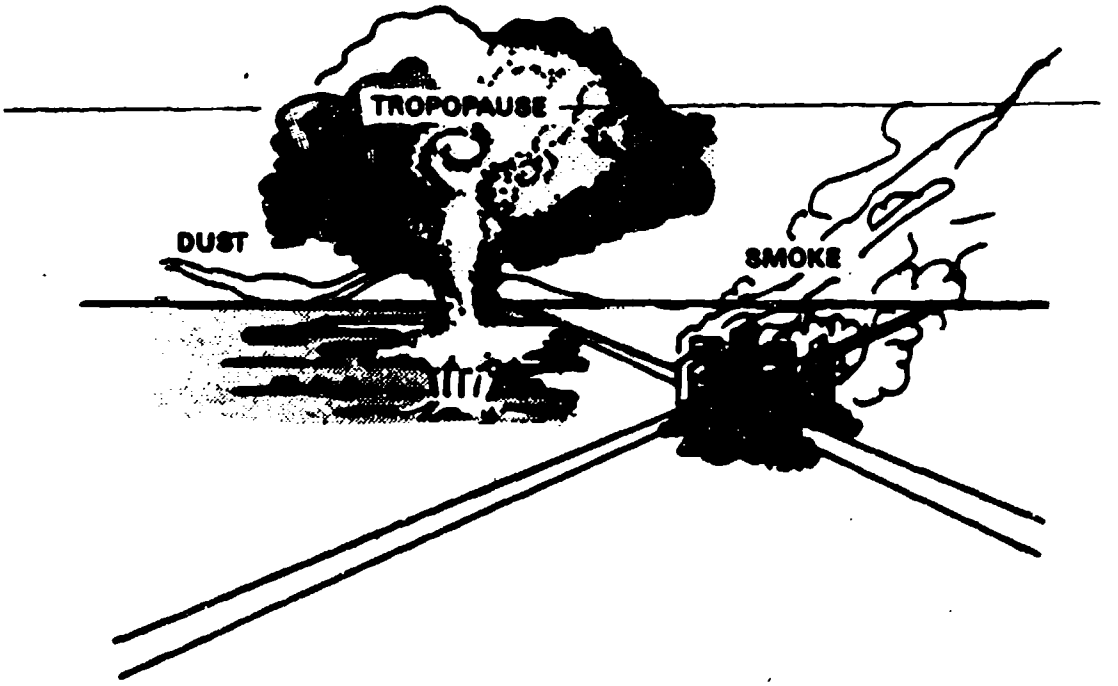

TYPE OF BURST	YIELD PER WARHEAD (megatons)	NUMBER OF BURSTS	YIELD EXPENDED (megatons)
Land surface	10	110	1100
Land surface	5	460	2280
Land near-surface	1	3000	3000
Low airburst	1	1000	1000
Exo-atmospheric	1	100	100
Low airburst	0.5	500	250
Low airburst	0.3	3000	900
Low airburst	0.2	3000	600
Water surface	0.2	1000	200
Low airburst	0.1	3000	300
Water surface	0.1	1000	100
		16160	9800

Figure 1. TTAPS Nuclear Exchange

assumptions concerning whether fires start at all, whether they spread significantly, whether firestorms occur and, if so, whether the smoke reaches the stratosphere have led to extreme variations in the severity of predicted outcomes.

While it may be true that the amplitude of dust induced climate effects is less severe, the longevity of stratospheric dust aerosols (as compared to longevity of smoke which is confined predominantly to the troposphere and is therefore subject to rapid removal by washout) prolongs the dust induced temperature drop for periods exceeding one year. Indeed, dust alone is sufficient to produce significant temperature changes according to the results of a TTAPS scenario in which no smoke was injected (figure 2). The relative significance of dust has been enhanced by declining estimates of urban fuel loading and the addition of scavenging to smoke removal models (6,7).

Although not as formidable as those for smoke, large uncertainties do exist in the parameters used for the modeling of dust effects. One of the largest of these uncertainties is the particle size distribution. The optical thickness of a given mass of dust is extremely sensitive to the size distribution of the dust. This is illustrated in Chapter II where the optical thickness is computed for three different size distributions as proposed by Nathans (and used by TTAPS), Ramaswamy (5), and Norment (8). The large differences in the magnitude and duration of the sunlight occlusion for the three selected size distributions and the obvious extreme sensitivity of optical thickness behavior to the dispersion of the size distribution are worrisome in that the relative effect on the climate ranges from nil (Norment) to potentially severe (Nathans, Ramaswamy).

B. Research Objective.

The objective of the present effort has been to reduce the uncertainties in the admissible weapon debris aerosol size distributions. While large uncertainties still remain with respect to the mass lofted vs. yield and burst height, the uncertainties in size distribution are more significant because they affect both the amplitude and duration of sunlight attenuation. Variance in the lofted mass affects only the amplitude of the attenuation and probably does not exceed an order of magnitude for surface bursts (1,3). This translates into a factor of ten uncertainty in the optical thickness. It is evident from figure 3 that larger uncertainties in the optical thickness can

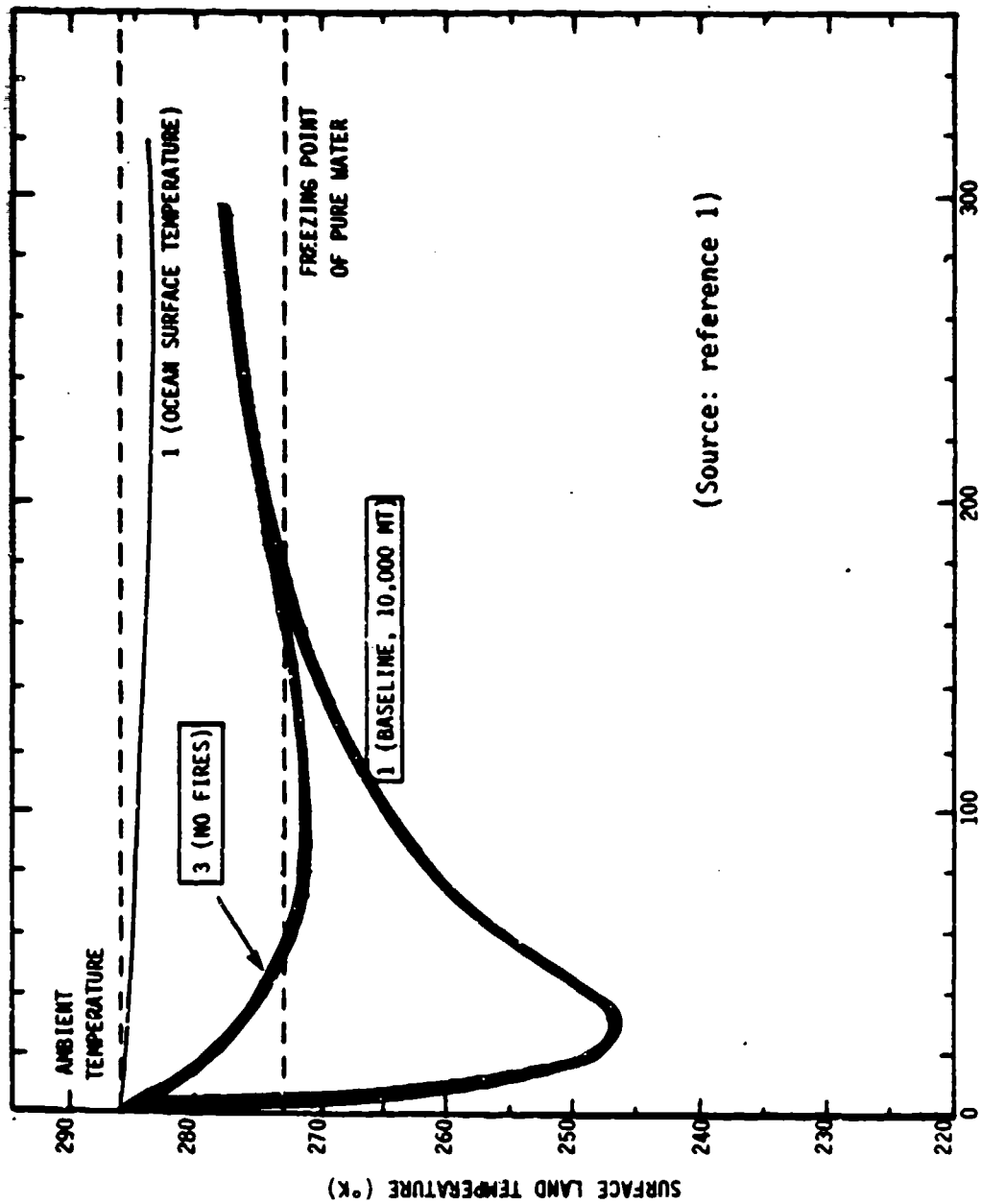

Figure 2. Dust vs Smoke Effects

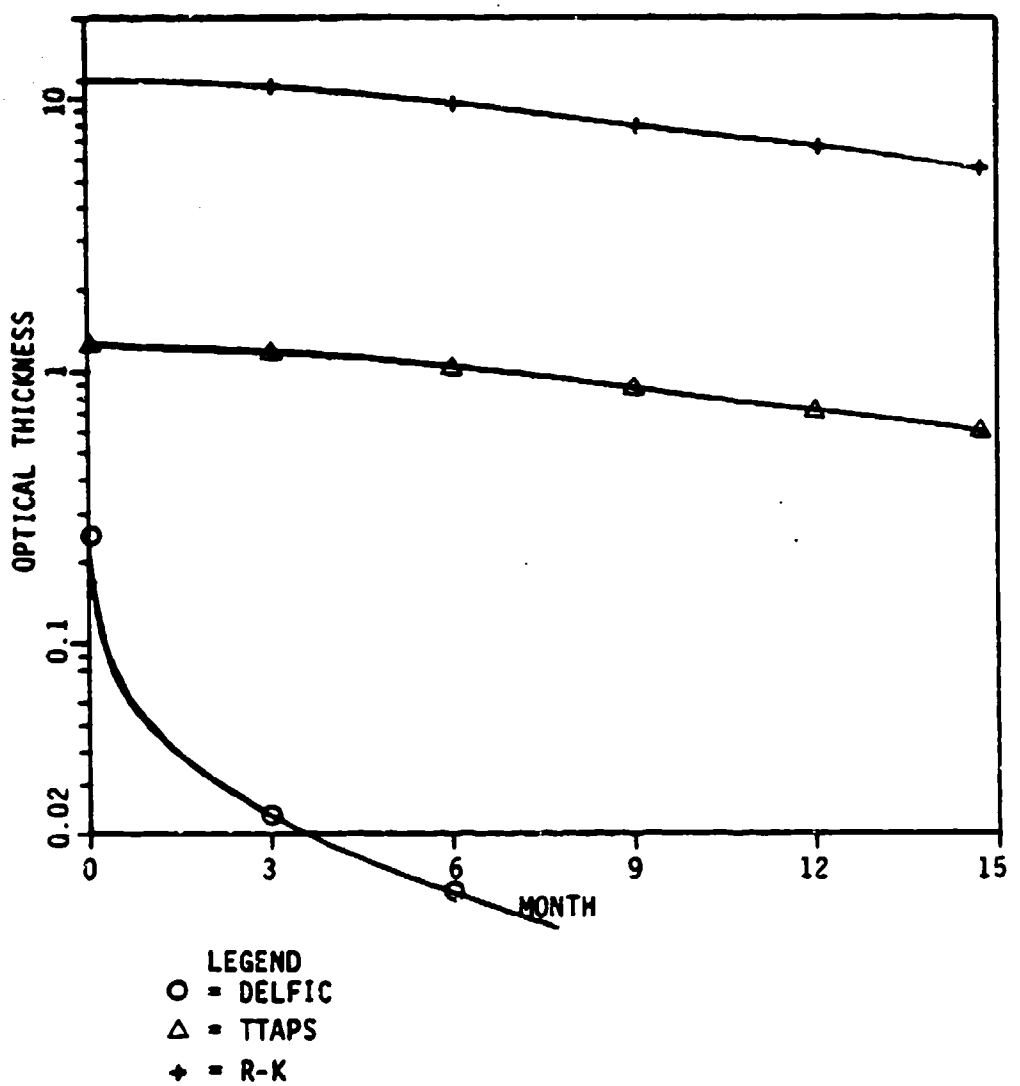

Figure 3. OT vs. Time, Cloud Initially Centered at 25 km

be attributed to variance in size distribution.

C. Approach.

This effort has used activity tracing to bound admissible size distributions. Activity tracing involved starting with historical data recording nuclear weapon fallout in the atmosphere and on the ground and then back-calculating the size distribution(s) which could have caused the measured activity transfer. This method of determining admissible size distributions has not been previously used.

The approach proceeded as follows. First, fallout removal/deposition mechanisms were modeled. The models were exercised against available data. Size distribution parameters were adjusted to achieve favorable comparisons between the models and the data. Care was taken to identify and resolve differences between the size distributions derived from activity tracing, and those previously reported (which were based upon microscopic techniques). A variety of historical data was used. Chapter IV contains a detailed discussion of the approach, how it differed from previous n(r) investigations, and how it was affected by the types of data available.

D. Other Methods.

Other methods have been used and are being developed to characterize size distributions. In the past, particle size distributions have been measured primarily by microscopic examination of fallout samples. Another method presently under development uses laser interferometry. Both methods are "direct" in that they measure the size of individual particles in isolated samples. By contrast, the activity tracing method is indirect in that size information is inferred from bulk activity transfer data.

D.1. Microscopic Techniques.

Particle size distributions have been primarily determined from the microscopic study of individual samples from clouds (particles collected on aircraft filters) or the ground (gummed paper, granular collectors). A discussion of aircraft sampling methods is contained in documentation of the DNA High Altitude Sampling Program (HASP) (9,10,11,12). A discussion of ground fallout collection methods is contained

in test director reports for many of the atmospheric test series (examples 13,14,15).

D.1.a. Nathans' Cloud Sample Analysis.

Nuclear winter studies have based their particle size distributions on Nathans' laboratory analysis of cloud samples from four ground bursts: Johnie Boy, Castle Bravo, Koon, and Zuni (16). In his experimental procedure, sections of the sampling filter paper were "ashed" leaving behind the debris particles plus some limited filter residue. Low temperature ashing was used when possible to avoid losing volatile fission products. Because small particles were masked by larger ones (diameters range over several orders of magnitude), samples were put into solution and separated via centrifuge into (typically ten) size fractions. About 100 particles from each size fraction were measured so that the size distribution of each sample was based on ~1000 particles. By adding the size distributions of the fractions weighted by number, composite size distributions were plotted. Apparently, histograms for these surface bursts were based upon irregularly shaped particles only. Spherical particles were present in significant numbers only in the three smallest size fractions of Johnie Boy and had a size distribution which differed from the irregulars. Nathans' results for samples from the four surface bursts appear in figures 4-6. His results include a slight correction for sedimentation (further discussion in Section V.E). The TTAPS and NRC particle size distributions were based on these results.

Nathans has also done a similarly meticulous evaluation of clouds from eleven air bursts (17,18) and finds in all cases a unimodal lognormal size distribution with a slope similar to that of the submicron surface burst cloud population, but having a smaller median radius on average (.07μ air burst vs .25μ surface burst). Nathans claims to have been able to detect particles down to and slightly below .02μ in diameter. Below 0.1μ he used activity to isolate the particles. For extremely small particles he developed a method to agglomerate several smaller particles in order to detect their presence (19). Nathans noted a lower cutoff diameter for debris particles in the vicinity of .02μ (18). Nathans' analysis included the correlation of specific activity (equivalent fissions per gram) with particle radius. This correlation was an essential input to the activity tracing method pursued in the present effort.

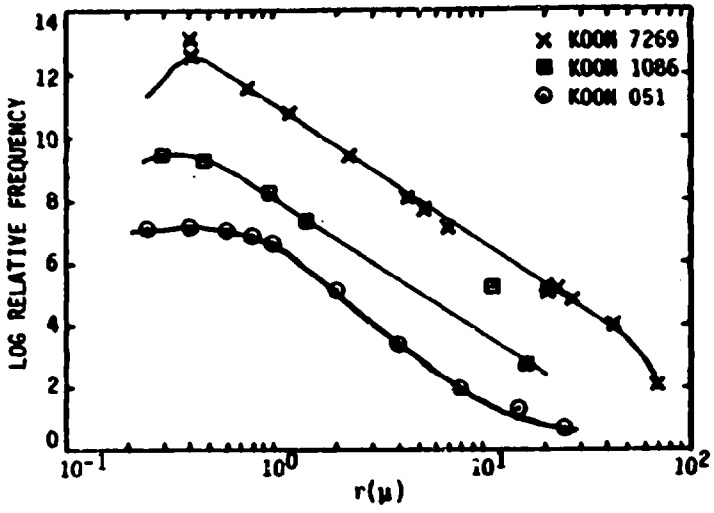

Figure 4. Size frequency curves for three Koon samples

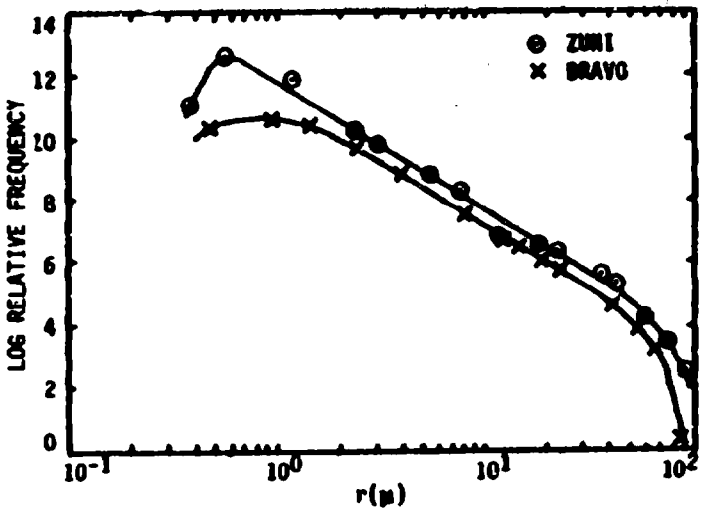

Figure 5. Size frequency curves for a Bravo and a Zuni sample

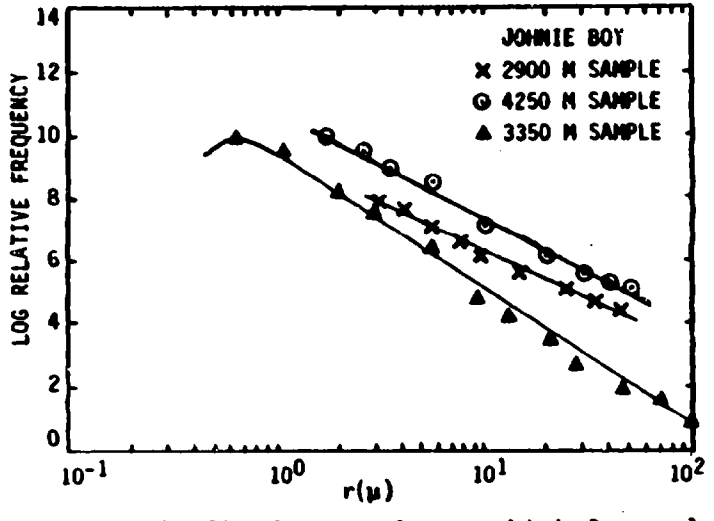

Figure 6. Size frequency for some Johnie Boy samples

D.1.b. Ground Sample Analysis.

Unfortunately, the documentation of n(r) analysis for ground samples is very sparse. Most analysis was concerned primarily with the radiochemical morphology of the particles and to a lesser extent with the size distribution. In addition, reported ground sample particle size distributions exhibit much more variability than do cloud samples. Norment's DELFIC nominal distribution, previously discussed (8), is a unimodal lognormal function with median radius, $r_m = .204\mu$ and a logarithmic slope = 4. Freiling (20) reports lognormal distributions with mass median radii of the order of 100μ and logarithmic slopes of 1.68 to 1.98. Tompkins (21) reports a mass median radius of 250μ and a logarithmic slope of 1.9 for a Small Boy sample 5.8 km from ground zero. At greater distances, his samples are not unimodal. The WSEG fallout model (22), based on ground deposition, uses an activity median of 60μ and slope of 2. The present research has developed evidence that the extreme variability in ground samples may well be due to cloud stratification caused by gravity sorting (see section V.E).

D.2. Laser Interferometry.

Optical methods involving laser interferometry are presently being perfected for analysis of nuclear cloud samples (23). In particular, Los Alamos is developing a method using the doppler shift of laser light to correlate the Brownian motion of particulates in solution, thereby determining particle size from diffusion velocity (24). While laser techniques have been successfully employed for in situ measurement of particle sizes during recent high explosive events, systematic studies of old nuclear cloud samples by such methods are not yet available. These techniques look very promising.

E. Some Problems Associated with Other Methods.

The advantages of the direct techniques are obvious. The analyst is measuring and counting observable particles from real samples. The analyst knows when and where the sample originated as well as which event (and relevant detonation parameters) was the primary contributor to observables. However, there are drawbacks. The size separation techniques may well affect particle size (some dissociation of

agglomerated particles may occur in the solution). There are questions about the degree to which the filter ash may mask the properties of the debris. In addition, there appear to be large variabilities between samples taken at different times and locations (even for cloud samples). The question then remains, "which sample is to be trusted as the most truly representative of the total cloud?" The analysis procedure is extremely tedious and very few events have been systematically characterized (five surface burst clouds, eleven air burst clouds). Surface burst data is of most importance for optical effects since air bursts loft little mass. Despite sample analysis for many events, ground fallout histograms are so highly variable it is difficult to construct a composite size distribution for any one event based upon microscopic techniques.

F. Purpose.

As stated above the purpose of this research was not to rework the direct methods described above, but rather to determine size distributions using a different approach. This approach, activity tracing, involved back-calculating the size distribution from recorded fallout data. The data and methods used to trace activity are presented in Chapters III and IV respectively.

II. Sensitivity of Optical Thickness to Dust Size

The optical properties of any aerosol are extremely sensitive to the population vs radius. Assuming a unimodal lognormal size distribution for the aerosol, it is possible to derive a relatively simple expression for the optical thickness of dust to illustrate this size sensitivity.

A. Optical Attenuation.

The attenuation of sunlight results from scattering and absorption by particulates lofted into the atmosphere. If a cloud of particles is separated into vertical lamina, then the differential change (due to absorption and scattering) in the number of photons traversing each lamina is related to the aggregate cross section of the particles in the laminar volume:

$$\frac{d\phi}{\phi} = \frac{\textit{aggregate particle area}}{\textit{cloud cross section}} = \frac{nA_c\,dz<\mu>}{A_c} \qquad (1)$$

A_c denotes cloud cross section, which is roughly equal to the area of the northern hemisphere ($1.14 \times 10^{14}\ m^2$) in a nuclear winter scenario; n is the particle number density; and $<\mu>$ represents the average optical cross section of the particles. Integration of equation (1) yields an exponential attenuation:

$$R = e^{-\frac{N_t}{A_c}<Q_e \pi r^2>} = e^{-OT} \qquad (2)$$

where OT is the "optical thickness" and N_t is the total number of particles in the cloud. Q_e is the Mie extinction efficiency which is a function of refractive index and the ratio of diameter to wavelength (25). The extinction efficiency is largest for submicron particles and averages about 2.5 at wavelengths of 0.5 μm for particle radii between 0.1 and 10 μ (figure 7). It is evident from this expression that the optical thickness is directly proportional to the aggregate surface area of the particles in the cloud. Thus, the rate of decay of OT with time is directly proportional to the decrease in the second moment of particle number distribution as particles are

removed from the atmosphere by gravity and diffusion, i.e.,

$$OT(t) \ \alpha \ \int_0^\infty \pi r^2 \hat{n}(r,t)dr \tag{3}$$

where

$$\int_0^\infty \hat{n}(r,0)dr = 1 \tag{4}$$

N_t is simply:

$$N_t = \frac{M_T}{\frac{4}{3}\pi < r^3 > \rho_s} \tag{5}$$

where M_t is the total mass lofted, ρ_s is the debris density, and

$$< r^3 > = \int_0^\infty r^3 \hat{n}(r,0)dr \tag{6}$$

Assuming a lognormal distribution (a discussion of the mathematical properties of lognormal distributions is provided in Appendix B):

$$\hat{n}(r,0) = \frac{1}{\sqrt{2\pi}\beta r} \exp\left[-\frac{1}{2}\left(\frac{ln(r) - ln(r_m)}{\beta}\right)^2\right] \tag{7}$$

then

$$< r^3 > = \exp\left[3ln(r_m) + \frac{9}{2}\beta^2\right] \tag{8}$$

Similarly,

$$< r^2 > = \exp\left[2ln(r_m) + 2\beta^2\right] \tag{9}$$

and the initial optical thickness can be expressed in terms of total mass lofted (roughly 10^{12} kg for the 5000 megaton TTAPS scenario), effective particle radius, cloud cross section, and particle density (2600 $\frac{kg}{m^3}$ according to Nathans, ref. 16):

$$OT_{t=o} = \frac{3M_T Q_e}{4r_e \rho_s A_c} \tag{10}$$

$$where \quad r_e = r_m \exp\left(\frac{5}{2}\beta^2\right)$$

Note that the optical thickness of the initial stabilized cloud is dependent on both the median radius and dispersion of the size distribution. The ratio of the initial optical thickness predicted by any two lognormal distributions is given by:

$$\frac{OT_1}{OT_2} = \frac{r_{m_2}}{r_{m_1}} \exp\left[-\frac{5}{2}\left(\beta_1^2 - \beta_2^2\right)\right] \tag{11}$$

A mode radius of .204μ and a slope of 4 is used as the nominal parameters in the Department of Defense Land Fallout Interpretive Code (DELFIC, ref. 8). Ramaswamy and Kiehl (5) use a pure lognormal number distribution with a median radius of .16μ and a slope of 2. A factor of 47 difference in optical thickness results which translates to a ~2 order of magnitude difference in predicted sunlight attenuation (using a radiative transfer algorithm in which full account is taken of multiply scattered radiation, refs. 26,27; figure 9). Note the exponential effect that the assumed slope has on the sunlight attenuation. As will become evident, the slope also has a dramatic effect on the rate of dust removal.

B. Submicron Particle Criticality.

B.1. Optical Efficiency.

As is evident from figure 7, the extinction efficiency is largest below 1μ at the peak solar wavelength. Ramaswamy (5) illustrates the importance of submicron particulates to optical attenuation by computing the optical thickness as the product of a mass attenuation coefficient, ψ_e (*units* m^2/g), and a columnar particle area density:

$$OT = \int_0^\infty \psi_e \left[\int_0^z m(r,z)\, dz\right] dr \tag{12}$$

where r is particle radius and m is the mass density of the aerosol. He then plots the ψ_e as a function of surface mode radius for assumed particle size distributions of slope 2. His results are graphed in figure 8 and vividly illustrate the contribution of the submicron particle population to the optical thickness. An attenuation maximum occurs at a surface mode radius of 0.2μ. Figure 8 also illustrates the very small

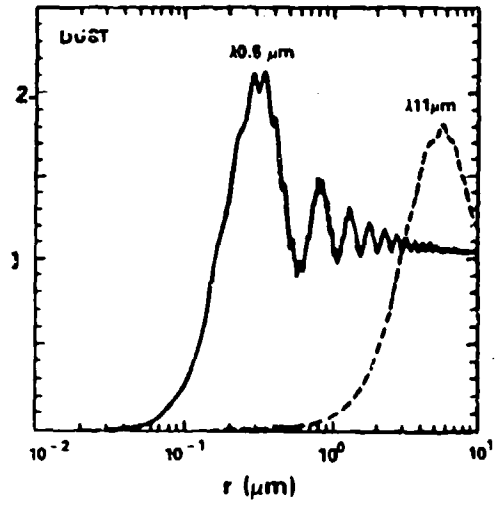

Figure 7. Extinction Efficiency of Dust Aerosols at Wavelengths of 0.5 and 11 μm, as a Function of Size

Source: *Journal of Geophysical Research*, Vol. 90, No. D3 p5598, Copyright American Geophysical Union

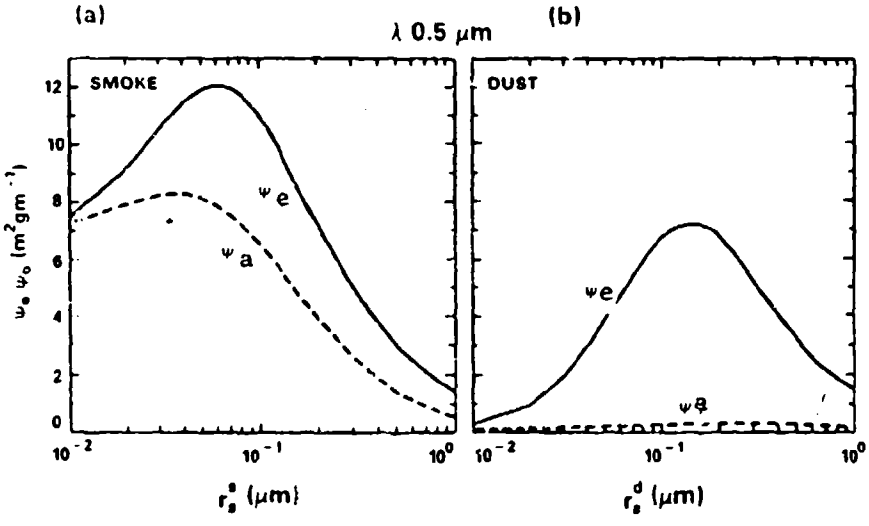

Figure 8. Dependence of the Specific Extinction and Absorption of (a) Smoke Aerosols and (b) Dust Aerosols at a Wavelength of 0.5 μm on the Mode Radius

Source, *Journal of Geophysical Research*, Vol. 90, No. D3, p5600, Copyright American Geophysical Union

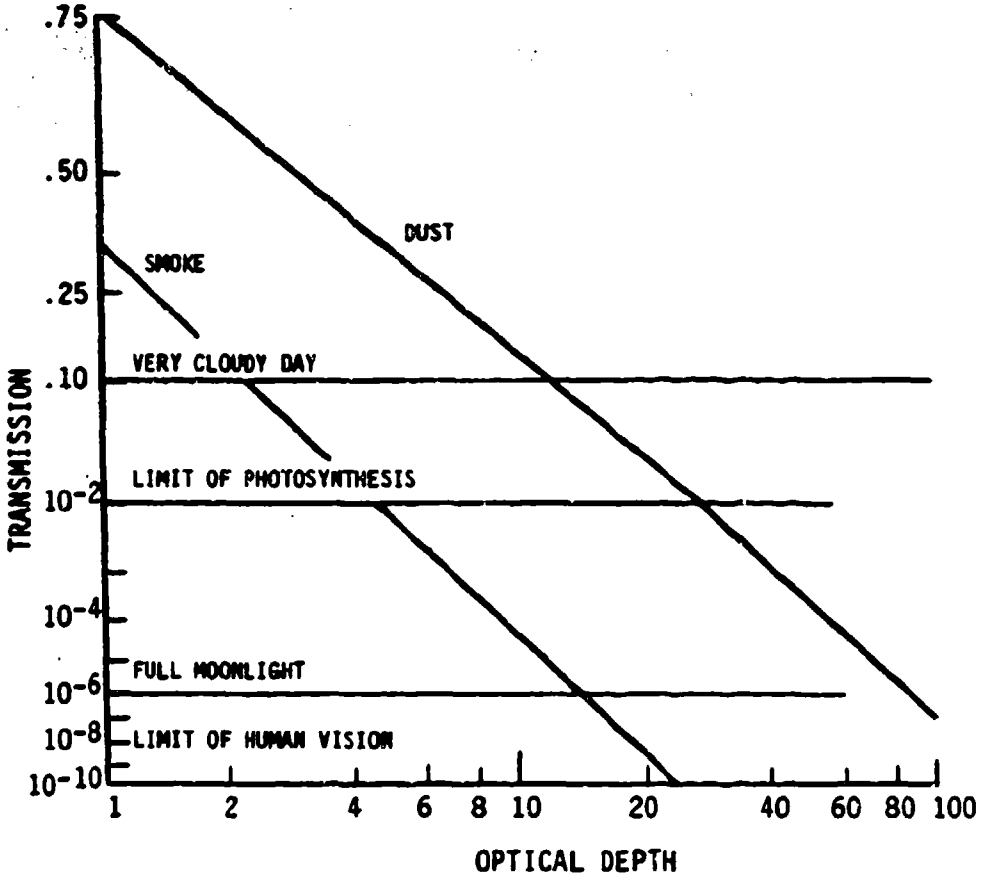

Source: Reference 3

Figure 9. Fraction of incident solar radiation reaching the surface as a function of extinction optical depth for smoke and dust particulates.

contribution of the absorption component, ψ_a, to the attenuation coefficient of dust. Dust is not highly absorbing, and the optical attenuation in dust clouds is primarily due to scattering. Thus for a given optical thickness, optical attenuation in dust is much lower than for smoke which *is* highly absorbing (figure 9).

B.2. Longevity.

Because of the extremely low sedimentation velocities of particles smaller than 1μ, the fraction of the particle ensemble in the submicron range governs the duration of optical attenuation over periods necessary to induce climate changes. For instance, a spherical 10μ particle falls from 20 km to the tropopause (average altitude 12 km) in approximately 3 days whereas a 1μ particle takes 190 days. A graph of fall time vs radius and altitude for spherical particles is included as figure 10. The graph is based upon Stokes-Davies-Macdonald fall mechanics model as described in Appendix A. It is clear from this graph that the submicron particle fraction, in addition to dominating the optical attenuation, also governs the duration of sunlight attenuation.

C. Ground vs Cloud Sample Dichotomy.

Depending upon the origin of particle samples, size distributions determined from the analysis of atmospheric test dust exhibit markedly different submicron fractions. Most available samples fall into two major categories: (1) local fallout (down within roughly 24 hours of event) ground samples, and (2) early time (within several hours) cloud samples.

The tendency has been to use cloud samples as representative of initially lofted particle distributions. Intuitively, one would expect that because of sedimentation, ground samples would be biased toward the larger end of the size spectrum and cloud samples would be oppositely biased. This seems to be true. However, one should also expect that since the origin of both cloud and ground samples for any event is ultimately the same explosion, there should be similarities in particle characteristics.

A point in favor of using ground sample distributions is that near ground zero, fallout appears to result from the vertical component of toroidal circulation within the cloud (as well as sedimentation). Ground samples near ground zero should

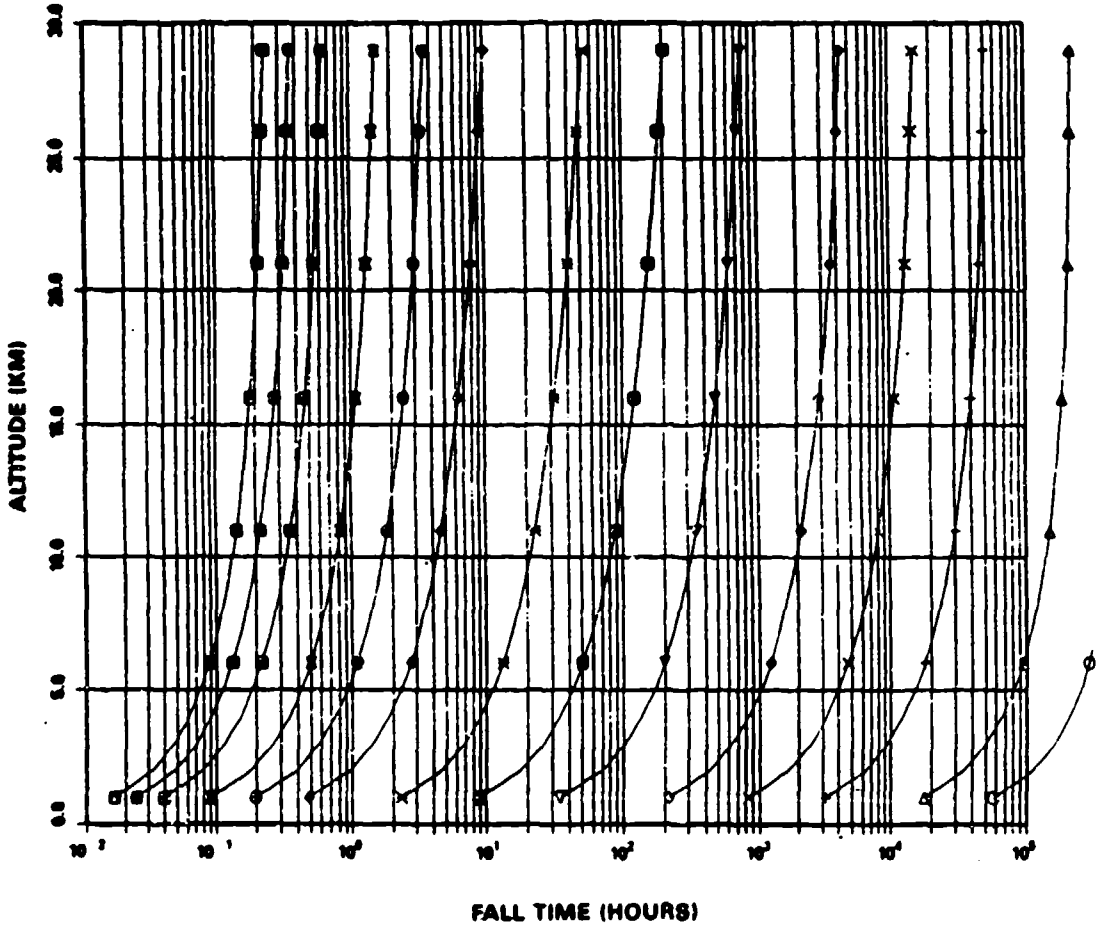

Figure 10. Fall Time versus Size and Altitude

therefore represent a homogeneous mixture of lofted particles, both large and small (28:51). Indeed, by ascribing ground sample size distributions to clouds and then modeling deposition by sedimentation, reasonable predictions of ground fallout contours are obtained (29,30,31,32). Ground samples cannot be easily dismissed as nonrepresentative of the particle population. In addition, since many cloud samples (16) were taken at altitudes considerably below the cloud vertical center (since for high yield events, the cloud eluded the altitude capabilities of sampling aircraft), these samples may also be nonrepresentative of the aggregate cloud population.

There is some additional cause for questioning the use of distributions derived from available analysis of surface burst cloud samples. The TTAPS and NRC studies used particle size distributions based upon surface burst cloud sample analysis of Marcel Nathans (16). Nathans measured and counted particles from four surface bursts: Johnie Boy, Castle Bravo, Koon, and Zuni. Of these, the high yield shots (of most interest for nuclear winter predictions) were detonated over coral. Johnie Boy, the only burst over silicate soil, was low yield (.5 kiloton) and slightly buried. Since the nuclear winter phenomenon is based on mass lofted by megaton surface bursts over silicate soil there is good reason to question the applicability of the measured size distributions. Admittedly, test ban restrictions have prevented extending the data base. Nonetheless, as the present research indicates, there is much more that can be learned from the existing atmospheric test data base.

To investigate the effect of differing size distributions on both the magnitude and longevity of optical effects, three distributions were selected for initial comparisons--one (the Defense Land Fallout Interpretive Code or DELFIC nominal distribution) representative of ground sample data, the other two (TTAPS, R-K) representative of cloud sample data. A discussion of the characteristics of each size distribution follows.

C.1. DELFIC Nominal Distribution.

DELFIC is a full physics, main frame fallout code developed by Hillyer Norment for the Defense Nuclear Agency (8). Although any size distribution may be used as input, a nominal or default unimodal lognormal distribution is provided which is based upon close-in ground fallout samples over the area out to the 10 rad/hr

contour from events Small Boy and Ess (33). Although his n(r) analysis has never been documented, Norment says that the close-in size distributions from these two events were very similar. This is somewhat surprising since Small Boy was a near-surface burst and Ess was buried. A graph of the DELFIC size distribution and its 2nd moment (proportional to surface area) and 3rd moment (proportional to mass) appears in figure 11. The median radius, r_m, and the logarithmic slope are .204μ and 4 respectively (r_m will always be used to designate median radius for the number distribution). The distinguishing characteristic of this distribution is its broad dispersion (large logarithmic slope). The median radius is quite similar to those of the TTAPS or R-K distributions. The submicron particle population accounts for 5% of the aggregate surface area of the DELFIC distribution.

C.2. Nathans/TTAPS Distribution.

In contrast to the simple unimodal DELFIC size distribution, the TTAPS distribution is a hybrid function in which the submicron population is fit to a lognormal function, and the supermicron population is fit to a power law "tail":

$$r<1\mu; \quad n(r) = n_o \frac{r_m}{r}\left(\frac{r_o}{r_m}\right)^{\frac{p+1}{2}} \exp\left[-\frac{1}{2}\left(\frac{\ln\frac{r}{r_m}}{\beta}\right)^2\right] \tag{13}$$

$$r\geq 1\mu; \quad n(r) = n_o \left(\frac{r_o}{r}\right)^p \tag{14}$$

The functions join at r_o which is chosen such that the functions and their first derivatives are continuous at the splice:

$$r_o = r_m \exp\left[(p-1)\beta^2\right] \tag{15}$$

The function was originally used by Nathans to fit his surface burst cloud data (34). TTAPS adopted Nathans function using parameters typical of Nathans' results: $r_m = .25\mu$, log *slope* =2, $p=4$ and $r_o = 1.06\mu$. The TTAPS number, area, and mass distributions are plotted in figure 12. Besides being more difficult to manipulate, the third moment of the power law tail (if $p \leq 4$) is not analytic unless a maximum particle radius is defined. If $p=4$,

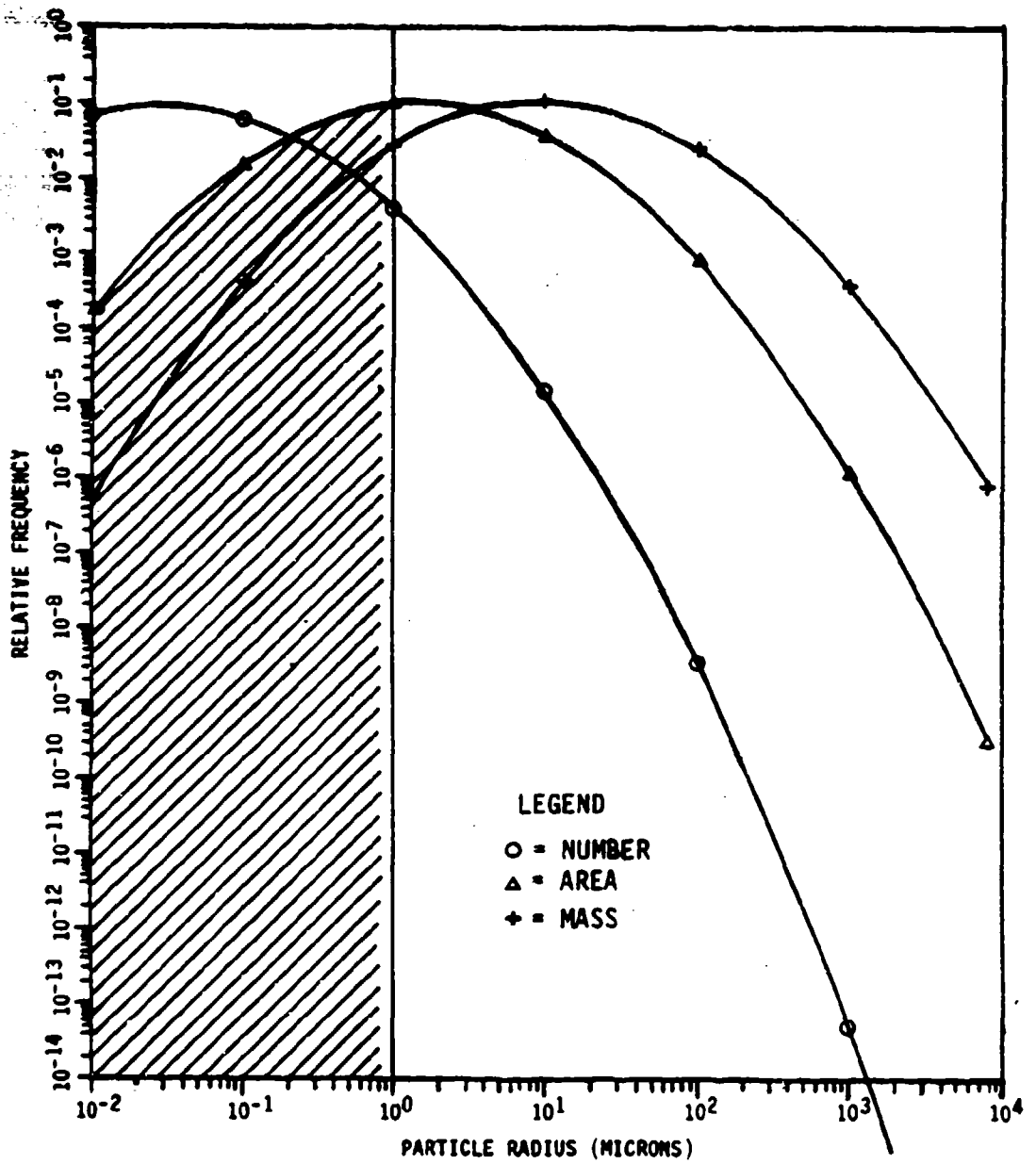

Figure 11. DELFIC Nominal Distribution

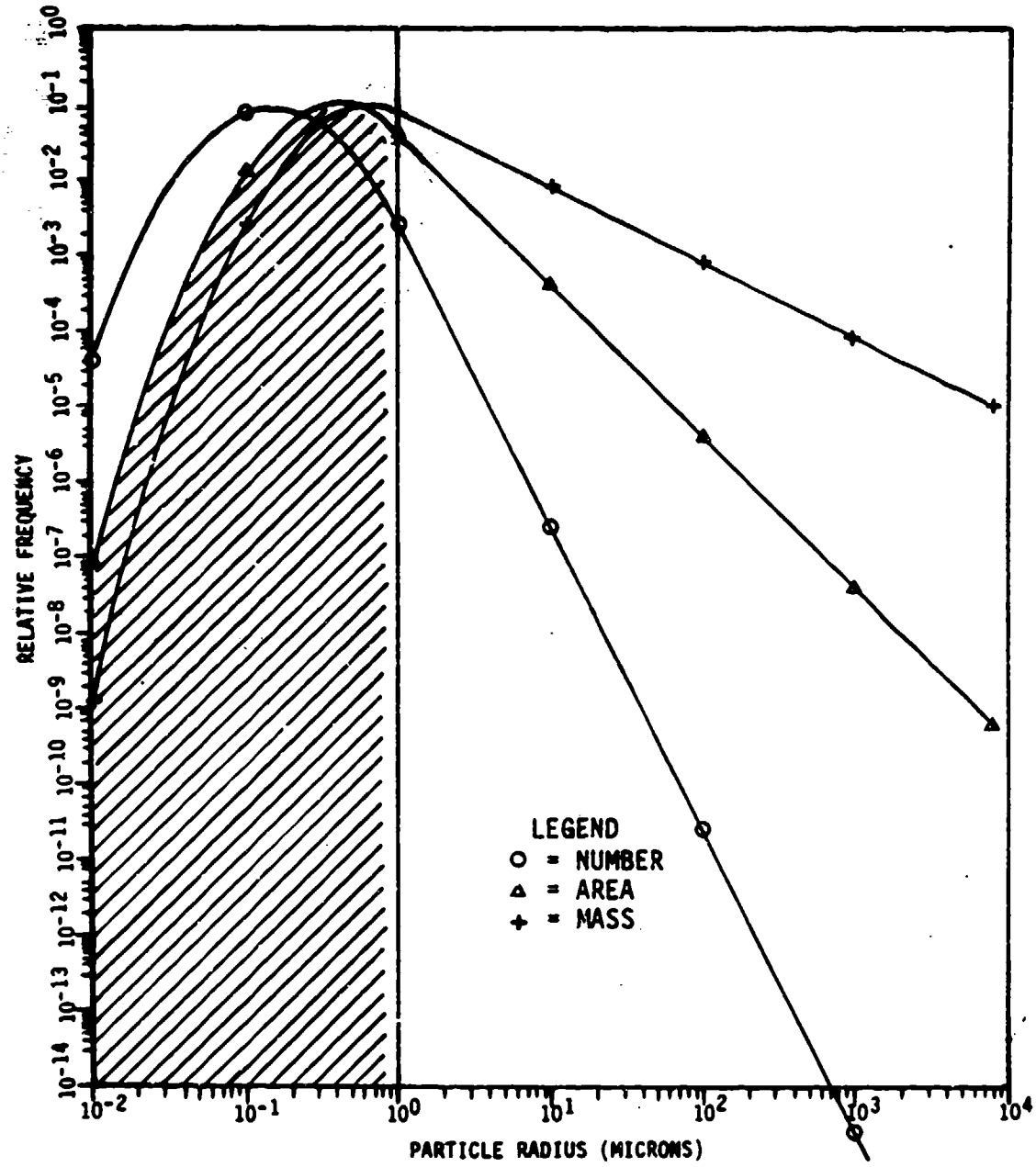

Figure 12. TTAPS Distribution

$$r_{max} = r_o \exp\left[\frac{\sqrt{2\pi}\beta(1-f_m)}{2f}\right] \tag{16}$$

where f_m is the mass fraction below r_o (see Appendix C for a more general expression for r_{max}). The TTAPS choice of parameters (r_o=1.06μ and f=.084) yields r_{max}= 1.3 cm. The fraction of surface area on particles below 1μ (roughly r_o) is given by:

$$f_s = \frac{\sqrt{2\pi}\beta e^{2\beta^2} r_o^{5/2} r_m^{1/2} CNF\left[\frac{\ln r_o - \ln r_2}{\beta}\right]}{\sqrt{2\pi}\beta e^{2\beta^2} r_o^{5/2} r_m^{1/2} CNF\left[\frac{\ln r_o - \ln r_2}{\beta}\right] + r_o \ln\left(\frac{r_{max}}{r_o}\right)} \tag{17}$$

where CNF denotes the cumulative normal function:

$$CNF[x] = \frac{1}{\sqrt{2\pi}} \int_{-\infty}^{x} e^{-\frac{1}{2}w^2}\, dw \tag{18}$$

and r_2 is the median radius of the second moment of the submicron population. A derivation of the Nathans' function and its moments is included in Appendix C.

The submicron population accounts for 60% of the total surface area of the TTAPS distribution. This large submicron surface fraction yields optical effects which are dramatically different in both magnitude and duration from those predicted using the DELFIC nominal distribution (figure 3).

C.3. Ramaswamy-Kiehl (R-K) Distribution.

The R-K distribution, like the DELFIC distribution, is a unimodal lognormal function. The R-K distribution, however, is more typical of particle populations observed in air burst clouds (17). Ramaswamy uses a surface mode radius of .26μ which translates into a median radius for the number distribution of .16μ. He uses a logarithmic slope of 2. Nathans has overlaid his results for multiple air burst clouds and determined that at a median radius of around .07μ and slope of 2.1 are reasonable averages (35).

The submicron population of the R-K distribution accounts for 90% of the surface area, larger even than the TTAPS distribution. Thus the R-K distribution predicts the largest initial optical thickness and the slowest decay with time.

D. Comparative Results.

To illustrate the relative magnitude and duration of optical effects among the DELFIC, TTAPS, and R-K distributions, OT vs time was computed for 10^{12} KG of dust distributed over a hemisphere (estimate based on 5000 MT exchange). The initial cloud vertical centroid was taken as 25 km (peak density altitude of the TTAPS study). For a description of the code used to compute stratospheric debris removal see section IV.A.3. The results (figure 3) clearly demonstrate the large differences in optical effects predicted by the three distributions. Note that the TTAPS and R-K distributions are removed at nearly identical rates (a residence half life of roughly 9 months). This is explained by the large fraction of surface area below 1 micron which is removed by the turbulent diffusion process rather than sedimentation. The broad DELFIC distribution, with its large fraction of particles above 1μ, is removed predominantly by sedimentation which accounts for its rapid decrease with time (half life roughly 1 week). The differences in OT behavior between the R-K and DELFIC distributions are predominantly a result of the factor of two difference in slope.

E. Summary.

It is obvious that the optical occlusion of sunlight energy responsible for climate effects is extremely sensitive to the modeled size distribution and that several plausible size distributions would produce effects ranging from scant to severe. It is also clear that the submicron population governs both the magnitude and duration of optical attenuation. The next chapter discusses activity injection into the atmosphere and the data types available for use in the activity tracing model.

III. Data.

A. Data Records.

The radioactive behavior of debris from nuclear events can be used to trace the rate of its removal from the atmosphere. Since sedimentation is a function of particle size, it is possible to derive particle size statistics from the observed bulk vertical transfer of radioactivity in the atmosphere. Two basic types of data are available:

Stratospheric Removal. The stratospheric burden of certain radionuclides has been recorded over long periods of time (9, 10, 11, 12, 36, 37, 38, 39, 40, 41, 42, 43, 44, 45, 46). Best records were kept for ^{90}Sr, ^{95}Zr, HTO, ^{14}C and ^{185}W. ^{90}Sr burdens have been recorded since 1954 and reflect the contributions of 92 high yield (megaton class and greater) events (38).

Ground Deposition. The downrange cloud arrival time was recorded for 30 events at the Nevada Test Site (47). The yields of these events ranged from .1 to 50 KT. From this information it was possible to determine activity grounded as a function of time. In addition, following the 1958 test moratorium, rough ^{90}Sr contours were plotted over the continental United States which reflect the contributions of roughly 75 Nevada shots up until that time (36).

B. Merits and Drawbacks of Activity Tracing.

There are major drawbacks to using activity tracing. Unlike microscopic techniques where actual debris is examined in detail, this is an indirect method. In order to extract size information from activity data, it was necessary to relate radioactive content to particle size via specific activity behavior. Nathans found that specific activity could in fact be correlated with of particle size using a single correlation function (17:62). Unfortunately, specific activity data is somewhat sparse, highly variable and, in some cases, difficult to interpret. This problem is the weak link in the activity tracing method and may explain why this approach has not been

previously used for particle size characterization.

However, there are some distinct advantages to the method particularly with respect to the nuclear winter problem. Nuclear winter is predicated on the average behavior of debris from hundreds of bursts, and in particular, the bulk removal of such material from the stratosphere. Indeed, the nature of the available activity trace data enables bounding the n(r) behavior governing depletion of the stratospheric debris from a very large number of events, both U.S. and foreign. Activity tracing data gives the bulk behavior of clouds and is not subject to the sample variance quandry associated with microscopic techniques. Activity tracing supplemented by comparisons with the results of previous microscopic analysis was used successfully in the present research to determine n(r) parameter bounds averaged over many events.

C. Fallout Formation and Removal.

An understanding of fallout formation and dispersal processes is important to interpreting activity data. When a nuclear weapon is detonated, fragments of fissionable material, unfissioned active material, the bomb tamper and casing are vaporized. This collection of material is referred to as bomb debris. Soil debris engulfed by the expanding fireball is also vaporized (the vaporization temperature of soil is ~1700° K). Other close-in soil debris is melted or partially melted while more distant soil particles within the range of the blast wave and subsequent gust is lofted in its solid form. The height (or depth) of the burst, the nature of the terrain, and the weapon's yield determine the relative amounts of soil debris which are vaporized, melted, or simply lofted.

In the case of a free air burst, where the rising fireball does not entrain surface dust, no soil debris is present in the highly radioactive fireball. The free air burst threshold altitude is ~700m for 1 KT (13:3-6). The fireball cools to debris vaporization temperatures within 1-5 seconds. Within 10 minutes the cloud of vapor condensate stabilizes at altitudes high enough (5-35 km depending upon yield) that virtually no local fallout occurs. Local fallout is defined as that occurring within 24 hours of detonation. The absence of local fallout in the case of free air bursts implies that the condensed bomb debris particles are very fine. Indeed, Nathans (17,18) measures distributions tightly clustered about a median radius of ~.1μ.

For a surface burst or low air burst of a given yield, even though the cloud rises to similar altitudes as for a free air burst, soil particles present provide the "carrier" for local fallout. The fact that roughly 60% of the activity falls within 24 hours (48:414) of a surface detonation is due mainly to the presence of larger particles, and to a lesser degree to the toroidal hydrodynamic motion which brings down a homogeneous mixture of particles close to the burst point. Since sedimentation velocity is a function of particle radius, it should be possible to correlate activity down vs time, A(t), with A(r) and thence infer n(r) from A(r). The larger particles are due to the presence of a large mass of molten earth drawn into the cloud of hot fission product vapor and mixed to a greater or lesser degree by the toroidal circulation within the cloud. Judging from specific activity behavior for surface bursts, the mass of melted or partially melted soil is at least an order of magnitude greater than the mass of material directly vaporized (49:388).

During the condensation phase, volatile mass chains with vaporization temperatures lower than soil (viz. As, Se, Br, Kr, Rb, Mo, Tc, Te, I, Xe, Cs, ref. 50) tend to coat the surface of the previously condensed soil particles and refractory nuclides (those with high condensation temperatures). The refractory nuclides (the products of the mass chains not listed above), tend to be volumetrically mixed in fallout particles. Thus, the relative concentration of volatile nuclides goes roughly as the square of the particle radius and the concentration of refractory nuclides goes roughly as the cube. The different nuclide condensation temperatures, different thermal histories of material, and mixing inhomogeneities within the cloud lead to nonuniform concentrations of the different nuclides on fallout particles. This phenomenon is known as "fractionation" and serves to complicate the activity tracing method. A further complication, noted by Nathans in his analysis of air burst debris, is that below 1μ, the specific activity in some cases grows very rapidly with decreasing radius (roughly as r^{-3}). The present effort has produced evidence that this "specific activity catastrophe" is probably due to the condensation of unmixed fission products to form high activity particles (section V.C.3).

D. Fallout Data Categories.

Fallout data may be grouped into three general categories: global fallout, intermediate fallout, and local fallout. By definition, local fallout is deposited within 24 hours of detonation and within roughly (depending upon prevailing winds) 500 km of ground zero. Intermediate fallout is not as precisely defined. For this research it was defined as falling between one and several days following the detonation and as deposited within roughly 5000 km of ground zero (continental scales). Global fallout is present only for large yield ($\geq 1MT$) weapons capable of lofting contaminated debris into the stratosphere. Fine material in the stratosphere lingers for months and circulates the globe many times before being removed by sedimentation and turbulent diffusion. The longevity of debris in the troposphere is limited by washout/rainout and thermal circulation to periods of less than 3 weeks (residence time is function of altitude). Because the rainout and washout mechanisms are not operative in the stratosphere, the lifetime of submicron particles reaches 6-12 months above ~12 km.

Each fallout data category is roughly associated with a certain range of particle sizes (figure 13). These associations become apparent by studying the graph in figure 10 for the case where particles start from an altitude of 10 km (~100 KT cloud vertical centroid). Within 24 hours particles 20μ and greater will have been removed by sedimentation and local fallout data will yield information on the fraction of particulates in this range. Within 1 week (intermediate fallout period), particles up to ~5 microns will have sedimented. Beyond a week, only particles less than 5 microns will remain aloft. Thus global fallout behavior reveals information on the submicron size fraction. These ranges are only approximate and depend upon the initial cloud height and wind velocities.

D.1. Global (Stratospheric) Fallout Data.

Several programs have been instituted over the years by the Department of Defense and Department of Energy to sample radionuclides in the stratosphere. Early estimates of stratospheric burden were based upon limited balloon sampling and global ground sampling. With the advent of thermonuclear weapons capable of lofting significant amounts of debris into the stratosphere, the advisability of continued testing demanded an evaluation of stress of this global fallout on the earth's

environment and ecology. In 1954, the Joint Chiefs of Staff instituted efforts at the Defense Atomic Support Agency (now the Defense Nuclear Agency) to quantify the concentration of radioactivity in the stratosphere (12). This led to the organization of the DoD High Altitude Sampling Program (HASP). An element of this program, Project Stardust, provided the stratospheric tracer data used in the present research. Beginning in 1957 Stardust flew up to two U2 aircraft sampling missions per week. Sampling occurred at altitudes up to 60,000 feet over the North and South American continents. A map of the HASP flight profiles appears in figure 14.

Following the 1962 test ban, the U.S. Atomic Energy Commission (later the Department of Energy) assumed responsibility for sampling and instituted its own High Altitude Sampling Program including the use of balloons (Project Ashcan) and B57 aircraft (Project Airstream) for sampling. The balloon probes sampled up to 35 km, while the aircraft sampling was between altitudes of 15-20 km with flight paths following the west coast of North and South American from 72° N to 50° S.

Sampling was accompanied by extensive radiochemical analysis. Nuclides which have yielded the most useful results for determining the removal of debris from the stratosphere include ^{90}Sr, ^{95}Zr, HTO (tritiated water vapor), ^{14}C (CO_2), and ^{185}W. Of these nuclides, ^{90}Sr has been studied in the most detail because of its long half life (28.1 years) and biological hazard. Spacial and temporal averaging of the data was used in plotting the stratospheric burden of ^{90}Sr shown in figure 15 (51). Of particular interest are the massive injections which occurred in the autumn of 1961 during a high yield Soviet test series. Because of the extreme altitude of the cloud (center around 35 km) and a debris residence time which spanned several years, the erratic effect of seasonal variations in the vertical diffusion constant was reduced. In addition, for high clouds, sedimentation was not totally masked by diffusion as it appears to be for debris near the tropopause (37). Since ^{90}Sr has noble gas precursors which condense late in the fallout formation process it is not the best choice for tracing fallout removal. Refractory nuclides, such as ^{95}Zr or ^{185}W, are expected to be more evenly mixed in the debris. In addition refractory nuclides tend to be mixed volumetrically in debris particles and are less subject to concentration variation due to fractionation. Although modeling ^{90}Sr removal provided interesting and useful results, it was deemed prudent to also model the bulk vertical transfer of a refractory nuclide.

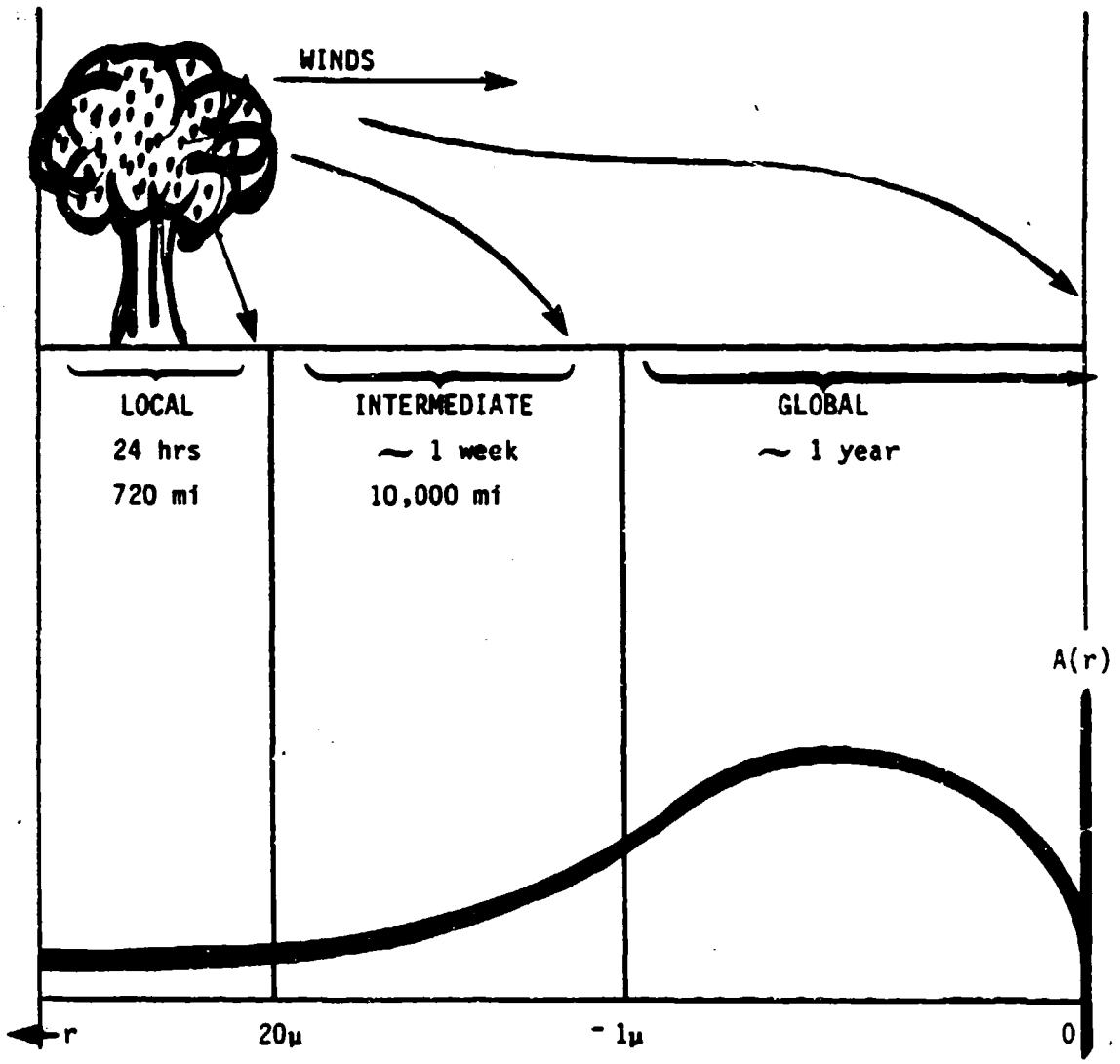

Figure 13. Fallout Data Categories

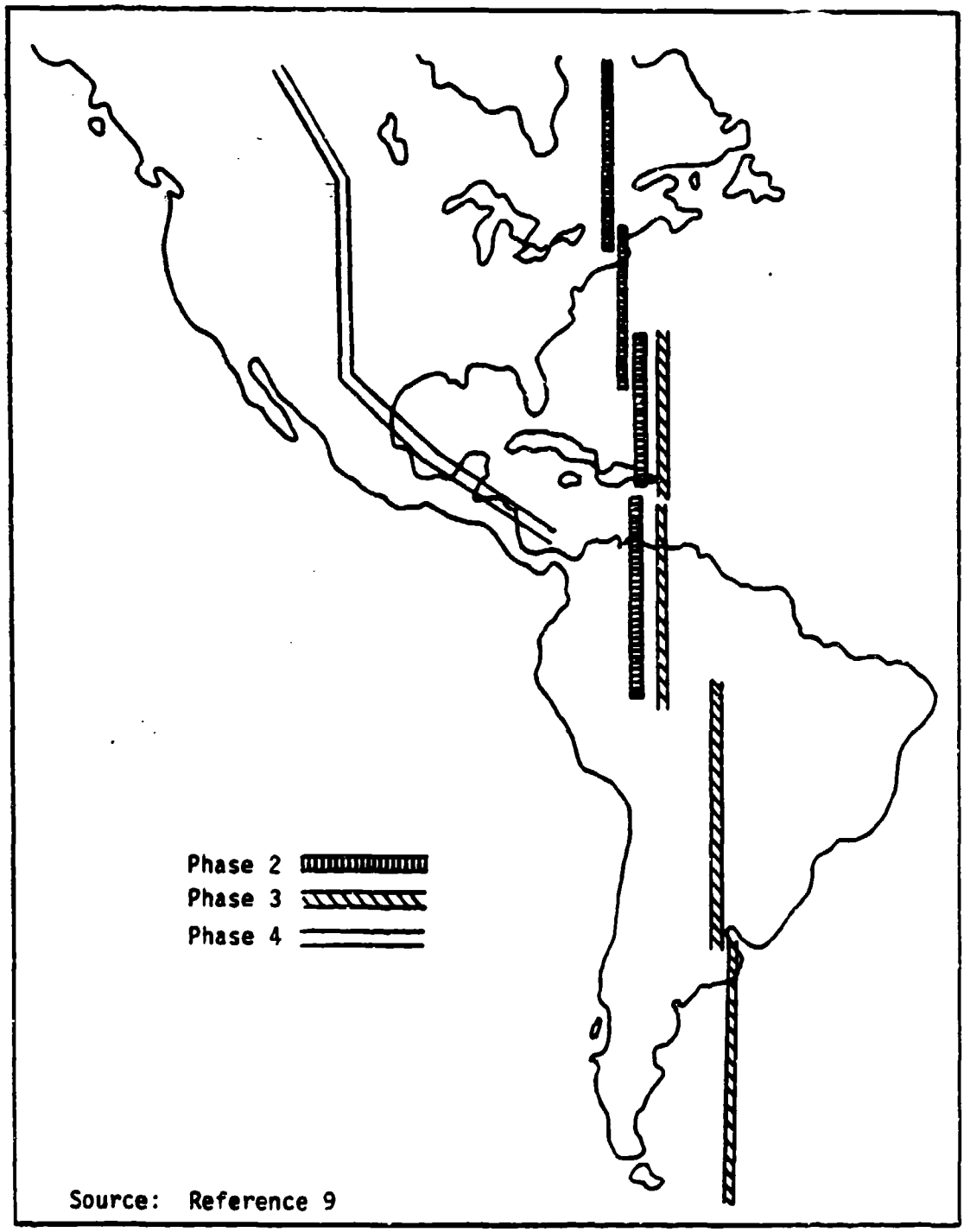

Figure 14. HASP Flight Tracks (DoD)

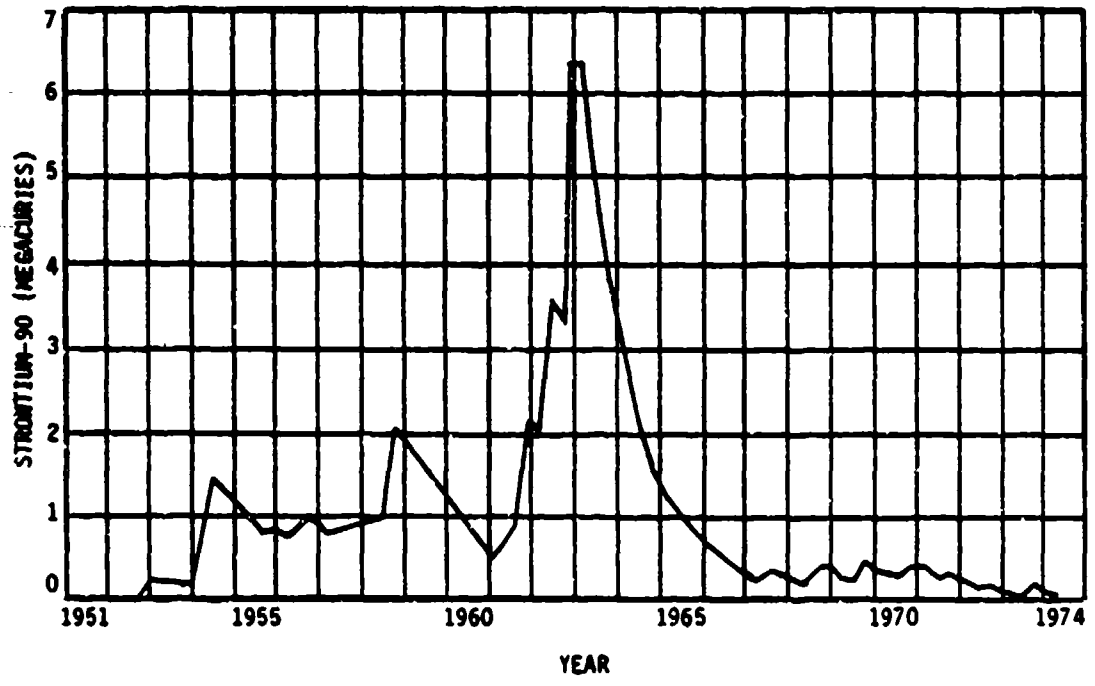

Figure 15. ^{90}Sr Stratospheric Inventory, 1951-1974

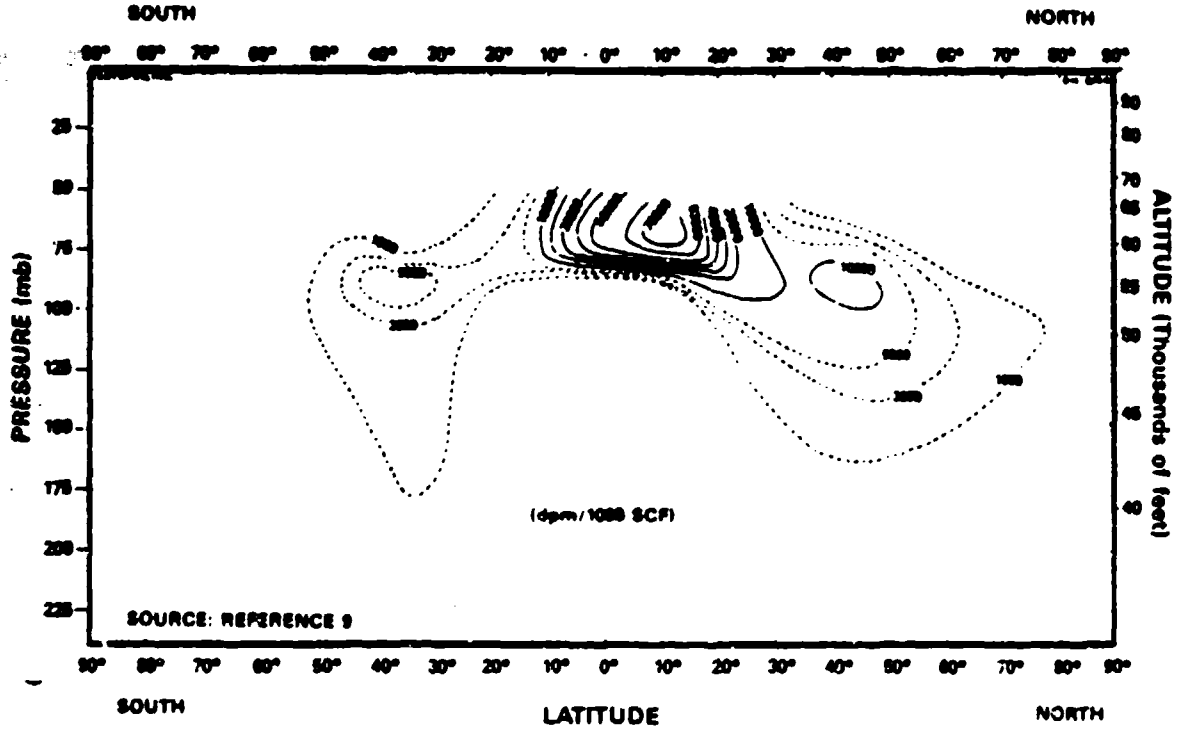

Figure 16. Mean Distribution of Stratospheric ^{185}W, Sept.-Oct. 1958

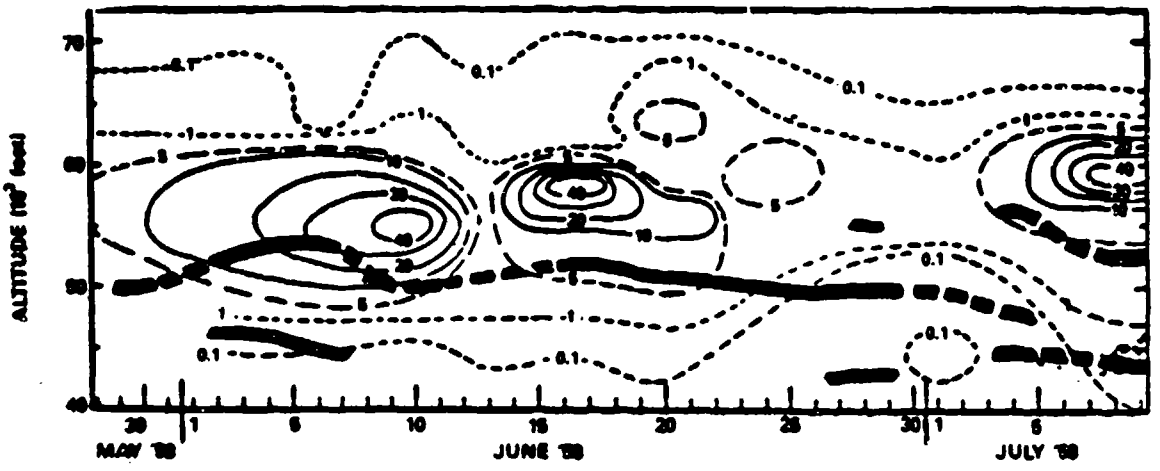

TUNGSTEN-185 ACTIVITY (dpm/SCF corrected to 15 Aug. 1958)

THE VARIATION INACTIVITY AT 18° NORTH DURING MAY - JULY 1958.
(TROPOPAUSES ARE SHOWN AS DARK BANDS)

Figure 17. Tungsten Cloud Movement

Source: Reference 10

For several reasons ^{185}W was selected as the refractory nuclide for this study. The nuclide was injected into the stratosphere only during a three month period in 1958 (mean injection date of 1 July). The tracer was an activation product unique to several devices in the Hardtack Series. The devices producing ^{185}W were detonated on barges containing silica sand (10:102). Project Stardust carefully monitored tungsten data to determine debris transfer mechanisms and removal rates in the stratosphere. Both the vertical and lateral diffusion rates of actual tungsten clouds were determined based on isopleths constructed from aircraft sampling data (figures 16,17). The stratospheric tungsten burden was charted for a 14 month period following injection (figure 18). The tungsten was injected at tropical latitudes where the effective vertical diffusion constant is low. Nonetheless, the stratospheric Tungsten burden decays relatively quickly, falling to half its initial value in 5 months. This indicates that sedimentation is an important factor in the activity transfer process since the diffusion half-life is 9 months on average. Mason et al (37) have shown that tritiated water vapor (HTO) and ^{95}Zr from midlatitude Chinese shots are removed at almost identical rates from the lower stratosphere (half residence time of 9 months) implying diffusion is the dominant factor in that case. A discussion of stratospheric removal processes is included in section IV.A.3.

D.2. Intermediate Fallout Data.

Intermediate fallout data was the least profuse of any category. Data taken and analyzed during the DoD High Altitude Sampling Program (36,52) was used. HASP computed the rate of deposition of stratospheric debris using ^{90}Sr soil concentrations collected from a world-wide network of sampling stations in 1959 (53). In order to discriminate the stratospheric fallout detected by U.S. stations it was necessary to subtract the Nevada Test Site contribution (all Nevada shots were less than 100 KT and did not contribute significantly to the stratospheric burden). Thus, it was necessary to construct isopleths of the ^{90}Sr deposition downwind of the Nevada Test Site through 1958. Combining measured soil concentrations with known rainfall data over the region, the contour plot shown in figure 19 was constructed (52). A combined total of 995 KT fission yield is estimated to have injected 100 kilocuries of ^{90}Sr through 1958 (very nearly 0.1 kilocurie/KT fission on average, ref. 36). An estimated 41 kilocuries of ^{90}Sr fell within the the 10 millicurie/mi^2 contour. Below 10

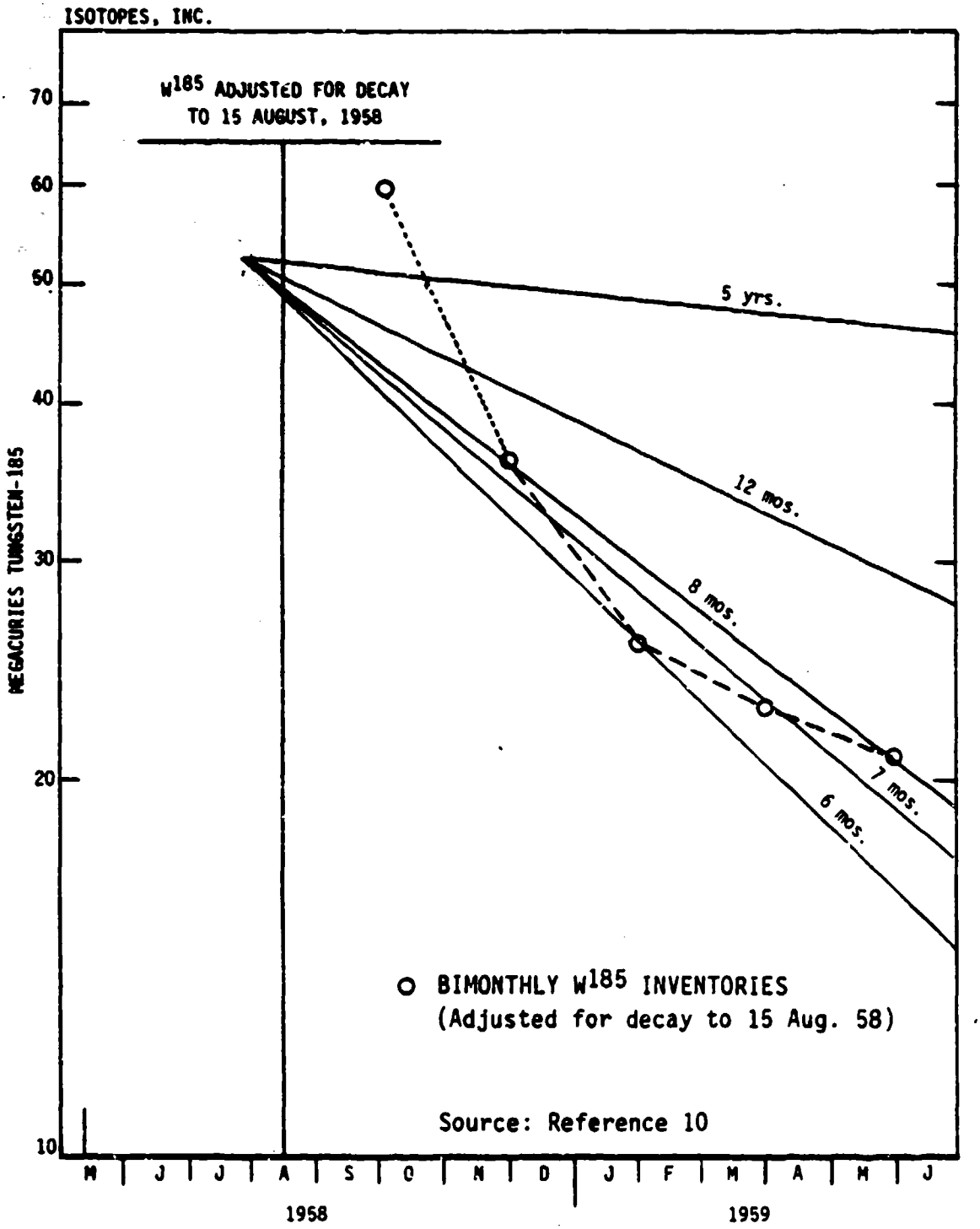

Figure 18. ^{185}W Stratospheric Inventory, 1958-1959

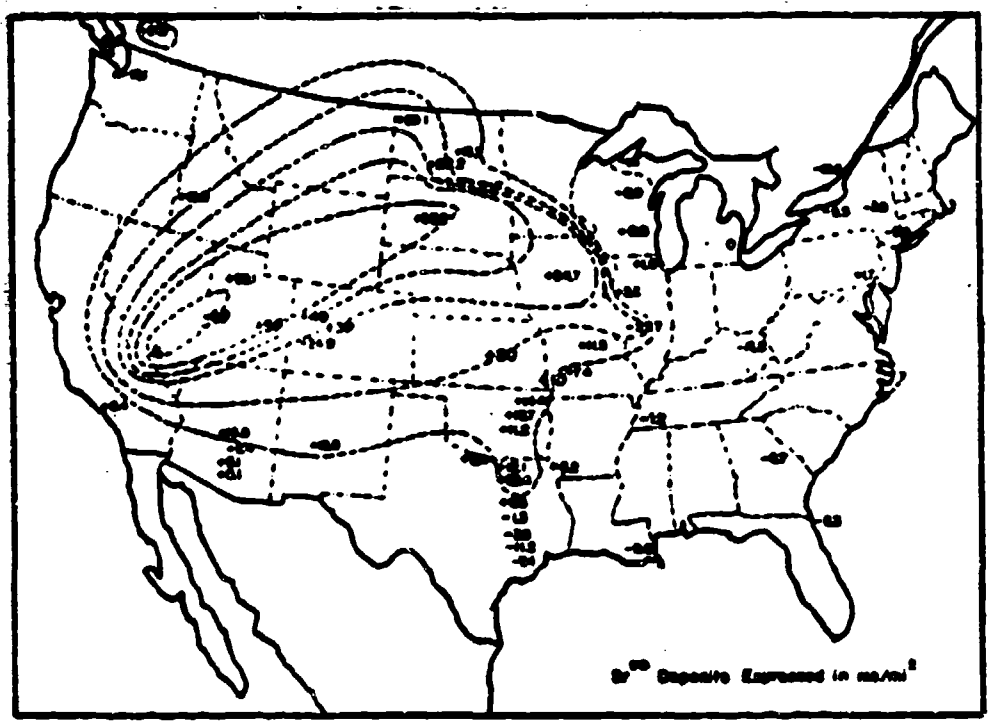

FIGURE 19. ^{90}Sr in U.S. Soils from Intermediate Fallout

Source: Reference 82

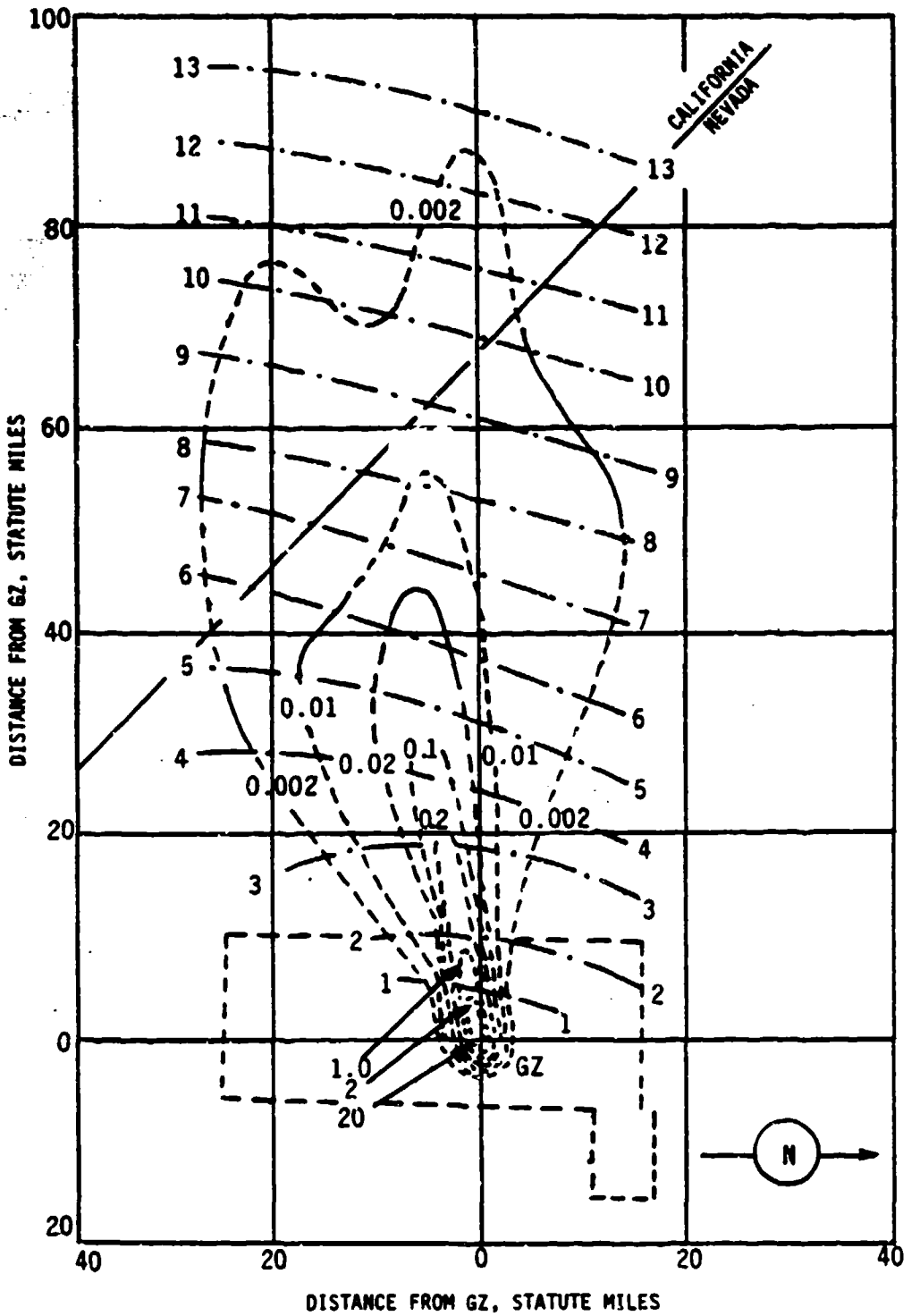

Source: Reference 47

Figure 20. Operation PLUMBBOB - Coulomb B.
Off-site dose rate contours in r/hr at H+1 hour.

millicuries/mi^2 it was not possible to discriminate NTS fallout from the world-wide fallout background. The uncertainty in the intermediate ^{90}Sr total is estimated to be 25% (52).

D.3. Local Fallout Data.

For many of the U.S. Nevada and Pacific shots, an effort was made to plot activity contours down wind from ground zero. An unclassified compendium of fallout data for U.S. atmospheric tests including ground deposition contours (when available) has been published by the Defense Nuclear Agency (47). For several events an approximate cloud location vs time is included with the fallout contours. An example is shown in figure 20. Unfortunately, most Nevada tests were air bursts and since large amounts of ground debris were not entrained in the fireball, only a very small part of the activity was deposited locally. Davis (54) has attempted to determine particle size distributions from local activity contours with some limited success (discussion section V.F).

E. Summary.

This chapter has surveyed the available data and discussed the intrinsic advantages and disadvantages of the activity tracing method. A strong point in favor of activity tracing is that data is available on the rate of activity depletion from the stratosphere over a period of more than a decade. The data reflects the behavior of debris from close to 100 high yield events. Since stratospheric material is the source of prolonged sunlight attenuation, this data is particularly germane to the nuclear winter problem.

IV. Modeling Global and Intermediate Fallout.

This chapter describes the modeling used to predict fallout, including both stratospheric depletion and ground deposition. The models used an assumed particle size, n(r), as input. The input was varied in a systematic way to make the calculated activity burden and deposition match the data summarized in the last chapter.

Two separate models were required. For stratospheric data comparisons, a model of tracer burden above the tropopause as a function of time was developed. To utilize intermediate fallout data a model of ground deposition vs time was required. The basic ingredient of each model was an algorithm to compute cloud sedimentation and diffusion in one dimension.

Admittedly the atmosphere is not one dimensional and thus any 1-D parameterization will have limited accuracy. However, in order to facilitate multiple variations in n(r) parameters, it was necessary to simplify the physics of the atmospheric transfer model. There is precedent for 1-D modeling. One dimensional codes have been used extensively in estimating the environmental impact of atmospheric pollutants. Bauer has used 1-D models to track the transfer of nuclear debris from the stratosphere with reasonable success (38,39). The TTAPS results were based on a 1-D model of the atmosphere. Detailed descriptions of the debris removal models used in this study follow.

A. Stratospheric Transfer Modeling.

A.1. Properties of the Stratosphere.

Megaton class nuclear detonations inject large portions of the resulting radioactive clouds into the stratosphere. Particle removal from the stratosphere is dominated by turbulent diffusion and sedimentation (38,39). The sedimentation process was modeled using Stokes or Davies-McDonald fall mechanics depending upon the particle size and altitude (discussed in appendix A).

The turbulent diffusion process is not yet totally understood but is strongly influenced by the characteristics of the tropopause (figure 21). Because of its stable temperature profile, there is very little vertical convective motion in the stratosphere itself. This is especially true at tropical latitudes where clouds from nuclear explosions can remain intact for several passes around the globe (47:445) with less than a two mile change in altitude. Figure 16 provides evidence of this behavior. However, there is considerable lateral transfer in the stratosphere which is influenced by the gaps in the tropopause in each temperate zone. The gap regions are extremely turbulent and it is believed that a considerable transfer of air between the stratosphere and troposphere occurs there (confirmed by higher ground activity concentrations at latitudes underneath the gap region, ref. 36). The gap region migrates north in the summer and south in the winter creating a "peeling" effect which is strongest in spring and autumn months as evidenced by more rapid global fallout during these periods (37,38,39,40,41,42). In addition, the tropopause rises and falls with the ground temperature which also adds to the seasonal variation in transfer rates.

Although the vertical diffusion process is stronger in the polar region (because of the gaps) than in the tropics, it is reasonable to define an average vertical diffusion constant since nuclear injections spread quite rapidly in the lateral direction. Lateral mixing coefficients are of the order of 10^5 $m^2 sec^{-1}$ (larger in the polar regions) which yields a meridional spread of 40^o in 6 months time (9). Thus, because of their large lateral span, clouds experience an effective diffusivity which is in effect averaged over latitude. Bauer (38) has plotted the eddy diffusivity profiles used in the one dimensional models of several researchers (figure 22). For this research, a seasonal average eddy diffusivity (K_z) of 0.5 m^2 sec^{-1} was used with a mean tropopause height of 12 km. This value of K_z predicts a diffusivity half life for submicron particles in the lower stratosphere (12-25 km) of about 9 months which agrees with the measured values reported by Mason for ^{95}Zr and ITO (37).

Naturally occurring stratospheric aerosols are extremely tenuous (the latent vertical optical depth at visible wavelengths is only .005). It is not expected that their presence significantly affected the formation or size distribution of nuclear debris particulates during the condensation phase. Thus it is reasonable to assume that radioactive tracers were attached to weapon debris rather than ambient particulates.

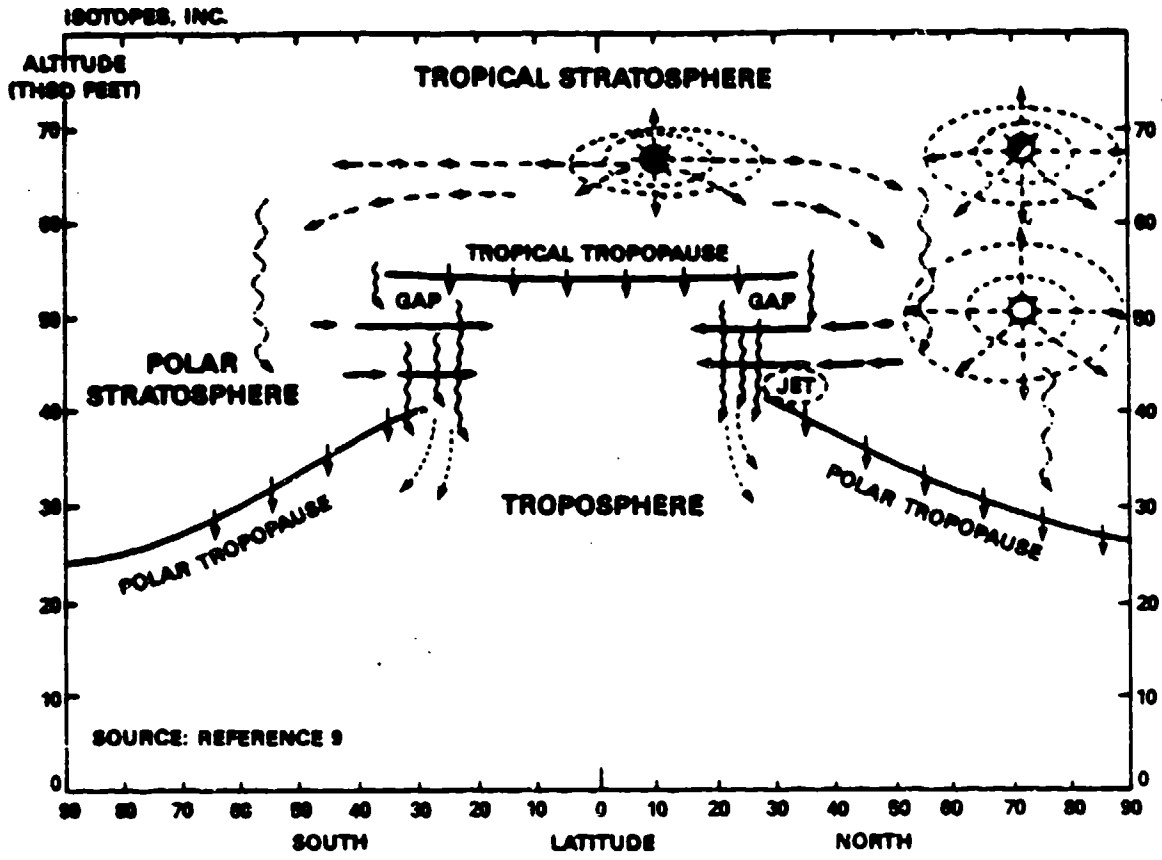

Figure 21. Hypothetical Model of Stratospheric Mixing and Transfer

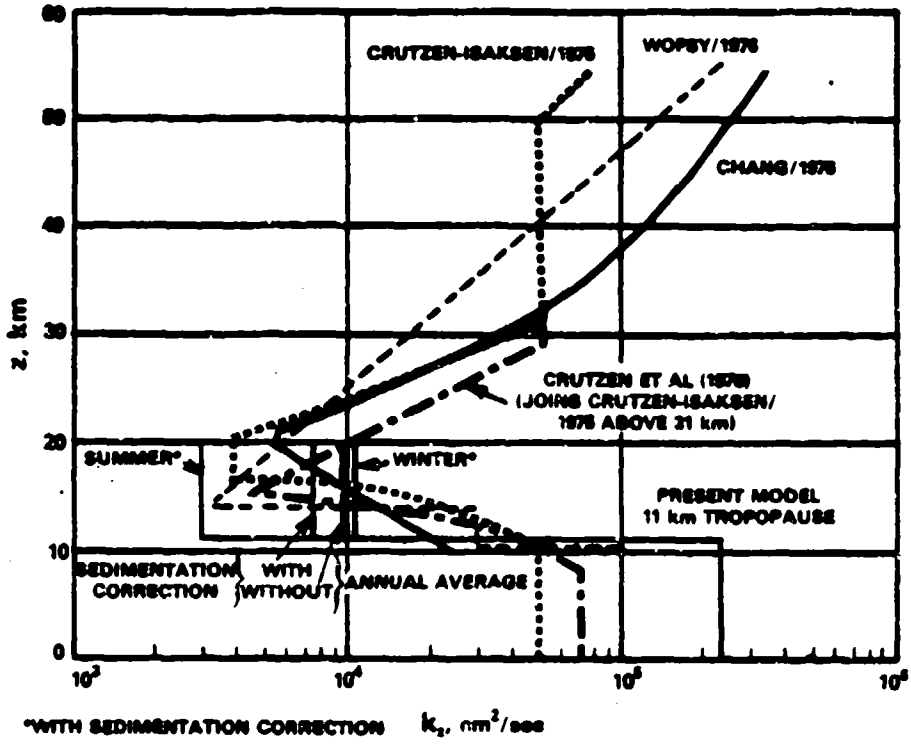

Figure 22. Eddy Diffusivity Profiles

(Source: Reference 28)

Source: *Journal of Geophysical Research*, Vol. 83, p4819, Copyright American Geophysical Union

A.2. Cloud Injection.

A.2.a. Injection Altitude.

Since the model computes cloud behavior over a period of weeks to months and since clouds stabilize in less than 10 minutes, it was reasonable to omit cloud rise physics and to initialize the computation at cloud stabilization time. At stabilization the cloud was given a Gaussian profile in altitude per Telegadas and Bauer (38:5-2):

$$f(z,0) = f_o \frac{\exp\left[-\frac{1}{2}\left(\frac{z-z_o}{\sigma_z}\right)^2\right]}{\sqrt{2\pi}\sigma_z} \tag{19}$$

where

$$f(z,t) = \frac{\textit{burden of tracer at } z \text{ and } t}{\textit{ambient air mass at } z} = \frac{n_s(z,t)}{n_a(z)} \tag{20}$$

and $\sigma_z = 2.15$ km for stratospheric injections. The computations are fairly insensitive to the choice of initial dispersion (38:5-3) since the total burden of tracer is being computed over months. Results are much more sensitive to the injection height and K_z.

There are several empirical models for cloud injection height vs yield. The Foley-Ruderman model used in the TTAPS study fits a power law to visible cloud extremities observed for U.S. tests (figure 23). Fits for cloud top and bottom were developed separately (43):

$$CT = 21.64\,Y^{.2}\ km \tag{21}$$

$$CB = 13.41\,Y^{.2}\ km \tag{22}$$

One drawback of the Foley-Ruderman model is that it is based upon the dimensions of the visible cloud. The cloud radioactivity profile may not match the visible cloud profile, and indeed Zuni rocket sampling indicates activity residing near the lower boundary of the visible cloud (22:24).

Seitz et al (44) estimated cloud top and bottom based upon the behavior of radioactive debris a few days after the 1961-62 U.S. and Soviet tests. Because data was not available much above an altitude or 24 km, Seitz arbitrarily assigned cloud

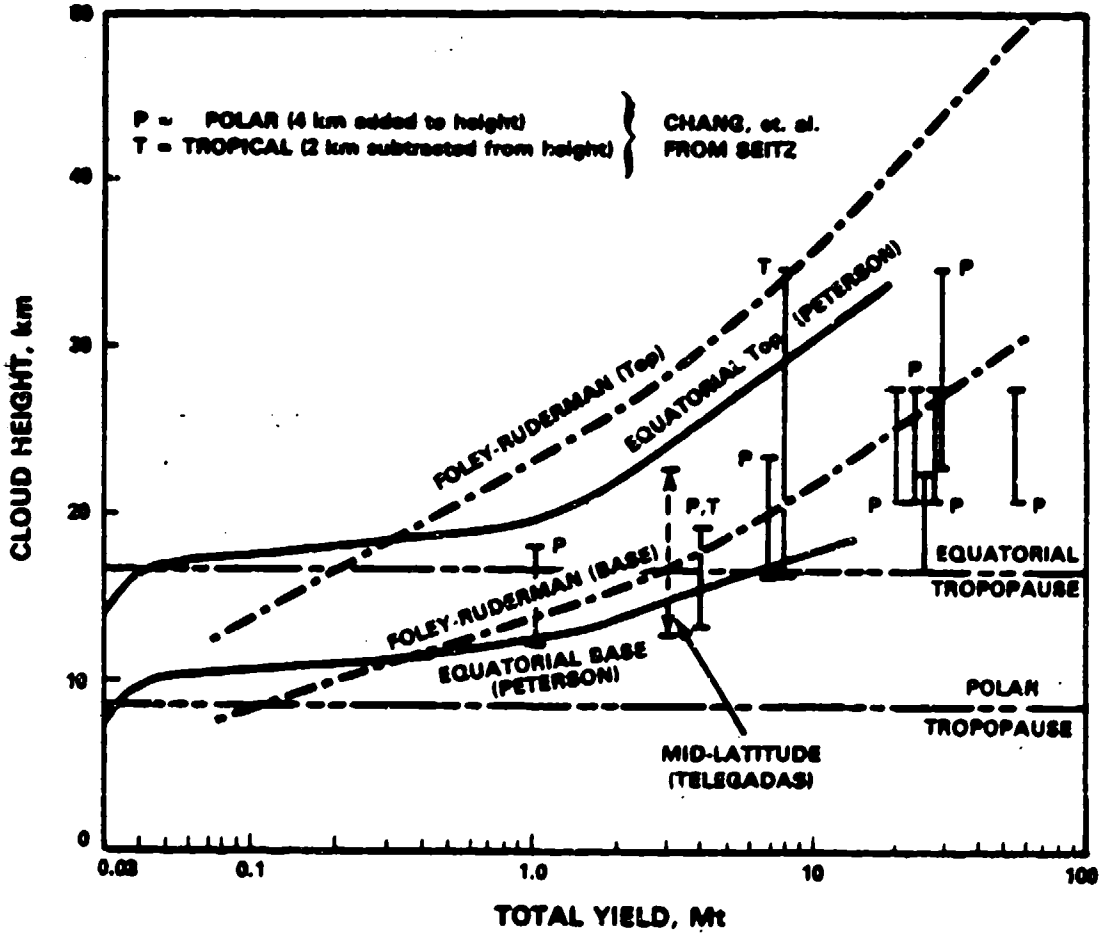

Figure 23. Nuclear Cloud Rise Height as a Function of Yield

Source: Reference 28

top altitudes of 24 km to high yield events. Thus Seitz' curve fits are systematically low, and should be used with caution (45). Peterson (46) has fit the clouds from U.S. tropical tests. However these clouds are consistently lower than those from similar bursts at northerly latitudes. Chang et al (45) conclude that the Foley-Ruderman model is useful as an upper bound, while the Seitz model is useful for a lower bound. Bauer (38) believes the Seitz model to be more realistic, but comes to this conclusion based upon a fast diffusion calculation of .1μ monosized particles in which sedimentation effects are negligible.

The Foley-Ruderman fit was used in the present effort to set cloud injection height. The fit is based on actual observations of U.S. events. There is limited evidence that the fit predicts the cloud injection height of the high yield Soviet shots (38:3-5). The fact that activity has been observed to concentrate low in the visible cloud may have been due to sedimentation prior to sampling time. In addition, since the cloud was modeled as being distributed normally with atmospheric pressure (equation 19), the modeled activity centroid is below the injection altitude, z_o (see section IV.A.3.b). Bauer's underprediction of transport from Foley-Ruderman altitudes is overcome if a finite spread is introduced into his particle size distribution. Indeed, the spread which best predicts bulk vertical transfer is nearly identical to microscopically observed dispersions for air burst samples (see section V.A).

A.2.b. Event Data Input.

During the 1950's and 1960's 97 atmospheric events lofted significant amounts of ^{90}Sr into the stratosphere. Yield information for most of these events is classified. To keep the results unclassified, events which occurred in close succession were grouped together. Bauer (38) and Seitz (44) have published unclassified grouping schemes. Bauer's event groups were used with slight modifications (tables I,II). A mean value of .1 kilocurie ^{90}Sr was injected per kiloton of fission yield (36:40, 50:321). Bauer's estimates of fission fractions were used (38:5-3).

^{185}W was injected by several events in the late spring and early summer of 1958. For classification reasons, the model treated these events as a single injection occuring on 1 July with a stabilized cloud center at 20 km. The stabilized cloud altitude was based on isopleths generated from U2 measurements (9).

TABLE I:

Grouping of 1950s Injections - ^{90}Sr						
Mean Injection Date	April 54	June 56	Sept 56	June 57	June 58	Oct 58
Country	US	US	USSR	USSR	US/UK	USSR
Location	Tropic	Tropic	mid-hi lat	mid-hi lat	Tropic	Arctic
Number of Events	5	5	4	5	30	10
Mean Yield	9.6MT	3.5MT	1.5MT	2.4MT	.7MT	3.6MT
Estimated ^{90}Sr Inj.	2.4MC	880KC	300KC	1.4MC	1.1MC	1.1MC
Foley-Ruderman Cloud Center	26km	21km	20km	21km	17km	23km

TABLE II:

Grouping of 1960s Injections - ^{90}Sr					
Mean Injection Date	Oct 61	Nov 61	Jul 62	Oct 62	Oct 62
Country	USSR	USSR	US	USSR	USSR
Number of Events	13	2	7	5	11
Mean Yield	2.8MT	41.5MT	5.3MT	25MT	6.8MT
Estimated ^{90}Sr Inj.	640KC	690KC	430KC	4.6MC	2.0MC
Foley-Ruderman Cloud Center	22km	38km	25km	35km	26km

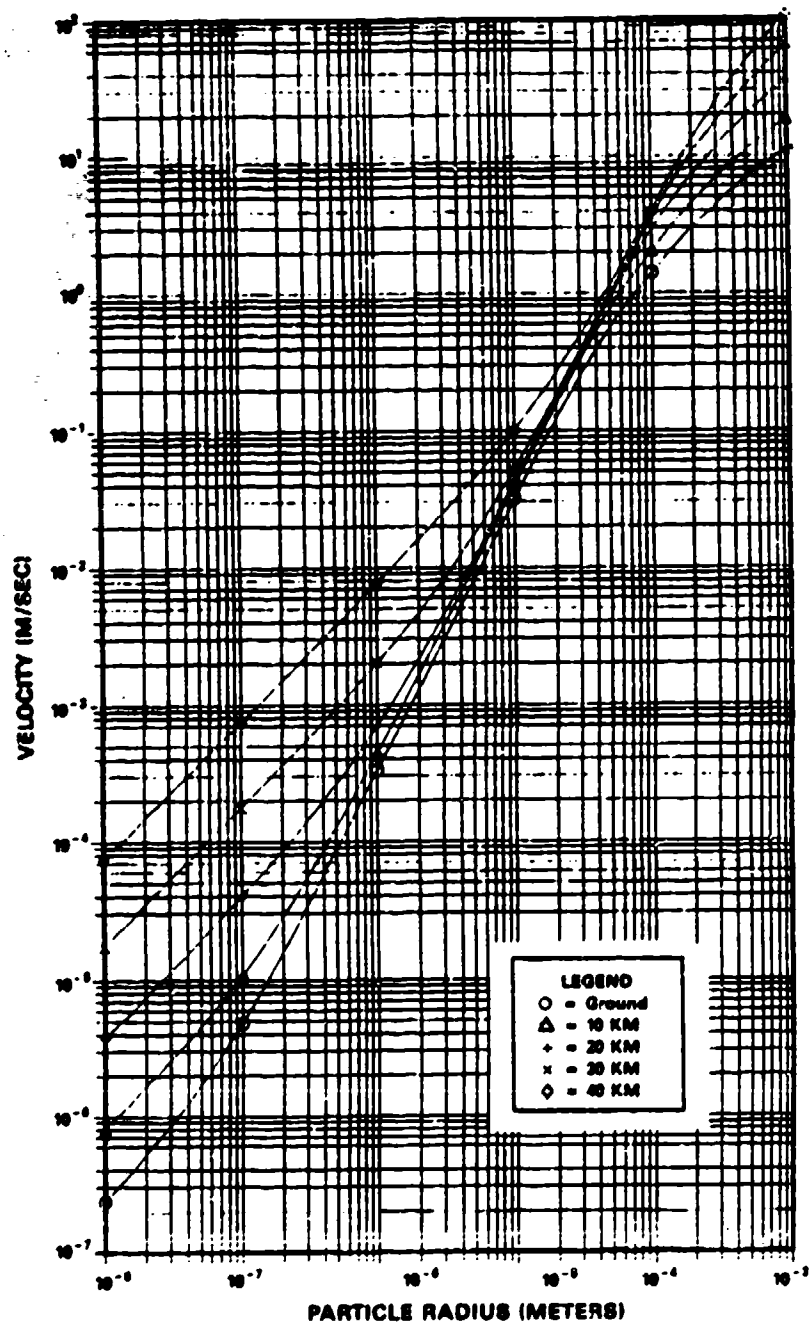

Figure 24. Velocity versus Radius and Altitude

A.3. Tracer Removal.

A.3.a. Sedimentation.

The particle sedimentation model is based on that used in the Defense Land Fallout Interactive Code (8). The Stokes, Davies-McDonald, and Beard equations were used depending upon the value of the Davies number:

$$Q_z = \frac{4\rho_a(\rho_s-\rho_a)gd^3}{3\eta^2} \tag{23}$$

where ρ_a is air density, ρ_s is particle density, g is the acceleration of gravity, d is particle diameter, and η is dynamic viscosity (see appendix A).

The atmosphere was modeled according to equations in the U.S. Standard Atmosphere publication (55). Hopkins (56) has shown that the U.S. atmosphere is also a reasonable approximation for the atmosphere over the Pacific test sites for purposes of fallout modeling.

Particles were treated as smooth spheres of density 2600 kg/m^3 (16) settling in still air. The Knudsen-Weber slip correction factor was used (57) which gives terminal velocities slightly smaller than the commonly used Cunningham slip. The Knudsen formula fits terminal velocity data over a wider range of d/λ_{MFP} (MFP denotes mean free path).

Appendix A presents the fall velocity equations used and includes a printout of the fall velocity subroutine. Figures 10 and 24 (fall velocity vs size and altitude) were generated using this subroutine.

A.3.b. Diffusion.

The diffusion model used is similar to Bauer's "model I" (39). Diffusion of a chemically inert tracer of mixing ratio f(z,t) is described by the following diffusion equation:

$$\frac{\partial}{\partial z}\left[n_a(z)\frac{\partial f(z,t)}{\partial z}\right] = n_a(z)\frac{\partial f(z,t)}{\partial t} \tag{24}$$

where $n_a(z)$ is the ambient atmosphere's number density, f(z,t) is described by eqn. 20 and K_d is the eddy diffusion coefficient. In this model, K_d was treated as constant

(.5 m^2/sec). The boundary at the tropopause was treated as an infinite sink because tropospheric washout/rainout is very rapid compared to stratospheric removal processes.

If the stratosphere is treated as isothermal, i.e.,

$$n_a(z) = n_o \exp\left[-(z-z_o)/z_{scale}\right] \tag{25}$$

where z_o is the cloud center altitude, z_{scale} is the atmospheric scale height, and n_o is the tracer density at z_o, then the diffusion equation (24) simplifies to:

$$K_d \frac{\partial^2 f(z,t)}{\partial z^2} - \frac{K_d}{z_{scale}} \frac{\partial f(z,t)}{\partial z} = \frac{\partial f(z,t)}{\partial t} \tag{26}$$

Solving the equation for a point source injection, we find:

$$f(z,t) = \frac{1}{\sqrt{2\pi}\,\sigma_z} \exp\left[-\frac{\sigma_z^2}{8}\left(\frac{1}{z_{scale}} + \frac{2\Delta}{\sigma_z^2}\right)\right] \tag{27}$$

where

$$\Delta = z_o - z \tag{28}$$

and

$$\sigma_z = \sqrt{2K_d\,t} \tag{29}$$

This f(z,t) is equivalent to an $n_s(z,t)$ of the following form:

$$n_s(z,t) = K_N \left[\frac{e^{-\frac{1}{2}(\Delta/\sigma_z)^2}}{\sqrt{2\pi}\,\sigma_z}\right]\left[e^{\left(\frac{\Delta}{z_{scale}}\right)}\right] \tag{30}$$

which may be thought of as the product of two probability distributions, the first relating to the diffusion profile of the tracer, the second relating to the atmospheric density gradient. K_N is a normalization factor which is a function of σ_z and z_{scale}. With some further manipulation it can be shown that $n_s(z,t)$ is also Gaussian:

$$n_s(z,t) = \frac{K_N}{\sqrt{2\pi}\,\sigma_z} \exp\left\{-\frac{1}{2}\left[\frac{z-\left(z_o - \frac{\sigma_z^2}{z_{scale}}\right)}{\sigma_z}\right]^2\right\} \tag{31}$$

The ambient atmospheric number density gradient effectively displaces the cloud

center below z_o by the factor σ_z^2/z_{scale}. As σ_z increases with time, the effective cloud center moves downward. Note that n_s has the same dispersion as f(z,t).

A.3.c. Transport.

Sedimentation and diffusion were combined in a multigroup transport computation. The cloud was separated into 60 velocity (or size) groups:

$$n_s(z,t) = \sum_{g=1}^{60} n_g \left[v_g(r_g, z_g), z, t \right] \tag{32}$$

where v_g is group sedimentation velocity and z_g is the vertical group centroid. The cloud was treated in effect as sixty rigid clouds with separate streaming and eddy diffusion characteristics. The initial vertical dispersion of each group was taken as the dispersion of the composite cloud (2.15 km). Because eddy diffusion is a bulk process, the same diffusion constant (K_d) was applied to each group. It was assumed that once the particles were formed during the thermal processes immediately after detonation, the particle size distribution stayed reasonably constant in time, i.e., agglomeration was not included. Turco et al estimate the effects of agglomeration on dust burden to be less than 10% (1:63). Yoon et al state that no clear evidence of nuclear debris particle agglomeration exists (13:3-43).

Streaming was governed by the sedimentation velocity of particles at altitude z_g. Since the sedimentation velocity is a function of altitude, treating the clouds as rigid (all particles at centroid velocity regardless of altitude) introduces some error into the streaming calculation. Since dv/dz increases with decreasing radius (see figure 24), so does the sedimentation error. An indication of the magnitude of the error is given in figure 25. The figure shows a comparison of the stratospheric burden predicted by rigid cloud descent vs the descent of a multigroup cloud (initially Gaussian) of monosize particles. The clouds were given an initial centroid height of 25 km and a dispersion of 2.15 km. For particles of radius $\geq 10\mu$, the error is small enough to be imperceptible given the large time increments (1-2 weeks) used in the stratospheric debris transfer calculations. In the submicron regime, the cloud dispersion decreases significantly (the cloud "bunches up") due to the increasing fall velocity with altitude. This bunching effect is reflected in the more sudden drop in burden for the multigroup treatment than for the rigid cloud approximation (figure 25b). The

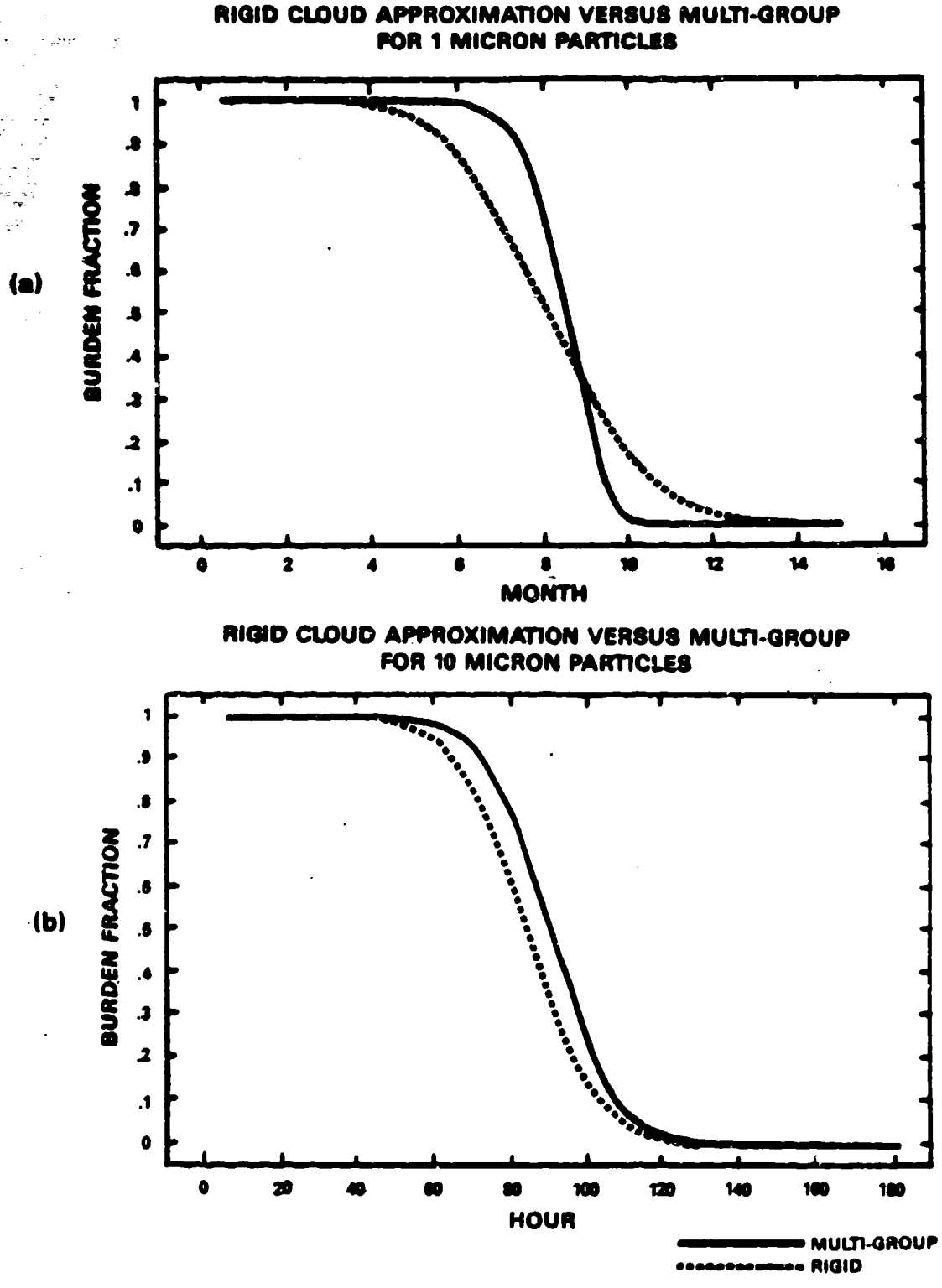

Figure 28. Sedimentation Error Introduced by Rigid Cloud Model

sedimentation half-life is roughly the same for the two calculations. The early time burden predicted by the rigid cloud approximation is accurate to within 30% of the multigroup treatment. At later times, the error is mitigated since for small particles turbulent diffusion is the dominant removal mechanism, especially as particles approach .1μ and less (the results in Chapter V show that in admissible size distributions most particles are submicron with a median radius of ~.1μ). Thus, the error introduced by the rigid cloud approximation is negligible above 10μ and probably less than a factor of 2 across the remaining size spectrum.

A.3.d. Burden Computation.

The transport was calculated using a Fortran subroutine (subroutine STRATFAL of Appendix D) which injected clouds at Foley-Ruderman altitudes and computed subsequent size group diffusion and sedimentation. Figure 26 depicts the transport of the 1μ group as computed by STRATFAL for the Castle Bravo event (area under curves normalized to 1). The stratospheric burden vs time, B(t) is:

$$B(t) = \sum_{g} \int_{z_{trop}}^{\infty} A_g(r_g, z, t)\, dz \tag{34}$$

where the activity, $A_g(r)$ is a function of $n_g(r)$ and the specific activity, S(r). A global mean tropopause height of 12 km was used. The stratospheric burden computed in equation 34 can be directly compared with atmospheric test data as depicted in figures 15 and 18.

A.4. Specific Activity Treatment.

In order to relate activity burden to number size distribution, a functional relationship must be determined relating the activity expected on a particle to its radius. Freiling has proposed a "radial model" of activity content in which refractory nuclide activity is approximately proportional to particle volume:

$$A_r(r) = K_r n(r) r^3 \tag{35}$$

and volatile nuclide activity is approximately proportional to particle surface:

$$A_v(r) = K_v n(r) r^2 \tag{36}$$

where K_r and K_v are constants of proportionality.

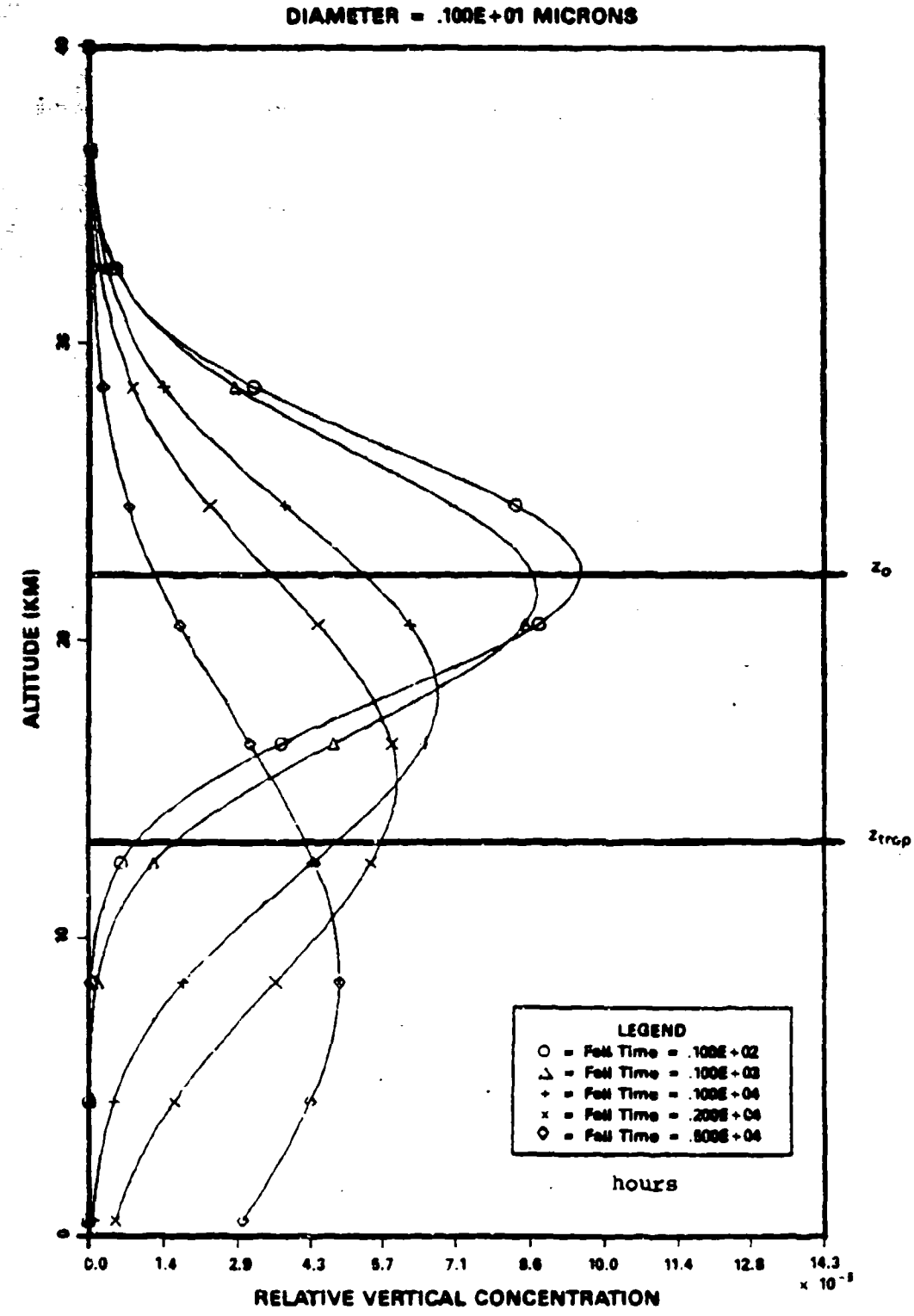

Figure 28. Group Fall Illustration

Available data on individual particle activity is usually presented in the form of equivalent fissions per gram, a quantity called specific activity. Some authors use "specific abundance" which is probably a better term, although less prevalent in the literature. An equivalent fission is defined as the number of fissions that must have occurred in a device to produce the amount of a particular radionuclide observed on a particle (49:382). There are 6.02×10^{23} nuclei in 235 grams of ^{235}U and each fission releases 180 MeV. Thus 1 ton (2.6×10^{22} MeV) of completely fissioned material when completely mixed with 1 ton of soil will yield particles with an average specific activity of 1.4×10^{14} fissions/g.

Observed particle activities vary between r^2 and r^3 over the range of particle sizes of interest for cloud modeling, conforming to Freiling's hypothesis. Some anomalous behavior has been noted and explained for large particles (100 - 1000μ) by R. C. Tompkins (21). In addition, as previously discussed in section IV.A.4, Nathans has observed a strong, non-Freiling radial dependence below .2μ in air burst debris. Since this phenomenon is probably due to the presence of unmixed fission products, a similar effect may not be present for surface bursts where much more mixing material (carrier) is available.

It was initially assumed that in the cloud most of the activity resided on particles between .01 and 10 microns and, further, that the specific activity in this size range obeyed Freiling's radial model. The first assumption was justified by what is known about size distributions from microscopic analysis. Since these analyses show the bulk of cloud particle surface and volume lies below 10μ, it was expected that the activity would probably behave likewise. The second assumption is confirmed from measured specific activity data (see for example figures 27-29). In most cases, specific activity varied between that expected for refractory and volatile species:

$$refractory: \quad S_r(r) \propto \frac{A_r(r)}{r^3} \propto constant \tag{37}$$

$$volatile: \quad S_v(r) \propto \frac{A_v(r)}{r^2} \propto \frac{1}{r} \tag{38}$$

Note from the example plots that for the same nuclide, S(r) behavior varies from event to event.

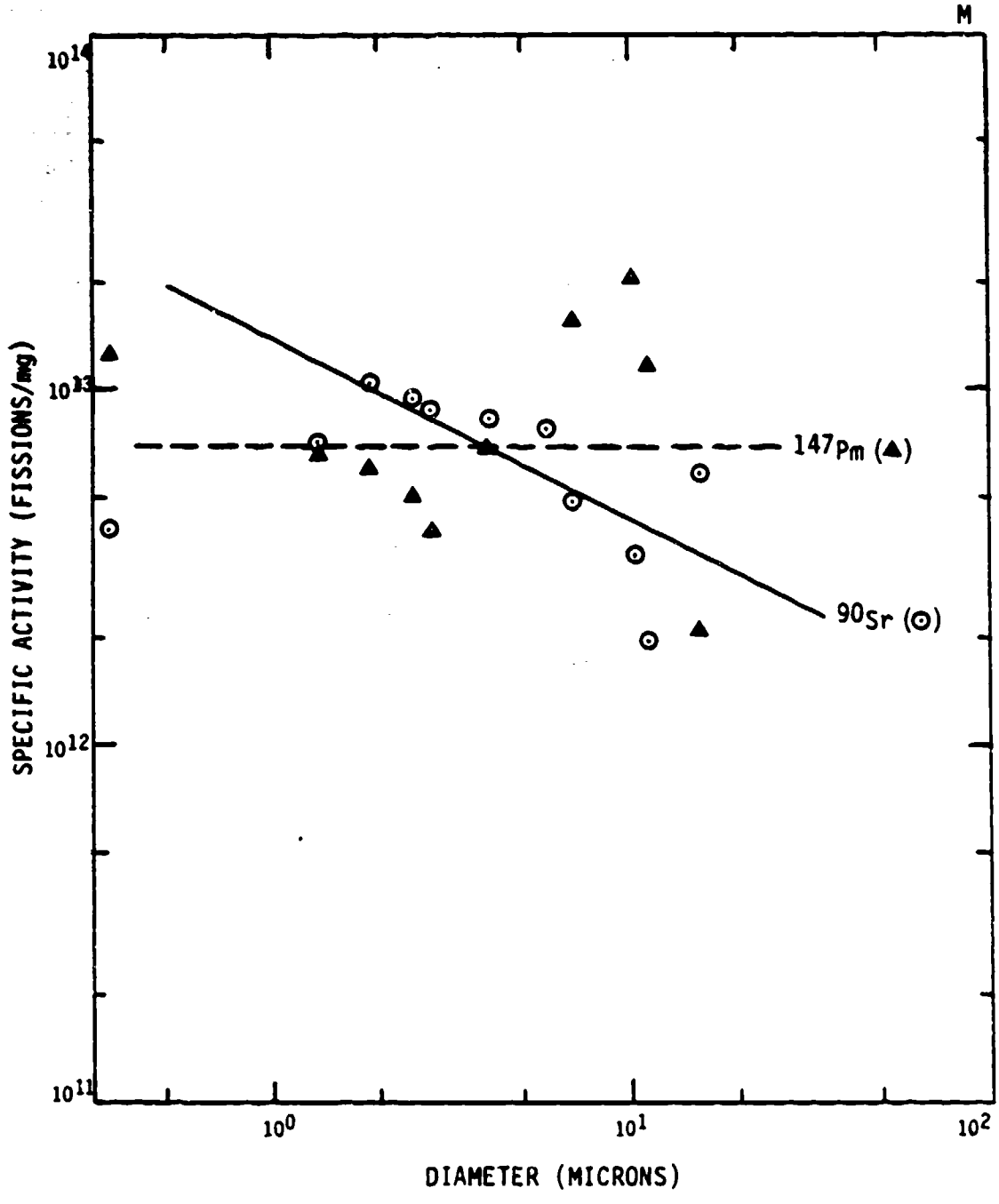

Figure 27. Specific Activities of ^{90}Sr and ^{147}Pm in a Tower Burst

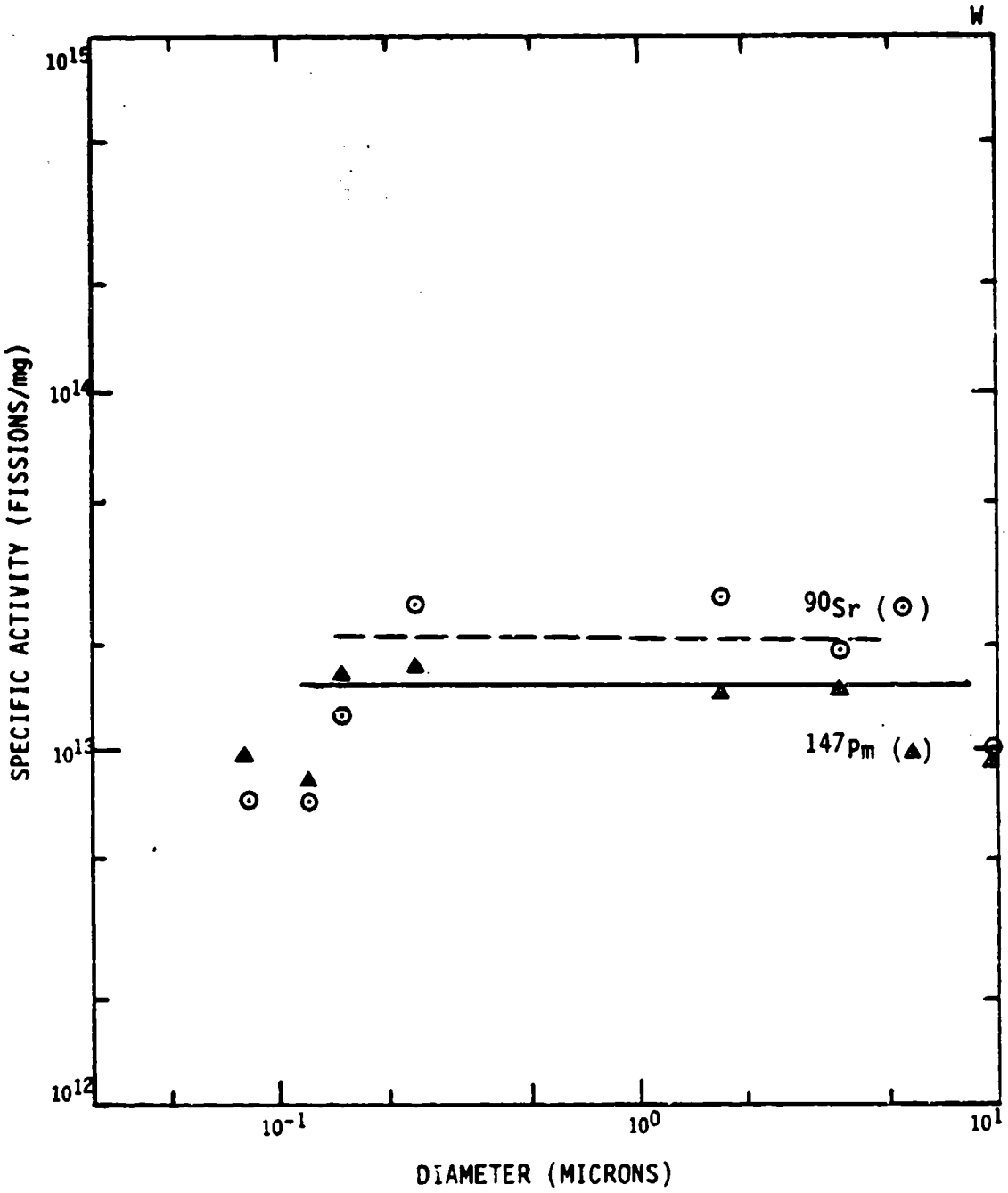

Figure 28. Specific Activities of ^{90}Sr and ^{147}Pm in a Wilson Sample

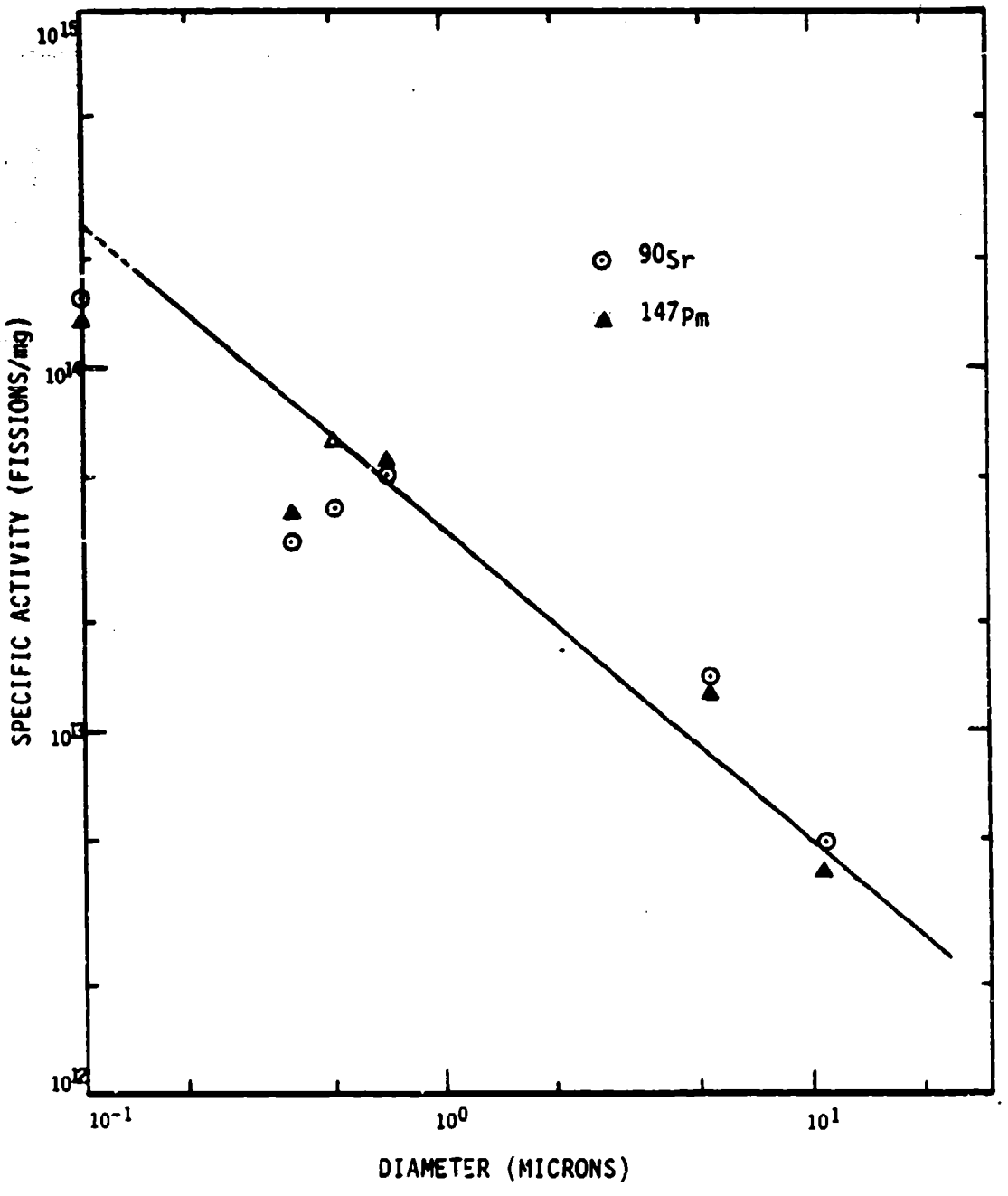

Figure 29. Specific Activities of ^{90}Sr and ^{147}Pm in a Hood Sample

In the computation of stratospheric burden, a normalized n(r) was converted to A(r) using:

$$A(r) \;\alpha\; n(r)r^{l} \tag{39}$$

From this relationship A_g, the fraction of activity in each group was computed from:

$$A_g = K_n \int_{r_{g-1}}^{r_g} \hat{n}(r)r^{l}\, dr \tag{40}$$

where

$$K_n = \left[\exp\left(l\ln(r_m)+\frac{l^2\beta^2}{2}\right)\right]^{-1} \tag{41}$$

in the case of lognormal distributions or

$$K_n = \left[\sqrt{2\pi}\beta e^{\frac{1}{2}l^2\beta^2} r_o^{5/2} r_m^{l-\frac{3}{2}} CNF\left(\frac{\ln r_o - \ln r_l}{\beta}\right) + \frac{r_o}{l-p+1}\left(r_{\max}^{l-p+1} - r_o^{l-p+1}\right)\right]^{-1} \tag{42}$$

in the case of Nathans' distribution. In the expression above, p is the exponent of the power law tail and r_l is the median radius of the lth moment of the log normal portion of the distribution:

$$r_l = r_m e^{l\beta^2} \tag{43}$$

For ^{90}Sr, l was set to a nominal 2.5 based upon Nathans' specific activity graphs. For the highly refractory ^{185}W, l was set to a nominal 3.0. A sensitivity study was performed by varying l between 2 and 3 for both nuclides. This variation altered the median radius bound by less than a factor of 2 for a lognormal n(r).

A.5. Matching the Model to the Stratospheric Data.

^{90}Sr data comparisons were carried out by main programs SHOT50 and SHOT60 (1950s and 1960s comparisons were run separately) which varied the n(r) parameters (r_m, β, p, f_m) and then called subroutines to set the activity distribution, inject the clouds from the combined events, and then compute activity removal with time. Appendix D lists the optimization program for the 1960s ^{90}Sr data comparisons. Similar programs were developed for 1950s ^{90}Sr and 1958-59 ^{185}W data comparisons. In all cases, optimum n(r) parameters were determined by maximizing a

figure of merit expressed by:

$$\chi = \left\{ \sum_j \left[B^+(t_j) - B(t_j) \right]^2 \right\}^{-1} \tag{44}$$

where $B^+(t_j)$ represented the measured stratospheric burden data from the last chapter and $B(t_j)$ represented the model results (eqn. 34). The program flow is shown in figure 30.

Three sets of optimization runs were performed. 1960s ^{90}Sr data was optimized in a separate run from the 1950s ^{90}Sr. The third set used the ^{185}W data from the 1958 Hardtack series. The ^{90}Sr data was split for two reasons:

(1) 1950s data was not as uniformly trustworthy as 1960s. Prior to Project Stardust (under which regular U2 sampling was conducted beginning in 1957), the ^{90}Sr burden estimates were based on ground samples and limited balloon sampling. Thus, estimated stratospheric burdens prior to 1957 were subject to considerable uncertainty.

(2) The 1950s high yield events were mostly contact surface bursts (detonated within 1 meter of surface). In the 1960's, although the exact burst heights were not available, they tended to be higher in general to avoid local fallout (58). Thus, running separate optimizations might identify systematic differences in particle size distributions between the two eras. Indeed, results indicate a larger size distribution for the 1950s events as compared to the 1960s but the difference is small enough that it could be due to uncertainties in the data and model.

Results from stratospheric n(r) optimization runs are presented in section V.A.

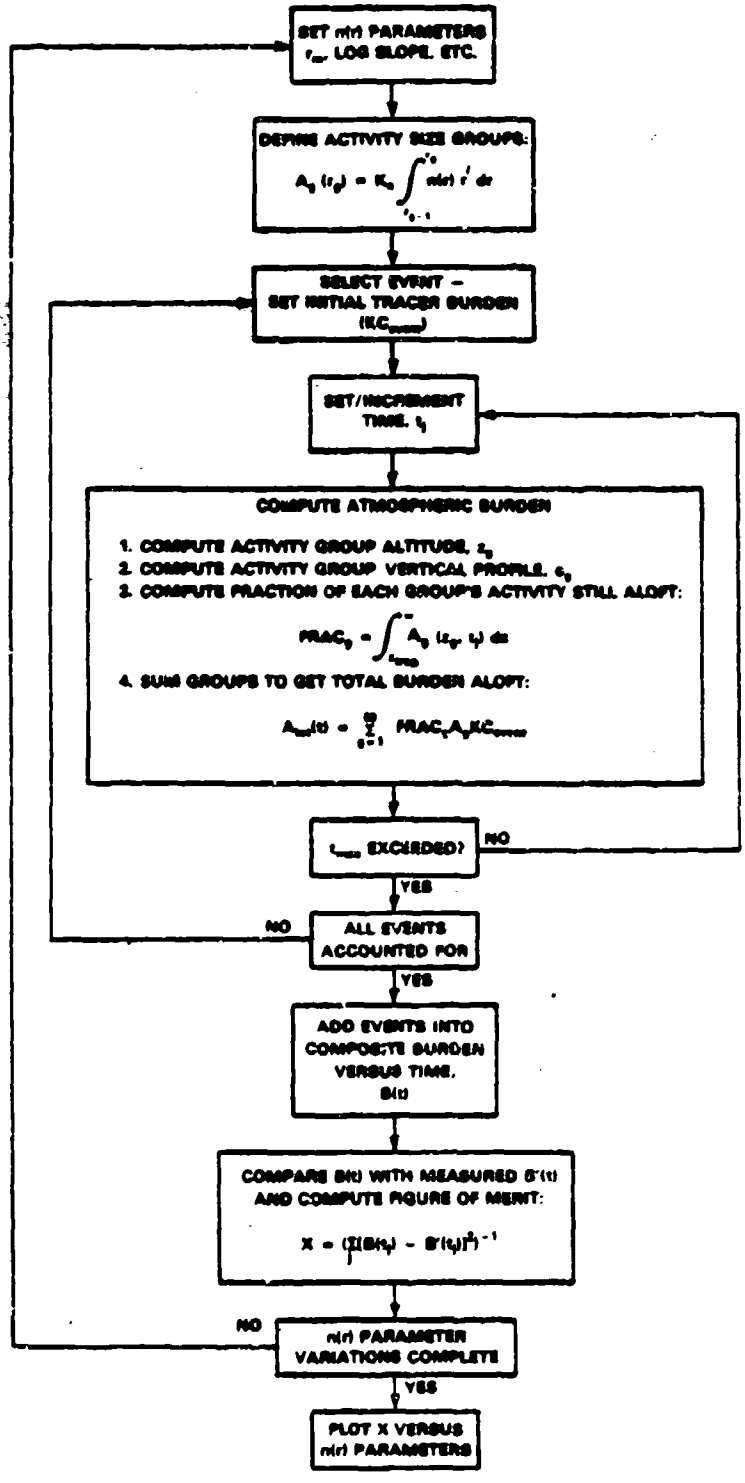

Figure 30. N(r) Optimization: Code Flow Diagram

B. Tropospheric (Local/Intermediate) Fallout Transfer Modeling.

B.1. Properties of the Troposphere.

Because of the unstable temperature profile in the troposphere, a different vertical transfer model was needed. Stronger vertical air currents exist and the hygroscopic nature of debris particles leads to removal by washout. Disregarding horizontal transport, the following equation governs particulate density in the troposphere (59:507):

$$K_d \frac{\partial^2 n}{\partial z^2} - an - bn^2 - w\frac{\partial n}{\partial z} = 0 \tag{45}$$

where K_d is the eddy diffusion coefficient, n is the vertical particle concentration, a is the washout removal rate (a is the reciprocal of the residence time, T), b is the coagulation coefficient, and w is the sedimentation velocity. According to Junge, washout is the predominant removal mechanism for naturally occurring particulates (average radius .03μ) below 5 km so that equation (45) may be simplified to:

$$K_d \frac{\partial^2 n}{\partial z^2} - an = 0 \tag{46}$$

By noting the altitude range over which n decreases by a factor of ten, Junge estimates residence time for particulates below 5 km to be somewhere between 1 and 10 days. Above 5 km, removal by washout diminishes and the effective particulate residence time increases. The TTAPS study used a tropospheric residence time of 10 days for smoke however this represented a global average. Since Junge's estimates were based upon data taken over the continental United States' midsection, the present model varied T between his bounds. Even though the average initial cloud center height was in the vicinity of 10 km for Nevada shots, sedimentation lowers the activity centroid to altitudes for which Junge's values were considered reasonable. Constant exponential washout was assumed.

Tropospheric sedimentation was modeled using the same algorithms developed for stratospheric sedimentation (Section IV.A.3). Based upon Junge's analysis, washout was assumed to dominate eddy diffusion effects.

B.2. Tropospheric Cloud Injection and Removal.

B.2.a. ^{90}Sr Injection.

The Foley-Ruderman model was not needed for intermediate fallout modeling. Since all events considered were low yield U.S., the measured cloud heights were available (47). The initial cloud centroid was taken as the mean of the reported cloud top and bottom.

Initially, an attempt was made to model injection and removal event by event. This approach proved extremely unwieldy since it was determined that 75 bursts contributed to offsite ^{90}Sr between 1951 and 1958 (Table III). Although wind data over the test site was readily available at shot time, properly modeling individual bursts would have required including wind and rain data over the central United States for 3 days following each event, a grueling proposition. Instead, the average behavior of the 75 bursts was determined and a composite injection of ^{90}Sr was modeled. Table III lists the contributing events and their injection parameters (based on information in reference 47).

The 75 events had a combined total yield of 995 KT and lofted roughly 99.5 kilocuries of ^{90}Sr. Yield weighted average injection parameters were as follows:

Y = 13 KT
Cloud center = 10.4 ± 1.2 km
Wind Speed = 70 ± 15 km/hr (at cloud center)
Wind Direction = 246° ± 24° (compass)

B.2.b. ^{90}Sr Removal.

The model included both sedimentation (same model as for stratospheric tracers) and washout. The change in the activity aloft as a function of time was described as follows:

$$\left(\frac{dA}{dt}\right)_{total} = -\lambda A(t) - \left(\frac{dA}{dt}\right)_{sed} \qquad (47)$$

where λ is the reciprocal of the washout residency time, T. The solution is of the form:

TABLE III

Events Contributing to Off-Site Fallout Through 1958

EVENT NAME	YIELD (kt)	CLOUD CENTER (kft)	WIND DIRECTION (°)	WIND SPEED (mph)	BURST HEIGHT (ft)
OPERATION:			RANGER		
Able	1	13 *	300	28	1060
Baker-1	8	33 *	290	38	1080
Easy	1	10 *	340	32	1080
Baker-2	8	26	290	51	1100
Fox	22	35	290	52	1435
OPERATION:			BUSTER-JANGLE		
Baker	3.5	27	50	24	1118
Charlie	14	34	30	20	1132
Dog	21	39	330	66	1417
Easy	31	43	340	52	1314
Sugar	1.2	13	210	51	3.5
Uncle	1.2	9 *	220	24	-17
OPERATION:			TUMBLER-SNAPPER		
Able	1	13 *	250	17	793
Baker	1	13	340	9	1109
Charlie	31	37	290	17	3447
Dog	19	36	260	47	1040
Easy	12	30 *	220	107	300
Fox	11	37 *	240	40	300
George	15	34 *	190	41	300
How	14	34 *	150	29	300
OPERATION:			UPSHOT-KNOTHOLE		
Annie	16	35	260	61	300
Nancy	24	34	210	50	300
Ruth	.2	12	300	17	305
Dixie	11	39	290	138	6022
Ray	.2	10	340	20	100
Badger	23	30	310	53	300
Simon	43	38	270	49	300
Encore	27	35	240	195	2423
Harry	32	35	290	72	300

*estimated

TABLE III continued

Events Contributing to Off-Site Fallout Through 1958

EVENT NAME	YIELD (kt)	CLOUD CENTER (kft)	WIND DIRECTION (°)	WIND SPEED (mph)	BURST HEIGHT (ft)
OPERATION:			UPSHOT-KNOTHOLE		
Grable	15	29	220	92	524
Climax	61	39	280	25	1334
OPERATION:			TEAPOT		
Wasp	1	18	320	76	762
Moth	2	20	300	62	300
Tesla	7	24	280	33	300
Turk	43	40	260	18	500
Hornet	4	33	280	43	300
Bee	8	35	310	47	500
Ess	1	10 *	340	29	-67
Apple-1	14	7	260	47	500
Wasp'	3	27 *	250	69	739
HA	3	33 *	320	35	Hi Alt
Post	2	14	350	8	300
Met	22	36	240	86	400
Apple-2	29	43	210	29	500
Zucchini	28	33	260	77	500
OPERATION:			PLUMBBOB		
Boltzman	12	28	160	23	500
Franklin	.14	15	220	6	300
Wilson	10	30	220	20	500
Priscilla	37	34	260	15	700
Hood	74	42	210	28	1500
Diablo	17	26	300	14	500
John	2	20 *	220	22	Hi Alt
Kepler	10	24	180	16	500
Owens	9.7	28	220	20	500
Stokes	19	32	200	76	1500
Shasta	17	24	300	7	500
Doppler	11	31	230	43	1500
Franklin'	4.7	27	220	40	750
Smoky	44	35 *	300	35	700
Galileo	11	27	70**	12	500

*estimated

**extremely erratic winds

TABLE III continued

Events Contributing to Off-Site Fallout Through 1958

EVENT NAME	YIELD (kt)	CLOUD CENTER (kft)	WIND DIRECTION (°)	WIND SPEED (mph)	BURST HEIGHT (ft)
OPERATION:			PLUMBBOB		
Wheeler	.2	15	120	120	500
Coulomb-B	.3	16 *	100	8	3
Laplace	1	17	200	9	750
Fizeau	11	34	120	22	500
Newton	12	26	250	51	1500
Whitney	19	24	60	10	500
Charleston	12	26	190	48	1500
Morgan	8	33	280	50	500
OPERATION:			HARDTACK II		
Mora	2	14	360	23	1500
Lea	1.4	14	110	3	1500
Socorro	6	23	220	19	1450
Wrangell	.115	8	220	16	1500
Rushmore	.188	7	140	5	500
Sanford	4.9	19	230	32	1500
De Baca	2.2	14	280	13	1500
Santa Fe	1.3	16	40	43	1500
averages:	13.3 kt	26.2 kft	238°	39 mph	99.5 ft

*estimated

$$A(t) = A_o e^{-\lambda t} - e^{-\lambda t} \int_o^t \left(\frac{dA}{dt'} \right)_{sed} e^{\lambda t'} \, dt' \tag{48}$$

where A_o is the initial atmospheric activity burden. A separate expression is needed for sedimentation rate since this is a function of particle radius (washout rate is not). If g(t) is defined as the fractional activity removal rate by sedimentation such that:

$$\left(\frac{dA}{dt'} \right)_{sed} = A_s(t) \frac{d\hat{a}}{dt'} = A_s(t') g(t') \tag{49}$$

where $\hat{a}$ is normalized activity and A_s as the activity remaining in the atmosphere from which sedimentation can still progress (the "sedimentation pool"), then A(t) becomes:

$$A(t) = e^{-\lambda t} \left[A_o - \int_o^t e^{\lambda t'} A_s(t') g(t') \, dt' \right] \tag{50}$$

But since the sedimentation pool is being exponentially depleted by washout:

$$A_s = A_o e^{-\lambda t} \tag{51}$$

we have finally:

$$A(t) = e^{-\lambda t} A_o \left[1 - \int_o^t g(t') \, dt' \right] \tag{52}$$

This expression was incorporated into Fortran program INTOPT (Appendix E) as the basis for intermediate fallout removal calculations.

B.3. Ground Contour Computation.

Equation 52 gives the rate of tracer removal. In order to compare with the available data (which is presented in the form of ground contours), fallout smearing was modeled. The Bridgman-Bigelow approximation (29:215) was adapted for this purpose. Bridgman and Bigelow developed a simple expression for ground activity surface density (A_ρ) which in terms of unit time reference activity (A_1) reduces to:

$$A_\rho(x,y) = \frac{A_1 f(y,t_a) g(t_a)}{v_z} \tag{53}$$

where the cloud is moving in the x direction, y is the transverse direction, t_a is the cloud arrival time, and $f(y,t_a)$ is the cloud spacial distribution in the transverse direction (assumed to be Gaussian). In order to include washout, the present model replaced the Bridgman-Bigelow g(t) function with $\left(\frac{dA}{dt}\right)_{total}$ (equation 47). Other modifications included ascribing a Gaussian vertical profile to the cloud and incorporating DELFIC fall mechanics (as described in section IV.A.3.). A constant wind velocity was assumed but the wind direction was changed according to the direction of the activity hotline (figure 31).

Given $A_\rho(x,y)$, contours were drawn using the linear interpolation routine contained in the *DISSPLA*$_{tm}$ graphics system (60). The model was checked by comparing contours with an example case computed by Bridgman and Bigelow (29:215-216).

B.4. Matching the Model to the Intermediate Fallout Data.

For reasons discussed in section IV.B., rigorous contour correlations between the data and the model were not performed. Instead, given the tremendous uncertainties inherent in the calculation, a simple comparison of activity grounded vs distance was used in an attempt to optimize n(r). The activity contours were subdivided by breaking the hotline into six segments as shown in figure 31. The activity deposited along each hotline segment was estimated assuming a Gaussian transverse distribution such that:

$$\Delta A_i = A_{\rho_i} \Delta x_i \sqrt{2\pi}\, \sigma_{y_i} \tag{54}$$

where A_{ρ_i} is the peak surface activity density along hotline segment i, Δx_i is the segment length, and σ_{y_i} was estimated from:

$$\sigma_{y_i} \approx Y_{10} \left(2 \ln \frac{A_{\rho_i}}{10}\right)^{-1/2} \tag{55}$$

Y_{10} was determined by bisecting each hotline segment and averaging the distance from the hotline to the 10 mC/mi^2 contour. While upper and lower bounds for the activity density were available for segments 2-6, no upper bound was available for segment 1. Possibly high values of activity density due to local fallout within the 60 mC/mi^2 contour would have made a large difference in the average activity

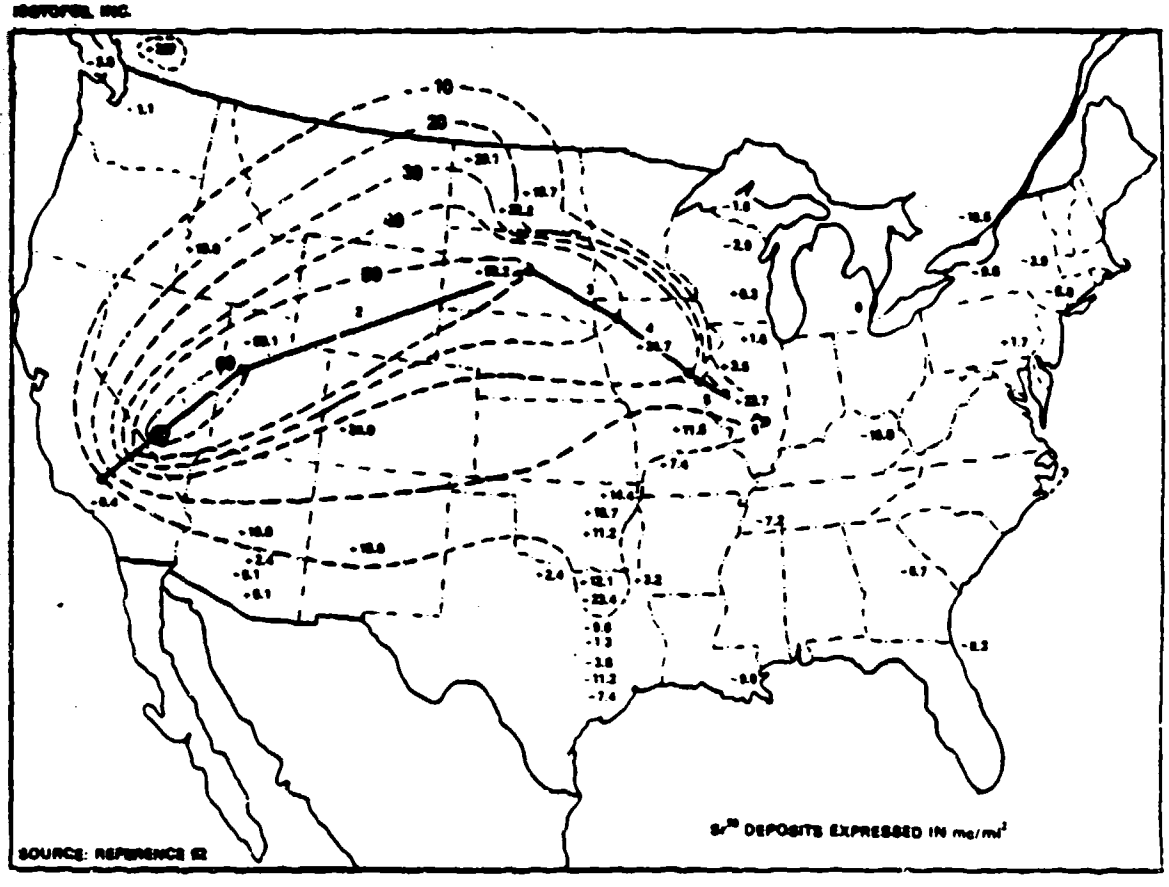

Figure 31. Distribution of Strontium-90 in U.S. Soils in Excess of World-Wide Fallout Amounts

TABLE IV

Incremental Intermediate Fallout Deposition				
segment number	A_{ρ_i} millicur/mi^2	Δx miles	σ_y miles	ΔA kilocuries
1	65	459	196	14.7
2	55	757	310	32.3
3	45	252	284	8.08
4	35	229	253	5.09
5	25	184	237	2.74
6	15	23	394	0.34

density along segment 1. Checks of local maps of ^{90}Sr deposition in Nevada and Utah revealed that 65 mC/mi^2 is a reasonable average (61,62). Table IV gives the deposition computed for each segment.

This method allows for the presence of activity outside the 10 mC/mi^2 contour (in contrast to roughly 40% computed within the 10 mC/mi^2). Isotopes, Inc. (52) constructed the intermediate fallout map used for the analysis and guessed that the bulk of the remaining 60% was deposited locally. The present analysis supports the opposite conclusion, namely that the remaining activity was still aloft.

The intermediate fallout n(r) optimization proceeded similarly to the stratospheric n(r) optimization (Section IV.A.5). The only difference was that the intermediate fallout n(r) optimization was based on ground activity fraction rather than the stratospheric fraction. Optimization was performed by a main program INTOPT which varied n(r) parameters, called subroutine INTFAL to compute tracer removal, and finally computed a figure of merit as in equation 44. The results of the optimization are discussed in section V.B.

V. Results.

The previous chapter described the modeling of vertical activity transfer in the stratosphere and troposphere and the approach used to optimize n(r). Chapter V presents the results of the optimization calculations. Chapter VI summarizes the findings and presents recommendations for their implementation.

A. Global (Stratospheric) Tracer Removal.

A.1. ^{90}Sr Removal.

The unaltered DELFIC size distribution was used as the initial n(r) input to the stratospheric fallout subroutine, STRATFAL (see listing, Appendix D). The DELFIC distribution was obviously too heavy to explain the data as is evident from figure 32. A combination of the 1950s and 1960s results are shown. If the activity were distributed according the the DELFIC ground fallout nominal, the stratospheric burden would have decayed in days rather than months. The DELFIC distribution is obviously biased much too strongly toward the heavy end of the particle size spectrum.

It was expected that the TTAPS distribution, with its larger activity fraction below 1μ, would better match the data. This was indeed the case, as shown in figure 33. Although some improvement was evident in comparison to the DELFIC nominal, even this distribution was too heavy to explain the data (the modeled stratospheric burden again drops too quickly). The critical parameter in Nathans' distribution is f_m, the mass fraction below r_o. This turns out to be a rather complicated function of Nathans' n(r) parameters:

$$f_m = \left[1 + \frac{\left(\frac{r_o}{r_{max}}\right)^{p-4} - 1}{\beta(4-p)e^{\beta^2(p-4)^2/2} CNF\left[\beta(p-4)\right]} \right]^{-1} \quad , \; p \neq 4 \tag{56a}$$

$$f_m = \left[1 + \frac{2 \ln \frac{r_{max}}{r_o}}{\sqrt{2\pi}\,\beta} \right]^{-1} \quad , \; p = 4 \tag{56b}$$

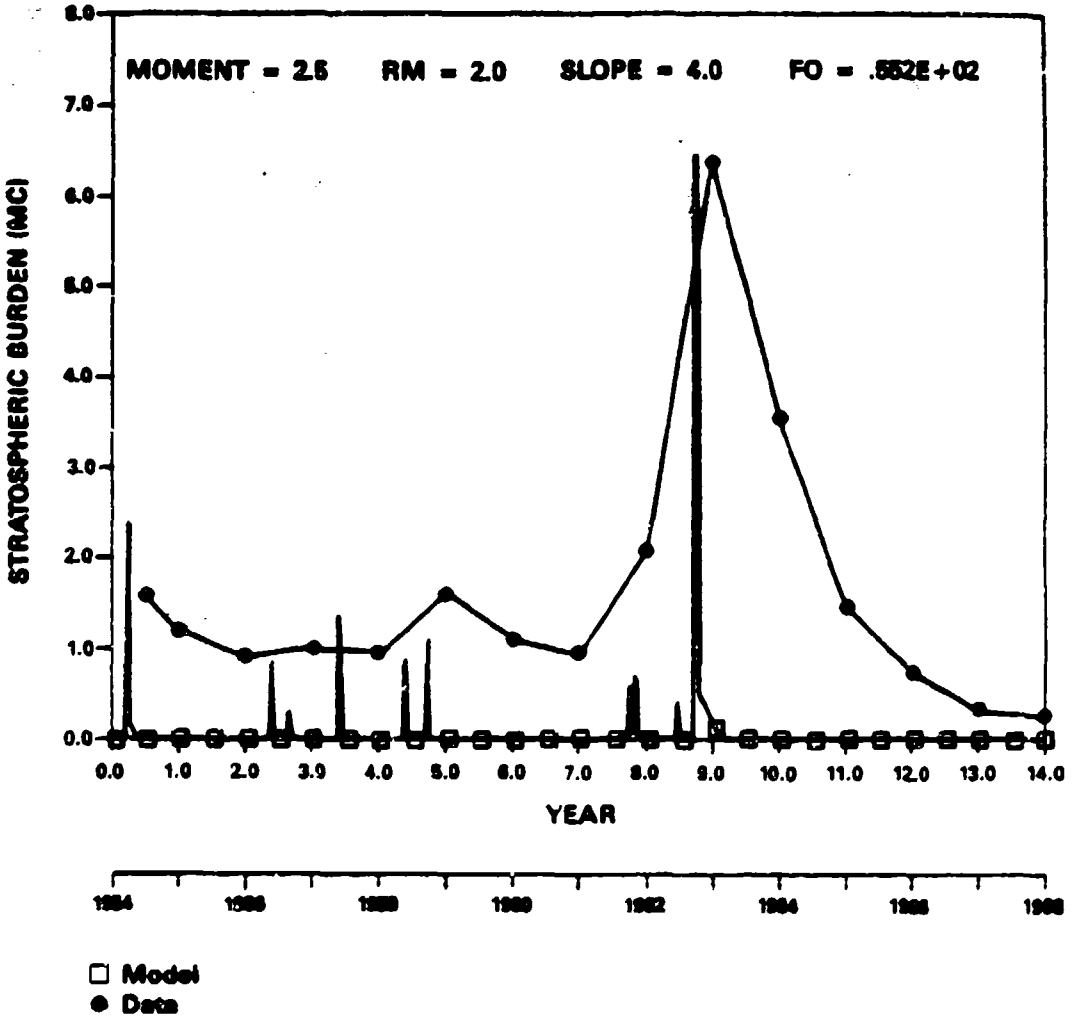

Figure 32. ^{90}Sr Burden from U.S. and Foreign Tests, DELFIC Nominal

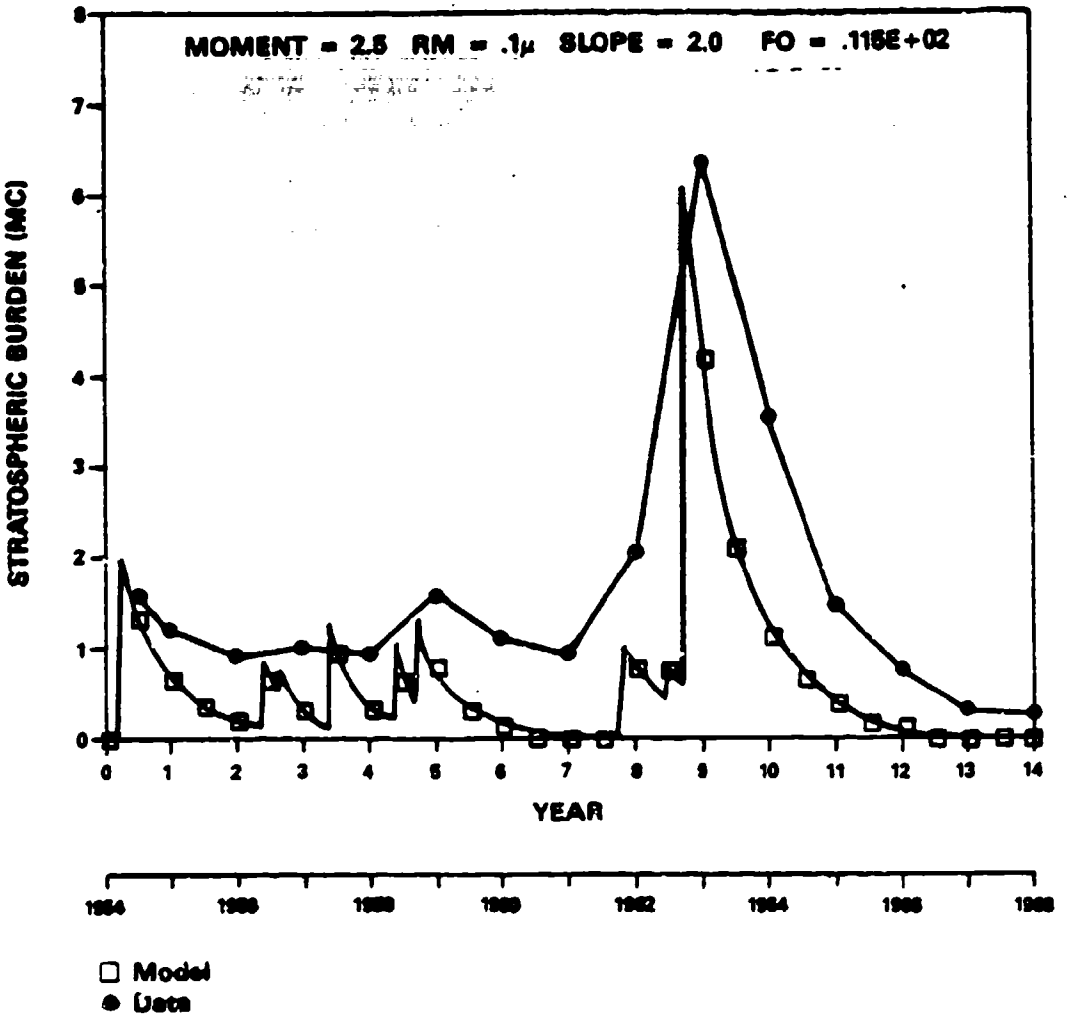

Figure 33. ^{90}Sr Burden from U.S. and Foreign Tests, Nathans' Distribution

R_o is a function of the power exponent, p, and varies between 0.7 and 1.7μ for $3 \leq p \leq 5$. Thus over the range of p bracketing Nathans' data, f_m is a good indicator of the fraction of mass in the submicron range.

Best fits to the stratospheric data were obtained when all of the mass was placed in the submicron regime ($f_m \rightarrow 1.0$). For fixed r_{max}, f_m is optimized for high values of p ($p \rightarrow \infty$). For fixed p, f_m is maximized as $r_{max} \rightarrow r_o$. In either case, best fits to the stratospheric data were obtained with $f_m = 1$ such that optimum r_{max} and p values are not physically reasonable. As an example, figure 34 depicts the data-model comparison with 100% of the mass below r_o. The fit looks good, but the size distribution is truncated at r_o. Thus, the Nathans' hybrid function does not adequately predict the removal of ^{90}Sr from the stratosphere .

Next, parameters for a pure lognormal distribution were optimized by varying r_m from .01 to 10μ and the slope from 1.01 to 4. A Gauss-Newton optimization was used at first but later abandoned because the data did not yield a unique solution (see figures 35, 36). It was more expedient to vary the parameters continuously and generate a three dimensional plot of the figure of merit, χ, vs r_m and slope. The figure of merit was defined as:

$$\chi(r_m,\beta) = \left\{\sum_j \left[B^+(t_j) - B(r_m,\beta,t_j)\right]^2\right\}^{-1} \qquad (57)$$

where $B^+(t_j)$ represents the measured stratospheric burden, and B(t) the model results.

Separate parameter variations were performed for 1950s and 1960s data. A total of 450 cases were run for each era. Figures 35 and 36 plot χ vs r_m and slope for 1950s ^{90}Sr removal and 1960s ^{90}Sr removal respectively. Note the lack of a unique solution (see figures 35, 36). Rather, for any slope, an optimum r_m is indicated. If the slope is ~2 (Nathans' value) the median radius is in the vicinity of .1μ for each optimization, somewhat lower than the r_m indicated by Nathans' surface burst sample analysis. The figure of merit improves slightly as r_m decreases. Thus the distribution which best predicts the removal of ^{90}Sr from the stratosphere is biased more toward smaller particles than even the TTAPS distribution and can be modeled as a simple lognormal function rather than a hybrid splice. Figure 37 plots model results

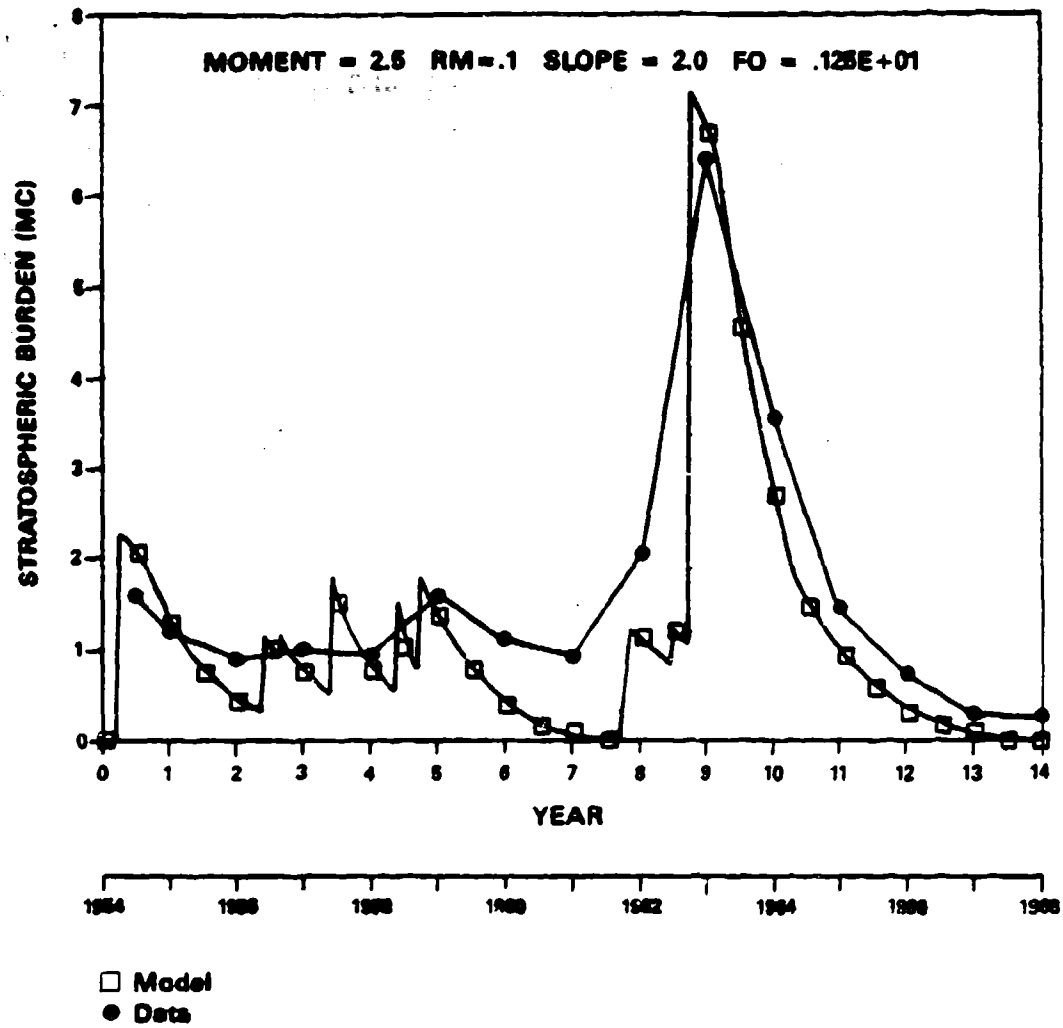

Figure 34. ^{90}Sr Burden from U.S. and Foreign Tests, $f_m = 1$ ($r_{max} = r_o$)

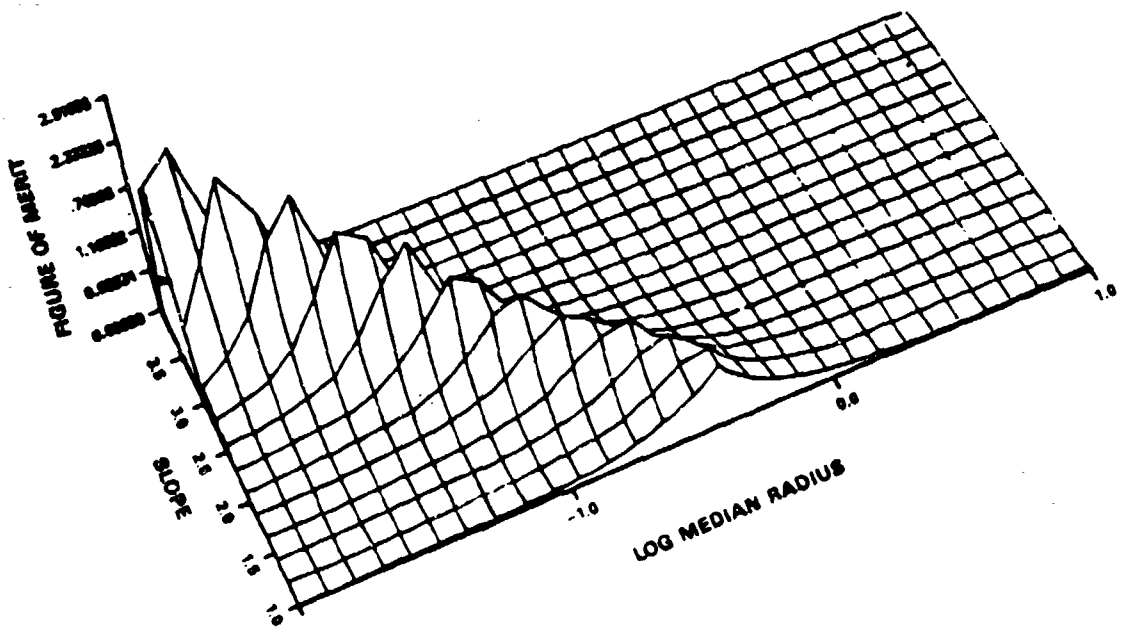

Figure 35. N(r) Parameter Variation, 1950s ^{90}Sr

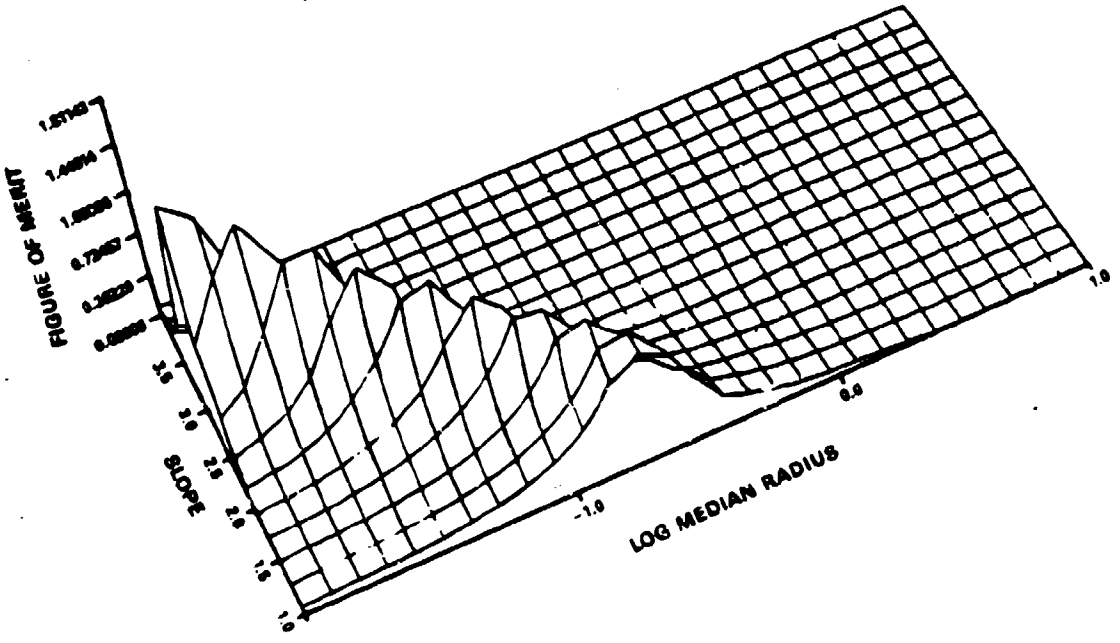

Figure 36. N(r) Parameter Variation, 1960s ^{90}Sr

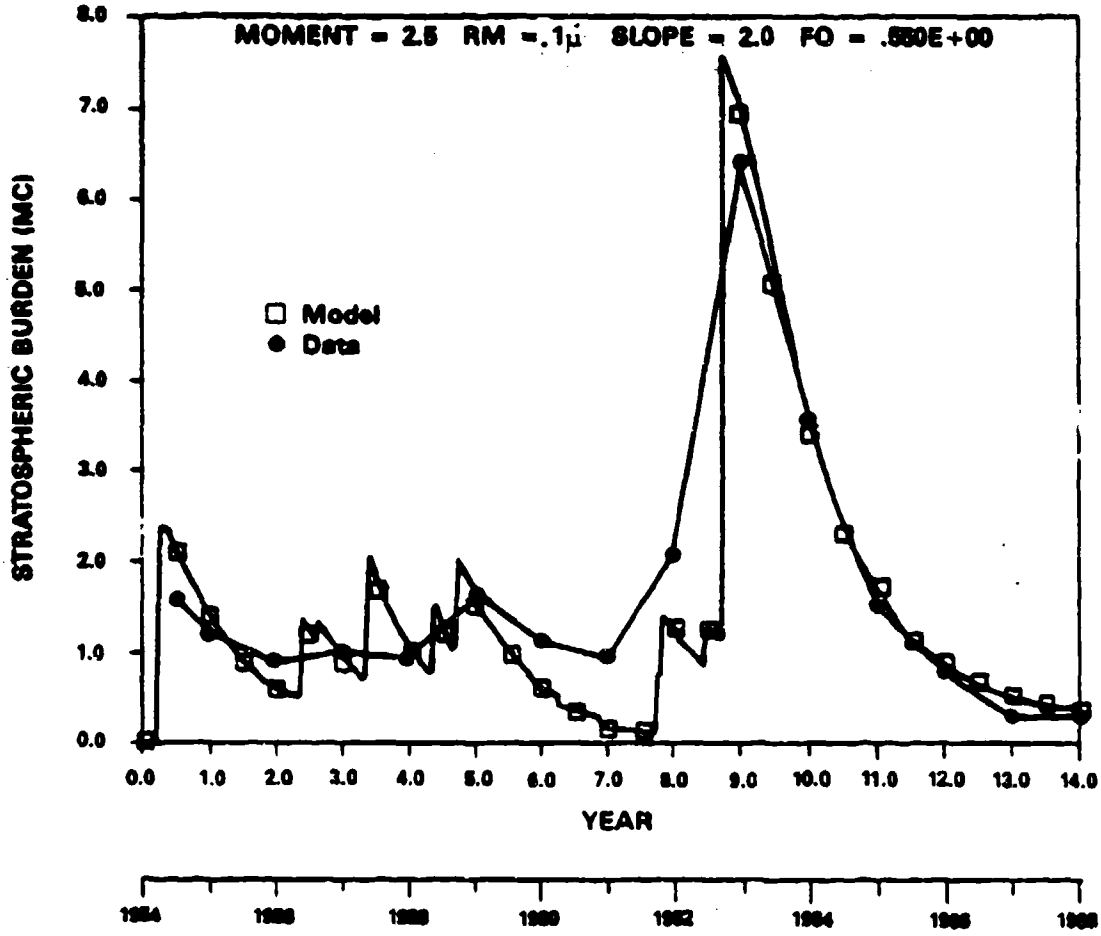

Figure 37. ^{90}Sr Burden from U.S. and Foreign Tests, Reasonable Fit

vs stratospheric data using $r_m = .1\mu$ and $\beta = \ln(2)$. The fit is quite reasonable given the large uncertainties in the stratospheric measurements. The disparity between model and data around 1960-61 is possibly explained by the arrival of debris from two high yield exoatmospheric bursts (250 km), Teak and Orange, which occurred in late 1958 (52:82). These bursts were not included in the burden calculations.

It might be argued that the bias toward a smaller particle distribution was a result of the volatility of ^{90}Sr precursors (63:3). The mass chain condenses late (roughly 5 minutes after detonation for megaton class weapons) such that the gaseous precursors, not heavily influenced by gravity, may have risen higher than early condensing chains. The rare gas precursors would have inhibited ^{90}Sr scavenging by local fallout. At the time of condensation, sedimentation would have lowered the concentration of the heaviest particles to some degree, such that condensation nuclei may have been generally smaller for ^{90}Sr. The best test of this possible explanation for the smallness of the particulates carrying the ^{90}Sr was to compare the behavior of a refractory nuclide. Fortunately, data on the stratospheric removal of ^{185}W, with one of the highest condensation temperatures on the periodic chart (therefore highly refractory), were available.

A.2. ^{185}W Removal.

The sequence of optimization trials for ^{185}W was identical to that used for ^{90}Sr. As in the case of ^{90}Sr, the nominal DELFIC distribution predicted a stratospheric removal rate which was much too rapid (figure 38). But again, surprisingly, the TTAPS distribution predicted a faster removal than indicated by stratospheric sampling data (figure 39). Indeed, the behavior of ^{185}W appeared to be very similar to that for ^{90}Sr, such that the TTAPS function again did not give satisfactory results except for non-physical values of n(r) parameters (see discussion in section V.A.1).

As with ^{90}Sr, parameters were optimized for a lognormal function based on a figure of merit as expressed in equation 57. The results were not extremely different from ^{90}Sr. Apparently, the two nuclides resided on similar debris particle distributions. A reasonable data-model comparison for ^{185}W is shown in figure 40 for $r_m = .2\mu$ and $\beta = ln(2)$. Figure 41 plots best fit r_m and logarithmic slope values from ^{90}Sr and ^{185}W optimization calculations. Notice that the ^{185}W results are

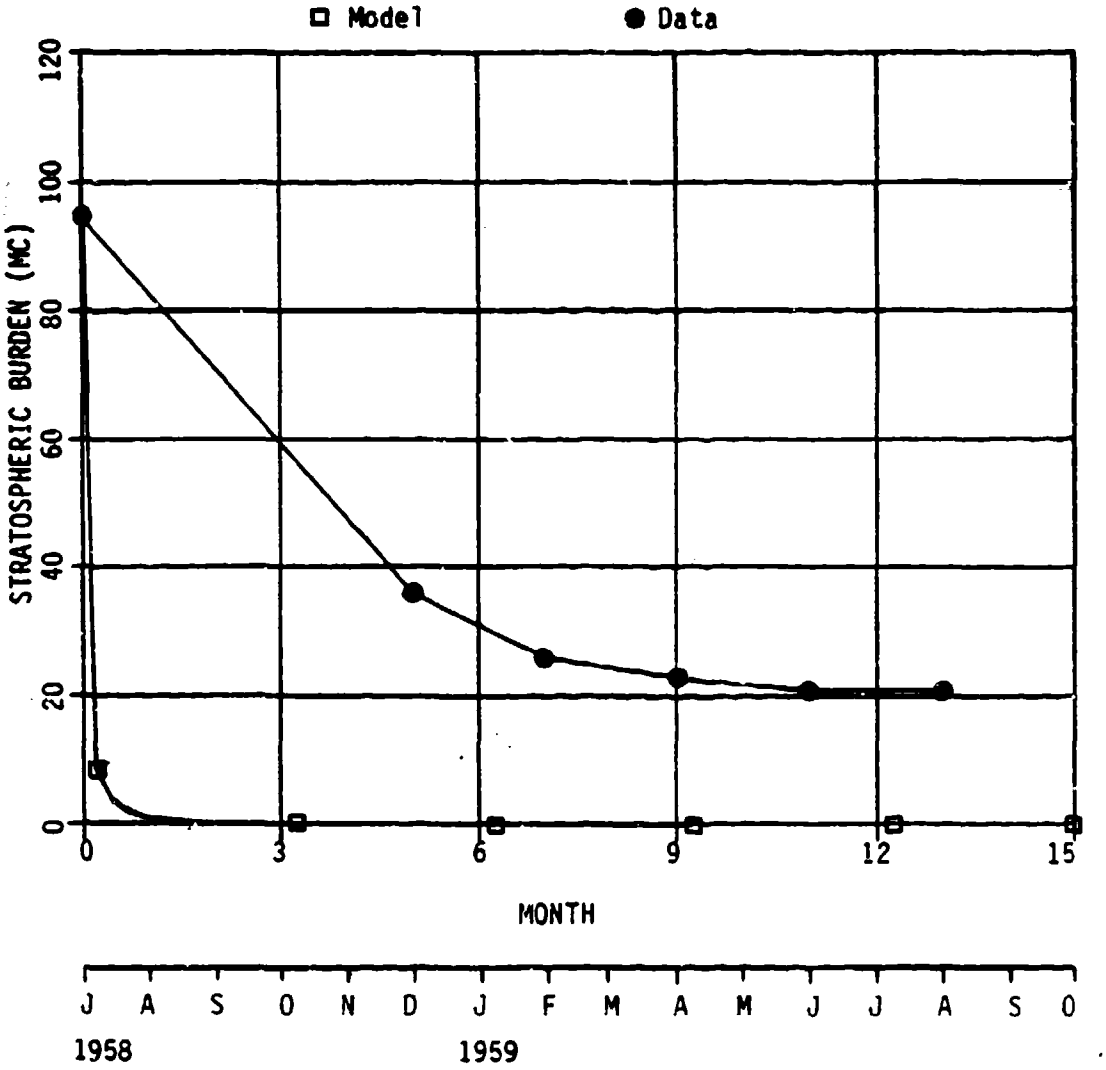

Figure 38. ^{185}W from Hardtack Series, DELFIC Nominal Distribution

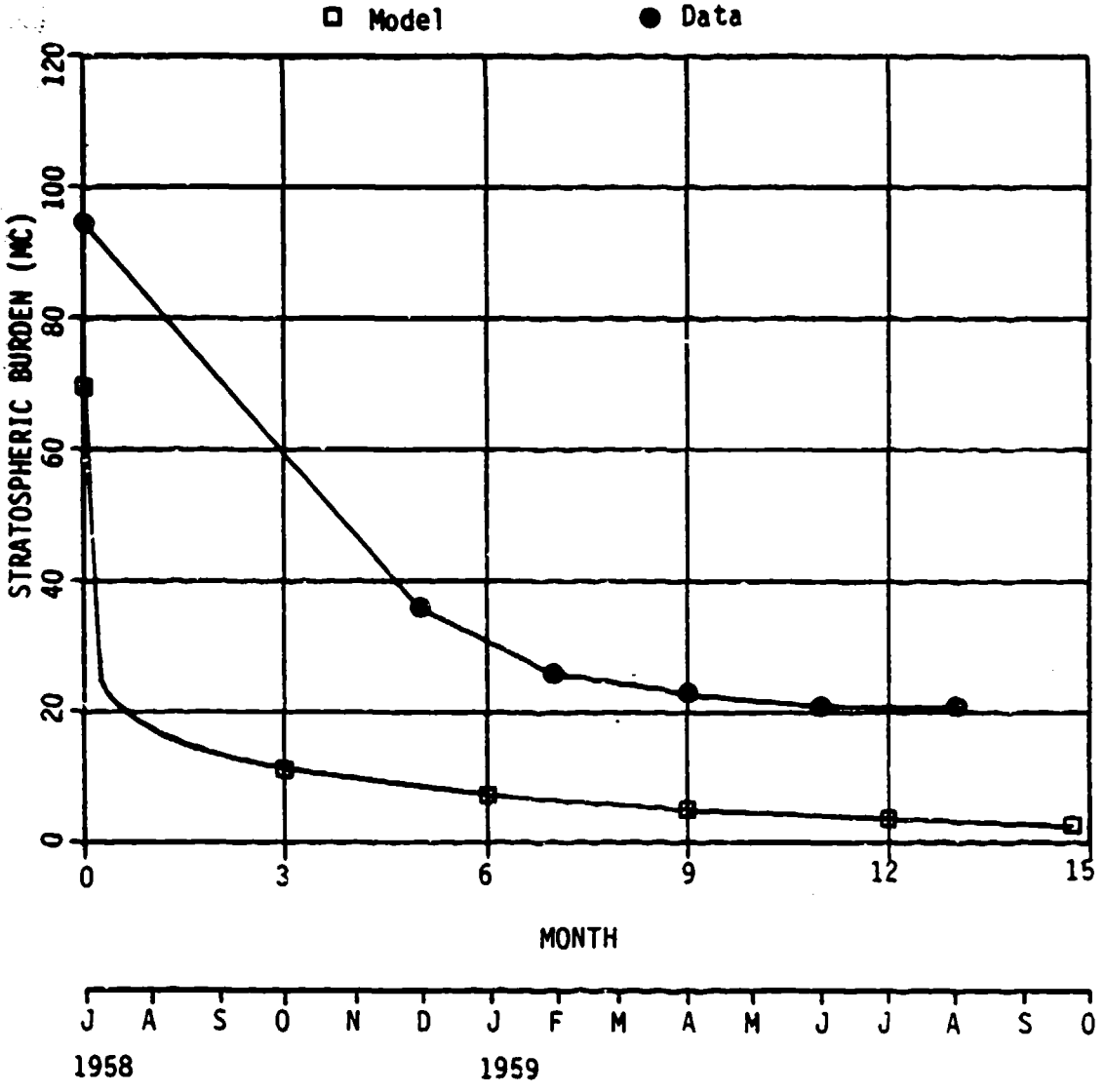

MOMENT=3.0 RM=25μ SLOPE=2.0

Figure 39. ^{185}W from Hardtack Series, Nathans' Distribution

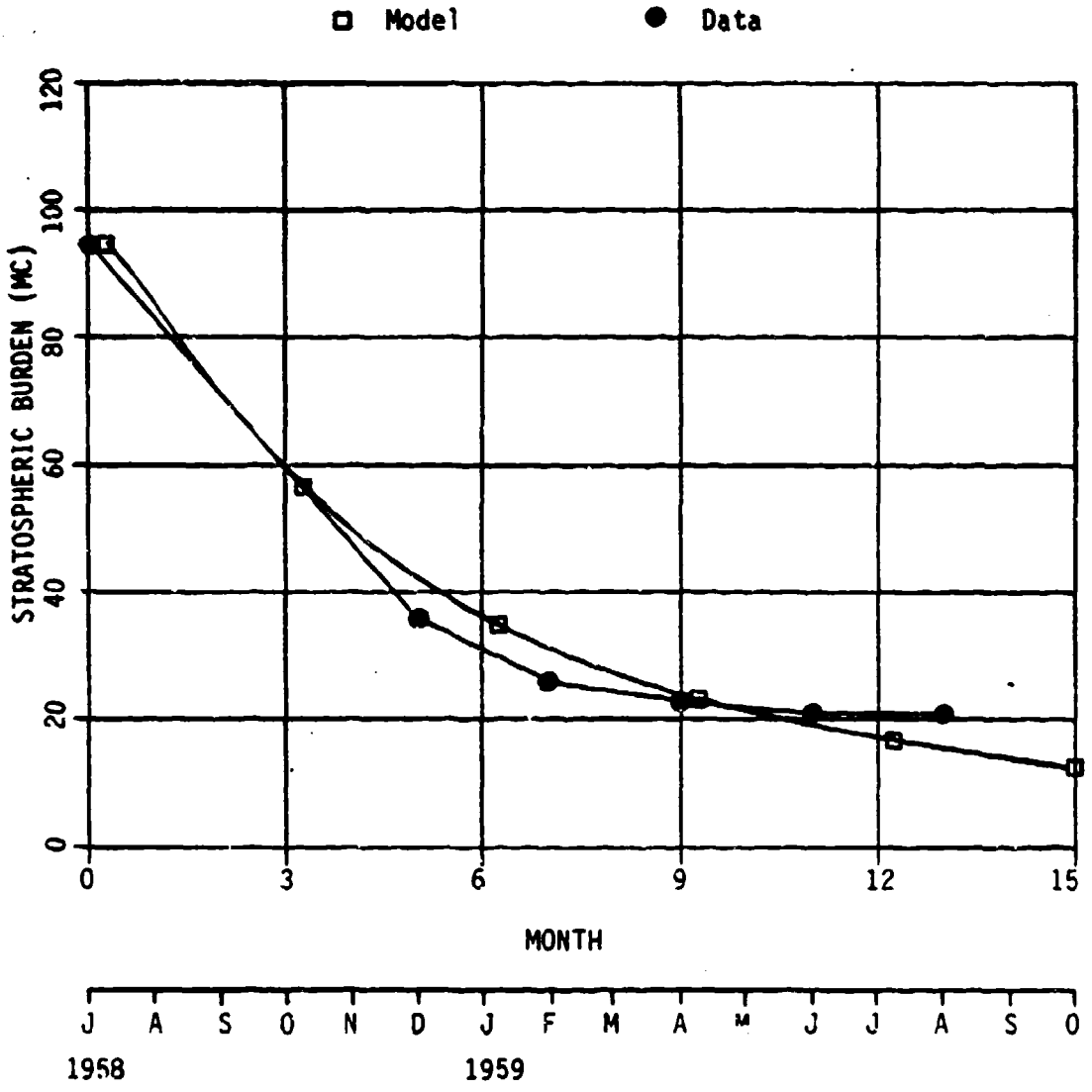

Figure 40. ^{185}W from Hardtack Series, Reasonable Fit

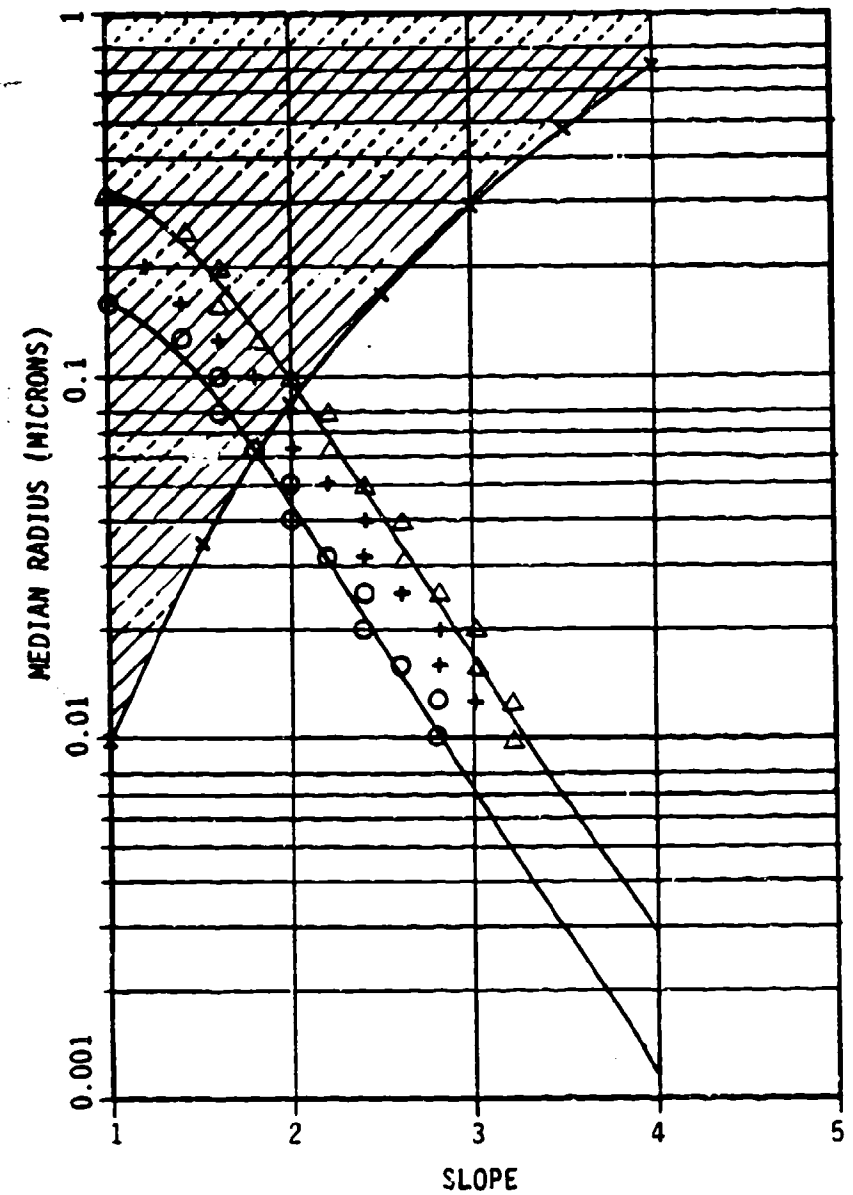

Figure 41. Stratospheric Strontium and Tungsten Removal, Best Fit Median Radius and Slope

straddled by the ^{90}Sr results, evidence that the tracers reside on similar particle populations despite differing mass chains and physical properties. These curves by themselves did not isolate a unique size distribution. In order to limit the range of admissible parameter values, another experimental observation was needed.

In his experience with test sample data, Nathans noted that he rarely if ever saw nuclear debris particles of radius less than .01μ (64). Since he based his size distribution statistics on samples of typically 1000 particles, the probability of the presence of particles $\leq .01\mu$ is at most .001. By plotting the locus of r_m vs slope which satisfy the inequality:

$$\frac{1}{\sqrt{2\pi}} \int_0^{.01\mu} \frac{1}{\beta r} \exp\left[-\tfrac{1}{2}\left(\frac{\ln r_m - \ln r}{\beta}\right)^2\right] dr \leq .001 \qquad (58)$$

it was possible to bound the admissible values of r_m and slope (figure 42 shaded area). Since for each nuclide the figure of merit improved with decreasing r_m, actual parameters are expected to lie closer to the lower boundary of the admissible area (lower r_m, higher logarithmic slope).

The particles which linger in the stratosphere obey a size distribution which may be described by a lognormal function and is smaller in general than either the DELFIC or TTAPS distributions. Thus, stratospheric particulates were initially expected to be removed at an even slower rate than the nuclear winter studies predicted (1,2,3,4,5). However, this conclusion turned out to be premature, and was contradicted by the intermediate and local fallout results.

An important clue to determining the true size distribution parameters was the fact that, for both ^{90}Sr and ^{185}W, the size distribution which predicted their long term behavior was quite similar to size distributions which Nathans determined for air bursts. This was despite the fact that all bursts producing ^{185}W were contact surface bursts, and that the 1950s events producing significant stratospheric ^{90}Sr were predominantly surface or near-surface bursts.

B. Intermediate Fallout.

As described in section IV.B, intermediate fallout data consisted of ^{90}Sr activity contours over the continental U.S. The initial comparison calculation used the n(r)

bounds determined from the analysis of stratospheric ^{90}Sr removal (nominally taken as $r_m = .1\ \mu$, B = ln(2)). The results were quite puzzling. Virtually no intermediate fallout due to sedimentation was predicted if the ^{90}Sr was carried by particles obeying a stratospheric size distribution. Washout appeared to be the only removal mechanism (figure 42). A reasonable comparison between predicted and actual contours was obtained by turning off the sedimentation effect entirely and using a washout e-folding time of 48 hours (figure 43).

Because of the tremendous uncertainties inherent in the computation of intermediate fallout (combining 75 bursts, assuming constant wind along the hot line, assuming exponential washout which may completely mask sedimentation effects), it was not possible to predict size distribution parameters from intermediate fallout data with any confidence. However one set of optimization calculations was made using plausible atmospheric parameters (constant wind speed of 40 mph, washout e-folding of 72 hours) to determine if the size distribution could be described with a lognormal function. Indeed it could, as shown in figure 44. A median radius of $.27\mu$ and slope of 3.1 optimized intermediate ^{90}Sr removal for the assumed atmospheric behavior.

As a point of interest, the model was exercised using the DELFIC nominal distribution and the TTAPS distribution, with results shown in figures 45 and 46. The DELFIC distribution obviously overpredicted grounded activity. Indeed, the DELFIC distribution by itself came close to predicting observed contours. However, it is extremely unlikely that the true distribution resembled the DELFIC n(r) since most of the 75 bursts contributing to off-site activity were air bursts and the nominal DELFIC distribution is based on contact surface and buried burst particles. The TTAPS distribution gave a reasonable fit but this was considered fortuitous given the uncertainties in the model. A rigorous optimization of the TTAPS distribution was considered to be unfruitful.

The most useful information from the intermediate fallout analysis was that the stratospheric distribution, based largely upon data from surface and near-surface burst injections, predicted virtually no fallout by sedimentation. This result was puzzling since significant local fallout was observed on clear days (no washout) for all surface and near-surface U.S. events (47). The intermediate fallout results implied

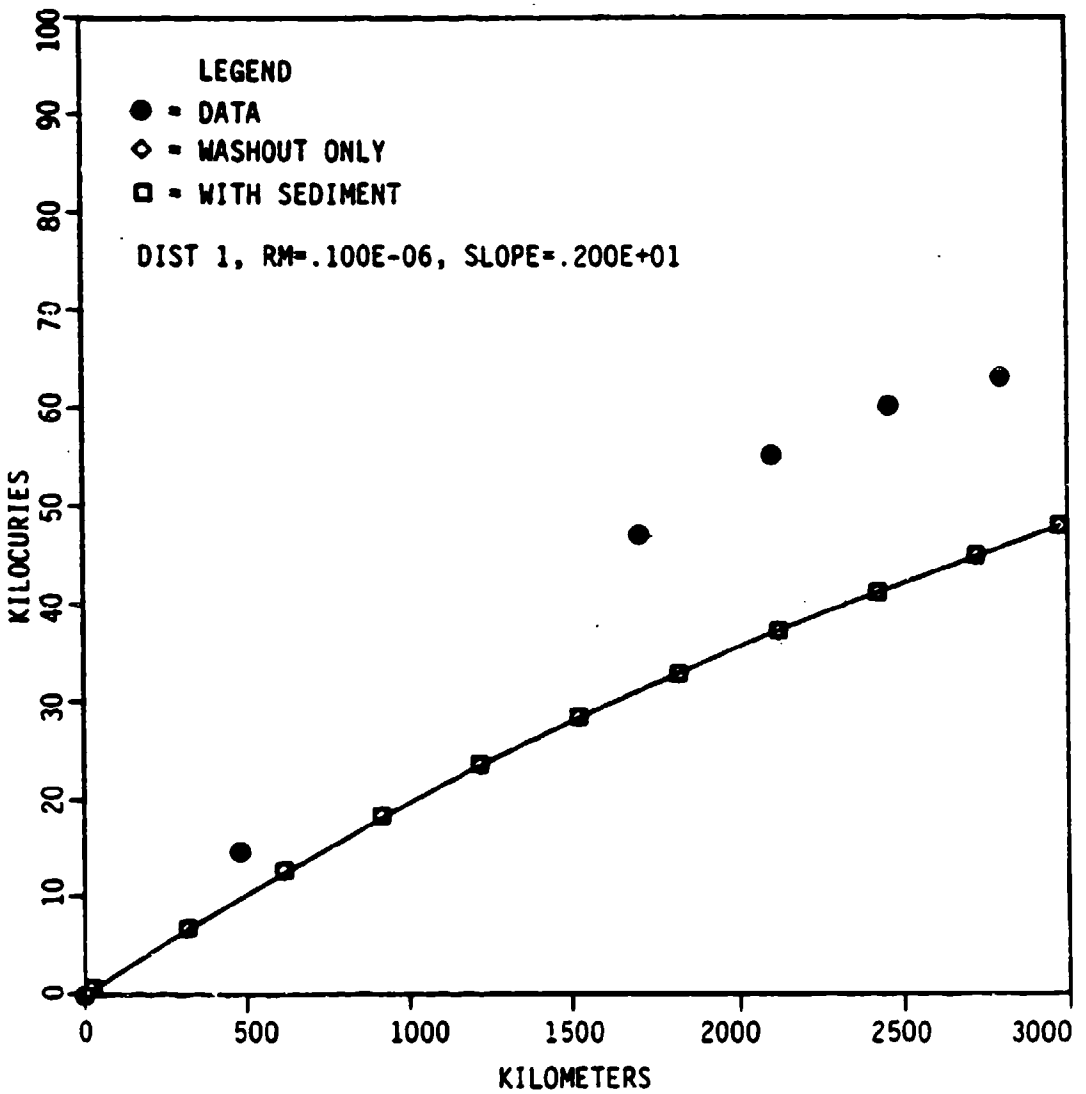

Figure 42. Activity Grounded vs. Distance, Stratospheric n(r) Parameters

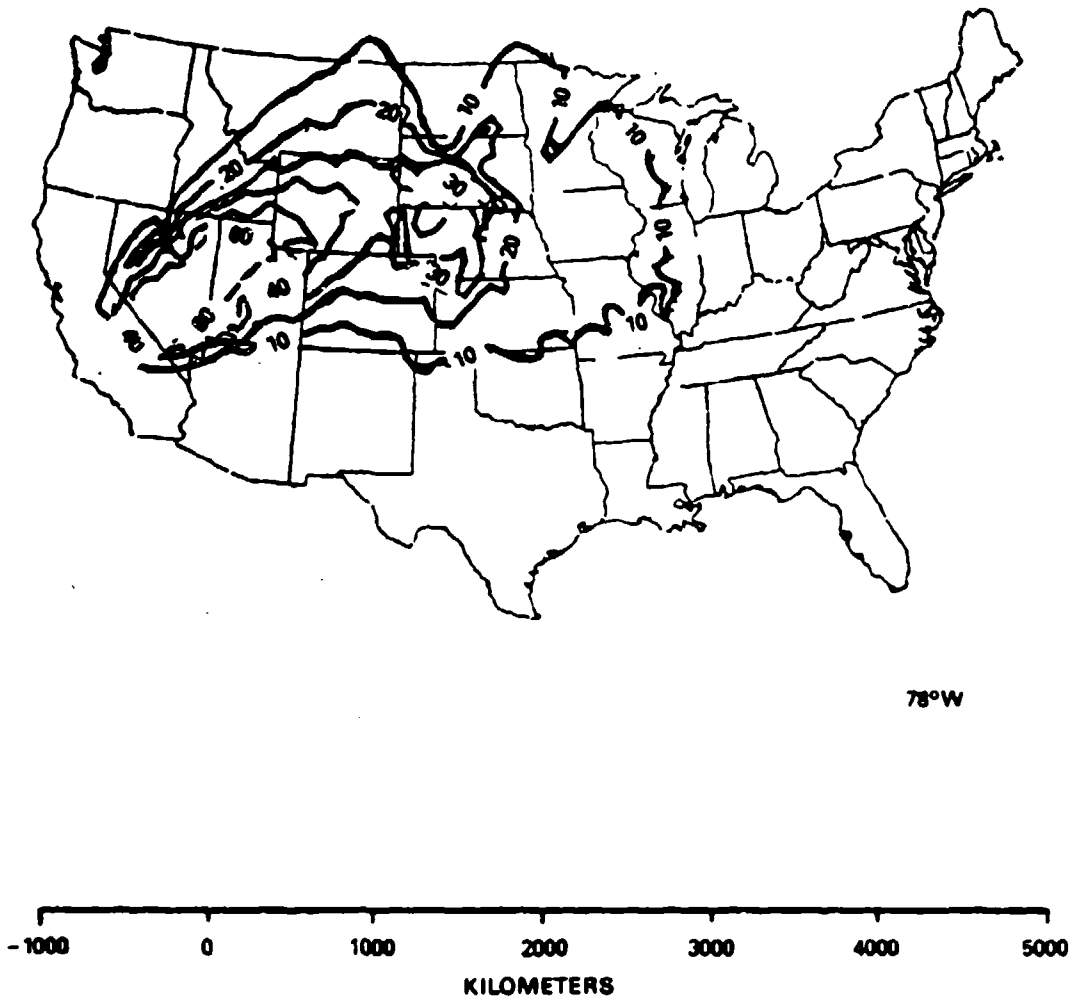

Figure 43. Composite Event Fallout Contours

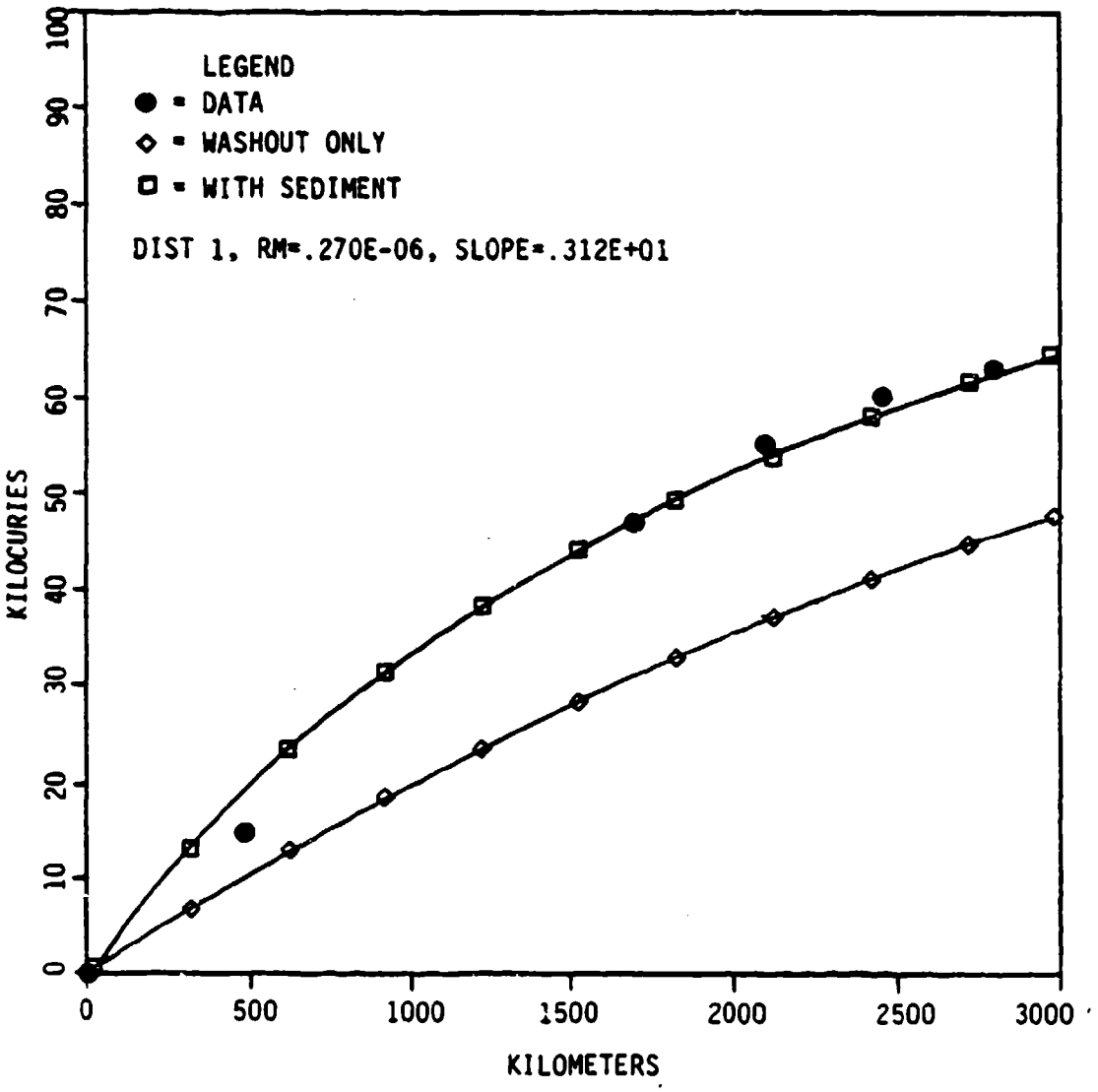

Figure 44. Activity Grounded vs. Distance, Best Fit n(r)

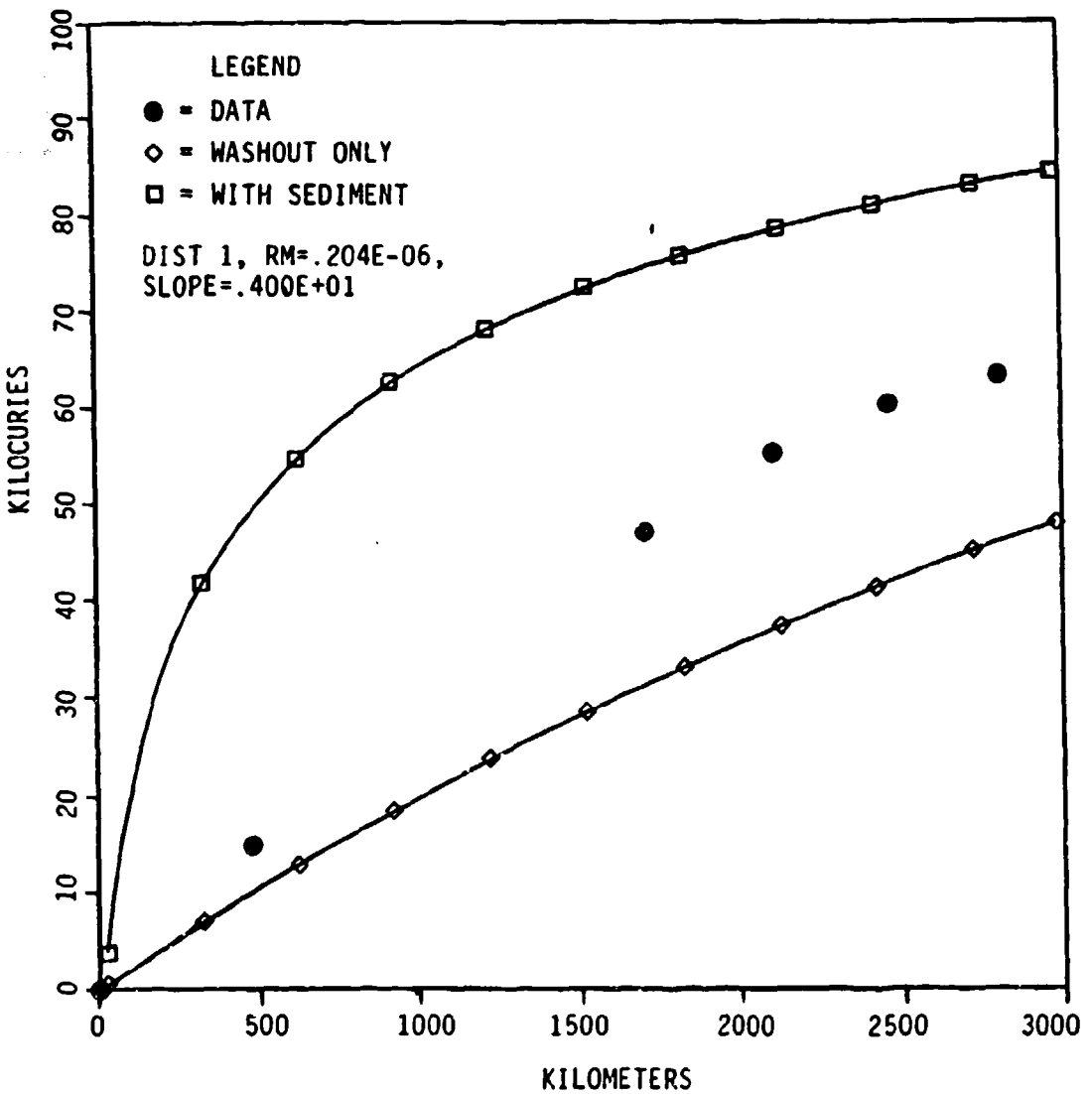

Figure 45. Activity Grounded vs. Distance, DELFIC Nominal.

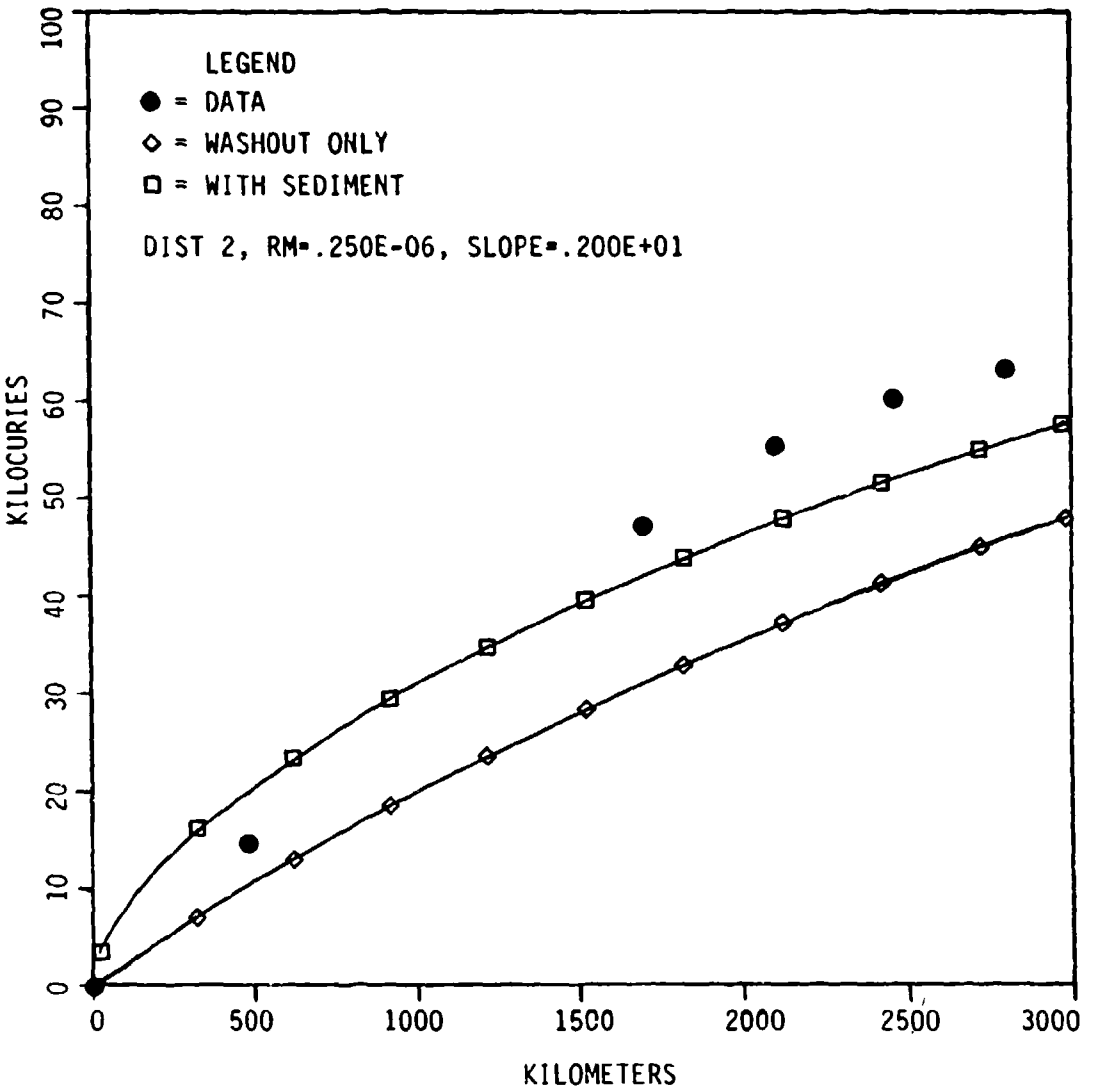

Figure 46. Activity Grounded vs. Distance, Nathans' Distribution

that the stratospheric n(r) did not represent the complete description of the actual particle size distribution for surface bursts.

C. Resolving the Global vs Local Fallout n(r) Dichotomy.

The stratospheric and intermediate fallout results were paradoxical. The stratospheric tracers resided on particles lofted predominantly by surface and near-surface bursts. Yet the stratospheric activity resided on particle distributions more representative of air bursts. The intermediate fallout model predicted no activity deposited via sedimentation when upper bound stratospheric size distributions were used thus contradicting observed local fallout particle size distributions from surface bursts (DELFIC being one example). These local size distributions are removed primarily by sedimentation as predicted by Bridgman-Bigelow (29) and others. Additional information was sought to explain coexistence of these different size distributions each of which explained one portion (global vs local) of the observed fallout but not the other.

C.1. Cloud Samples vs Ground Samples.

The differences observed between particles from cloud and ground samples provided an important clue to resolving the size distribution dichotomy. Tompkins et al have published a comparative study (49:381-400) of cloud and ground samples from four events in which they superimposed plots of specific activity (S) vs particle size for cloud and close-in fallout samples. Figures 47-50 show these superpositions for ^{141}Ce, ^{99}Mo, ^{140}Ba, and ^{45}Ca respectively. A careful examination of these plots reveals that, invariably, $S(r)$ is lower for ground samples than for cloud/distant samples by a significant margin (roughly a factor of 5 for refractory chains when averaged over radius; less pronounced for volatile chains). *Thus it appears that for the same event specific activity is bivariate,* and fundamental differences exist in the physical properties of particles deposited locally vs particles remaining in the cloud or deposited at some distant location.

The existence of these fundamental differences is further supported by Tompkins' separation of ground samples from the 5 megaton barge-mounted Tewa event (samples were from a location 17.5 km upwind and probably represent debris which fell

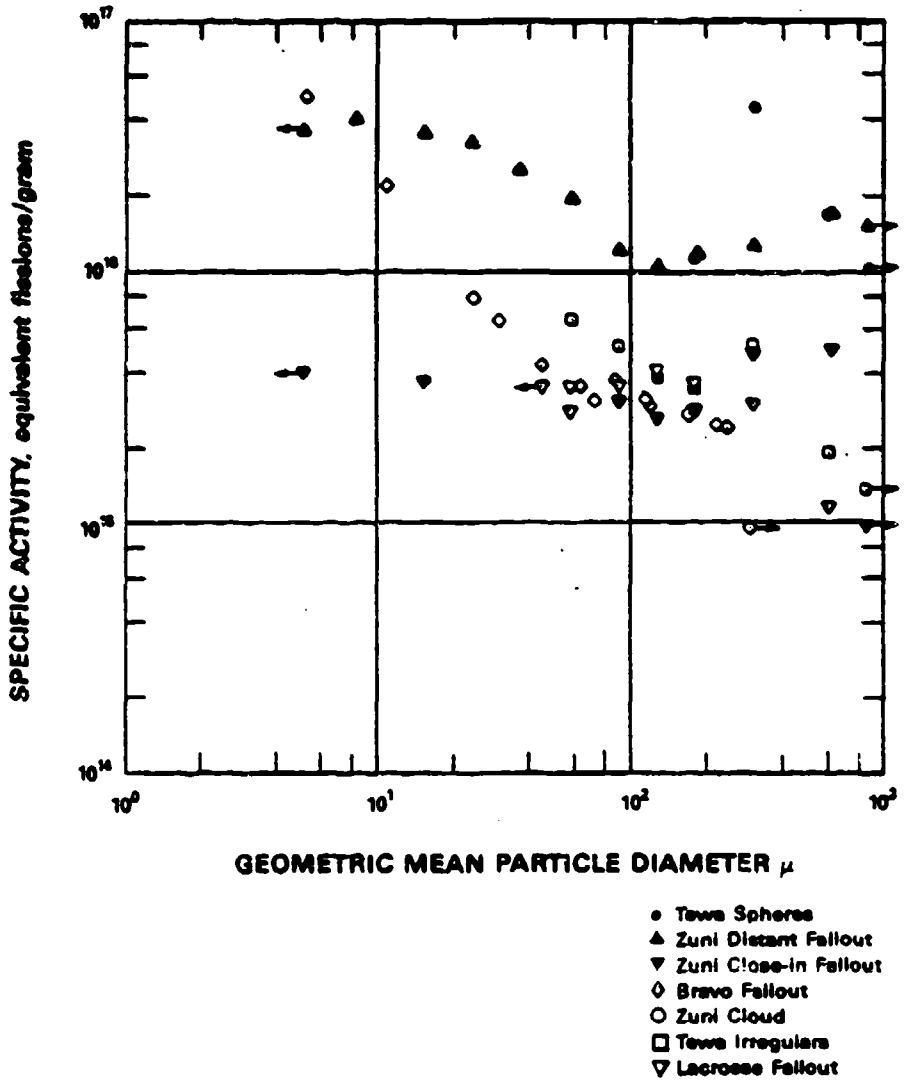

Figure 47. Specific Activity of ^{144}Ce in Fallout versus Particle Size

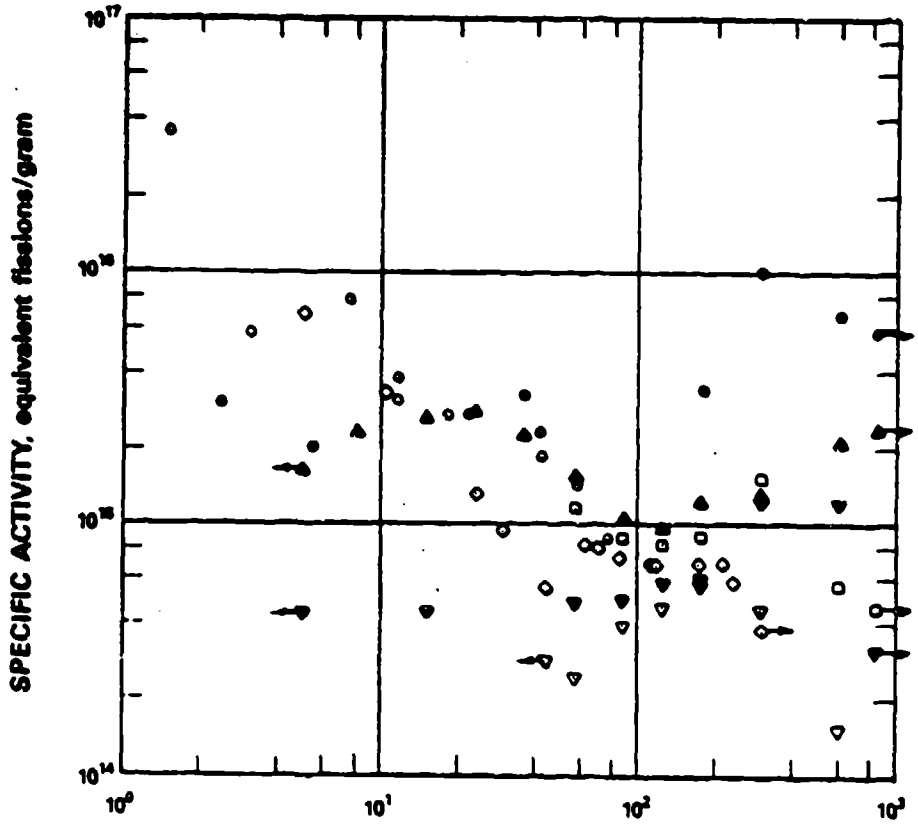

Figure 48. Specific Activity of ^{99}Mo in Fallout and ^{147}Pm in Cloud versus Particle Size

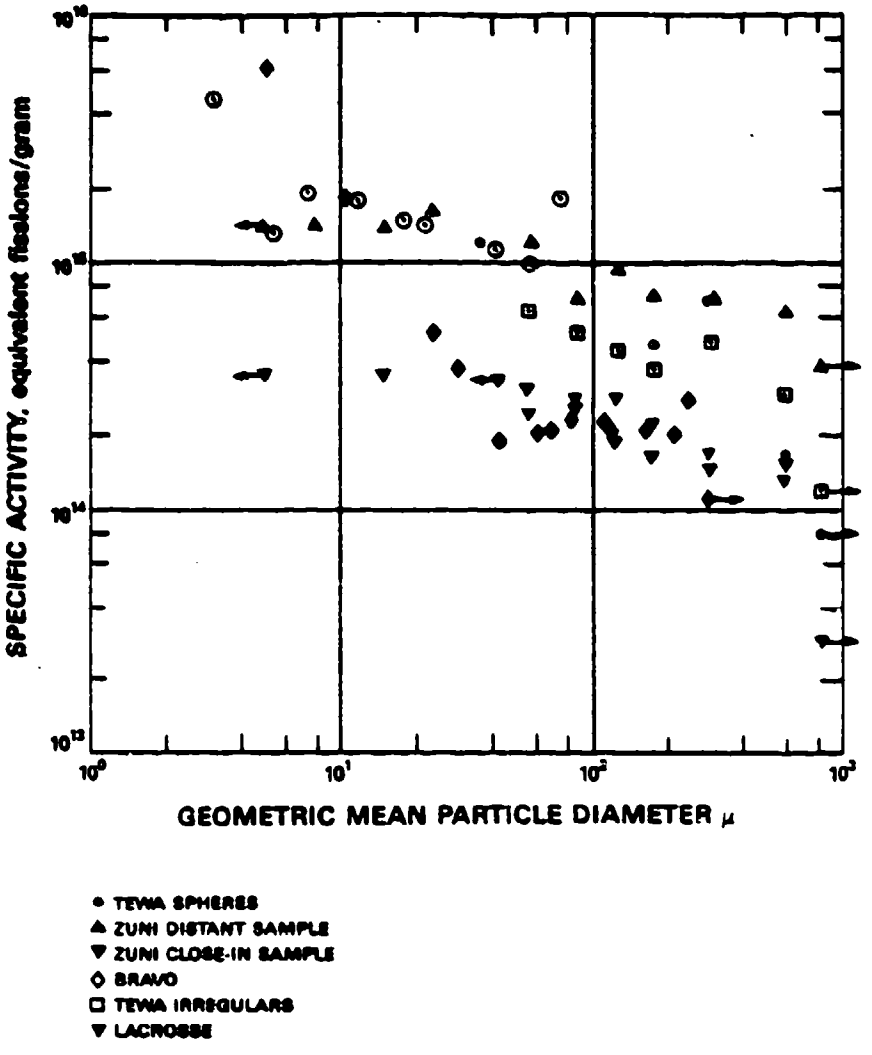

Figure 49. Specific Activity of ^{140}Ba in Fallout and ^{90}Sr in Cloud versus Particle Size

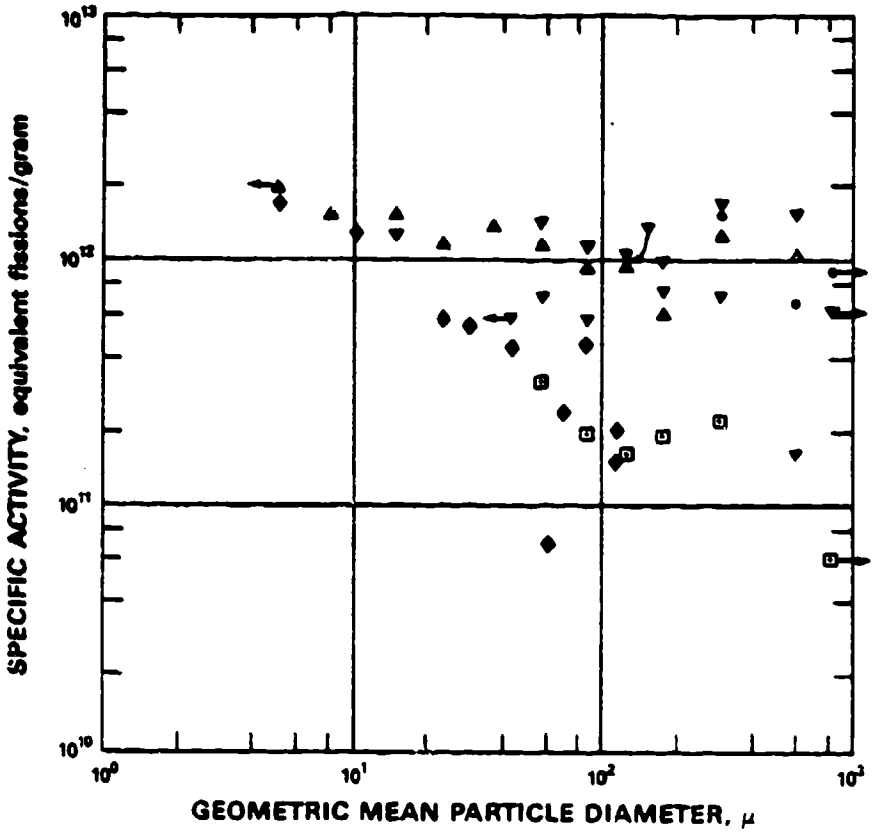

Figure 50. Specific Activity of ^{45}Ca in Fallout versus Particle Size

within 1 hour of detonation) into spherical and irregular fractions. The specific activity of these fractions are overlaid in figure 48. It is interesting that the higher specific activity of the spherical particles (over their admittedly limited size range) more closely matches that of the cloud particles while the lower specific activity of the irregular particles more closely matches that of the ground samples. Thus even though Tompkins did not separate cloud samples into spherical and irregular fractions, one might expect that cloud samples would be richer in spherical particles and close-in samples would be richer in irregular particles. Tompkins concluded that the high specific activity of the spherical particles was the result of a more intense thermal history such that refractory chains were incorporated in the spherical particles during a hot early phase which the irregular particles never experienced (49:395). Apparently the spheres originated from the condensation of material vaporized in the fireball at a time when the fission product concentration was very high. The irregular particles did not reach fireball temperatures and probably were unmelted or partially melted soil particles whose material was not homogeneously mixed with fission products, hence they exhibited a lower specific activity.

C.2. Spherical and Irregular Particles in Cloud Samples.

Nathans confirmed the existence of spherical and irregular particles in debris clouds by separating cloud samples into spherical and irregular particles on two silicate surface bursts of yield .5 KT and 10 KT (16:367;64). He found that his smaller size fractions were richer in spherical particles, and that the bulk of radioactivity was carried by the spheres (as a consequence of their higher specific activity). For the 10 KT event, he performed independent size statistics for spherical and irregular particles and found that they obeyed different lognormal distributions (figure 51). The spherical particles tended to be smaller with median radius of 0.1μ and a logarithmic slope of 2. The irregular particles tended to be larger and more disperse with median radius of $.17\mu$ and a logarithmic slope of 3. For both events he found that spheres outnumbered irregulars in cloud samples approximately 2.3:1. The larger irregular particle ensemble would sediment more rapidly than the smaller more narrow spherical particle distribution. It is interesting that the size distribution of spherical particles is typical of the size distributions Nathans measured for air bursts (17). This fact, taken together with the optimum distribution derived for stratospheric debris,

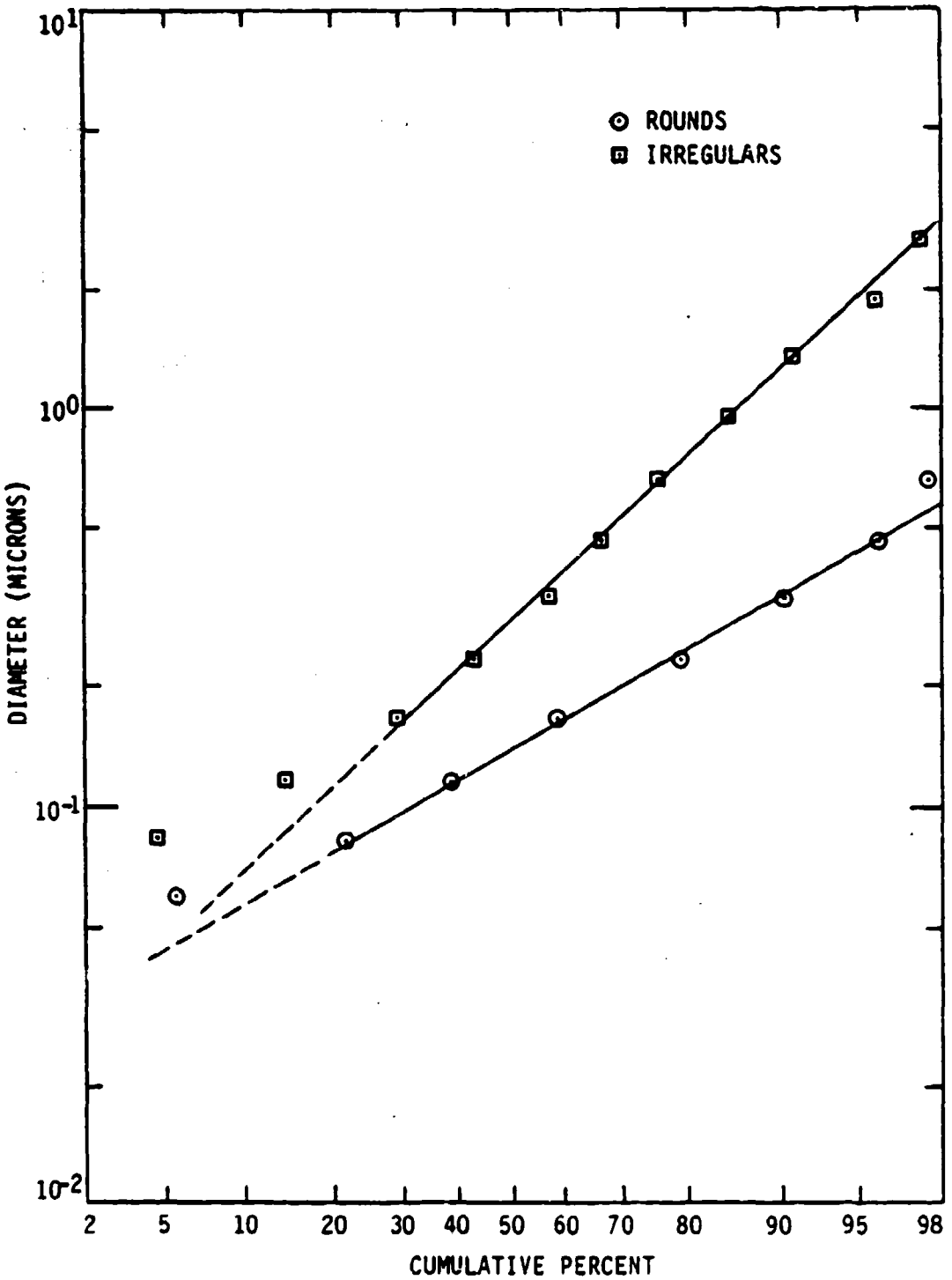

Figure 51. Round vs. Irregular Particle Distributions

implies that surface burst particle distributions contain a component which is similar if not identical to the size distribution for free air bursts (in which little or no soil is mixed with the weapon debris and all debris reaches fireball temperature).

C.3. Specific Activity Catastrophe.

From free air burst data it is apparent that debris which reaches fireball temperature tends, through hydrodynamic processes, toward a characteristic size distribution with $r_m \approx .1\mu$, $\beta \approx ln(2)$. This behavior is corroborated by the size distribution of what appears to be unmixed fission products in air burst debris. Nathans observed that below 1μ the specific activity of particles increased rapidly with decreasing radius (64) in a manner uncharacteristic of the Freiling radial behavior (in which activity increases as the 2nd or 3rd moment of the number size distribution, refs. 66, 67). An example of this behavior for Promethium is shown in figure 52. Nathans described the effect, which leads to extremely high specific activities at low radius, as a "catastrophe" which he was unable to explain. For the several airbursts which he studied, the specific activity for submicron particles was observed to vary between $r^{-2.5}$ and $r^{-3.5}$ for refractory chains.

The effect was of concern for the present research because the fraction of total activity carried by submicron particles could be dramatically affected by the catastrophe. The effect can be explained if at the time of detonation a totally random fission product dispersion occurs such that nuclide concentrations on individual particles are roughly independent of radius. Particle specific activity would then be scattered about r^{-3}, as observed. In one study (64) Nathans overlaid ^{95}Zr specific activity data for a range of yields. A linear fit to his points in log space reveals that the submicron specific activity obeys the following relation roughly independent of yield:

$$S(r) \approx \frac{16 \times 10^{17}}{r^{2.5}} \frac{fissions}{gram} \qquad (r \text{ in microns}) \tag{59}$$

It is hypothesized that the submicron particles are pure fission products, and that they therefore obey the characteristic size distribution for high temperature debris. If the fission product dispersion is totally random, it is useful to compute an average activity per gram. This average, if indeed the particles are composed of pure

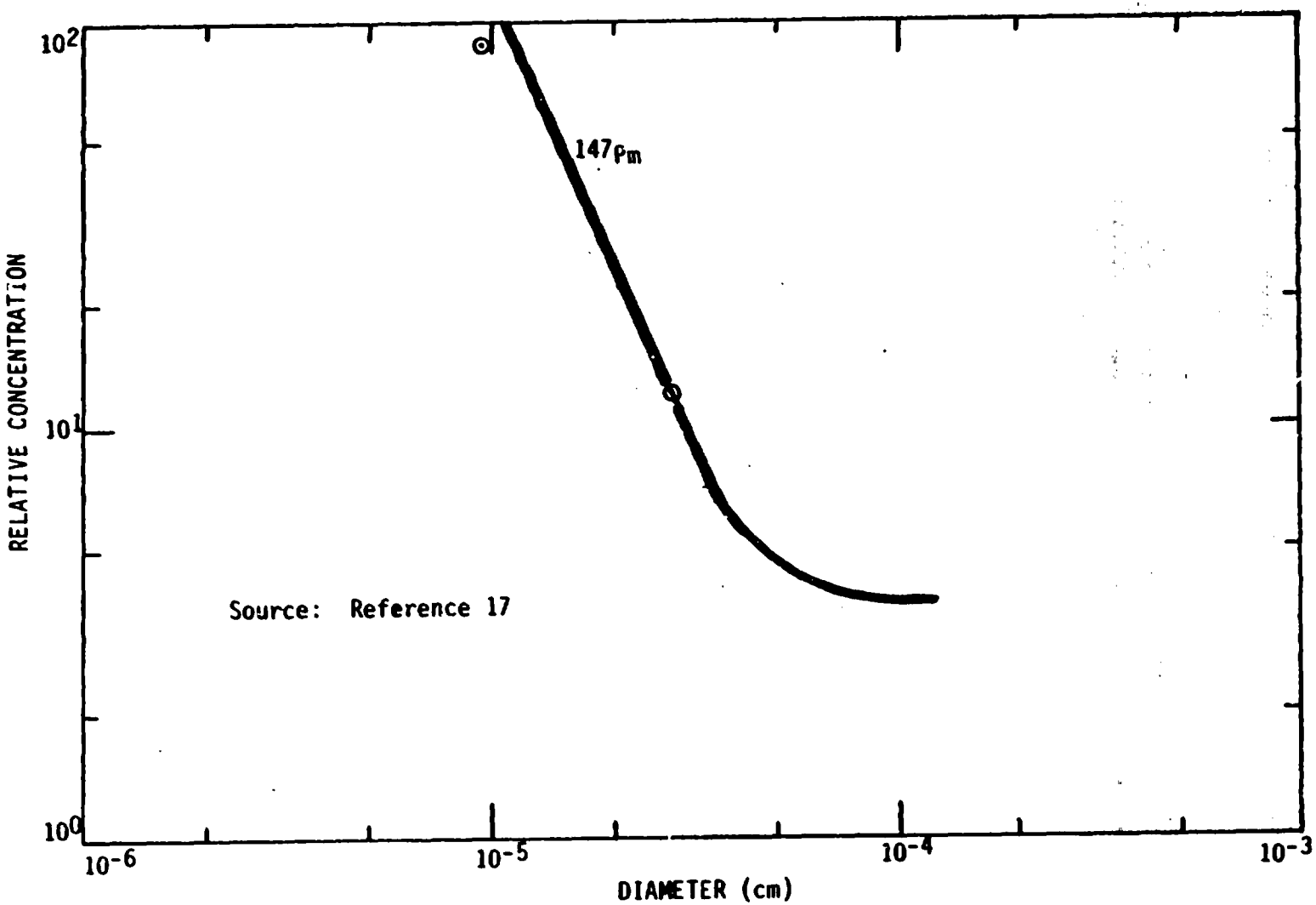

Figure 52. Specific Activity Catastrophe Example

fissioned material, should equal the total activity available (1.4×10^{26} fissions/megaton) divided by the mass of totally fissioned bomb material (5.7×10^{4} g/megaton). Using the number size distribution characteristic of stratospheric surface burst debris and air burst debris, the average specific activity is in fact within 10% of this quotient, i.e.:

$$<S(r)> = \int_{o}^{\infty} S(r)\hat{n}(r)dr \approx \frac{1.4 \times 10^{26}}{5.7 \times 10^{4}} \frac{fissions}{gram} \tag{60}$$

where,

$$\hat{n}(r) = \frac{1}{\sqrt{2\pi}(ln\ 2)r} \exp\left[-\tfrac{1}{2}\left(\frac{\ln(.1) - \ln(r)}{\ln 2}\right)^2\right] \tag{61}$$

The equality expressed by equation 60 lends further credence to the parameter values believed to govern the high temperature debris size distribution.

D. Proposed Cloud Distribution.

The evidence discussed in section V.A, V.B, and V.C supports the existence of a bimodal cloud particle distribution for surface bursts:

$$n(r) = n_1(r) + n_2(r) \tag{62}$$

where n_1 represents high activity spherical particles formed from the condensation of vaporized bomb and surface materials. The second mode, n_2, represents irregularly shaped particles of unmelted or partially melted (low temperature history) surface material with a lower activity concentration in general.

Such a distribution explains the apparent differences in size distributions governing the behavior of fallout at early and late times. In the stratosphere at late times, an n_1 type distribution governs tracer removal as demonstrated by the ^{90}Sr and ^{185}W optimization results of section V.A. The early cloud (within several hours of detonation) particles represent both n_1 and n_2 behavior as indicated by Nathans' analysis of surface burst clouds (16,64). As should be expected, close-in ground sample particles are more characteristic of n_2 as noted by Tompkins (predominantly irregular in shape, ref. 49:396) and Norment (DELFIC distribution more closely approximates n_2, ref. 8). Air bursts with little or no surface material present such that all debris reaches fireball temperatures produce an n_1 type distribution almost

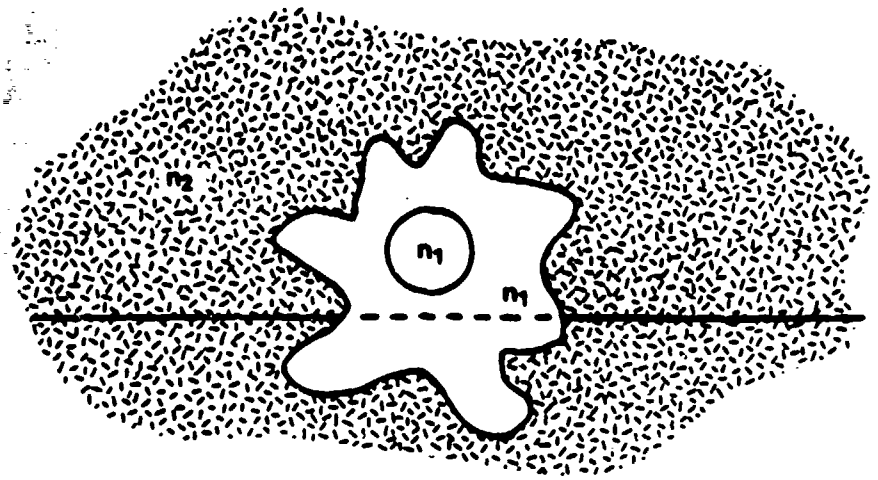

$$n(r) = n_1(r) + n_2(r)$$

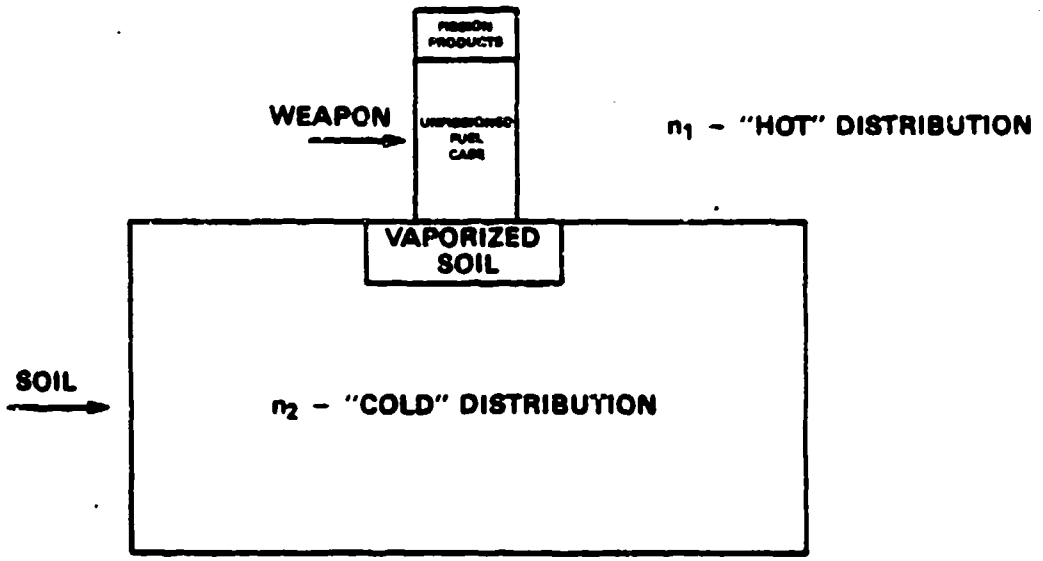

Figure 53. Debris Composition, Conceptual Picture

without exception (exceptions include some tower shots, and lower air bursts with some limited surface material contamination). A heuristic illustration of the origin of the n_1 and n_2 distributions appears in figure 53.

The n_1 parameters are well established by the independent results previously discussed-- namely, a lognormal distribution with r_m of .1 μ and slope of 2 describes the behavior of stratospheric tracers, air burst debris, and unmixed fission products. The establishment and corroboration of n_2 parameters was not as straightforward.

E. Characterization of n_2.

The most direct evidence available for an actual n_2 size distribution is Nathans' analysis of cloud samples from the 10 KT silicate surface burst discussed in section V.C.2. Nathans divided his samples into spherical and irregular particle fractions and characterized their size distributions separately. The results for one sample are shown in figure 51. His n_2 distribution is lognormal with a median radius of .17 μ and a slope of 2. Unfortunately, this is the only instance in which he intentionally characterized spherical and irregular particle size distributions separately (68).

Nathans did characterize what is purported to be the undifferentiated size distributions of clouds from four surface bursts (Johnie Boy, Koon, Zuni, and Bravo, ref. 16). However, a careful reading of his documentation reveals that (for undisclosed reasons) he included only irregular particles in his size analysis (16:367). Thus, the particle size statistics for these events were used to get additional information on n_2.

A puzzling aspect of Nathans' particle statistics for the four surface bursts was the power law behavior (not lognormal) of the size distributions above 1μ diameter (see figures 4-6). This behavior can be explained by noting the position of the aircraft with respect to the cloud at the time of sampling. Apparently the sampling aircraft could not get up to the cloud altitude. In all but two of Nathans' samples for the four events, samples were extracted at altitudes below the visible cloud (see table V). Only Johnie Boy samples 827L and 842L, although lower than the cloud vertical centroid, were within the visible cloud. It was apparent that the low sampling altitudes affected the size distribution of the samples vis-a-vis the aggregate cloud.

Nathans did correct for sedimentation in plotting his size distributions (16:379). However, his correction factor did not account for a variable vertical cloud

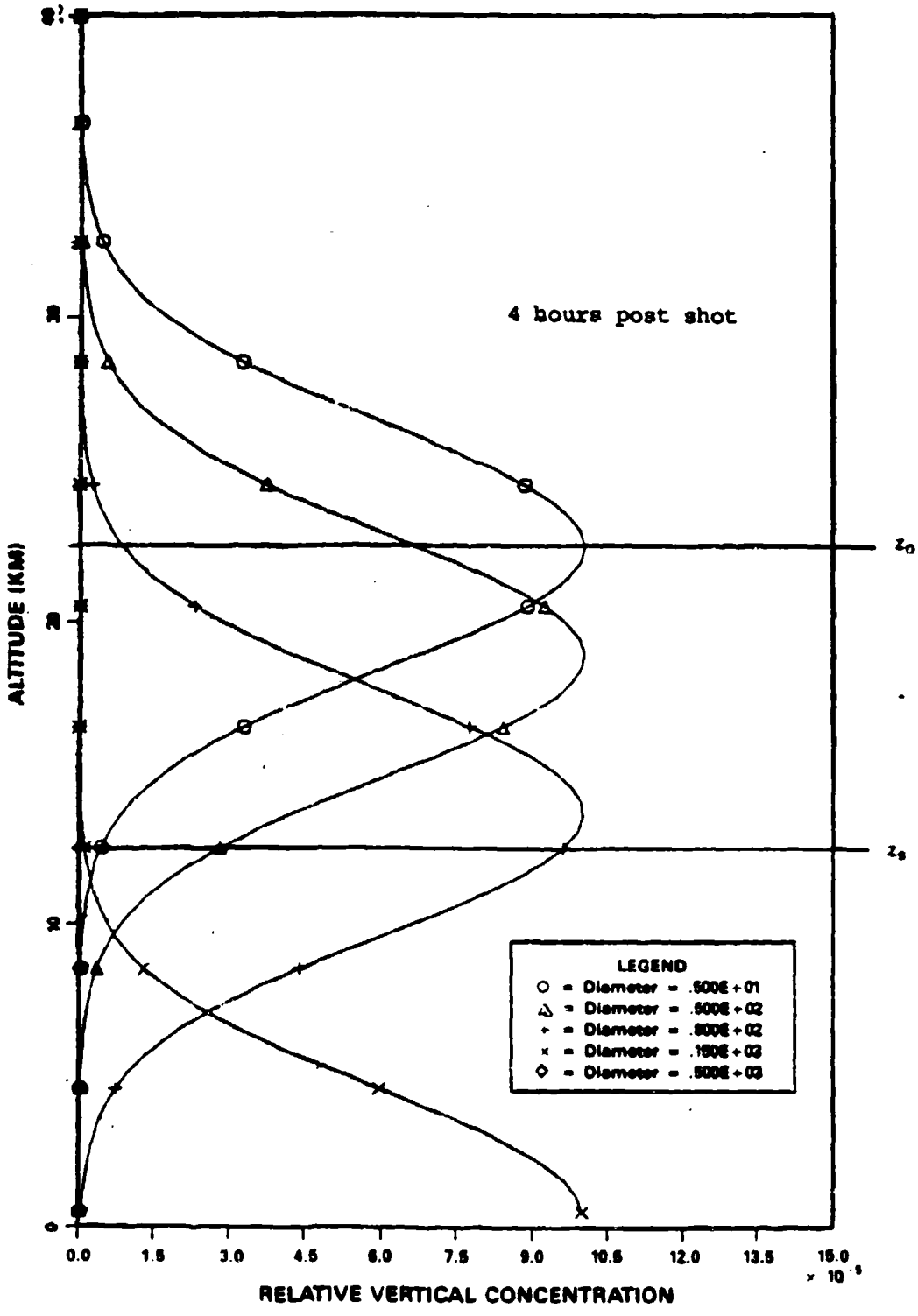

Figure 54. Group Fall Illustration

Table V

Nathans' Samples: Bravo, Zuni, Koon, Johnie Boy

Event/sample	Yield	Soil	Cloud Top[a]	Cloud Bottom	Sample Time	Sample Altitude
Bravo (1954)	15 MT	coral	34km	16.6km	4hrs	15.5km
Zuni (1956)	3.4 MT	coral	24.5km	15km	3.1hrs	12.7km
Koon (1954)	150 KT	coral	16.5km	--[b]		
/1086					3.1hrs	11.95km
/051					3.1hrs	11.95km
/7269					3.1hrs	11.95km
Johnie Boy (1962)	.5KT	silicate	5.18km	3.81km		
/842R					.6hrs	2.95km
/842L					.4hrs	3.4km
/245L					.8hrs	3.7km
/827L					.35hrs	4.35km

[a] In fallout calculations, the cloud centroid was taken as the mean of top and bottom altitudes. The stabilized cloud was modeled as Gaussian in the vertical dimension with $\sigma_z = 1/4(CT - CB)$

[b] A strong wind shear at about 11km directed the bottom portion of the cloud away from the remainder of the cloud.

concentration profile and consequently was not very large (less than a factor of 2 in all cases). Thus, his corrected distributions are very nearly equal to what was actually measured. Nathans' correction factor does account for the vertical velocity gradient which does not produce as large an effect as the vertical concentration gradient (Section A.3.c).

Nathans used aircraft samples taken between .4 - 4 hours after detonation. Figure 54 illustrates size group stratification predicted (assuming Gaussian dispersion and using subroutine STRATFAL) at 4 hours following the Bravo event. The graph is plotted with n(r) as constant so that only variations due to the vertical concentration gradient are depicted. Note that at any sampling altitude, z_s (a 12 KM sampling altitude is marked), the sample n(r) is greatly affected by the vertical stratification. At time t=0, assuming that all size groups are distributed uniformly in the z direction, a distribution, $n_o(r_j, t=0, z_s)$, proportional to the true cloud distribution would be measured at any altitude. If a sample is taken at a later time, a distribution of $n_s(r_j, t_s, z_s)$ is measured. It is then possible to relate n_o to n_s by using the correction factor, C_j:

$$n_o(r_j, 0, z_s) = \frac{n_s(r_j, t_s, z_s)}{C_j} \tag{63}$$

C_j is defined as

$$C_j = \frac{f(z_j - z_s)}{f(z_o - z_s)} \tag{64}$$

where f is the vertical distribution function. In this case, analogous to equation 30,

$$f(z - z_s) = \left[e^{-\frac{1}{2}\frac{\sigma_t^2}{z_{scale}}}\right]\left[\frac{e^{-\frac{1}{2}\left[\frac{z-z_s}{\sigma_z}\right]^2}}{\sqrt{2\pi}\,\sigma_z}\right]\left[e^{-\frac{z-z_s}{z_{scale}}}\right] \tag{65}$$

C_j for Bravo is plotted in figure 55 (DELFIC fall mechanics were used). Note that the correction factor peaks at that particle diameter which has just reached aircraft altitude at sampling time. The apparent population at this diameter would be enhanced in the sample. The sample would be depleted in larger particles since they would have fallen past the sampling altitude. The smallest particles would be present in their true proportions ($C_j = 1$).

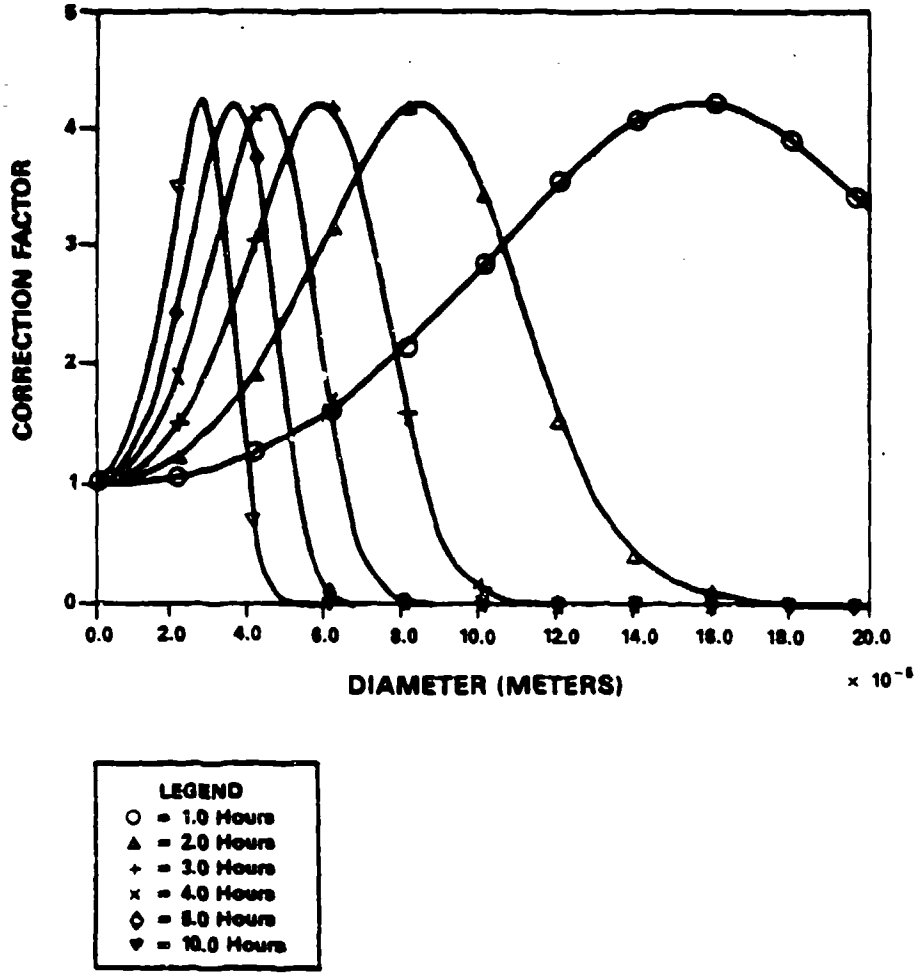

Figure 55. Size Distribution Correction Factor

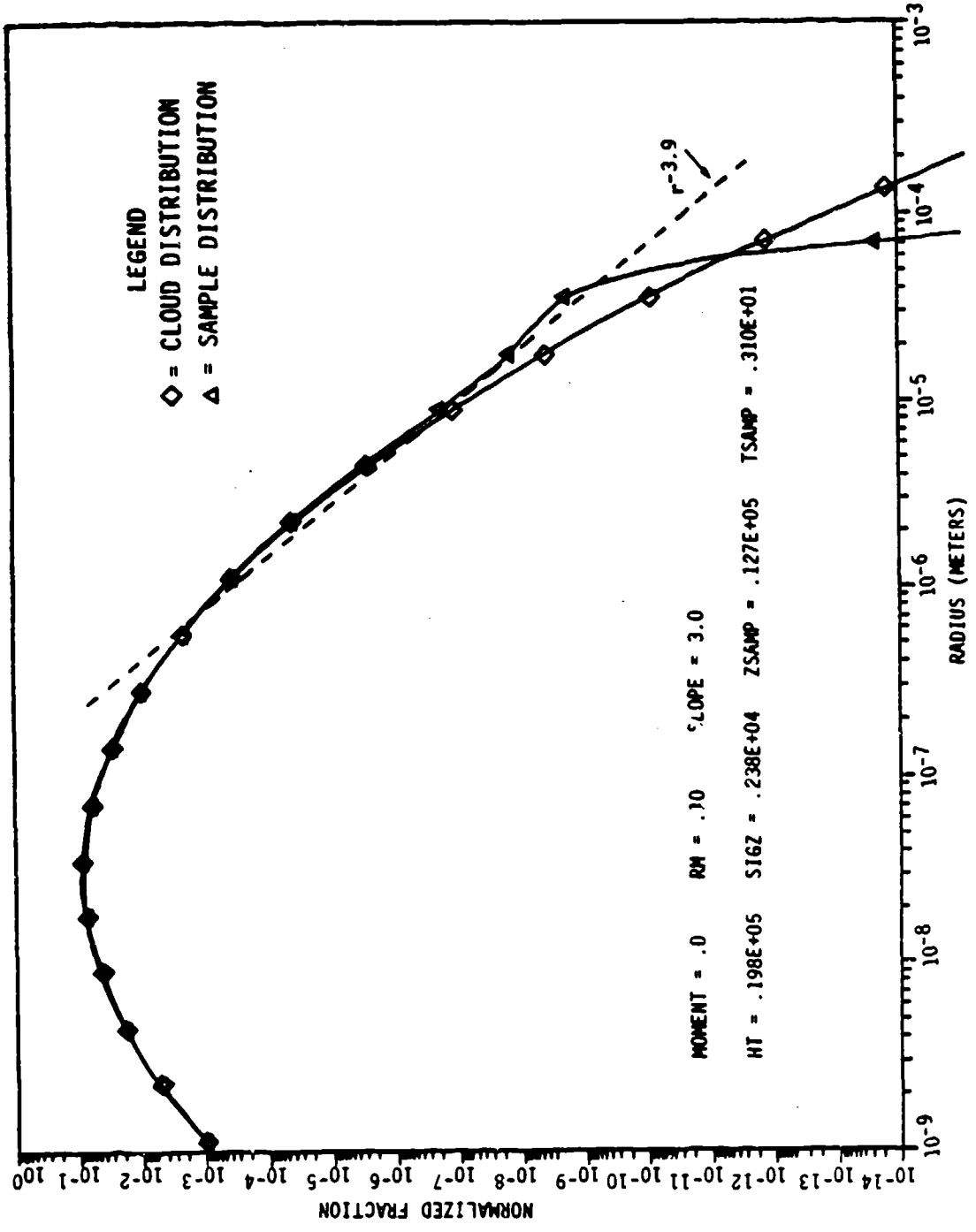

Figure 56. Zuni Cloud vs. Sample Distribution

It is suspected that this correction factor boosted the population in Nathans' samples in the 10-100μ range and that this effect causes a lognormal distribution to approximate a power law. This possibility was investigated by using Nathans' lognormal characterization of irregular particles for the 10 KT silicate surface burst as the aggregate cloud n_2 distribution for the four events. For the 10 KT event, Nathans realized that sedimentation had affected the population of particles larger than 10μ in his samples and therefore confined his analysis to particles of diameter 2μ and smaller (see figure 52). Gravity sorting would not have significantly affected the relative population of these small particles at sampling time (figure 10). Thus the 10 KT particle statistics were a reasonable standard of comparison. It was suspected that the lognormal parameters developed for $\leq 2\mu$ particles would also describe the larger particle population.

Starting with a lognormal aggregate cloud distribution, the correction factor was applied to determine the sample population at the time and altitude of extraction. The calculation for Zuni sample 049 is illustrated in figure 56. Application of the correction factor to the lognormal distribution yields a curve that does in fact approximate a power law function. Indeed, a straight line fit to the curve falls as $r^{-3.9}$ (Nathans' fit yielded an exponent of -4.07). Similar results are obtained for the other samples. In each case, the correction factor applied to a lognormal distribution with $r_m = .17\ \mu$ and $\beta = \ln(3)$ masquerades as a power law function. In order to determine the best slope, r_m was held constant and β was varied until the slope of the corrected lognormal distribution matched Nathans' power law exponent. In each case a logarithmic slope of ¯3 provided the best fit (see figures 57-59). Varying r_m between .1$\rightarrow$.5μ did not significantly affect the optimum β.

The correction factor as expressed in equation 64 did not explain the depletion of submicron particles in Nathans' samples (figures 4-6). A more elaborate correction, taking into account variations in f(z) with size group is probably needed. Since Nathans did not find spherical particles in samples taken underneath the visible cloud, there is reason to believe that smaller particles were more tightly clustered at the cloud center (smaller σ_z) such that their presence at sampling altitude would have been considerably diminished (65:3). Such clustering could be caused by the centrifugal action of the toroidal cloud motion which should preferentially disperse the

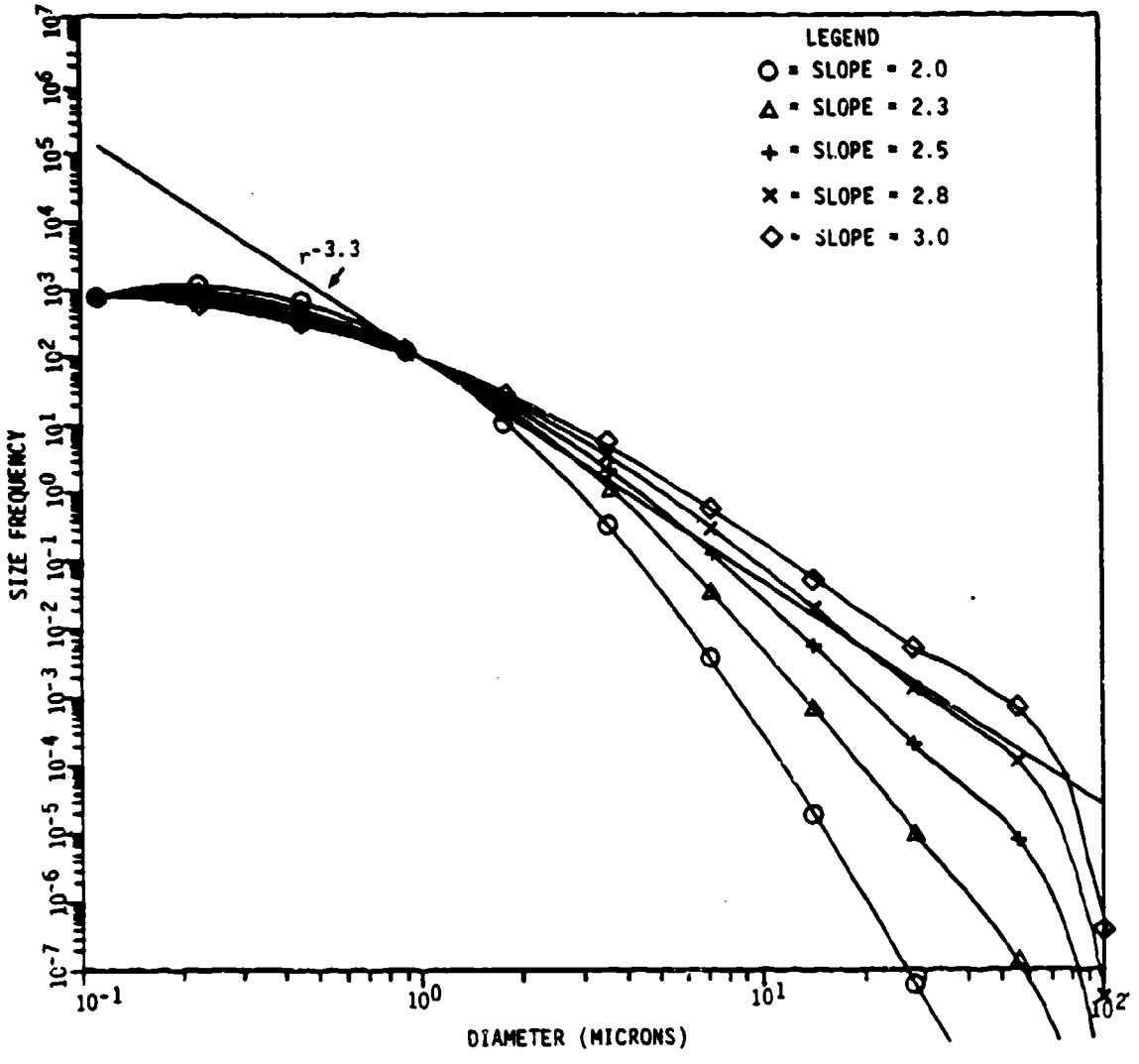

Figure 57. Lognormal vs. Power Law Fit, Johnie Boy Sample 245L

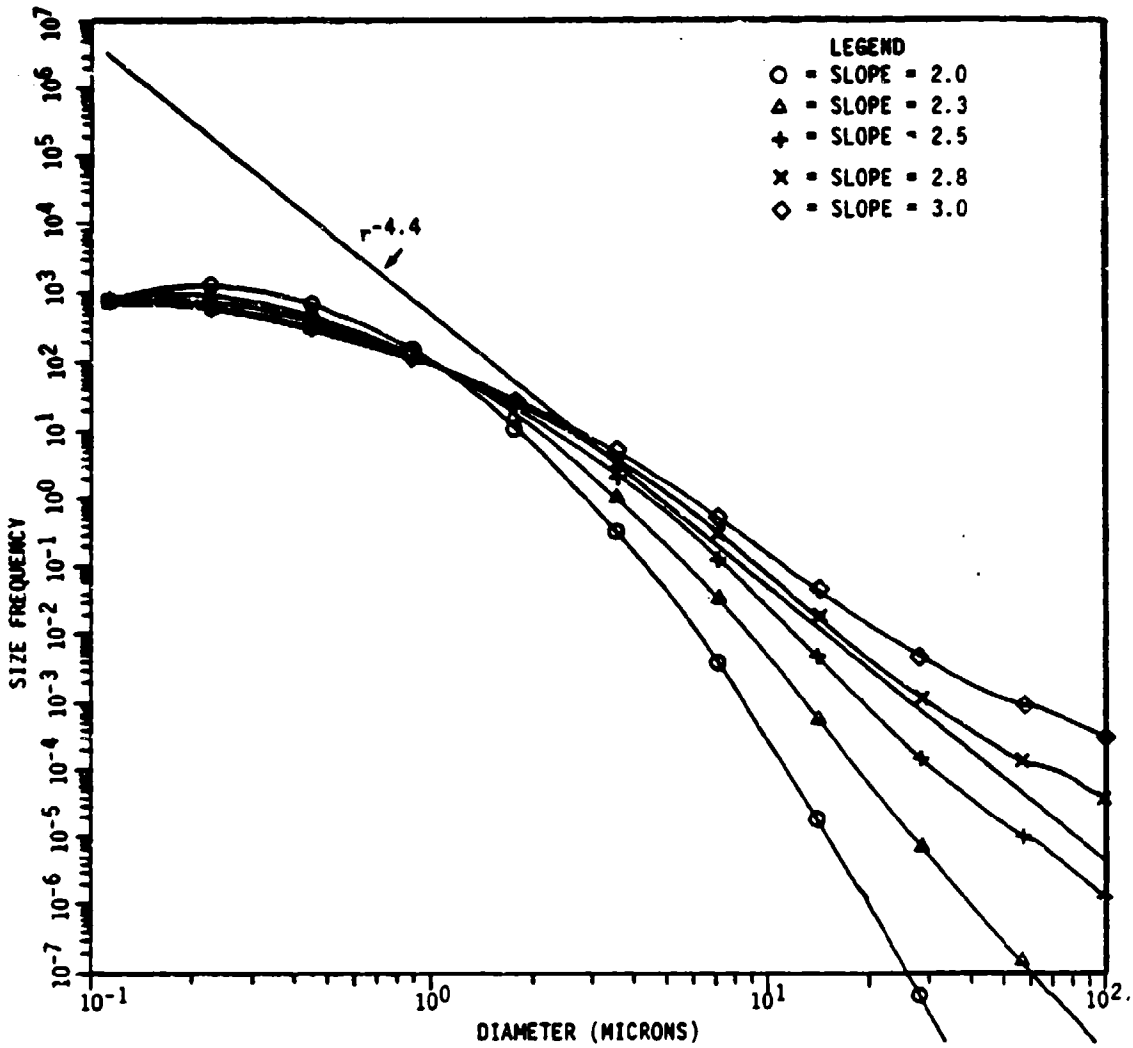

Figure 58. Lognormal vs. Power Law Fit, Johnie Boy Sample 842L

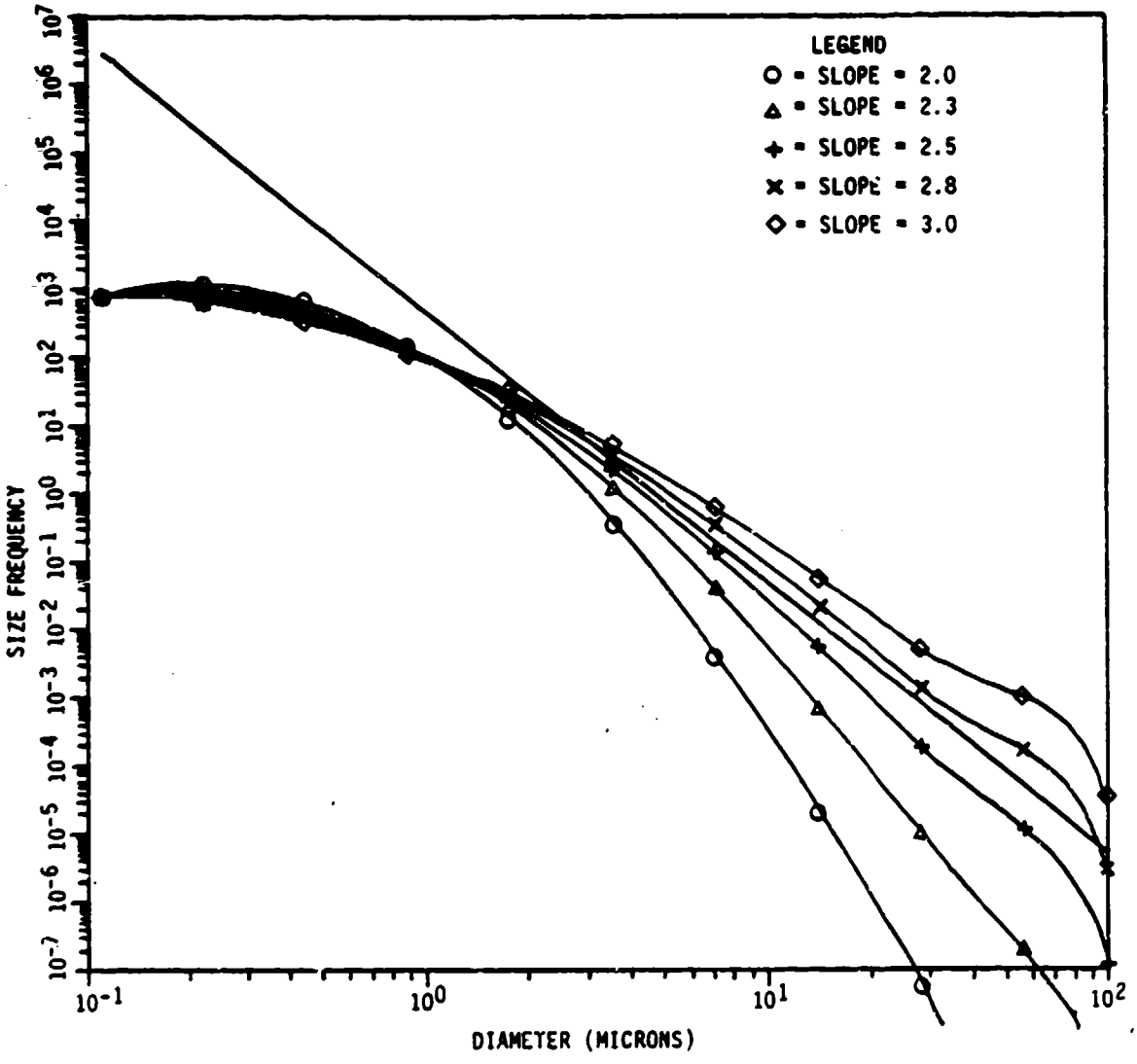

Figure 59. Lognormal vs. Power Law Fit, Bravo Sample

heavier particles. This phenomenon would explain the absence of spherical particles in Bravo, Koon, and Zuni samples (all significantly below the cloud centroid) and the presence of spherical particles in Johnie Boy samples (taken near the could centroid). Another possible explanation for small particle depletion is agglomeration due to differences in group fall velocity. The relatively motionless small particles might have been depleted by sticking to larger particles falling through their midst.

Admittedly there are many remaining questions concerning the n_2 distribution. Only one instance (10 KT silicate burst) was found in which n_2 was intentionally analyzed as a separate, independent entity. It appears that only n_2 type particles were analyzed for Johnie Boy, Bravo, Zuni and Koon. It is puzzling that few if any spherical particles were present in the Bravo, Zuni, and Koon samples. A possible explanation has been offered but there may be others. For instance, Pacific events may not have produced significant numbers of spherical particles (although some were observed on the ground near Tewa). Even though present results indicate a fairly consistent n_2 parameter values among events, significant excursions are expected since these particles originate from surface materials which differ considerably in morphology and thermal history (n_1 originates from fireball vapors whose initial temperature is nearly independent of surface material and yield). Indeed there is evidence that for buried bursts n_2 is multimodal (69). And Norment's nominal DELFIC distribution implies that larger logarithmic slopes exist.

Nathans' 10 KT silicate surface burst results provide the most solid evidence for the existence of an independent n_2 distribution. The 10 KT results are consistent with Nathans' distributions for Johnie Boy, Bravo, Zuni, and Koon if a Gaussian cloud stratification correction factor is applied. Assuming these n_2 parameters to be representative of clouds, an important remaining question is what are the relative populations of n_1 and n_2? The relative number (or mass) of particles in each distribution determines the optical properties and longevity of nuclear clouds.

F. The $n_1 - n_2$ Split.

The measured n_1/n_2 ratio for cloud samples from the two silicate surface bursts discussed in section V.E were nearly identical. The ratio was 2.3 for Johnie Boy and 2.2 for the 10 KT silicate surface burst. These ratios would not have been

significantly affected by sedimentation since nearly 100% of the population lies below 5μ for both n_1 and n_2. The mass ratio may then determined from:

$$\frac{M_1}{M_2} = \frac{\frac{4}{3}\pi\rho_1 \int_o^\infty N_1 \hat{n}_1(r) r^3 dr}{\frac{4}{3}\pi\rho_2 \int_o^\infty N_2 \hat{n}_2(r) r^3 dr} = \frac{N_1}{N_2} \frac{<r_1^3>}{<r_2^3>} \tag{66}$$

assuming particle densities (ρ_1, ρ_2) are roughly the same between the modes. Using a lognormal n_1 with r_m of .1 μ and slope of 2, and a lognormal n_2 with r_m of .17 μ and slope of 3, and $N_1/N_2 = 2.2$, the result is:

$$\frac{M_1}{M_2} = 1.7 \times 10^{-2} \tag{67}$$

Thus, even though n_1 has a higher population, it represents only 1.7% of the mass lofted. The mass ratio expressed in equation 67 can be used to compute the combined fraction of mass below 1μ, f_m, which equals 5.8%. This result is close to the TTAPS value of 8.4%.

Since the mass of soil lofted decreases with height of burst (13:3-7), M_1/M_2 should increase accordingly. An indication of increase with HOB may be obtained by estimating the fraction of activity carried by n_1 *vs* n_2. Local fallout data can be used to get an indication of the activity split. Davis (54) has attempted to derive size distributions from local activity deposited vs time. Unable to model air burst deposition using a unimodal lognormal distribution, he found that a bimodal distribution could explain the data. He fit the observed rate of local activity deposition for actual events of varying scaled height of burst using the following expression:

$$A(t) = A_o \left[F_1 \int_{r(t)}^\infty a_1(r) dr + F_2 \int_{r(t)}^\infty a_2(r) dr \right] \tag{68}$$

where A_o is the total activity lofted, r(t) is the radius of particles grounded at time t, F_2 is the fraction of activity carried by n_2, and $F_1 = 1 - F_2$. By fixing n_1 (lognormal with $r_m = .1\mu$ and slope=2) and assigning n_2 an r_m of .2 μ Davis obtained the results in Table VI (plotted in figure 60). The results indicate that 10 - 100% of the activity is carried by n_2 for a $\leq$3 foot scaled height of burst (SHOB=HOB*$KT^{-1/3}$)

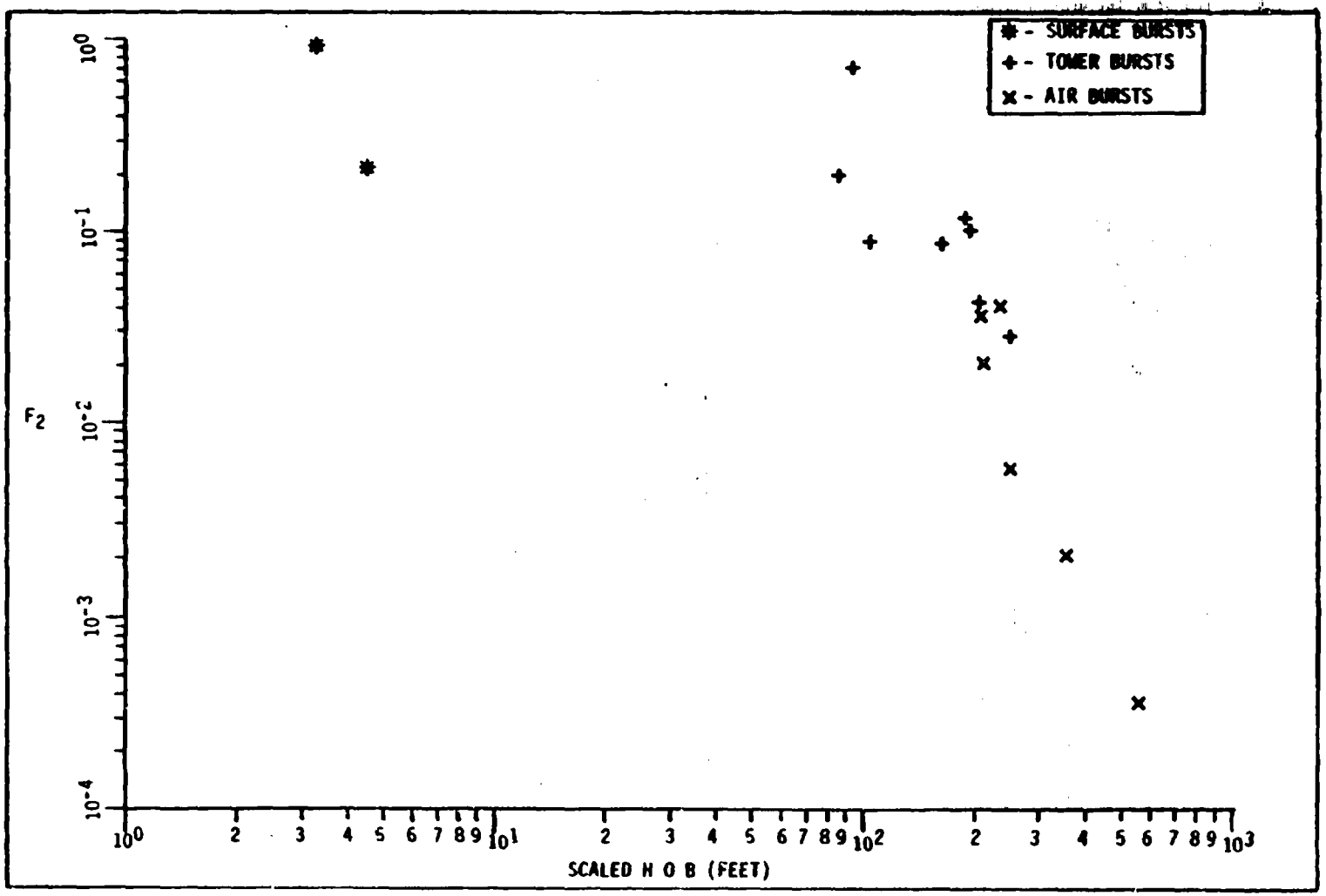

Figure 60. Fraction of Activity on n_2 vs. Scaled Height of Burst

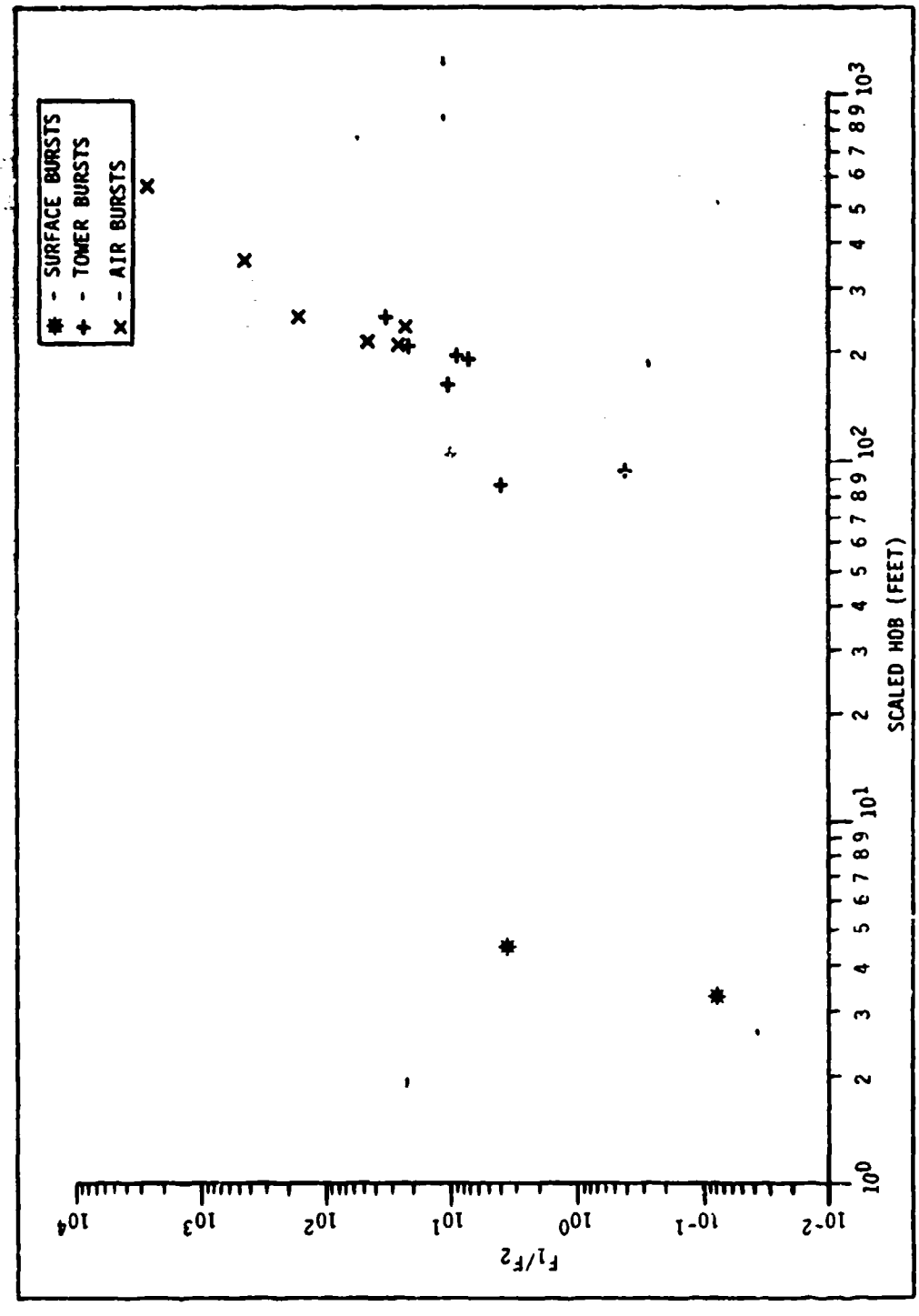

Figure 61. F_1/F_2 vs. Scaled Height of Burst

but that the fraction drops rapidly above 100 scaled feet. If the activity is distributed as the mass of particles, then $S_1(r)$ and $S_2(r)$ are constant and the mass ratio is proportional to the activity ratio:

$$\frac{F_1}{F_2} = \frac{\frac{4}{3}\pi\rho_1 \int_0^\infty n_1(r) r^3 S_1(r) dr}{\frac{4}{3}\pi\rho_2 \int_0^\infty n_2(r) r^3 S_2(r) dr} \approx \frac{<S_1>}{<S_2>} \frac{M_1}{M_2} \tag{69}$$

Davis' F_1/F_2 vs scaled height of burst is plotted in figure 61. These results will of course change with assumed particle size parameters and should be used with caution. However, the indicated trends are correct. It is interesting that the functional form of F_2 vs SHOB (figure 60) is reminiscent of Carpenter's fit to the total mass lofted vs SHOB (ref. 70, figure 62). This is logical since, for higher bursts, less surface mass is available to mix with fission products, hence F_2 should decrease roughly proportional to mass lofted. It is interesting that Davis' cliff in mass lofted occurs at ~200 scaled feet, noticeably lower than the ~700 ft. cliff exhibited by Carpenter's fit.

Notice that if the activity is radially distributed on particles it is not necessary to know specific activities, but rather mass ratios can be determined from number ratios via simple scaling relations:

$$\frac{M_1}{M_2} = \frac{A_1/<S_1>}{A_2/<S_2>} = \frac{N_1}{N_2} \frac{<r_1^3>}{<r_2^3>} \tag{70}$$

These number ratios can be readily determined from microscopic examination of fallout samples preserved from atmospheric tests. If size distributions are known then average specific activity ratios may be determined from a knowledge of the total activity carried by each mode. Aggregate area fractions also obey a simple scaling relation:

$$\frac{Area_1}{Area_2} = \frac{M_1}{M_2} \frac{<r_2^3>}{<r_1^3>} \frac{<r_1^2>}{<r_2^2>} \tag{71}$$

The lognormal behavior of n_1 and n_2 further simplifies the moments calculations.

The results in Table VI give evidence of the suspected variability of n_2. The logarithmic slope varies from 3.2 to 6, with a mean of 4.2 which is near the DELFIC nominal value of 4.0. While the uncertainties inherent in Davis' calculations are large

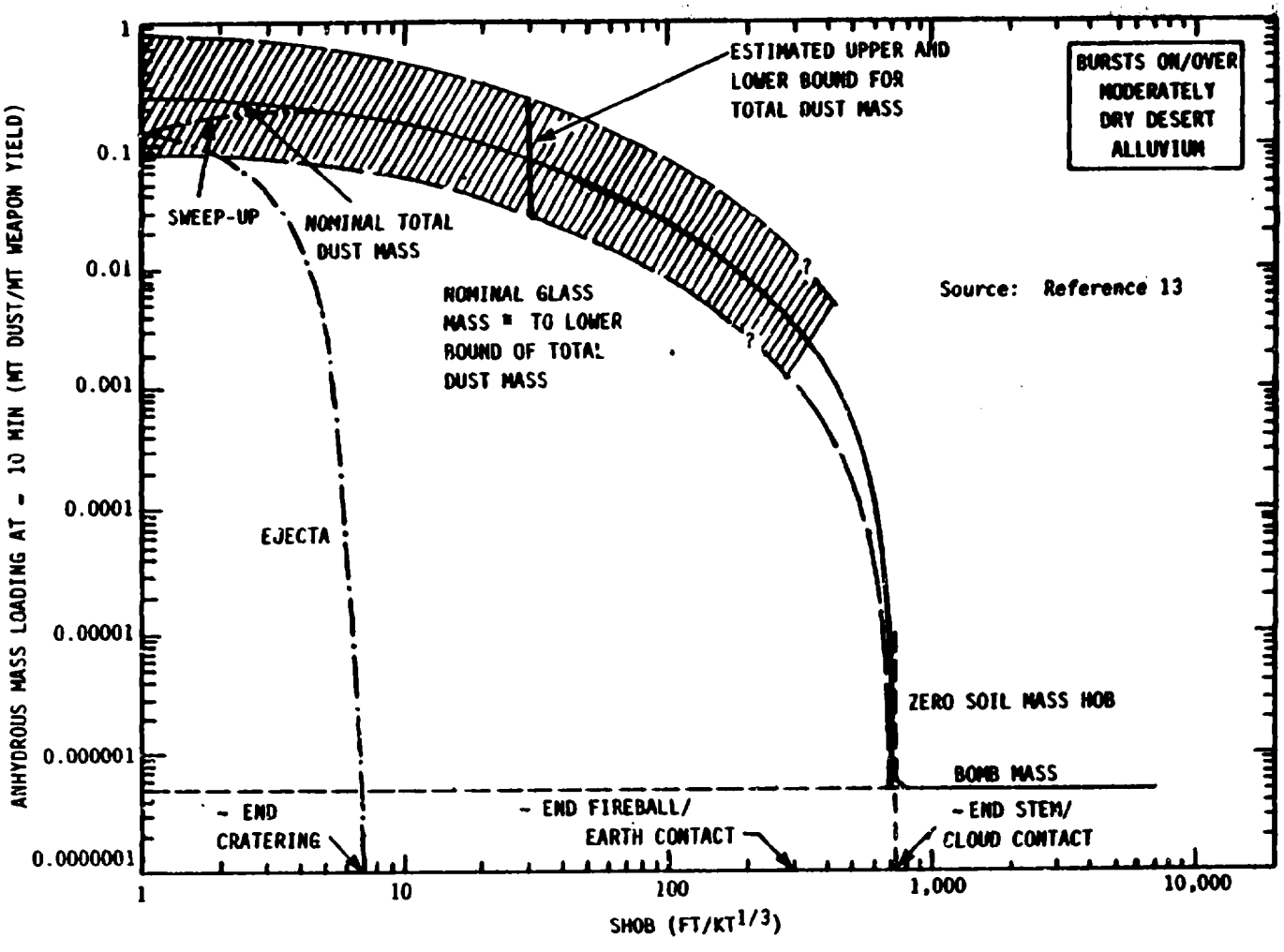

Figure 62. Dust Mass Lofted into the Stabilized Cloud (Showing Estimated Fraction of Glass and Relative Contributions of Blast Ejecta and Sweep-up)

Table VI

Lognormal Parameters: Bimodal Distribution[a]			
Event	F_2	Median Radius r_{m_2}	Log Slope (e^{β_2})
	Surface Bursts		
PLUMBBOB Coulomb-B	0.214	0.2	4.7
BUSTER-JANGLE Sugar	0.924	0.2	4.6
	Tower Bursts		
TEAPOT Hornet	0.115	0.2	5.2
TEAPOT Bee	0.0282	0.2	6.0
TEAPOT Apple	0.0404	0.2	4.4
PLUMBBOB Shasta	0.0994	0.2	4.8
UPSHOT-KNOTHOLE Nancy	0.0871	0.2	4.3
TEAPOT Apple II	0.0852	0.2	4.1
UPSHOT-KNOTHOLE Harry	0.703	0.2	3.4
UPSHOT-KNOTHOLE Simon	0.195	0.2	3.6
	Air Bursts		
PLUMBBOB Morgan	0.00583	0.2	4.7
PLUMBBOB Owens	0.0407	0.2	3.2
UPSHOT-KNOTHOLE Grable	0.0240	0.2	3.4
PLUMBBOB Stokes	0.00036	0.2	4.1
PLUMBBOB Priscilla	0.0366	0.2	3.3
PLUMBBOB Hood	0.00212	0.2	4.0

[a] Nominal n_1 assumed with $r_{m_1} = .1\mu$ and $\beta_1 = \ln 2$

and difficult to quantify, his results give further support to the existence of a bimodal particle distribution in clouds and also give a rough indication of activity partitioning between the modes.

VI. Summary and Conclusions.

This chapter will discuss the ramifications of Chapter V results and suggest further applications of atmospheric test data to the nuclear winter problem.

A. Bimodal Cloud Debris.

The major conclusion of this study is that cloud debris behavior can be explained by the existence of a bimodal size distribution. The puzzling dichotomy between early time and late time debris sedimentation (vividly demonstrated by the failure of the stratospheric size distribution to produce appreciable intermediate/local fallout by the sedimentation process) can be explained if:

$$n(r) = n_1(r) + n_2(r) = \frac{N_1 e^{-\frac{1}{2}\left[\frac{\ln(r)-\ln(r_{m1})}{\beta_1}\right]^2}}{\sqrt{2\pi}\,\beta_1} + \frac{N_2 e^{-\frac{1}{2}\left[\frac{\ln(r)-\ln(r_{m2})}{\beta_2}\right]^2}}{\sqrt{2\pi}\,\beta_2} \quad (72)$$

where n_1 governs the late time behavior of activity removal and n_2 governs the early time behavior. Figure 63 plots n(r) as expressed above using Nathans' measured 10 KT silicate surface burst parameters. The TTAPS and DELFIC distributions are included for comparison. Supporting evidence for the bimodal distribution includes the size distribution indicated by the bulk vertical transfer of stratospheric tracers over a period of months to years (section V.A) and Nathans' analysis of early time cloud debris from surface bursts (section V.C). The n_1 (or "hot") component of cloud debris appears to originate from the condensation of material vaporized in the fireball and is present for both surface and air bursts. The n_2 (or "cold") component appears to be unmelted or partially melted surface material which never reached fireball temperatures. The n_2 component is not present in cloud samples from free air bursts. Table VII contrasts the properties of n_1 and n_2.

The microscopically measured size distribution parameters for the n_1 component are fairly consistent from event to event (17). It is significant that the parameters properly predicting the removal of activity from the stratosphere are consistent with

Table VII

Characteristics of N_1 vs N_2 Particles	
N_1	N_2
spherical	irregular
high specific activity $S_1(r) \ \alpha \ r^3$	low specific activity $S_2(r) \ \alpha \ r^2$
Origin: vaporized material weapon mass + soil	Origin: unmelted/partially melted material soil
Size Distribution: lognormal $r_m \approx .1\mu$ $\beta \approx ln(2)$	Size Distribution: lognormal $r_m \approx .2\mu$ $\beta \approx ln(3) - ln(5)$
Stratospheric Removal: Sedimentation + Diffusion	Stratospheric Removal: Sedimentation
PRESENCE[6]: Air burst..... yes Low air/tower...varies with HOB Surface...small fraction of mass	 .....no .....varies with HOB ...large fraction of mass

[6]Reference 76

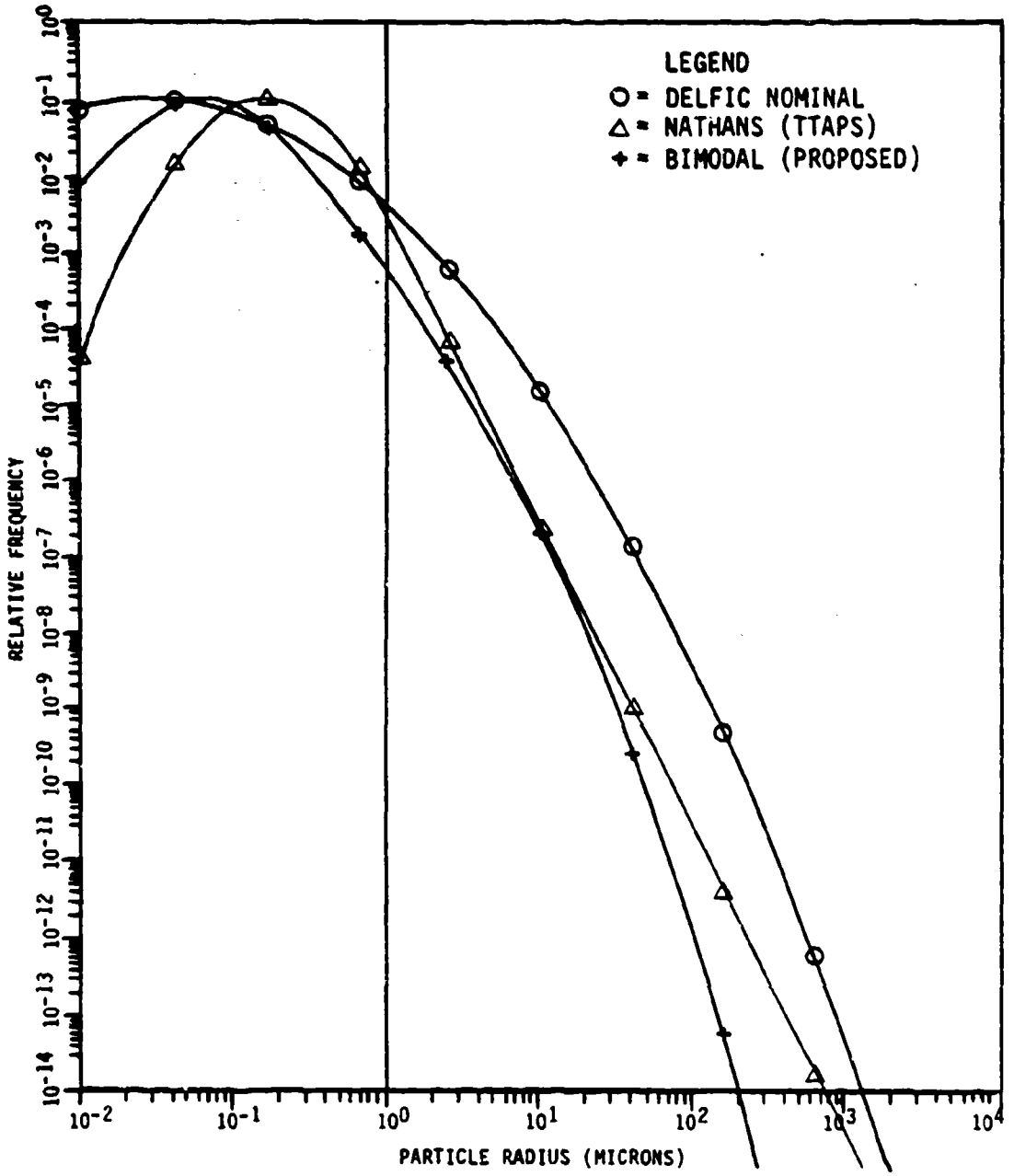

Figure 63. Bimodal Distribution Compared to Nathans' and DELFIC

the microscopically measured size distributions for hot particles from air and surface bursts (figures 35,39,42). Representative values for the median radius and slope are .1μ and 2 respectively. These values predict the average behavior of stratospheric ^{90}Sr debris injected by 97 events over a 15 year period.

Characterization of n_2 has been less satisfactory due to data limitations and the expected variation in n_2 parameters with surface material and burst height. Analysis of limited data for surface bursts provided by Nathans indicates a median radius and slope in the vicinity of .17μ and 3 for the n_2 component. Davis' results (54) indicate that logarithmic slopes may vary considerably about a mean of ~4. Clearly, more work is needed to bound the size and mass properties of the "cold" distribution. It may be that n_2 is itself multimodal, especially for buried bursts (69). In addition the relation of n_2 fraction to burst height needs to be resolved with confidence. This relation is bound up with the problem of determining mass lofted per kiloton.

The existence of a bimodal cloud distribution leads to a new equation for computing the total mass lofted:

$$M_T = A_T \left[\frac{F_1}{<S_1>} + \frac{F_2}{<S_2>} \right] \tag{73}$$

The present effort has not investigated the full implications of this equation which enables computation of mass lofted based upon a knowledge of total activity deposited. Reasonable estimates of F_1 and F_2 should be possible from a careful evaluation of existing fallout data. For example, Tompkins (71) has developed fits for the fraction of activity deposited locally based upon data from several Nevada events. Since a large part of the n_2 distribution and almost none of the n_1 distribution falls in 24 hours, Tompkins' fraction roughly approximates F_2, at least for above ground shots.

There is considerable uncertainty in the average specific activity parameters. The data required to narrow these uncertainties does not appear to be plentiful, particularly for determining the variation of $<S_1>$ and $<S_2>$ with height of burst. However data from surface bursts and free air bursts are available, which taken together with some reasonable physics could be used to develop a credible model. For purposes of illustration, consider an approximate calculation for Johnie Boy whose fission yield was .5 KT (equivalent to ~7 x 10^{22} fissions). Tompkins (71)

indicates that ~70% of the activity from Johnie Boy was deposited locally. Using this as a rough value for F_2 and estimating $<S_1>$ and $<S_2>$ to be $\sim 10^{16}$ and $\sim 10^{15}$ respectively, then $M_T \approx .051\ KT$. This translates to .12 kilotons of dust lofted per kiloton of yield.

B. Cloud Stratification Effects.

An important conclusion from the investigation of the power tail behavior of samples from Johnie Boy, Bravo, Zuni and Koon (section V.E) is that size distributions vary tremendously with sample location and time due to sedimentation induced vertical cloud stratification. Consequently, extreme caution should be exercised in generalizing a cloud distribution from the distributions of isolated samples. The results show specifically that clouds whose total particle ensemble is lognormally distributed can yield sample distributions which obey a power law function. It is quite possible that Natl .ns' power law distributions originated from clouds whose aggregate population was closer to lognormal.

Cloud stratification effects on sample distributions become extremely pronounced with increasing distance from the cloud centroid. The stratification effect may in fact explain the narrow distributions observed for ground samples which seem to vary so much with distance downwind. An example of the size distribution which would be measured on the ground 12 hours post shot underneath a Gaussian cloud with a standard devia. on of 700m is shown in figure 64. The distribution peaks at 35μ with a half-width of only 5μ. The half-width is a function of the sedimentation correction factor (equation 61) which is in turn a function of the cloud vertical density distribution. Thus, it may be possible to learn something about the vertical density of clouds by studying the half width of particle size distributions of ground samples.

C. Optical Depth Implications.

Using the bimodal size distribution expressed in equation 73, it is possible to compute the optical thickness vs time for a stratospheric dust cloud representative of the TTAPS 5000 Megaton exchange. Analogous to equation 10:

$$OT = \left[\frac{3M_T Q_e}{4\rho_s A_c}\right]\frac{<r^2>}{<r^3>} \tag{74}$$

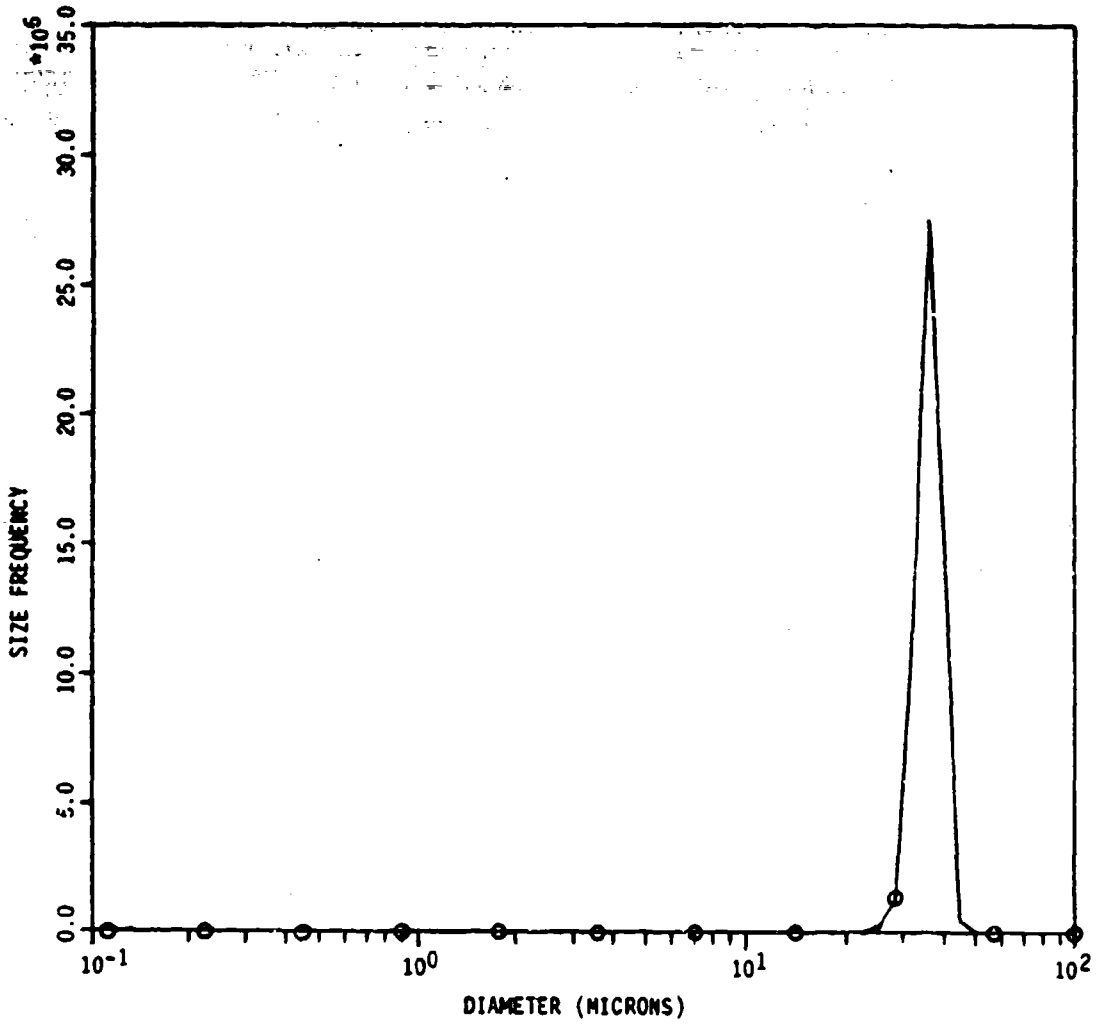

Figure 64. Ground Sample Distribution, 12 Hours Post-Shot

Using equations 6 and 7 for the 2nd and 3rd moments of the lognormal distributions n_1 and n_2 the following expression for the initial optical thickness results

$$OT = \left[\frac{3M_T Q_e}{4\rho_e A_c}\right]\left[\frac{\frac{N_1}{N_2}e^{2\ln(r_{m1}+2\beta_1^2)} + e^{2\ln(r_{m2}+2\beta_2^2)}}{\frac{N_1}{N_2}e^{3\ln(r_{m1}+\frac{9}{2}\beta_1^2)} + e^{3\ln(r_{m2}+\frac{9}{2}\beta_2^2)}}\right] \tag{75}$$

Using the cloud parameter values from section I.B.1 ($A_c = 1.14\ x\ 10^{14}\ m^2$, $\rho_e = 2600\ kg/m^3$, and $Q_e = 2.5$) the initial optical thickness is 2.0. This is comparable to the initial dust optical thickness of 1.25 computed by the TTAPS group. Recall (figure 3) that the nominal DELFIC n(r) predicts an initial O.T. of .25, and the Ramaswamy-Kiehl (R-K) distribution predicts 11.6. The bimodal distribution was used in subroutine STRATFAL to predict the rate of decay of optical thickness for a cloud initially centered at 25 KM. The results are overlaid with DELFIC, TTAPS, and R-K in figure 65. The bimodal distribution optical attenuation is initially higher than the TTAPS result, but decays more rapidly leveling off to a value of ~½ of the TTAPS optical thickness (the factor of ½ is certainly within model uncertainties). The curves are parallel at late times because the remaining particles are small enough that their removal is governed by the exponential turbulent diffusion effect. Thus, the size distribution derived in this research, although different than the size distribution used in the TTAPS study, yields similar estimates of optical thickness magnitude and decay (other effects being equal). Although the power law behavior may well be an aberration of cloud stratification, Nathans' distribution appears to provide a reasonable estimate of sunlight attenuation magnitude and duration. The similarity of the results is due to the fact that the submicron fractions are comparable.

D. Recommendations.

1. The evidence supports the existence of a bimodal particle size distribution in nuclear clouds. The distribution expressed in equation 72 should be seriously considered for predicting optical attenuation effects and fallout removal. The existence of distributions of different consistencies and thermal origins (Table VII) warrants an investigation of possibly large differences in optical properties as well.

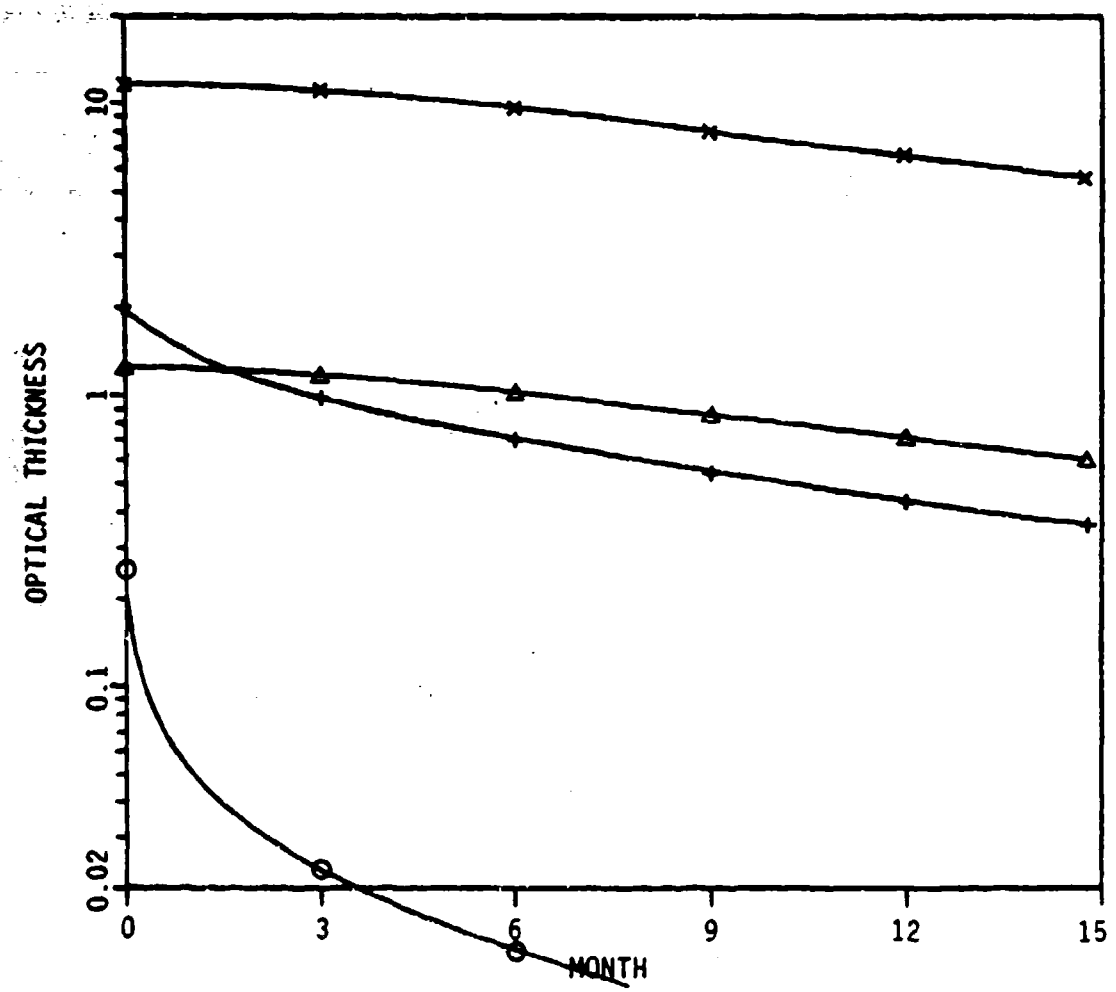

Figure 65. OT vs. Time, Cloud Initially Centered at 25 km

2. Work is needed to characterize n_2(r). This research has uncovered only one instance of separate size analysis of spherical and irregular particles. There may be others. If not, it is recommended that further analysis of samples from atmospheric test clouds be conducted and that any such analysis develop separate statistics for spherical and irregular particles. The n_2 parameter values used here (median radius .17μ and slope of 3) are based on analysis of actual data by Marcel Nathans, and are certainly reasonable values to use in the interim for estimates of surface burst effects. Indications are that the slope ranges higher. Thus the nominal DELFIC distribution is also a plausible representation of n_2.

3. Computations of mass lofted per kiloton should be reexamined in light of the bimodal nature of the cloud distribution. An attempt should be made to quantify the parameters of equation 73 based upon test data over a range of scaled burst height/depth. It is reasonable to expect that the uncertainty in estimates of mass lofted vs yield and height of burst can be considerably reduced.

4. It would be useful to run the rigorous models of climate effects from nuclear war using the bimodal n(r) function and parameters developed in the present research. Although it appears that optical effects are not drastically different from TTAPS, the effect on temperature drop needs to be investigated. The higher initial magnitude and more rapid decay rate may cause larger differences in the predicted temperature changes.

APPENDIX A

TREATMENT OF FALL MECHANICS

Fall mechanics involves the solution of the one dimensional force balance equation including a viscosity term:

$$F(t) = fu - m\frac{du}{dt} \tag{A.1}$$

where m is the particle's mass, u is its velocity, and f is the viscous damping coefficient. Particles are assumed to be spherical. The functional relationship between the viscous force, fu, and particle diameter varies with particle size and altitude. At sea level, for particles less than 10μ, Stoke's law applies:

$$f = 6\pi\eta r \tag{A.2}$$

and the force balance equation becomes:

$$6\pi\eta r = \frac{4}{3}\pi r^3 \rho g \tag{A.3}$$

where η is the dynamic viscosity (kg/sec/m) and r is the particle's radius. Note that the resisting force is proportional to radius. Solving for terminal velocity:

$$u_{term} = \frac{2r^2\rho g}{9\eta} \tag{A.4}$$

For particles greater than ~10μ, aerodynamic drag is significant and the force balance equation becomes:

$$\tfrac{1}{2}\rho_a u^2 C_d \pi r^2 = \frac{4}{3}\pi r^3 \rho g \tag{A.5}$$

The solution of this equation is complicated by the fact that C_d is a function of the particle's velocity. McDonald (73) suggested a method of solution by defining u in terms of the Reynolds number:

$$u = \frac{R_e \eta}{2\rho_a r} \tag{A.6}$$

McDonald then defined a quantity, Q:

$$Q = R_e^2 C_d = \frac{32\rho_a(\rho - \rho_a)gr^3}{3\eta^2} \tag{A.7}$$

which Davies (74) has fit to various polynomial expressions depending upon its magnitude. Q is referred to as the"Davies number"). For a given altitude, the fall velocity is computed by calculating Q, finding R_e from Davies' polynomial fits, and then computing u from R_e. Polynomial fits for determining R_e are as follows:

for 140 < Q ≤ 4.5E7:

$$\log_{10}R_e = -1.29536 + .986 log_{10}Q + .046677\log_{10}^2 Q + 1.1235E{-}3\log_{10}^3 Q \tag{A.8}$$

for 84.175 < Q ≤ 140:

$$R_e = Q(\ 4.166667E{-}2 - 2.3383E{-}4Q + 2.0154E{-}6Q^2 - 6.9105Q^{3)} \tag{A.9}$$

for .3261 ≤ Q ≤ 84.175:

$$R_e = \exp[-3.18657+.992696lnQ-.153193E{-}2ln^2Q-.987059E{-}3ln^3Q-.578876E{-}3ln^4Q + .855176E{-}4ln^5Q-.327815E{-}5ln^6Q] \tag{A.10}$$

for Q < .3261

Stokes equation (A.5) applies.

For particle diameters approaching the mean free path (L) of air molecules, the drag for a given velocity is less than predicted by the polynomial fits and a slip correction factor must be introduced. For example, when d/L=10 the Stokes equation underestimates u by about 15 percent (9). At 50,000 ft, L=.4 microns, so it is clear that the slip factor is important for gravity fall calculations.

The Cunningham slip correction factor used in HASP analysis (10) and DELFIC (8) was derived for d/L ratios between 2 and 100. Knudsen and Weber (57) proposed a general formula that fits data over a wider range of d/L values:

$$C = 1 + \frac{L}{r}\left[A_1 + A_2 exp\left(\frac{-2A_3 r}{L}\right)\right] \tag{A.11}$$

where A_1=1.644, A_2=.552, and A_3=.656. The Knudsen- Weber slip correction formula was incorporated into the fall velocity model.

The equations in this appendix were encoded as shown in the listing which follows. Computed terminal velocities compare to within 20% of those computed by models used in the High Altitude Sampling Program for particle diameters ranging from .001 -10μ (10:154).

```
      FUNCTION VEL(ZB,RP)
C     COMPUTES TERMINAL VELOCITY OF SPHERICAL PARTICLES USING
FULL DELFIC
C     FALL MECHANICS AND U.S. STANDARD ATMOSPHERE EQUATIONS
C     SUBROUTINE ATMOS RETURNS DENSITY, VISCOSITY AND MEAN FREE
PATH AT ALT ZB
      REAL MFP,LOGREY
C     EXTERNAL ATMOS
      CALL ATMOS(ZB,DENS,VISC,MFP)
      DENSF=2600.
      G=9.8
      QZ=4*DENS*(DENSF-DENS)*G*(2.*RP)**3/(3.*VISC*VISC)
C     WRITE(6,1051)QZ,DENS,VISC,MFP
C1051 FORMAT('QZ,DENS,VISC,MFP',4(E10.3))
      YY=ALOG(QZ)
C     DENSF IS PARTICLE DENSITY, G IS GRAV, QZ IS DAVIES NUMBER
DEFINED IN
C     DNA TR-5159F-1, P24
           IF(QZ .LE. .3261)THEN
                VEL=VISC*QZ/(24.*DEN3*2.*RP)
                GO TO 1100
                ENDIF
           IF((QZ .GT. .3261) .AND. (QZ .LE. 84.175))THEN
                VEL=(VISC/(DENS*2.*RP))*EXP(-3.18657+.992696*YY-
     ^
1.53193E-3*YY**2-9.87059E-4*YY**3-5.78878E-4*YY**4
     ^          +8.551759E-5*YY**5-3.27815E-6*YY**6)
                GO TO 1100
                ENDIF
           IF((QZ .GT. 84.175) .AND. (QZ.LT.140))THEN
                VEL=VISC*QZ*(4.166667E-2-2.3363E-4*QZ+2.0154E-6*Q
Z**2
     ^          -6.9105E-9*QZ**3)/(DENS*2.*RP)
                GO TO 1100
                ENDIF
           IF((QZ .GE. 140) .AND. (QZ .LT. 4.5E7))THEN
                LOGREY=-1.29536+.986*YY/2.303-.046677*(YY/2.303)*
*2
     ^          +.0011235*(YY/2.303)**3
                REYNOL=10.**LOGREY
                VEL=REYNOL*VISC/(2.*DENS*RP)
                ENDIF
C          KNUDSEN SLIP CORRECTION
 1100        IF(RP.GT.100.*MFP) THEN
         EXPFAC=0.
         ELSE
         EXPFAC=EXP(-.656*2.*RP/MFP)
         ENDIF
            VEL=VEL*(1.+(1.644+.552*EXPFAC)*MFP/
     ^          (2.*RP))
      RETURN
      END
C*************************************************************
*************
```

```
C*****************************************************************
***************
      SUBROUTINE ATMOS(ZB,DENS,VISC,MFP)
C     SUBROUTINE CALCULATES ATMOSPHERIC TEMPERATURE, PRESSURE AND
VISCOSITY
C     FOR ALTITUDES UP TO 84,852 METERS (MKS UNITS EMPLOYED)
      REAL LK,NUMDEN,MFP
      IF(ZB .LE. 11000.)THEN
           LK=-.006545
           TK=288.15
           PK=101300.
           TB=TK+LK*ZB
           PB=PK*(TK/TB)**(.034164/LK)
           GO TO 1240
           ENDIF
      IF((ZB .GT. 11000.) .AND. (ZB .LE. 20000.))THEN
           ZK=11000.
           TK=216.65
           PK=22690.
           LK=0.
           TB=TK
           PB=PK*EXP(-.034164*(ZB-ZK)/TK)
           GO TO 1240
           ENDIF
      IF((ZB .GT. 20000.) .AND. (ZB .LE. 32000.))THEN
           ZK=20000.
           TK=216.65
           PK=5528.
           LK=.001
           TB=TK+LK*(ZB-ZK)
           PB=PK*(TK/TB)**(.034164/LK)
           GO TO 1240
           ENDIF
      IF((ZB .GT. 32000.) .AND. (ZB .LE. 47000.))THEN
           ZK=32000.
           TK=228.65
           PK=888.8
           LK=.0028
           TB=TK+LK*(ZB-ZK)
           PB=PK*(TK/TB)**(.034164/LK)
           GO TO  1240
           ENDIF
      IF((ZB .GT. 47000.) .AND. (ZB .LE. 51000.))THEN
           ZK=47000.
           TK=270.65
           PK=110.873
           LK=0.
           TB=TK
           PB=PK*EXP(-.034164*(ZB-ZK)/TK)
           GO TO 1240
           ENDIF
      IF((ZB .GT. 51000.) .AND. (ZB .LE. 71000.))THEN
           ZK=51000.
           TK=270.65
```

```
            PK=66.9218
            LK=-.0028
            TB=TK+LK*(ZB-ZK)
            PB=PK*(TK/TB)**(.034164/LK)
            GO TO 1240
            ENDIF
      IF((ZB .GT. 71000.) .AND. (ZB .LE. 84852.))THEN
            ZK=71000.
            TK=214.65
            PK=3.95536
            LK=-.002
            TB=TK+LK*(ZB-ZK)
            PB=PK*(TK/TB)**(.034164/LK)
            GO TO 1240
            ENDIF
      IF((ZB .GT. 84852))THEN
            WRITE (6,1230)
            GO TO 1241
            ENDIF
 1230 FORMAT('PARTICLE ALTITUDE BEYOND RANGE OF PROGRAM
APPLICABILITY')
 1240 VISC=1.46E-6*TB**1.5/(TB+110.4)
      DENS=.003484*PB/TB
      NUMDEN=DENS*2.55E25/1.23
C             PER CUBIC METER: 2.55E25 MOLECULES PER CUBE AT SEA
LEVEL.
C             DENSITY AT SEA LEVEL IS 1.23 KG/CUBE
      MFP=1/(1.414*NUMDEN*4.5E-19)
C             MFP=1/(ROOT2*N*SIGMA)
 1241 RETURN
      END
  END OF FILE
```

APPENDIX B

THE LOGNORMAL DISTRIBUTION AND ITS MOMENTS

The lognormal distribution derives from the normal distribution if the variable of integration is replaced by its logarithm: if

$$r \longrightarrow ln(r),$$

then

$$dN = \frac{dr}{\sqrt{2\pi}\,\sigma}\exp\left[-\tfrac{1}{2}\left(\frac{r-r_o}{\sigma}\right)^2\right] \tag{B.1}$$

$$\longrightarrow dN = \frac{dr}{\sqrt{2\pi}\beta r}\exp\left[-\tfrac{1}{2}\left(\frac{ln(r)-ln(r_m)}{\beta}\right)^2\right] \tag{B.2}$$

where r_m is the median radius of the number distribution (50% of particles are smaller than r_m) and β governs the dispersion of the distribution:

$$\beta = \exp\left[\frac{r_{84.13\%}}{r_m}\right] = \exp\left[\frac{r_m}{r_{15.87\%}}\right] = \exp\left[\,S\,\right] \tag{B.3}$$

S is known as the "logarithmic slope" (or sometimes just "slope") of the distribution.

The distribution function appears in several forms:

$$\frac{dN}{d(lnr)} = \frac{1}{\sqrt{2\pi}\beta}\exp\left[-\tfrac{1}{2}\left(\frac{ln(r)-ln(r_m)}{\beta}\right)^2\right] \tag{B.4}$$

or

$$\frac{dN}{dr} = \frac{1}{\sqrt{2\pi}\beta r}\exp\left[-\tfrac{1}{2}\left(\frac{ln(r)-ln(r_m)}{\beta}\right)^2\right] \tag{B.5}$$

or

$$\hat{n}(r) = \frac{1}{\sqrt{2\pi}\beta r}\exp\left[-\tfrac{1}{2}\left(\frac{ln(r)-ln(r_m)}{\beta}\right)^2\right] \tag{B.6}$$

The last expression is used in the present research. The symbol " ^ " denotes the function as normalized, i.e.

$$\int_0^\infty \hat{n}(r)dr = 1 \tag{B.7}$$

The mode radius of a lognormal distribution lies below r_m:

$$r_{mode} = r_m e^{-\beta^2} \tag{B.8}$$

The mean radius lies above r_m:

$$r_{mean} = r_m e^{\frac{1}{2}\beta^2} \tag{B.9}$$

Any moment of a lognormal distribution is itself lognormal (true for both positive and negative moments). This can be demonstrated by successive substitutions for the variable of integration. Consider the lth moment:

$$\begin{aligned} A(r) &= \int_0^r \tilde{r}^l \hat{n}(\tilde{r})\, d\tilde{r} \\ &= \int_0^r \tilde{r}^l \frac{1}{\sqrt{2\pi}\beta\tilde{r}} \exp\left[-\tfrac{1}{2}\left(\frac{ln(\tilde{r})-ln(r_m)}{\beta}\right)^2\right] d\tilde{r} \end{aligned} \tag{B.10}$$

letting

$$z = \left(\frac{ln(r)-ln(r_m)}{\beta}\right) \tag{B.11}$$

A(r) becomes:

$$A(r) = e^{l(lnr_m)} \int_{-\infty}^{\frac{lnr-lnr_m}{\beta}} \frac{1}{\sqrt{2\pi}} e^{-\frac{1}{2}(z^2 - 2lz\beta)} dz \tag{B.12}$$

completing the square in the exponent of the integrand yields:

$$A(r) = \frac{1}{\sqrt{2\pi}} e^{l^2\beta^2/2} e^{l(lnr_m)} \int_{-\infty}^{\frac{lnr-lnr_m}{\beta}} e^{-\frac{1}{2}(z-l\beta)^2} dz \tag{B.13}$$

changing variables again, let

$$w = z - l\beta \tag{B.14}$$

Then:

$$A(r) = \left[e^{\frac{1}{2}l^2\beta^2}\, e^{l(\ln\, r_m)}\right]\frac{1}{\sqrt{2\pi}} \int_{-\infty}^{\frac{\ln r-(\ln r_m + l\beta^2)}{\beta}} e^{-\frac{1}{2}w^2}dw \qquad \text{(B.15)}$$

Letting

$$r_l = \ln\, r_m + l\beta^2 \qquad \text{(B.16)}$$

yields a very useful integral expression for A(r):

$$A(r) = \left[e^{\frac{1}{2}l^2\beta^2} e^{l(\ln r_m)}\right]\frac{1}{\sqrt{2\pi}} \int_{-\infty}^{\frac{\ln r-\ln r_l}{\beta}} e^{-\frac{1}{2}w^2}dw \qquad \text{(B.17)}$$

The expression above is readily evaluated using approximations in Abramowitz and Stegun (72: 932-933). Equation B.17 can be manipulated further into lognormal form by letting:

$$w = \frac{\ln r - \ln\, r_l}{\beta} \qquad \text{(B.18)}$$

Then,

$$A(r) = e^{\frac{1}{2}l^2\beta^2 + l(\ln r_m)} \int_0^r \frac{e^{-\frac{1}{2}\left[\frac{\ln r' - \ln r_l}{\beta}\right]^2}}{\sqrt{2\pi}\beta r'}dr' \qquad \text{(B.19)}$$

Differentiating,

$$\frac{dA(r)}{dr} = e^{\frac{1}{2}l^2\beta^2 + l(\ln\, r_m)} \frac{e^{-\frac{1}{2}\left[\frac{\ln\, r - \ln\, r_l}{\beta}\right]}}{\sqrt{2\pi}\beta r}dr \qquad \text{(B.20)}$$

$$= a(r) \quad (\textit{analogous to eqn. B.6})$$

Thus the lth moment is lognormal with the same dispersion (β) but a different median radius, r_l:

$$r_l = r_m\, e^{l\beta^2} \qquad \text{(B.21)}$$

Normalized expressions for a(r) are:

$$\hat{a}(r) = \frac{1}{\sqrt{2\pi}\beta r} e^{-\frac{1}{2}\left[\frac{\ln r - \ln r_l}{\beta}\right]^2} \qquad \text{(B.22a)}$$

$$= \frac{\frac{r^l}{\sqrt{2\pi}\beta r} e^{-\frac{1}{2}\left(\frac{\ln r - \ln r_m}{\beta}\right)^2}}{e^{\frac{1}{2}l^2\beta^2 + l\ln(r_m)}} \tag{B.22b}$$

Note that the average value of r^l is:

$$\langle r^l \rangle = \int_0^\infty r^l \hat{n}(r)dr = A(\infty) = e^{\frac{1}{2}l^2\beta^2 + l\ln r_m} \tag{B.23}$$

The ease of manipulating the moments of the lognormal distribution greatly simplifies n(r) parameter analysis.

APPENDIX C

NATHANS' DISTRIBUTION AND ITS MOMENTS

Nathans fit his particle size data to a function of the following form:

$$n(r) = n_A(r) = n_o \left(\frac{r_m}{r}\right)\left(\frac{r_o}{r_m}\right)^{\frac{p+1}{2}} \exp\left[-\tfrac{1}{2}\left(\frac{ln(r)-ln(r_m}{\beta}\right)^2\right], \quad r < r_o$$

$$= n_B(r) = n_o \left(\frac{r_o}{r}\right)^p, \quad r \geq r_o \tag{C.1}$$

where $n_o = n(r_o)$.

The transition radius, r_o, is found by requiring that the number size distribution and its first derivative be continuous there. This radius is given by:

$$r_o = r_m \exp[(p-1)\beta^2] \tag{C.2}$$

Note that the 3rd moment (mass distribution) of n(r) is not analytic for $p \leq 4$, i.e.,

$$\int_o^\infty n_o \left(\frac{r_o}{r}\right)^p r^3 dr \rightarrow \infty, \quad p \leq 4 \tag{C.3}$$

This problem is mitigated by defining a maximum radius, r_{max} as a function of the mass fraction (f_m) below r_o. Starting with:

$$f_m = \frac{\int_o^{r_o} n_A(r) r^3 dr}{\int_o^{r_o} n_A(r) r^3 dr + \int_o^{r_{max}} n_B(r) r^3 dr} \tag{C.4}$$

Solving for r_{max}:

$$r_{max} = \left[r_o(1 - 1/f_m)(p-4)e^{\frac{1}{2}\beta^2(p-4)^2}\sqrt{2\pi}\beta CNF[\beta(n-4)] + 1\right]^{\frac{1}{4-n}}, \quad p < 4$$

$$= r_o \exp\left[\sqrt{2\pi}\beta(1 - f_m/2f_m\right], \quad p = 4 \tag{C.5}$$

where CNF designates the normal or Gaussian probability function:

$$CNF(x) = \int_{-\infty}^{x} \frac{1}{\sqrt{2\pi}} e^{-\frac{1}{2}y^2} dy \tag{C.6}$$

Having defined r_{max} for the 3rd moment, the lower moments must be normalized assuming no particles exist with radius greater than r_{max}.

The normalized moments of n(r) are:

$$\hat{A}(r) = \frac{\int_{o}^{r} n_a(\tilde{r})\tilde{r}^l \, d\tilde{r}}{I_A + I_B}, \quad r < r_o \tag{C.7a}$$

$$= \frac{\int_{o}^{r_o} n_A(r)\tilde{r}^l \, dr + \int_{r_o}^{r} n_B(\tilde{r})\tilde{r}^l \, d\tilde{r}}{I_A + I_B}, \quad r \geq r_o \tag{C.7b}$$

where

$$I_A = \int_{o}^{r_o} n_A r^l \, dr = \sqrt{2\pi}\beta e^{\frac{1}{2}l^2\beta^2} r_o^{5/2} r_m^{l-3/2} CNF\left(\frac{\ln(r_o) - \ln(r_l)}{\beta}\right) \tag{C.8}$$

and

$$I_B = \int_{r_o}^{r_{max}} r^l \left(\frac{r_o}{r}\right)^p dr = \frac{r_o^p}{l-p+1}\left(r_{max}^{l-p+1} - r_o^{l-p+1}\right), \quad l \neq p-1 \tag{C.9a}$$

$$= r_o^p \ln\left(\frac{r_{max}}{r_o}\right), \quad l = p-1 \tag{C.9b}$$

Thus,

$$\hat{A}(r) = \frac{\sqrt{2\pi}\beta e^{\frac{1}{2}l^2\beta^2} r_o^{5/2} r_m^{l-3/2} CNF\left(\frac{ln(r) - lnr_l)}{\beta}\right)}{I_A + I_B}, \quad r < r_o \tag{C.10a}$$

$$= \frac{I_A + \frac{r_o^p}{l-p+1}\left[r^{l-p+1} - r_o^{l-p+1}\right]}{I_A + I_B}, \quad r \geq r_o, \; l \neq p-1 \tag{C.10b}$$

$$= \frac{I_A + r_o^p \ln(r/r_o)}{I_A + I_B}, \quad r \geq r_o, \; l = p-1 \tag{C.10c}$$

These equations are the basis for the activity group computation in subroutine SIZNAT (see Appendix E for a listing).

APPENDIX D

Program SHOT60 Listing

```
      PROGRAM
SHOT60(INPUT,OUTPUT,TAPE5=INPUT,TAPE6=OUTPUT,TAPE2,TAPE4,
     ^PLFILE=0)
C     PROGRAM IDENTIFIES BEST VALUES OF MOMENT, MEDIAN RADIUS,
AND BETA OF
C    ^LOG NORMAL STRATOSPHERIC PARTICLE SIZE DISTRIBUTION BASED
UPON
C    ^ATMOSPHERIC TEST DATA
      DIMENSION TRUEDA(20),BURDEN(20),RCOUNT(336),MONTH(336)
      DIMENSION RO(20),R(20),TRUEYR(20),YEAR(336)
      DIMENSION A(8,8),B(8,8),DELTA(8,8)
      COMMON RGROUP(60),WEIGHT(60),OFFSET(11),Y(11),MC(11)
      REAL MO, MO1, MONTH, MC, LOGR
      INTEGER OFFSET
C OPEN AUXILIARY DATA FILE
      OPEN(2,FILE='F1')
C     FIRST ESTABLISH VALUES FOR DATA (TRUE) AGAINST WHICH TO
OPTIMIZE
      TRUEDA(1)=1.60
      TRUEDA(2)=1.20
      TRUEDA(3)=.903
      TRUEDA(4)=1.00
      TRUEDA(5)=.933
      TRUEDA(6)=1.62
      TRUEDA(7)=1.10
      TRUEDA(8)=.933
      TRUEDA(9)=2.07
      TRUEDA(10)=6.41
      TRUEDA(11)=3.56
      TRUEDA(12)=1.47
      TRUEDA(13)=.750
      TRUEDA(14)=.310
      TRUEDA(15)=.280
      TRUEYR(1)=6./12.
      TRUEYR(2)=12./12.
      TRUEYR(3)=24./12.
      TRUEYR(4)=36./12.
      TRUEYR(5)=48./12.
      TRUEYR(6)=60./12.
      TRUEYR(7)=72./12.
      TRUEYR(8)=84./12.
      TRUEYR(9)=96./12.
      TRUEYR(10)=108./12.
      TRUEYR(11)=120./12.
      TRUEYR(12)=132./12.
      TRUEYR(13)=144./12.
      TRUEYR(14)=156./12.
      TRUEYR(15)=168./12.
C INPUT OFFSET,YIELD,SR90 FOR ATMOSPHERIC "EVENTS"
      OFFSET(1)=6
      OFFSET(2)=58
      OFFSET(3)=64
      OFFSET(4)=82
      OFFSET(5)=106
```

```
      OFFSET(6)=114
      OFFSET(7)=186
      OFFSET(8)=188
      OFFSET(9)=204
      OFFSET(10)=210
      OFFSET(11)=210
      Y(1)=9.6
      Y(2)=3.5
      Y(3)=1.5
      Y(4)=2.4
      Y(5)=.7
      Y(6)=3.6
      Y(7)=2.8
      Y(8)=41.5
      Y(9)=5.3
      Y(10)=25.
      Y(11)=6.8
      MC(1)=2.4
      MC(2)=.88
      MC(3)=.3
      MC(4)=1.4
      MC(5)=1.1
      MC(6)=1.1
      MC(7)=.644
      MC(8)=.689
      MC(9)=.427
      MC(10)=4.56
      MC(11)=1.95
C     SET VALUES FOR THE MOMENT, MEDIAN RADIUS, AND SLOPE (BE1)
C     BETA IS THE NATURAL LOG OF THE SLOPE
        WRITE(6,*)' INPUT NDIST (1=LOG NORM, 2=NATHANS HYBRID)'
        READ(5,*)NDIST
      WRITE(6,*)' INPUT MOMENT'
      READ(5,*)MO1
      I=0
      DO 20 BE1=1.01,4.,.2
        I=I+1
        J=0
      DO 10 LOGR=-2.,1.,.1
        J=J+1
        RM1=10.**LOGR
  5     FORMAT (A)
         IF(NDIST.EQ.2)WRITE(6,*)' INPUT FMASS (P1=4) '
         IF(NDIST.EQ.2)READ(5,*)F
      F0=0.
      CALL STRATF(NDIST,MO1,RM1,BE1,F,BURDEN,RCOUNT)
      DO 30 K=10,15
      R0(K)=BURDEN(K)-TRUEDA(K)
      R0(K)=R0(K)*R0(K)
      F0=F0+R0(K)
 30   CONTINUE
      WRITE(6,32) I,J,BE1,RM1,F0
      WRITE(2,50)I,J,LOGR,BE1,F0
 50   FORMAT( I4,I4,E12.5,E12.5,E12.5)
```

```
 10   CONTINUE
 20   CONTINUE
 32   FORMAT( ' I',I4,' J',I4,' B',E8.3,' R',E8.3,' FO',E8.3)
      DO 40 I=1,336
      MONTH(I)=FLOAT(I)/2.
      YEAR(I)=MONTH(I)/12.
 40   CONTINUE
      GO TO 999
C     DISSPLA PLOTTING CALLS FOLLOW
 77   CALL COMPRS
      CALL XNAME('YEAR$',100)
      CALL YNAME('STRATOSPHERIC BURDEN (MC)$',100)
      CALL PAGE(8.5,11.)
      CALL AREA2D(5.1,4.)
      CALL HEADIN('SR90 BURDEN FROM U.S.  FOREIGN
TESTS$',100,1.,1)
      CALL INTAXS
      CALL GRAF(0.,1.,14.,0.,1.,8.)
      CALL THKFRM(.02)
      CALL FRAME
      CALL MARKER(15)
      CALL CURVE(TRUEYR,TRUEDA,15,1)
      CALL MARKER(0)
      CALL CURVE(YEAR,RCOUNT,336,12)
      CALL GRID(1,1)
      ENCODE(60,15,LABEL)MO1,RM1,BE1,FO
  15  FORMAT('MOMENT=',F4.1,'  RM=',F4.1,'  SLOPE=',F4.1,
     ^    ' FO=',E9.3,'$')
      CALL RLMESS(LABEL,100,1.,7.)
      CALL XDTAXS(540101,4HYEAR,680101,5.1,'$',100,0.,-.75)
      CALL ENDPL(0)
      CALL DONEPL
 999  END
CCCCCCCCCCCCCCCCCCCCCCCCCCCCCCCCCCCCCCCCCCCCCCCCCCCCCCCCCCCCCCCC
CCCCCCCCCCCC
CCCCCCCCCCCCCCCCCCCCCCCCCCCCCCCCCCCCCCCCCCCCCCCCCCCCCCCCCCCCCCCC
CCCCCCCCCCCC
CCCCCCCCCCCCCCCCCCCCCCCCCCCCCCCCCCCCCCCCCCCCCCCCCCCCCCCCCCCCCCCC
CCCCCCCCCCCC
      SUBROUTINE MTXEQ(A,X,B,N,K)
C
C     MATRIX EQUATION SOLVER
C
C     USAGE...

C
C     TO SOLVE THE LINEAR SYSTEM      AX=B
C
C     CALL MTXEQ(A,X,B,N,K)
C
C        WHERE A MUST BE DIMENSIONED N X N
C              X MUST BE DIMENSIONED N X K
C              B MUST BE DIMENSIONED N X K
C              N IS THE NO. OF EQUATIONS (ROWS IN A,X,B)
```

```
C               K IS THE NO. OF SOLUTION VECTORS (COLS. IN X,B)
C
C
C     NOTE...   TO CHANGE DIMENSIONS OF ARRAYS C AND PIV, ALSO
C             CHANGE VALUES OF NMAX AND NKMAX IN DATA STATEMENT.
C
C
C
C DECLARATIONS
C
      INTEGER KP,NP,J,I,IFROM,IP1,IPIV,ITO,L,NP1,NPJ,NPK
      REAL A(8,8),B(8,8),X(8,8)
      REAL PIV(16),C(8,16),ATPE,RM
      DATA     NMAX, NKMAX/ 8, 16/
C
C     GET ARGUMENTS N AND K
C
      NP=N
      KP=K
C
C     TEST N AND K FOR CORRECT RANGE
C
      IF(NP.LE.0.OR.NP.GT.NMAX) GO TO 190
      IF(KP.LE.0.OR.(NP+KP).GT.NKMAX) GO TO 190
C
C     MOVE ARRAYS A(I,J) AND B(I,J) INTO C(I,J)
C
      DO 10 J=1,NP
      DO 10 I=1,NP
 10   C(I,J)=A(I,J)
      DO 20 J=1,KP
      NPJ=NP+J
      DO 20 I=1,NP
 20   C(I,NPJ)=B(I,J)
C
C     SET TO PERFORM N ELIMINATION SWEEPS (I=1,N)
C
      NP1=NP+1
      NPK=NP+KP
      DO 120 I=1,NP
      IP1=I+1
C
C     SEARCH FOR NEXT PIVOT ROW (I-TH PIVOT IS IN COL. I)
C
      ATPE=0.
      DO 40 J=I,NP
      IF (ABS(C(J,I))-ATPE) 40,30,30
 30   ATPE=ABS(C(J,I))
      IPIV=J
 40   CONTINUE
C
C     OPERATE ON THE PIVOT ROW
C
      IF (ATPE) 210,210,50
```

```
 50    DO 60 J=IP1,NPK
         IF (C(IPIV,I) .EQ. 0) THEN
           WRITE(6,302)
           WRITE(6,327)
           STOP
         ELSE
           PIV(J)=C(IPIV,J)/C(IPIV,I)
         ENDIF
  60   CONTINUE
C
C      PERFORM ELIMINATIONS BELOW THE DIAGONAL (COL. I)
C
       IFROM=NP
       ITO=NP
 70    IF (IFROM-IPIV) 80,100,80
 80    RM=-C(IFROM,I)
       DO 90 J=IP1,NPK
 90    C(ITO,J)=C(IFROM,J)+RM*PIV(J)
       ITO=ITO-1
 100   IFROM=IFROM-1
       IF (IFROM-I) 110,70,70
C
C      PUT THE I-TH PIVOT ROW IN THE VACATED ROW I
C
 110   DO 120 J=IP1,NPK
 120   C(I,J)=PIV(J)
C
C      NOW DO THE BACK SOLUTION
C
       I=NP
 130   IP1=I
       I=I-1
       IF (I) 160,160,140
 140   DO 150 J=NP1,NPK
       DO 150 L=IP1,NP
 150   C(I,J)=C(I,J)-C(I,L)*C(L,J)
       GO TO 130
C
C      MOVE THE SOLUTION TO ARRAY X(I,J)
C
 160   DO 170 J=1,KP
       NPJ=NP+J
       DO 170 I=1,NP
 170   X(I,J)=C(I,NPJ)
 180   RETURN
C
 190   WRITE(6,1000) NP, KP
C       CALL SYSTEM (200,'L')
       STOP
 210   WRITE(6,1001)
C       CALL SYSTEM (200,'L')
       STOP
 302   FORMAT(4(/),51H *** DIVISION BY ZERO OCCURED IN SUBROUTINE
MTXEQ -
```

```
     *,32H DURING EVALUATION OF PIV(J) ***)
 327  FORMAT(24H PLEASE CHECK YOUR INPUT,4(/))
 1000 FORMAT(3HON=,I12,3H K=,I12,35H ARE INCORRECT FOR SUBROUTINE
MTEQ )
 1001 FORMAT (37HODET(A)=0 IN CALL TO SUBROUTINE MTXEQ)
      END
C      SUBROUTINE SYSTEM
C      RETURN
C      END
CCCCCCCCCCCCCCCCCCCCCCCCCCCCCCCCCCCCCCCCCCCCCCCCCCCCCCCCCCCCCCCCCC
CCCCCCCCCCCC
CCCCCCCCCCCCCCCCCCCCCCCCCCCCCCCCCCCCCCCCCCCCCCCCCCCCCCCCCCCCCCCCCC
CCCCCCCCCCCCC
      SUBROUTINE
STRATF(NDIST,MOMENT,RMICRON,SLOPE,F,BURDEN,RCOUNT)
C     VERSION TO GENERATE PSEUDO DATA TO CHECK OPTIMIZATION TECHN
C     TAPE5 FROM KEYBOARD,TAPE6 TO SCREEN,TAPE2=EVENT
DATA,TAPE3=DATA OUT FOR PBBBR
C     PLOT
      DIMENSION CONTR(60), ZGROUP(60)
      DIMENSION GRPSUM(11,336), RCOUNT(336), GCOUNT(336),
FALL(336)
      DIMENSION PLTEAU(336), TVEL(60)
      DIMENSION BURDEN(20),HOC(11)
      COMMON RGROUP(60),WEIGHT(60),OFFSET(11),Y(11),MC(11)
      REAL MONTH,LNY,MOMENT,MC
      INTEGER OFFSET,EVENT,CONTR,TABS,TAB
      EXTERNAL STRAF,VEL
      RM=RMICRON*1.E-6
      B=ALOG(SLOPE)
C     OPEN AUXILIARY DATA FILES
C      OPEN(2,FILE='EV60',STATUS='OLD')
C      OPEN(3,FILE='PSEUDA')
C     INPUT RUN PARAMETERS FROM KEYBOARD
C         WRITE(6,5) ' WHAT IS TROPOPAUSE ALT (M) ?'
            ZTROP=12000.
C          READ(5,*) ZTROP
C           WRITE(6,6)ZTROP
 5         FORMAT(A)
 6         FORMAT( ' TROPOPAUSE ALTITUDE (M)=',E10.3)
C     INITIALIZE ARRAYS
          DO 10 TABS=1,336
                PLTEAU(TABS)=0.
                RCOUNT(TABS)=0.
                GCOUNT(TABS)=0.
                FALL(TABS)=0.
 10             CONTINUE
          DO 20 EVENT=1, 11
             DO 30 INCRE=1,336
 30             GRPSUM(EVENT,INCRE)=0.
 20          CONTINUE
C     DEFINE PHYSICAL CONSTANTS
          G=9.8
C     SET UP SIZE GROUPS, LOG NORMAL, OR LOG NORMAL + EXPONENTIAL
```

```
TAIL
           NGROUP=60
           IF (NDIST.EQ.2)CALL SIZNA25(RM,B,MOMENT,F)
           IF(NDIST.EQ.1)CALL SIZCNF(RM,B,MOMENT)
C      INPUT TERMINAL VELOCITIES FOR EACH GROUP AT TROPOPAUSE
           DO 190 J=1, NGROUP
           TVEL(J)=VEL(ZTROP,RGROUP(J))
C          WRITE(6,191) RGROUP(J),TVEL(J)
 190       CONTINUE
 191       FORMAT( 2E10.3)
C      DEFINE DETONATION PARAMETERS
           NBURST=11
       HOC(1)=26000.
       HOC(2)=21000.
       HOC(3)=20000.
       HOC(4)=21000.
       HOC(5)=17000.
       HOC(6)=23000.
       HOC(7)=22000.
       HOC(8)=38000.
       HOC(9)=25000.
       HOC(10)=35000.
       HOC(11)=26000.
CCCCCCCCCCCCCCCCCCCCCCCCCCCCCCCCCCCCCCCCCCCCCCCCCCCCCCCCCCCCCCCCC
CCCCCCCCCCCCCCCCCCCCCCCCCCCCCCCCCCCCCCCCCCCCCCCCCCCCCCCCCCCCCCCCC
C      FOR EACH EVENT COMPUTE STRATOSPHERIC BURDEN VS TIME
       DO 710 EVENT=7,11
C          COMPUTE STABILIZATION ALTITUDE AND INITIAL Z
DISPERSION. Y IN MT
C                USING HOPKINS FORMULA
                 LNY=ALOG(Y(EVENT)*1000.)
C
ZOM=EXP(7.889+.34*LNY+.001226*LNY**2-.005227*LNY**3
C    ^                    +.000417*LNY**4)
               ZOM=HOC(EVENT)
                 SIGZ0=2.15E3
C          DETERMINE WHICH SIZE GROUPS HAVE HIT THE GROUND WITHIN
1 DELTAT
                 DELTAT=365.25/24.
                 DELSEC=DELTAT*24.*3600.
                 DO 420 J=1,NGROUP
                   TFALMX=ZOM/TVEL(J)
                   IF(TFALMX.LT.DELSEC)THEN
                      CONTR(J)=0
                      ELSE
                      CONTR(J)=1
                      ENDIF
                   IF((CONTR(J).EQ.0) .AND. (CONTR(J-1).EQ.1))THEN

                      JCUT=J-1
                      ENDIF
 420             CONTINUE
C          SET INITIAL ALTITUDE OF EACH GROUP TO ZOM
              DO 440 J=1,NGROUP
```

```
                ZGROUP(J)=ZOM
 440            CONTINUE
C          FIND INITIAL FRACTION OF EACH CONTRIBUTING GROUP IN
THE STRATOSPHERE
               INCRE=1
               TLAPSE=0.
               TABS=OFFSET(EVENT)
C               WRITE(6,479) ZGROUP(1),SIGZ0,TLAPSE
 479           FORMAT( 'ZGROUP,SIGZ0,TLAPSE',3E10.3)
               FRAC=STRAF(ZGROUP(1),SIGZ0,TLAPSE,ZTROP)
               DO 480 J=1, JCUT
                    GRPSUM(EVENT,INCRE)=GRPSUM(EVENT,INCRE)+WEIG
HT(J)*
                    FRAC*MC(EVENT)
 480                CONTINUE
               RCOUNT(TABS)=RCOUNT(TABS)+GRPSUM(EVENT,INCRE)
               DO 495 TAB=OFFSET(EVENT), 336
                    PLTEAU(TAB)=PLTEAU(TAB)+MC(EVENT)-
                                GRPSUM(EVENT,INCRE)
 495                CONTINUE
C               WRITE(6,500) FRAC, TABS, RCOUNT(TABS),
MC(EVENT),
C                    GRPSUM(EVENT,INCRE),PLTEAU(TABS)
 500           FORMAT (
'FRAC',E10.3,'TAB',I4,'COUNT',E10.3,'MC',
     E10.3,'GROUPSUM',E10.3,'PLATEAU',E10.3)
C          SET TIME, INCREMENT IN STEPS OF 1/24 YEAR (TWO WEEKS)
 510           INCRE=INCRE+1
               TABS=INCRE+OFFSET(EVENT)-1
               IF(TABS.GT.336)THEN
                    GO TO 710
                    ENDIF
               IF((GRPSUM(EVENT,INCRE-1)).LT.1.E-1)THEN
                    GO TO 710
                    ENDIF
               TLAPSE=INCRE*DELTAT
C              COMPUTE NEW Z(T) FOR EACH CONTRIBUTING GROUP
               DO 680 J=1,JCUT
                    RP=RGROUP(J)
                    IF(ZGROUP(J).GT.0.)THEN
                       ZB=ZGROUP(J)
                       ELSE ZB=0.
                       ENDIF
                    DZ=VEL(ZB,RP)*DELSEC
                    ZGROUP(J)=ZGROUP(J)-DZ
                    GRPSUM(EVENT,INCRE)=GRPSUM(EVENT,INCRE)+
     ^
STRAF(ZGROUP(J),SIGZ0,TLAPSE,ZTROP)*WEIGHT(J)
     ^                   *MC(EVENT)
C                   WRITE(6,679)EVENT,INCRE,J,ZB,VEL(ZB,RP),
C     ^               STRAF(ZGROUP(J),SIGZ0,TLAPSE,ZTROP),
C     ^                  GRPSUM(EVENT,INCRE)
 679                FORMAT( ' EV',I3,' INCRE',I4,' J',I3,
     ^            ' ZB',E10.3,' VEL',E10.3,' STRAF',E10.3,'
```

```
GSUM',E10.3)
 680              CONTINUE
                  RCOUNT(TABS)=RCOUNT(TABS)+GRPSUM(EVENT,INCRE)*
                  EXP(-6.78E-5*TLAPSE)
 700         GO TO 510
 710         CONTINUE
              DO 810 I=1,15
              K=I*24-24
              BURDEN(I)=RCOUNT(K)
 810          CONTINUE
 850            FORMAT( F5.1,E10.3,E10.3)
C               ENDFILE 3
       RETURN
       END
C**********************************************************************
**************
C**********************************************************************
**************
C**********************************************************************
**************
       SUBROUTINE SIZCNF(RM,B,MOMENT)

C      PROGRAM TO PARTITION PARTICLE MASS DISTRIBUTIONS INTO
GROUPS
       COMMON RCENTR(60),MASFRA(60),OFFSET(11),Y(11),MC(11)
       DIMENSION RLEFT(60),RRIGHT(60),MASCNF(60)
       REAL MASCNF,MASFRA,MOMENT,MC
       INTEGER GROUP,OFFSET
       EXTERNAL CNF
C      CNF IS THE CUMULATIVE NORMAL
FUNCTION(RADIUS,RM,BETA,MOMENT)
C      OPEN(7,FILE='TAPE7')
C      DEFINE LOG NORMAL FUNCTION PARAMETERS, RM  BETA
 30    FORMAT (I3,4(E10.3))
C      WRITE (6,40)
 40    FORMAT(' GROUP  RLEFT      RRIGHT    RCENTROID  MASS FRAC')
       EXPON=-9.
       GROUP=1
             RLEFT(GROUP)=0.
             RRIGHT(GROUP)=10.**EXPON
             RCENTR(GROUP)=RRIGHT(GROUP)
C    WRITE(6,60) RRIGHT(GROUP),RM,B
C60    FORMAT ( 3E10.3)
             MASCNF(GROUP)=CNF(RRIGHT(GROUP),RM,B,MOMENT)
             MASFRA(GROUP)=MASCNF(GROUP)
       DO 130 GROUP=2,60
             EXPON=EXPON+.10
             RRIGHT(GROUP)=10.**EXPON
             RLEFT(GROUP)=RRIGHT(GROUP-1)
             RCENTR(GROUP)=SQRT(RLEFT(GROUP)*RRIGHT(GROUP))
             R=RRIGHT(GROUP)
             MASCNF(GROUP)=CNF(R,RM,B,MOMENT)
             MASFRA(GROUP)=MASCNF(GROUP)-MASCNF(GROUP-1)
C            WRITE (6,30)
```

```
GROUP,RLEFT(GROUP),RRIGHT(GROUP),RCENTR(GROUP)
C     ^     ,MASFRA(GROUP)
 130  CONTINUE
      RETURN
      END
C*****************************************************************
**************
C*****************************************************************
***************
      SUBROUTINE SIZNA25(RM,B,MOMENT,F)
      COMMON RCENTR(60),ACTFRA(60)
C     SUBROUTINE PARTITIONS NATHANS R4 DISTRIBUTION INTO ACTIVITY
GROUPS
      DIMENSION RLEFT(60),RRIGHT(60),ACTCUM(60)
      REAL MOMENT,PI,MC
      INTEGER GROUP,OFFSET
      EXTERNAL CNF
C     CNF IS THE CUMULATIVE NORMAL FUNCTION
C     DEFINE NATHANS PARAMETERS
           R0=RM*EXP(3.*B*B)
           R25=RM*EXP(2.5*B*B)
           PI=3.14159
           R2PI=SQRT(2.*PI)
           RMAX=R0*EXP(R2PI*B*(1.-F)/2./F)
 30   FORMAT (I3,5(E10.3))
      WRITE(6,40)
 40   FORMAT(' GROUP RLEFT     RRIGHT    RCENTR     ACTV FRAC
CUM')
      EXPON=-9.1
      GROUP=0
 60   FORMAT ( 3E10.3)
      DO 280 GROUP=1, 49
           EXPON=EXPON+.1
           RRIGHT(GROUP)=10.**EXPON
            IF (GROUP.EQ.1) THEN
                RLEFT(GROUP)=0.
                RCENTR(GROUP)=RRIGHT(GROUP)
                ELSE
                RLEFT(GROUP)=RRIGHT(GROUP-1)
                RCENTR(GROUP)=SQRT(RLEFT(GROUP)*RRIGHT(GROUP))
           END IF
           RT=RRIGHT(GROUP)
C     CALCULATE DENOMINATOR WHICH IS PROPORTIONAL TO TOTAL
ACTIVITY
           DENOM=R2PI*B*RM*R0**2.5*EXP(3.125*B*B)*CNF(R0,RM,B,MOM
ENT)
     ^     +R0**4*2.*(1./SQRT(R0)-1./SQRT(RMAX))
C     NOW CALCULATE NUMERATOR WHICH IS PROPORTIONAL TO ACTIVITY
DOWN
           IF (RT.LT.R0) THEN
                CNFPART=CNF(RT,RM,B,MOMENT)
                ELSE
                CNFPART=CNF(R0,RM,B,MOMENT)
           END IF
```

```
            ST=R2PI*B*RM*RO**2.5*EXP(3.125*B*B)*CNFPART
            BT=RO**4*2.*(1./SQRT(RO)-1./SQRT(RT))
            IF (RT.LT.RO) BT=0.
            XNUM=ST+BT
            ACTCUM(GROUP)=XNUM/DENOM
            IF (GROUP.EQ.1) THEN
                 ACTFRA(GROUP)=ACTCUM(GROUP)
                 ELSE
                 ACTFRA(GROUP)=ACTCUM(GROUP)-ACTCUM(GROUP-1)
            END IF
            WRITE(6,30)
GROUP,RLEFT(GROUP),RRIGHT(GROUP),RCENTR(GROUP)
     ^    ,ACTFRA(GROUP),ACTCUM(GROUP)
 280  CONTINUE
C     DEFINE GROUP WHICH LUMPS BIG PARTICLES TOGETHER WITH
RCENTR=100 MICRONS
          GROUP=50
          RLEFT(GROUP)=RRIGHT(GROUP-1)
          RRIGHT(GROUP)=RMAX
          RCENTR(GROUP)=RRIGHT(GROUP-1)
          ACTFRA(GROUP)=  -ACTCUM(GROUP-1)
          ACTCUM(GROUP    TCUM(GROUP-1)+ACTFRA(GROUP)
          WRITE(6,30)
GROUP,RLEFT(GROUP),RRIGHT(GROUP),RCENTR(GROUP)
     ^    ,ACTFRA(GROUP),ACTCUM(GROUP)
     RETURN
     END
C*************************************************************************
**************
C*************************************************************************
***************
      FUNCTION CNF(R,RM,B,MOMENT)
C     COMPUTES CUMULATIVE NORMAL FUNCTION FOR MASS DISTRIBUTION
           REAL MOMENT
           R3=RM*EXP(MOMENT*B*B)
           Z=(ALOG(R)-ALOG(R3))/B
C          WRITE(6,50) Z
C 50       FORMAT (' Z=',E10.3)
           IF (Z) 1060,1050,1050
 1050      CNF=1.-.5/(1.+.196854*Z+.115194*Z**2 +.000344*Z**3
+.019527*Z
     ^                  **4 )**4
           GO TO 1070
 1060        Z=-Z
           CNF=.5/(1.+.196854*Z+.115194*Z**2+.000344*Z**3+.019527
*Z**4)
     ^               **4
 1070 RETURN
      END
C*************************************************************************
**************
C*************************************************************************
***************
      FUNCTION STRAF(ZB,SIGZO,TLAPSE,ZTROP)
```

```
      REAL KDZ
      KDZ=.5
      ZSCALE=6.5E3
      SIGZ=SIGZ0+SQRT(2.*KDZ*TLAPSE*24.*3600.)
      DELTZ=(ZB-SIGZ*SIGZ/ZSCALE)-ZTROP
      A=DELTZ/SIGZ
      IF (A) 1060,1050,1050
 1050    CUMNF=1.-.5/(1.+.196854*A+.115194*A**2 +.000344*A**3
+.019527*A
     ^         **4 )**4
               GO TO 1070
 1060     A=-A
          CUMNF=.5/(1.+.196854*A+.115194*A**2+.000344*A**3+.01952
7*A**4)
     ^     **4
 1070 STRAF=CUMNF
      RETURN
      END
C*************************************************************************
**************
C*************************************************************************
**************
      FUNCTION VEL(ZB,RP)

C     COMPUTES TERMINAL VELOCITY OF SPHERICAL PARTICLES USING
FULL DELFIC
C     FALL MECHANICS AND U.S. STANDARD ATMOSPHERE EQUATIONS
C     SUBROUTINE ATMOS RETURNS DENSITY, VISCOSITY AND MEAN FREE
PATH AT ALT ZB
      REAL MFP,LOGREY
C     EXTERNAL ATMOS
      CALL ATMOS(ZB,DENS,VISC,MFP)
      DENSF=2600.
      G=9.8
      QZ=4*DENS*(DENSF-DENS)*G*(2.*RP)**3/(3.*VISC*VISC)
C     WRITE(6,1051)QZ,DENS,VISC,MFP
C1051 FORMAT('QZ,DENS,VISC,MFP',4(E10.3))
      YY=ALOG(QZ)
C     DENSF IS PARTICLE DENSITY, G IS GRAV, QZ IS DAVIES NUMBER
DEFINED IN
C     DNA TR-5159F-1, P24
           IF(QZ .LE. .3261)THEN
                VEL=VISC*QZ/(24.*DENS*2.*RP)
                GO TO 1100
                ENDIF
           IF((QZ .GT. .3261) .AND. (QZ .LE. 84.175))THEN
                VEL=(VISC/(DENS*2.*RP))*EXP(-3.18657+.992696*YY-
     ^
1.53193E-3*YY**2-9.87059E-4*YY**3-5.78878E-4*YY**4
     ^          +8.551759E-5*YY**5-3.27815E-6*YY**6)
                GO TO 1100
                ENDIF
           IF((QZ .GT. 84.175) .AND. (QZ.LT.140))THEN
                VEL=VISC*QZ*(4.166667E-2-2.3363E-4*QZ+2.0154E-6*Q
```

```
Z**2
     ^          -6.9105E-9*QZ**3)/(DENS*2.*RP)
                GO TO 1100
                ENDIF
           IF((QZ .GE. 140) .AND. (QZ .LT. 4.5E7))THEN
                LOGREY=-1.29536+.986*YY/2.303-.046677*(YY/2.303)*
*2
     ^          +.0011235*(YY/2.303)**3
                REYNOL=10.**LOGREY
                VEL=REYNOL*VISC/(2.*DENS*RP)
                ENDIF
C          KNUDSEN SLIP CORRECTION
 1100        IF(RP.GT.100.*MFP) THEN
          EXPFAC=0.
          ELSE
          EXPFAC=EXP(-.656*2.*RP/MFP)
          ENDIF
             VEL=VEL*(1.+(1.644+.552*EXPFAC)*MFP/
     ^          (2.*RP))
       RETURN
       END
C*****************************************************************
**************
C*****************************************************************
**************
       SUBROUTINE ATMOS(ZB,DENS,VISC,MFP)

C      SUBROUTINE CALCULATES ATMOSPHERIC TEMPERATURE, PRESSURE AND
VISCOSITY
C      FOR ALTITUDES UP TO 84,852 METERS (MKS UNITS EMPLOYED)
       REAL LK,NUMDEN,MFP
       IF(ZB .LE. 11000.)THEN
            LK=-.006545
            TK=288.15
            PK=101300.
            TB=TK+LK*ZB
            PB=PK*(TK/TB)**(.034164/LK)
            GO TO 1240
            ENDIF
       IF((ZB .GT. 11000.) .AND. (ZB .LE. 20000.))THEN
            ZK=11000.
            TK=216.65
            PK=22690.
            LK=0.
            TB=TK
            PB=PK*EXP(-.034164*(ZB-ZK)/TK)
            GO TO 1240
            ENDIF
       IF((ZB .GT. 20000.) .AND. (ZB .LE. 32000.))THEN
            ZK=20000.
            TK=216.65
            PK=5528.
            LK=.001
            TB=TR+LK*(ZB-ZK)
```

```
      PB=PK*(TK/TB)**(.034164/LK)
      GO TO 1240
      ENDIF
    IF((ZB .GT. 32000.) .AND. (ZB .LE. 47000.))THEN
      ZK=32000.
      TK=228.65
      PK=888.8
      LK=.0028
      TB=TK+LK*(ZB-ZK)
      PB=PK*(TK/TB)**(.034164/LK)
      GO TO  1240
      ENDIF
    IF((ZB .GT. 47000.) .AND. (ZB .LE. 51000.))THEN
      ZK=47000.
      TK=270.65
      PK=110.873
      LK=0.
      TB=TK
      PB=PK*EXP(-.034164*(ZB-ZK)/TK)
      GO TO 1240
      ENDIF
    IF((ZB .GT. 51000.) .AND. (ZB .LE. 71000.))THEN
      ZK=51000.
      TK=270.65
      PK=66.9218
      LK=-.0028
      TB=TK+LK*(ZB-ZK)
      PB=PK*(TK/TB)**(.034164/LK)
      GO TO 1240
      ENDIF
    IF((ZB .GT. 71000.) .AND. (ZB .LE. 84852.))THEN
      ZK=71000.
      TK=214.65
      PK=3.95536
      LK=-.002
      TB=TK+LK*(ZB-ZK)
      PB=PK*(TK/TB)**(.034164/LK)
      GO TO 1240
      ENDIF
    IF((ZB .GT. 84852))THEN
      WRITE (6,1230)
      GO TO 1241
      ENDIF
 1230 FORMAT('PARTICLE ALTITUDE BEYOND RANGE OF PROGRAM
APPLICABILITY')
 1240 VISC=1.46E-6*TB**1.5/(TB+110.4)
      DENS=.003484*PB/TB
      NUMDEN=DENS*2.55E25/1.23
C             PER CUBIC METER: 2.55E25 MOLECULES PER CUBE AT SEA
LEVEL.
C             DENSITY AT SEA LEVEL IS 1.23 KG/CUBE
      MFP=1/(1.414*NUMDEN*4.5E-19)
C             MFP=1/(ROOT2*N*SIGMA)
 1241 RETURN
```

```
      END
C*************************************************************************
************
C*************************************************************************
************
      SUBROUTINE SIMGROU(RM,B,MOMENT)
C PROGRAM TO PARTITION PARTICLE ACTIVITY DISTRIBUTION INTO GROUPS

C USES SIMPSON INTEGRATION
      COMMON RCENTR(60),FRAC(60),MC
      DIMENSION R(60)
      REAL MOMENT,MC,LRL1
      EXTERNAL GRANDLN
C GRANDLN COMPUTES NORMAL FUNCTION INTEGRAND FOR SIMPSON
INTEGRATION
C
C            WRITE (6,*)' GROUP  LEFT    RRIGHT   CENTROID  ACT
FRAC'
      LRL1=ALOG(RM)+(MOMENT-1.)*B*B
C     (MUST DECREMENT MOMENT TO COMPENSATE FOR LOGARITHMIC R
INCREMENTS)
      J=0
      SUM=0.
      DP=.1
      DO 130 POWER=-9.,-3.,DP
           J=J+1
           R(J)=10.**POWER
           RUP=10**(POWER+DP)
           DR=RUP-R(J)
           RCENTR(J)=SQRT(R(J)*RUP)
           ARG=R(J)
           F1=GRANDLN(ARG,LRL1,B)
           ARG=.5*(R(J)+R(J)+DR)
           F2=GRANDLN(ARG,LRL1,B)
           ARG=R(J)+DR
           F3=GRANDLN(ARG,LRL1,B)
           DNDR=(1./6.)*(F1+4.*F2+F3)
           FRAC(J)=DNDR*DR
           SUM=SUM+FRAC(J)
C           WRITE (6,30) J,R(J),RUP,RCENTR(J),FRAC(J)
 30   FORMAT (I3,4(E10.3))
 130  CONTINUE
      RETURN
      END
C*************************************************************************
******
C*************************************************************************
******
      FUNCTION GRANDLN(R,LRL1,B)
C COMPUTES LOG NORMAL FUNC AS INTEGRAND OF SIMPSON INTEGRATION
PROCEDURE
      REAL LRL1
      R2PI=SQRT(2*3.14159)
      EXPARG=-.5*(ALOG(R)-LRL1)**2/B/B
```

```
      IF(EXPARG.LT.-200.)EXPARG=-200.
      GRANDLN=1./R2PI/B/R*EXP(EXPARG)
      RETURN
      END
END OF FILE
```

APPENDIX E

Program INTOPT Listing

```
      PROGRAM
INTOPT1(INPUT,OUTPUT,TAPE5=INPUT,TAPE6=OUTPUT,PLFILE=0)
C COMBINES 75 EVENTS INTO ONE EVENT BASED UPON PARAMETER
STATISTICS
C PROGRAM COMPUTES INTERMEDIATE FALLOUT FROM ATMOSPHERIC TEST
SERIES AT NEVADA
C PROGRAM USES MODIFIED BRIDGMAN-BIGELOW SMEARING EQUATION TO
INCLUDE VERTICAL
C SPREAD IN CLOUD SPACIAL DISTRIBUTION
      COMMON RCENTR(33),WEIGHT(33),WORK(10000)
      EXTERNAL VEL
      DIMENSION
ACT(150,101),ZGROUP(33),ATRUE(6),XTRUE(6),IPKRAY(60)
      DIMENSION ACTCENT(150),ACTCUM(100,100),WASH(149),X(149)
      REAL LOGNOR,NATHAN,MOMENT,MC,PIVX,PIVY
      INTEGER EVENT
      DATA((ACTCUM(I,J),I=1,100),J=1,100)/10000*0./
      ACTMAX=0.
C     EVENT DATA FOR INTERMEDIATE FALLOUT COMPUTATION
C     PARAMETERS FOR SINGLE REPRESENTATIVE BURST FOLLOW (YIELD
WEIGHTED AVGS)
         YIELD=13.27
         ZOKFT=34.1
         VECTOR=246.
         VWIND=27.5
C        MPH--->KM/HR
         VWIND=VWIND*1.609
         SHEAR=5.38
C SET WASHOUT TIME CONSTANT,HRS (REF. C. E. JUNGE, JOURNAL OF
METEOROLOGY)
      WRITE(5,*)'INPUT TWASH (HRS)'
      READ(6,*)TWASH
C        SET UP SIZE GROUPS, LOG NORMAL, OR LOG NORMAL +
EXPONENTIAL TAIL
            NGROUP=33
            WRITE(6,*)'INPUT NDIST (1>LOG NORMAL, 2>NATHANS
W/TAIL)'
            READ(5,*)NDIST
 12         IF(NDIST.EQ.2)WRITE(6,*)'INPUT ROLLOFF N AND RMAX
(MICRONS)'
            IF(NDIST.EQ.2)READ(5,*)P1,RMAX
            IF(NDIST.EQ.2)RMAX=RMAX*1.E-6
 11         WRITE(6,*)'INPUT RM (MICRONS) AND SLOPE'
            READ(5,*)RM,SLOPE
            IF(RM.LT.0.)STOP
            RM=RM*1.E-6
C            DO 1001 RM=.1E-6,1.E-6,.1E-6
C            DO 1000 SLOPE=1.5,3.5,.25
            B=ALOG(SLOPE)
            MOMENT=2.5
            IF(NDIST.EQ.2)CALL SIZNAT(RM,B,MOMENT,P1,RMAX)
            IF(NDIST.EQ.1)CALL SIZCNF(RM,B,MOMENT)
C  BEGIN EVENT LOOP                                    <----------
      DO 710 EVENT=1,1
```

```
      WRITE(6,*)' EVENT=',EVENT
C        SET UP BURST PARAMETERS (MT,TOTAL CURIES)
            Y=YIELD/1000.
C           MEGATONS
            FF=1.
            MC=75.*Y*.1*FF*1.E9
C           MILLICURIES
C        SET UP WIND CONDITIONS (ANGLE IN DEGREES, VELOCITY IN
KM/HR)
            VECTOR=-VECTOR+270.
C        SET INITIAL CLOUD HEIGHT, Z DISPERSION, YY DISPERSION
            INX=0
             SIGY0=50.
C            SIGY0=1.609*
C     ^       EXP(.7+ALOG(Y)/3.-(3.25/(4.+(ALOG(Y)+5.4)**2.)))
C           WSEG FORMULA
C
Z0KFT=44.+6.1*ALOG(Y)-.205*(ALOG(Y)+2.42)*ABS(ALOG(Y)+2.42)
            Z0M=Z0KFT/3.28*1000.
C           USING HOPKINS FORMULA
C           LNY=ALOG(Y(EVENT)*1000.)
C           Z0M=EXP(7.889+.34*LNY+.001226*LNY**2-.005227*LNY**3
C     ^     +.000417*LNY**4)
             DO 100 K=1,NGROUP
             ZGROUP(K)=Z0M
 100         CONTINUE
            SIGZ0=.18*Z0M/1000.
            TC=12.*Z0KFT/60.-2.5*(Z0KFT/60.)**2
C        BEGIN X INCREMENT LOOP
<----------
            DELTX=20.
C           SET XX=DISTANCE DOWNWIND FROM GZ, COMPUTE ARRIVAL
TIME
               DO 700 INX=1,149
               GRPSUM=0.
               XX=FLOAT(INX)*DELTX
      GO TO 670
 669             PIVX=0.
                 PIVY=0.
                 VECTOR=38.
                 XXSTART=0.
                 IF(..X.GT.443.) THEN
                  VECTOR=24.
                  XXSTART=443.
                  PIVX=443.*COSD(38.)
                  PIVY=443.*SIND(38.)
                  ENDIF
                 IF(XX.GT.1662.) THEN
                  VECTOR=-30.
                  XXSTART=1662.
                  PIVX=PIVX+(1662.-443.)*COSD(24.)
                  PIVY=PIVY+(1662.-443.)*SIND(24.)
                  ENDIF
                 IF(XX.GT.2069.) THEN
```

```
                    VECTOR=-40.
                    XXSTART=2069.
                    PIVX=PIVX+(2069.-1662.)*COSD(-30.)
                    PIVY=PIVY+(2069.-1662.)*SIND(-30.)
                    ENDIF
 670              TA=XX/VWIND
                  DELTAT=DELTX/VWIND
                  DELSEC=DELTAT*3600.
C                 COMPUTE CLOUD DISPERSION IN YY DIRECTION (KM)
                    TSTAR=MIN(3.,TA)
C                   SIGY=SQRT
C     ^
C
(SIGY0**2.*(1.+(8.*TSTAR/TC))+.5*(SHEAR*SIGZ0*TA)**2.)
                    SIGY=50.+555.*(EXP(-TA/40.)-EXP(-TA/10.))
C                    WRITE(6,*)' ZOM=',ZOM,' SIGY=',SIGY,' TA=',TA
C                 COMPUTE ALTITUDE OF EACH CONTRIBUTING PARTICLE
SIZE GROUP
                    DO 680 K=1,NGROUP
                    RP=RCENTR(K)
                    IF(ZGROUP(K).GT.0.)THEN
                       ZB=ZGROUP(K)
                       ELSE ZB=0.
                       ENDIF
                    DZ=VEL(ZB,RP)*DELSEC
                    IF((ZGROUP(K).GT.0. ).AND.
((ZGROUP(K)-DZ).LT.0.))
     ^              RDEP=RCENTR(K)
                    ZGROUP(K)=ZGROUP(K)-DZ
                    GRPSUM=GRPSUM+
     ^              GRNDF(ZGROUP(K),SIGZ0,TA,0.)*WEIGHT(K)
     ^              *MC
C                   WRITE(6,679)INX,K,ZB,DZ,
C     ^             GRNDF(ZGROUP(K),SIGZ0,TA,0.),GRPSUM
 679               FORMAT( ' INX',I3,' GP',I3,' ZB',E10.3,'
DZ',E10.3,
     ^             ' GRNDF',E10.3,' GRPSUM',E10.3)
 680                CONTINUE
C                 SET VALUE OF CUMULATIVE ACTIVITY ON
CENTERLINE(MILLICURIES)
                    SED=GRPSUM*EXP(-TA/TWASH)
                    WASH(INX)=MC*(1.-EXP(-TA/TWASH))
                    ACTCENT(INX)=WASH(INX)+SED
C                    WRITE(6,685)XX,TA,SED,WASH(INX),RDEP
 685               FORMAT( ' XX=',E8.3,' TA=',E8.3,' SED=',E8.3
     ^             ,' WASH=',E8.3,' RDEP=',E8.3)
C                    WRITE(6,*)'INX=',INX,' ACTCENT=',ACTCENT(INX)
       GO TO 390
C                 COMPUTE ACTIVITY/AREA ON THE GROUND ('ACT' IN
CURIES/SQ M)
C                   FOR EACH XX POSITION, VARY YY OUT TO +-100 KM
                       DO 380 J=1,101
                       YY=FLOAT(J-1)*20.-1000.
                        EXPON=.5*(YY/SIGY)**2.
                        IF (EXPON.GT.100.) THEN
```

```
                        EXPFAC=0.0
                        ELSE
                        EXPFAC=EXP(-EXPON)
                        ENDIF
                       FYTA=(SQRT(2.*3.14159)*SIGY)**(-1.)*EXPFAC
                       IF(INX.EQ.1) THEN
                          ACT(INX,J)=ACTCENT(INX)
     ^                    *FYTA/DELTX*2.59
C                          MILLICURIES PER SQUARE MILE
                          ELSE
                          ACT(INX,J)=(ACTCENT(INX)
     ^                    -ACTCENT(INX-1))*FYTA/DELTX
                          ENDIF
C                         UPDATE CUMULATIVE ACTIVITY
                          XC=PIVX+(XX-XXSTART)*COSD(VECTOR)
     ^                       -YY*SIND(VECTOR)
                          YC=PIVY+(XX-XXSTART)*SIND(VECTOR)
     ^                       +YY*COSD(VECTOR)
                          IC=INT((XC+3000.)/60.)-2000./60.
                          IF(IC.LE.0) GO TO 690
                          JC=INT((YC+3000.)/60.)
                          ACTCUM(IC,JC)=ACTCUM(IC,JC)+ACT(INX,J)/9.

                       ACTMAX=MAX(ACTMAX,ACTCUM(IC,JC))
 690                   CONTINUE
C                 WRITE(6,*)' XX=',XX,' YY=',YY,' ACT=',ACT(INX,J)
 380             CONTINUE
 390             CONTINUE
 700              CONTINUE
 710  CONTINUE
      WRITE(6,*)'ACTMAX=',ACTMAX
      GO TO 212
C COMPUTE ACTIVITY ENCLOSED BY EACH CONTOUR
C  EACH 60 X 60 KM CELL IS 1390 SQUARE MILES
 208  DATA DOWN10,DOWN20,DOWN30,DOWN40,DOWN50,DOWN60 /6*0./
      AREA10=0.
      DO 200 I=1,100
      DO 210 J=1,100
      IF(ACTCUM(I,J).GT.10.)AREA10=AREA10+1390.
      IF(ACTCUM(I,J).GT.60.) THEN
         DOWN60=DOWN60+1390.*ACTCUM(I,J)
         ACTCUM(I,J)=60.
         ENDIF
      IF((ACTCUM(I,J).GT.50.).AND.(ACTCUM(I,J).LE.60.))
     ^DOWN50=DOWN50+1390.*ACTCUM(I,J)
      IF((ACTCUM(I,J).GT.40.).AND.(ACTCUM(I,J).LE.50.))
     ^DOWN40=DOWN40+1390.*ACTCUM(I,J)
      IF((ACTCUM(I,J).GT.30.).AND.(ACTCUM(I,J).LE.40.))
     ^DOWN30=DOWN30+1390.*ACTCUM(I,J)
      IF((ACTCUM(I,J).GT.20.).AND.(ACTCUM(I,J).LE.30.))
     ^DOWN20=DOWN20+1390.*ACTCUM(I,J)
      IF((ACTCUM(I,J).GT.10.).AND.(ACTCUM(I,J).LE.20.))
     ^DOWN10=DOWN10+1390.*ACTCUM(I,J)
 210  CONTINUE
```

```
 200  CONTINUE
      CUM10=DOWN60+DOWN50+DOWN40+DOWN30+DOWN20+DOWN10
      WRITE(6,209)DOWN60,DOWN50,DOWN40,DOWN30,DOWN20,DOWN10
 209  FORMAT( ' DOWN60-10=',6(E10.3))
      WRITE(6,*) 'CUMULATIVE DOWN UP TO CONTOUR 10=',CUM10
      WRITE(6,*)'CUMULATIVE AREA UP TO CONTOUR 10=',AREA10
 212  CONTINUE
C COMPUTE FIGURE OF MERIT FOR SIZE DISTRIBUTION OPTIMIZATION
      DATA
(ATRUE(I),I=1,6)/0.,14.7E6,47.1E6,55.2E6,60.3E6,63.3E6/
      DATA(XTRUE(I),I=1,6)/C.,480.,1700.,2100.,2460.,2800./
      F0=0.
      F0=(ATRUE(2)-ACTCENT(24))**2.
      F0=F0+(ATRUE(3)-ACTCENT(85))**2.
      F0=F0+(ATRUE(4)-ACTCENT(105))**2.
      F0=F0+(ATRUE(5)-ACTCENT(123))**2.
      F0=F0+(ATRUE(6)-ACTCENT(140))**2.
      WRITE(6,*)ATRUE(2),ACTCENT(24)
      WRITE(6,*)ATRUE(3),ACTCENT(85)
      WRITE(6,*)ATRUE(4),ACTCENT(105)
      WRITE(6,*)ATRUE(5),ACTCENT(123)
      WRITE(6,*)ATRUE(6),ACTCENT(140)
      WRITE(6,*)'RM= ',RM,' SLOPE=',SLOPE,' F0=',F0
 1000 CONTINUE
 1001 GO TO 11
      GO TO 800
C DISSPLA CONTOUR PLOTTING CALLS FOLLOW---------
C PACKAGE PLOTS ACTIVITY GROUNDED VS TIME
 799  CALL COMPRS
      CALL PAGE(8.5,11.)
      CALL AREA2D(5.,5.)
      CALL LINES('DATA,',IPKRAY,1)
      CALL LINES('WASHOUT ONLY,',IPKRAY,2)
      CALL LINES('WITH SEDIMENT,',IPKRAY,3)
      CALL HEADIN('ACTIVITY GROUNDED VS DISTANCE,',100,1.75,1)
      CALL INTAXS
      CALL XNAME('KILOMETERS,',100)
      CALL YNAME('KILOCURIES,',100)
      CALL GRAF(0.,500.,3000.,0.,10.,100.)
      ENCODE(100,15,LABEL)NDIST,RM,SLOPE
   15 FORMAT(' DIST',I2,', RM=',E8.3,', SLOPE=',E8.3,',')
      CALL RLMESS(LABEL,100,100.,75.)
      CALL THKFRM(.02)
      CALL FRAME
      DO 10 I=1,149
      X(I)=20.*FLOAT(I)
      WASH(I)=WASH(I)/1.E6
      ACTCENT(I)=ACTCENT(I)/1.E6
C     MILLICURIES-->KILOCURIES
   10 CONTINUE
      DO 20 I=1,6
```

```
      ATRUE(I)=ATRUE(I)/1.E6
   20 CONTINUE
      CALL MARKER(15)
      CALL CURVE(XTRUE,ATRUE,6,-1)
      CALL MARKER(5)
      CALL CURVE(X,WASH,149,15)
      CALL MARKER(17)
      CALL CURVE(X,ACTCENT,149,15)
      CALL LEGEND(IPKRAY,3,.25,4.)
      CALL ENDPL(0)
      CALL DONEPL
      STOP
 800  CONTINUE
      END
C*************************************************************************
*************
C*************************************************************************
*************
C*************************************************************************
*************
      SUBROUTINE SIZCNF(RM,B,MOMENT)
C     SUBROUTINE TO PARTITION PARTICLE MASS DISTRIBUTIONS INTO
GROUPS
      COMMON RCENTR(33),MASFRA(33)
      DIMENSION RLEFT(33),RRIGHT(33),MASCNF(33)
      REAL MASCNF,MASFRA,MOMENT,MC
      INTEGER GROUP,OFFSET
      EXTERNAL CNF
C     CNF IS THE CUMULATIVE NORMAL
FUNCTION(RADIUS,RM,BETA,MOMENT)
C     DEFINE LOG NORMAL FUNCTION PARAMETERS, RM  BETA
 30   FORMAT (I3,5(E10.3))
C      WRITE(6,*) 'RM=',RM, '  B=',B,'  MOMENT=',MOMENT
       WRITE(6,*)'PURE CUMULATIVE NORMAL SIZE DISTRIBUTION
OPERATIVE'
C      WRITE(6,40)
 40   FORMAT(' GROUP  RLEFT  RCENTROID   RRIGHTOID  ACTV FRAC
CUMULA')
      EXPON=-6.
      GROUP=1
           RLEFT(GROUP)=0.
           RRIGHT(GROUP)=10.**EXPON
           RCENTR(GROUP)=RRIGHT(GROUP)
C   WRITE(6,60) RRIGHT(GROUP),RM,B
C60   FORMAT ( 3E10.3)
           MASCNF(GROUP)=CNF(RRIGHT(GROUP),RM,B,MOMENT)
           MASFRA(GROUP)=MASCNF(GROUP)
      DO 130 GROUP=2, 32
           EXPON=EXPON+.1
           RRIGHT(GROUP)=10.**EXPON
           RLEFT(GROUP)=RRIGHT(GROUP-1)
           RCENTR(GROUP)=SQRT(RLEFT(GROUP)*RRIGHT(GROUP))
           R=RRIGHT(GROUP)
           MASCNF(GROUP)=CNF(R,RM,B,MOMENT)
```

```
            MASFRA(GROUP)=MASCNF(GROUP)-MASCNF(GROUP-1)
 130   CONTINUE
C      LUMP LARGE SIZES TOGETHER IN GROUP WITH RCENTR=1000 MICRONS

            K=33
            RRIGHT(K)=999.
       RLEFT(K)=RRIGHT(K-1)
            RCENTR(K)=RRIGHT(K-1)
            MASFRA(K)=1.-MASCNF(K-1)
            MASCNF(K)=CNF(RRIGHT(K),RM,B,MOMENT)
C OUTPUT GROUP DIVISIONS
       DO 140 K=1,33
C
WRITE(6,30)K,RLEFT(K),RCENTR(K),RRIGHT(K),MASFRA(K),MASCNF(K)
 140   CONTINUE
       RETURN
       END
C*************************************************************************
*************
C*************************************************************************
**************
       SUBROUTINE SIZNAT(RM,B,MOMENT,P1,RMAX)
       COMMON RCENTR(33),ACTFRA(33)
C      SUBROUTINE PARTITIONS NATHANS R4 DISTRIBUTION INTO ACTIVITY
GROUPS
       DIMENSION RLEFT(33),RRIGHT(33),ACTCUM(33)
       REAL MOMENT,MC,IA,IB
       INTEGER GROUP,OFFSET
       EXTERNAL CNF
C      CNF IS THE CUMULATIVE NORMAL FUNCTION
C      DEFINE NATHANS PARAMETERS
            RO=RM*EXP((P1-1.)*B*B)
            R2PI=SQRT(2.*3.14159)
 30    FORMAT (I3,5(E10.3))
C       WRITE(6,40)
 40    FORMAT(' GROUP RLEFT     RRIGHT    RCENTR     ACTV FRAC
CUM')
       EXPON=-6.1
       GROUP=0
 60    FORMAT ( 3E10.3)
       DO 280 GROUP=1, 32
            EXPON=EXPON+.1
            RRIGHT(GROUP)=10.**EXPON
             IF (GROUP.EQ.1) THEN
                  RLEFT(GROUP)=0.
                  RCENTR(GROUP)=RRIGHT(GROUP)
                  ELSE
                  RLEFT(GROUP)=RRIGHT(GROUP-1)
                  RCENTR(GROUP)=SQRT(RLEFT(GROUP)*RRIGHT(GROUP))
            END IF
            RP=RRIGHT(GROUP)
C      CALCULATE DENOMINATOR WHICH IS PROPORTIONAL TO TOTAL
ACTIVITY
               IA=RO**(P1/2.+.5)*RM**( 5-P1/2.)*RM**(MOMENT)*B*R2P
```

```
I*
     ^          EXP(.5*MOMENT*MOMENT*B*B)*CNF(RO,RM,B,MOMENT)
                IF (MOMENT.EQ.(P1-1.)) THEN
                  IB=RO**P1*ALOG(RMAX/RO)
                  ELSE
                  IB=RO**P1*(RMAX**(MOMENT-P1+1.)-RO**(MOMENT-P1+1.
))
     ^            /(MOMENT-P1+1.)
                  END IF
                DENOM=IA + IB
                F=IA/(IA + IB)
C     NOW CALCULATE NUMERATOR WHICH IS PROPORTIONAL TO ACTIVITY
DOWN
                IF (RP.LT.RO)THEN
                  CNFPART=CNF(RP,RM,B,MOMENT)
                  ELSE
                  CNFPART=CNF(RO,RM,B,MOMENT)
                  END IF
                VIA=RO**(.5+P1/2.)*RM**(.5-P1/2.)*RM**(MOMENT)*B*R2
PI*
     ^          EXP(MOMENT*MOMENT*B*B*.5)*CNFPART
                IF (RP.LT.RO)THEN
                  VIB=0.
                  GO TO 250
                  END IF
                IF (MOMENT.EQ.(P1-1.))THEN
                  VIB=RO**P1*ALOG(RP/RO)
                  ELSE
                  VIB=RO**P1*(RP**(MOMENT-P1+1.)-RO**(MOMENT-P1+1.)
)
     ^                 /(MOMENT-P1+1.)
                  END IF
 250            CONTINUE
                ACTCUM(GROUP)=(VIA+VIB)/DENOM
              IF (GROUP.EQ.1) THEN
                  ACTFRA(GROUP)=ACTCUM(GROUP)
                  ELSE
                  ACTFRA(GROUP)=ACTCUM(GROUP)-ACTCUM(GROUP-1)
              END IF
C              WRITE(6,30)
GROUP,RLEFT(GROUP),RRIGHT(GROUP),RCENTR(GROUP)
C     ^    ,ACTFRA(GROUP),ACTCUM(GROUP)
 280  CONTINUE
C     DEFINE GROUP WHICH LUMPS BIG PARTICLES TOGETHER WITH
RCENTR=1000 MICRONS
           GROUP=33
           RLEFT(GROUP)=RRIGHT(GROUP-1)
           RRIGHT(GROUP)=RMAX
           RCENTR(GROUP)=RRIGHT(GROUP-1)
           ACTFRA(GROUP)=1.-ACTCUM(GROUP-1)
           ACTCUM(GROUP)=ACTCUM(GROUP-1)+ACTFRA(GROUP)
           WRITE(6,30)
GROUP,RLEFT(GROUP),RRIGHT(GROUP),RCENTR(GROUP)
     ^   ,ACTFRA(GROUP),ACTCUM(GROUP)
```

```
      RETURN
      END
C*************************************************************************
*************
C*************************************************************************
*************
      FUNCTION CNF(R,RM,B,MOMENT)
C     COMPUTES CUMULATIVE NORMAL FUNCTION FOR ACTIVITY
DISTRIBUTION
            REAL MOMENT
            R3=RM*EXP(MOMENT*B*B)
            Z=(ALOG(R)-ALOG(R3))/B
C           WRITE(6,50) Z
C 50        FORMAT (' Z=',E10.3)
            IF (Z) 1060,1050,1050
 1050       CNF=1.-.5/(1.+.196854*Z+.115194*Z**2 +.000344*Z**3
+.019527*Z
     ^                  **4 )**4
            GO TO 1070
 1060         Z=-Z
            CNF=.5/(1.+.196854*Z+.115194*Z**2+.000344*Z**3+.019527
*Z**4)
     ^              **4
 1070 RETURN
      END
C*************************************************************************
*************
C*************************************************************************
*************
      FUNCTION GRNDF(ZB,SIGZ0,TA,ZTROP)
      REAL KDZ
      KDZ=0.
      SIGZ=SIGZ0*1000.+SQRT(2.*KDZ*TA*3600.)
      DELTZ=ZB-ZTROP
      A=DELTZ/SIGZ
      IF (A) 1060,1050,1050
 1050    CUMNF=1.-.5/(1.+.196854*A+.115194*A**2 +.000344*A**3
+.019527*A
     ^         **4 )**4
               GO TO 1070
 1060     A=-A
          CUMNF=.5/(1.+.196854*A+.115194*A**2+.000344*A**3+.01952
7*A**4)
     ^       **4
 1070 GRNDF=1.-CUMNF
      RETURN
      END
C*************************************************************************
*************
C*************************************************************************
*************
      FUNCTION VEL(ZB,RP)
C     COMPUTES TERMINAL VELOCITY OF SPHERICAL PARTICLES USING
FULL DELFIC
```

```
C     FALL MECHANICS AND U.S. STANDARD ATMOSPHERE EQUATIONS
C     SUBROUTINE ATMOS RETURNS DENSITY, VISCOSITY AND MEAN FREE
PATH AT ALT ZB
      REAL MFP,LOGREY
C     EXTERNAL ATMOS
      CALL ATMOS(ZB,DENS,VISC,MFP)
      DENSF=2600.
      G=9.8
      QZ=4*DENS*(DENSF-DENS)*G*(2.*RP)**3/(3.*VISC*VISC)
C     WRITE(6,1051)QZ,DENS,VISC,MFP
C1051 FORMAT('QZ,DENS,VISC,MFP',4(E10.3))
      YY=ALOG(QZ)
C     DENSF IS PARTICLE DENSITY, G IS GRAV, QZ IS DAVIES NUMBER
DEFINED IN
C     DNA TR-5159F-1, P24
           IF(QZ .LE. .3261)THEN
                VEL=VISC*QZ/(24.*DENS*2.*RP)
                GO TO 1100
                ENDIF
           IF((QZ .GT. .3261) .AND. (QZ .LE. 84.175))THEN
                VEL=(VISC/(DENS*2.*RP))*EXP(-3.18657+.992696*YY-
     ^
1.53193E-3*YY**2-9.87059E-4*YY**3-5.78878E-4*YY**4
     ^          +8.551759E-5*YY**5-3.27815E-6*YY**6)
                GO TO 1100
                ENDIF
           IF((QZ .GT. 84.175) .AND. (QZ.LT.140))THEN
                VEL=VISC*QZ*(4.166667E-2-2.3363E-4*QZ+2.0154E-6*Q
Z**2
     ^          -6.9105E-9*QZ**3)/(DENS*2.*RP)
                GO TO 1100
                ENDIF
           IF((QZ .GE. 140) .AND. (QZ .LT. 4.5E7))THEN
                LOGREY=-1.29536+.986*YY/2.303-.046677*(YY/2.303)*
*2
     ^          +.0011235*(YY/2.303)**3
                REYNOL=10.**LOGREY
                VEL=REYNOL*VISC/(2.*DENS*RP)
                ENDIF
C          KNUDSEN SLIP CORRECTION
 1100      IF(RP.GT.100.*MFP) THEN
             EXPFAC=0.
             ELSE
             EXPFAC=EXP(-.656*2.*RP/MFP)
             ENDIF
           VEL=VEL*(1.+(1.644+.552*EXPFAC)*MFP/
     ^          (2.*RP))
      RETURN
      END
C*************************************************************
**********
C*************************************************************
**********
      SUBROUTINE ATMOS(ZB,DENS,VISC,MFP)
```

```
C     SUBROUTINE CALCULATES ATMOSPHERIC TEMPERATURE, PRESSURE AND
VISCOSITY
C     FOR ALTITUDES UP TO 84,852 METERS (MKS UNITS EMPLOYED)
      REAL LK,NUMDEN,MFP
      IF(ZB .LE. 11000.)THEN
           LK=-.006545
           TK=288.15
           PK=101300.
           TB=TK+LK*ZB
           PB=PK*(TK/TB)**(.034164/LK)
           GO TO 1240
           ENDIF
      IF((ZB .GT. 11000.) .AND. (ZB .LE. 20000.))THEN
           ZK=11000.
           TK=216.65
           PK=22690.
           LK=0.
           TB=TK
           PB=PK*EXP(-.034164*(ZB-ZK)/TK)
           GO TO 1240
           ENDIF
      IF((ZB .GT. 20000.) .AND. (ZB .LE. 32000.))THEN
           ZK=20000.
           TK=216.65
           PK=5528.
           LK=.001
           TB=TK+LK*(ZB-ZK)
           PB=PK*(TK/TB)**(.034164/LK)
           GO TO 1240
           ENDIF
      IF((ZB .GT. 32000.) .AND. (ZB .LE. 47000.))THEN
           ZK=32000.
           TK=228.65
           PK=888.8
           LK=.0028
           TB=TK+LK*(ZB-ZK)
           PB=PK*(TK/TB)**(.034164/LK)
           GO TO  1240
           ENDIF
      IF((ZB .GT. 47000.) .AND. (ZB .LE. 51000.))THEN
           ZK=47000.
           TK=270.65
           PK=110.873
           LK=0.
           TB=TK
           PB=PK*EXP(-.034164*(ZB-ZK)/TK)
           GO TO 1240
           ENDIF
      IF((ZB .GT. 51000.) .AND. (ZB .LE. 71000.))THEN
           ZK=51000.
           TK=270.65
           PK=66.9218
           LK=-.0028
           TB=TK+LK*(ZB-ZK)
```

```
            PB=PK*(TK/TB)**(.034164/LK)
            GO TO 1240
            ENDIF
      IF((ZB .GT. 71000.) .AND. (ZB .LE. 84852.))THEN
            ZK=71000.
            TK=214.65
            PK=3.95536
            LK=-.002
            TB=TK+LK*(ZB-ZK)
            PB=PK*(TK/TB)**(.034164/LK)
            GO TO 1240
            ENDIF
      IF((ZB .GT. 84852))THEN
            WRITE(6,1230)
            GO TO 1241
            ENDIF
 1230 FORMAT('PARTICLE ALTITUDE BEYOND RANGE OF PROGRAM
APPLICABILITY')
 1240 VISC=1.46E-6*TB**1.5/(TB+110.4)
      DENS=.003484*PB/TB
      NUMDEN=DENS*2.55E25/1.23
C             PER CUBIC METER: 2.55E25 MOLECULES PER CUBE AT SEA
LEVEL.
C             DENSITY AT SEA LEVEL IS 1.23 KG/CUBE
      MFP=1./(1.414*NUMDEN*4.5E-19)
C             MFP=1./(ROOT2*N*SIGMA)
 1241 RETURN
      END
END OF FILE
```

REFERENCES

1. R. P. Turco, O. B. Toon, T. P. Ackerman, J. B. Pollack, C. Sagan, **The Global Atmospheric Consequences of Nuclear War** , unpublished, R and D Associates, Marina del Rey, CA, 1983. ("TTAPS" report)
2. R. P. Turco, O. B. Toon, T. P. Ackerman, J. B. Pollack, C. Sagan, "Nuclear Winter: Global Consequences of Multiple Nuclear Explosions," **Science** . Volume 222, Number 4630, 23 Dec 1983, p1283-1292.
3. National Research Council, Frank Press, Chairman, **The Effects on the Atmosphere of a Major Nuclear Exchange** , National Academy Press, Washington, DC, 1985.
4. C. Covey, S. H. Schneider, and S.L. Thompson, "Global Atmospheric Effectsof Massive Smoke Injections from a Nuclear War: Results from General Circulation Model Simulations," **Nature** , 308:21-25, 1984.
5. V. Ramaswamy and J. T. Kiehl, "Sensitivities of the Radiative Forcing Due to Large Loadings of Smoke and Dust Aersols," **Journal of Geophysical Research** , Vol. 90, No. D3: 5597-5613, June 20 1985.
6. W. R. Cotton, G. Tripoli, C. Chen, **Recent Results of Convective Response to Fire Storms** , Presentation, Defense Nuclear Agency Global Effects Program Technical Review, February 1986.
7. D. S. Simonett, **A Critical Examination of Methods of Estimating the Spatial Distribution and Magnitudes of Urban Fuel Loadings** , Presentation, Defense Nuclear Agency Global Effects Program Technical Review, February 1986.
8. H. G. Norment, **DELFIC: Department of Defense Fallout Prediction System** , Volumes I and II, DNA 5159F, 31 December 1979.
9. A. K. Stebbins, **Third Annual HASP Briefing** , DASA-531 (DTL005840), 15 December 1959.
10. A. K. Stebbins, **A Special Report on the High Altitude Sampling Program** , DASA-532B, June 1960.
11. A. K. Stebbins, **Second Special Report on the High Altitude Sampling Program** , DASA-539B, August 1961.
12. J. P. Friend, H. W. Feely, P. W. Krey, J. Spar, A. Walton, **High Altitude Sampling Program Purpose and Methods** , DASA 1300, Volume 1, August 1961.
13. B. L. Yoon, G. D. Wilensky, D. C. Yoon, M. K. Grover, **Nuclear Dust and Radiation Cloud Environments for Aircraft and Optical Sensors** ,RDA-TR-135603-001,April 1985,Contract DNA-001-85-C-0022, R & D Associates, Marina del Rey, CA.
14. K. H. Larson et al, **Distribution, Characteristics, and Biotic Availability of Fallout, Operation Plumbbob** ,WT-1488, Laboratory of Nuclear Medicine and Radiation Biology, University of California at Los Angeles, 26 July 1966.
15. C. T. Rainey, J. W. Neel, H. M. Mork, K. H. Larson, **Distribution and Characteristics of Fall-out at Distances Greater Than 10 Miles from Ground Zero, March and April 1953** , WT-811, March-June 1953.
16. M. W. Nathans, R. Thews, I. J. Russell, "The Particle Size Distribution of Nuclear Cloud Samples, " **Advances in Chemistry Series: Radionuclides in the Environment** , No. 93 : 360-380, 1970.

17. M. W. Nathans, **The Determination of the Homogeneity of Nuclear Clouds from Airbursts** , TLW-6100, Part I, Contract AT (04-3)682 Mod. 4, United States Atomic Energy Commission, May 1971.

18. M. W. Nathans, unpublished.

19. M. W. Nathans, private communication.

20. E. C. Freiling, **Fractionation III. Estimation of Degree of Fractionation and Radionuclide Partition for Nuclear Debris** , USNRDL-TR-680 (AD423725), 12 September 1963.

21. R. C. Tompkins, **Radiochemical Interpretations of Small Boy Fallout** , BRLR 1623 (AD908895), November 1972.

22. G. E. Pugh, R. J. Galiano, **An Analytic Model of Close-in Deposition of Fallout for Use in Operational Type Studies** , WSEG Research Memorandum No. 10 , 15 October 1959 (AD261752).

23. E. D. Hirleman, "Nonintrusive Laser-Based Particle Diagnostics," Paper 83-1514, American Institute of Aeronautics and Astronautics 18th Thermophysics Conference, 1-3 June 1983.

24. Mason, A. S., private communication.

25. Van de Hulst, H. C., **Light Scattering by Small Particles** , New York, Wiley: 1957.

26. Pollack, J. B., O. B. Toon, C. Sagan, A. Summers, B. Baldwin, and W. VanCamp, "Volcanic Explosions and Climatic Change: A Theoretical Assessment," **Journal of Geophysical Research** , 81: 1071-1083, 1976.

27. J. B. Pollack., O. B. Toon, T. P. Ackerman, C. P. McKay, and R. P. Turco, "Environmental Effects of an Impact-generated Dust Cloud: Implications for the Cretaceous-Tertiary Extinctions," **Science** , 219:287-289, 1983.

28. W. B. Heidt, E. A. Schuert, W. W. Perkins, R. L. Stetson, **Nature, Intensity, and Distribution of Fall-out from Mike Shot** , WT-615, Armed Forces Special Weapons Project, November 1952.

29. C. J. Bridgman, W. S. Bigelow, "A New Fallout Prediction Model," **Health Physics** , Vol. 43, No. 2: 205-218, August, 1982.

30. D. K. Winegardner, **PROFET: a Rapid Method for Generating Fallout Predictions from Field Data** , NDL-TR-124, U. S. Army Nuclear Defense Laboratory, May 1969 (AD852969).

31. A. D. Anderson, **Application of Theory for Close-in Fallout to Low-yield Land Surface and Underground Nuclear Detonations** , USNRDL-TR-289, U. S. Naval Radiological Defense Laboratory, 12 January 1959(AD234359).

32. J. T. McGahan, E. J. Kownacki, **Sensitivity of Fallout Predictions to Initial Conditions and Model Assumptions** , DNA 3439F, December 1974 (AD/A-002464).

33. H. G. Norment, private communication.

34. M. W. Nathans, private communication.

35. M. W. Nathans, unpublished.

36. J. P. Friend, H. W. Feely, P. W. Krey, J. Spar, A. Walton, **The High Altitude Sampling Program** , DASA 1300, Volume 4: Application of HASP Data, 31 August 1961 (AD267613).

37. A. S. Mason, G. Hut, K. Telegadas, "Stratospheric HTO and 95Zr Residence Times," **Tellus** , 34: 369-375, 1982.

38. E. Bauer, **A Study of Stratosphere-to-Troposphere Transfer Using Radioactive Tracer Data in a One-dimensional Parameterisation** , FAA-EE-80-06, IDA-P-1456, February 1980 (ADA092841).

39. E. Bauer, R. C. Oliver, W. Wasylkiwskyj, "On the Use of Zr-95 Data from Chinese Atmospheric Thermonuclear Explosions to Study Stratospheric Transport in a 1-D Parameterization," **Journal of Geophysical Research** , 83: 4019, 1978.

40. A. S. Mason, H. G. Ostlund, **Stratospheric Tritium Sampling** , Final Report, LA-10546-PR, Los Alamos National Laboratory, September 1985.

41. K. Telegadas, **Radioactivity Distribution in the Stratosphere from the Chinese High Yield Nuclear Test of June 27, 1973** , HASL-298, U. S. Energy Research and Development Administration, Washington, D.C., January 1976.

42. K. Telegadas, **An Estimate of Maximum Credible Atmospheric Radioactivity Concentrations from Nuclear Tests** , HASL-328, U. S. Energy Research and Development Administration, Washington, D.C., October 1977.

43. H. M. Foley, M. A. Ruderman, **Stratospheric Nitric Oxide Production from Past Nuclear Explosions and its Relevance to Projected SST Pollution** , P-894, Institute for Defense Analyses, August 1972 (DTL113178).

44. H. Seitz, B. Davidson, J. P. Friend, H. W. Feeley, **Numerical Models of Transport, Diffusion and Fallout of Stratospheric Radioactive Material** , Final Report on Project Streak, NYO-3654-4, U. S. Atomic Energy Commission, Washington, D. C., 31 May 1968(DTL111249).

45. J. S. Chang, W. H Duewer, D. J Wuebbles, "The Atmospheric Nuclear Tests of the 1950's and 1960's: A Possible Test of Ozone Depletion Theories," **Journal of Geophysical Research** , Vol. 84, No. C4, 20 April 1979.

46. Peterson, K. R., "An Empirical Model for Estimating World-Wide Deposition from Atmospheric Nuclear Detonation," **Health Physics** , 18: 357-378, 1970.

47. H. A. Hawthorne, **Compilation of Local Fallout Data from Test Detonations 1945-1962 Extracted from DASA 1251** , Vol I-II, DNA 1251-1-EX and DNA 1251-2-EX, May 1979.

48. S. Glasstone, P. J. Dolan, **The Effects of Nuclear Weapons** , 1977.

49. R. C. Tompkins, I. J. Russell, M. W. Nathans, "A Comparison between Cloud Samples and Close-in Ground Fallout Samples from Nuclear Ground Bursts," **Radionuclides in the Environment , Advances in Chemistry Series** , American Chemical Society, 93: 381-400, 1970.

50. M. Eisenbud, **Environmental Radioactivity** , New York: Academic Press, 1973.

51. National Academy of Sciences, **Environmental Impact of Stratospheric Flight: Biological and Climatic Effects of Aircraft Emissions in the Stratosphere** , Washington, DC, 1975.

52. A. Walton, R. E. Fried, **Studies of Nuclear Debris in Precipitation (Summary Report)** , NYO-9530, Isotopes, Inc., 15 August 1961 (DTL013292).

53. L. T. Alexander et al, **Strontium-90 on the Earth's Surface** , HASL-88, USAEC, 1 July 1960.

54. Capt N. C. Davis, **Particle Size Determination from Local Fallout** , MS thesis, AFIT/GNE/ENP/86D-1, Air Force Institute of Technology, Wright-Patterson AFB OH, December 1986.

55. **U. S. Standard Atmosphere Supplements** , U. S. Government Printing Office, Washington, D.C., 1966.

56. Capt A. T. Hopkins, **A Two Step Method to Treat Variable Winds in Fallout Smearing Codes** , MS Thesis, AFIT/GNE/PH/82M-10, School of Engineering, Air Force Institute of Technology (AU), Wright-Patterson AFB OH, March 1982.

57. M. Knudsen, S. Weber, **Ann. Physik** , 36: 981, 1911.

58. H. Mitchell, R and D Associates, private communication.

59. C. E. Junge, "Vertical Profiles of Condensation Nuclei in the Stratosphere," **Journal of Meteorology** , Vol. 18, No. 4, 501-509, August 1961.

60. **DISSPLA User's Manual** , Version 9.0, Integrated Software Systems Corporation, San Diego, CA, 1981.

61. J. H. Harley, "Results of Analysis of Nevada Soils," HASL Memorandum, 25 August 1958.

62. K. H. Larson et al, **A Report of Sr90 and Total Beta Contamination in Eleven Areas in Nevada and Utah as of August, 1958** , University of California, 24 November 58.

63. J. P. Friend, H. W. Feely, P. W. Krey, J. Spar, A. Walton, **High Altitude Sampling Program Purpose and Methods** , DASA 1300, Volume 3, August 1961.

64. M. W. Nathans, unpublished.

65. C. F. Miller, **Biological and Radiological Effects of Fallout from Nuclear Explosions** , URS-702-1, Office of Civil Defense, Office of the Secretary of the Army, Washington, D.C., May 1969(AD688940).

66. E. C. Freiling, **Fractionation III. Estimation of Degree of Fractionation and Radionuclide Partition for Nuclear Debris** , USNRDL-TR-680, 12 September 1963 (AD423725).

67. E. C. Freiling, M. A. Kay, J. V. Sanderson, **Fractionation IV. Illustrative Calculations of the Effect of Radionuclide Fractionation on Exposure-Dose Rate from Local Fallout** , USNRDL-TR-715, 6 January 1964 (AD431227).

68. M. W. Nathans, private communication.

69. R. E. Heft, "The Characterization of Radioactive Particles from Nuclear Weapon Tests," **Advances in Chemistry Series: Radionuclides in the Environment** , No. 93 : 255-399, 1970.

70. Carpenter, H. J., Letter to E. Sevin, et al., (DNA) on dust-loading in the stabilized cloud from a nuclear burst, R D Associates, Marina del Rey, CA, 14 December 1982.

71. R. C. Tompkins, **Effect of Depth of Burial on Fallout from Atomic Demolition Munitions** , BRL-MR-2317, U.S. Army Ballistic Research Laboratory, August 1973 (AD913991).

72. M. Abramowitz and I. A. Stegun, **Handbook of Mathematical Functions** , National Bureau of Standards Applied Mathematics Series, #55, U. S. Government Printing Office, 1964.

73. J. E. McDonald, "An Aid to Computation of Terminal Fall Velocities of Spheres," **Journal of Meteorology** , 17: 463, 1960.

74. C. N. Davies, "Definitive Equations for the Fluid Resistance of Spheres," **Proceedings of the Physical Society** , 57: 259-270, London, 1945.

75. E. Cunningham, **Proceedings of the Physical Society** , 83-1: 357, London, 1910.

76. E. C. Freiling, **Physical and Radiochemical Properties of Fallout Particles** , U. S. Naval Radiological Defense Laboratory, USNRDL-TR-899, 15 June 1965 (AD623485).

VITA

George H. Baker III was born 23 March 1949 in Cheverly, Maryland. He graduated from Aberdeen High School (Maryland) and earned a B.A. in physics from Western Maryland College. In 1974 he received his M.S. degree (physics) from the University of Virginia. During 1973-1977 he investigated nuclear electromagnetic effects on tactical communications and field artillery at the U. S. Army Harry Diamond Laboratories. Since 1977 he has conducted the EMP effects and hardening programs for the Defense Nuclear Agency. Major efforts there have included MX vulnerability and hardening, strategic defense system vulnerability, and basic EMP technology development. The Defense Nuclear Agency sponsored his participation in the doctoral program at the Air Force Institute of Technology beginning in September 1984. He is a member of the American Physical Society.

Permanent address: 10858 Hampton Road
Fairfax Station, VA 22039

AD-A182 607

SECURITY CLASSIFICATION OF THIS PAGE

REPORT DOCUMENTATION PAGE

Form Approved OMB No. 0704-0188

1a. REPORT SECURITY CLASSIFICATION: Unclassified	1b. RESTRICTIVE MARKINGS
2a. SECURITY CLASSIFICATION AUTHORITY	3. DISTRIBUTION/AVAILABILITY OF REPORT: Approved for public release; distribution unlimited
2b. DECLASSIFICATION/DOWNGRADING SCHEDULE	
4. PERFORMING ORGANIZATION REPORT NUMBER(S): AFIT/DS/ENP/87-1	5. MONITORING ORGANIZATION REPORT NUMBER(S)
6a. NAME OF PERFORMING ORGANIZATION: School of Engineering; 6b. OFFICE SYMBOL (If applicable): AFIT/ENP	7a. NAME OF MONITORING ORGANIZATION: Defense Nuclear Agency
6c. ADDRESS (City, State, and ZIP Code): Air Force Institute of Technology, Wright-Patterson AFB, Ohio 45433	7b. ADDRESS (City, State, and ZIP Code): Washington, D.C. 20305
8a. NAME OF FUNDING/SPONSORING ORGANIZATION: Defense Nuclear Agency; 8b. OFFICE SYMBOL (If applicable): RAEE	9. PROCUREMENT INSTRUMENT IDENTIFICATION NUMBER
8c. ADDRESS (City, State, and ZIP Code): Washington, D.C. 20305	10. SOURCE OF FUNDING NUMBERS: PROGRAM ELEMENT NO. / PROJECT NO. / TASK NO. / WORK UNIT ACCESSION NO.

11. TITLE (Include Security Classification): see box 19

12. PERSONAL AUTHOR(S): Baker, George H.

13a. TYPE OF REPORT	13b. TIME COVERED	14. DATE OF REPORT (Year, Month, Day)	15. PAGE COUNT
PhD Dissertation	FROM _____ TO _____	1987 February 25	183

16. SUPPLEMENTARY NOTATION

17. COSATI CODES			18. SUBJECT TERMS (Continue on reverse if necessary and identify by block number)
FIELD	GROUP	SUB-GROUP	
19	11		Nuclear Winter; Nuclear Debris; Fallout; Atmospheric Physics; Dust Effects
04	01		

19. ABSTRACT (Continue on reverse if necessary and identify by block number)

Title: Implications of Atmospheric Test Fallout Data for Nuclear Winter
Advisory Committee Chairman: Charles J. Bridgman
Abstract: Historical atmospheric nuclear test data has been examined to gain information germane to nuclear winter. The size distribution of the nuclear debris aerosol is shown to govern the magnitude and duration of sunlight attenuation. By modeling the removal of nuclear debris from the atmosphere it has been possible to bound the admissible distribution of lofted particulates. This distribution bound reflects the average behavior of particulates from 97 tests contributing debris to the stratosphere. The results should be useful for fallout and dust effects modeling as well as nuclear winter studies.

20. DISTRIBUTION/AVAILABILITY OF ABSTRACT: ☐ UNCLASSIFIED/UNLIMITED ☒ SAME AS RPT. ☐ DTIC USERS	21. ABSTRACT SECURITY CLASSIFICATION: Unclassified
22a. NAME OF RESPONSIBLE INDIVIDUAL: Charles J. Bridgman	22b. TELEPHONE (Include Area Code): (513) 255-2012; 22c. OFFICE SYMBOL: AFIT/ENP

DD Form 1473, JUN 86 — Previous editions are obsolete. — SECURITY CLASSIFICATION OF THIS PAGE